高炉内ホールドアップとガス透過率の関係，並びに材料評価から得られる特殊鋼の安定生産に向けた充填層小型化モデルの研究

DISSERTATION

Study on the Relationship of Particle Hold-Up and Gas Permeability in Blast Furnace by Using Miniaturized Packed Bed Model to Maintain Stable Production of Special Steel from the View Point of Material Assessment

Siahaan Andrey Stephan

Graduate School of Engineering
Division of Production System Engineering
Muroran Institute of Technology
Muroran Hokkaido, Japan
2021

Study on the Relationship of Particle Hold-Up and Gas Permeability in Blast Furnace by Using Miniaturized Packed Bed Model to Maintain Stable Production of Special Steel from the View Point of Material Assessment

Siahaan Andrey Stephan

Graduate School of Engineering
Division of Production System Engineering
Muroran Institute of Technology
Muroran Hokkaido, Japan
2021

Study on the Relationship of Particle Hold-Up and Gas

Permeability in Blast Furnace by Using Miniaturized Packed Bed Model to Maintain Stable Production of Special Steel from the View Point of Material Assessment

by

Siahaan Andrey Stephan

DISSERTATION

Submitted in partial fulfillment of the requirements for the degree

DOCTOR OF ENGINEERING

Graduate School of Engineering
Division of Production System Engineering
Muroran Institute of Technology
Muroran Hokkaido, Japan
2021

Acknowledgements

I would like to express my gratitude to Professor Hideki Kawai, my major supervisor, with his knowledge and advice about my research topic, has guided me along this doctoral

journey. His unpretentious and cheerful personality left a deep impression on my life and made this doctoral course unforgettable and a meaningful.

I also would like to express my appreciation to Assistant Professor Yoshihiko Oishi with his help in laboratory. Also to Professor Daimaruya with his support and encouragement with my research regarding strength of material. I also feel grateful to Professor Fujiki Hiroyuki with his help in my research and as the one that introduce me to the badminton club. As long as I remember whenever I had a match with Sensei, I never, even once won the game. I have to admit that Fujiki Sensei is too strong.

I would like to acknowledge Professor Hiroshi Nogami that helped me to get more comprehension regarding DEM-CDF analysis and encourage me to write journals. I really grateful with your kindness and courtesy during my internship period in Tohoku University. I also would like to express my gratitude to your family with their warm welcome during my stay in your house in the last day of my internship. Professor Shibata from CRD Center really helped me a lot with my research regarding the material. His support and motivation really encourage me, I really grateful for that. I also would like to express my appreciation to Mr. Muramoto from Monotzukuri Center, his 'god' hand really helped me to overcome the problem with my experimental device.

Deep appreciation also to all Fluid Engineering Laboratory Members. Five years and a half already passed since I joined this laboratory. Some people graduated and some new members come. First, I would like to say my thank you to my peers Ohnuma, Kato, Tatsuya, and Takeuchi. Their kindness and mix personalities really cheer me and help me to adjust my life when at the first time I start my overseas life. I also would like to express my gratitude to my junior especially to Haga Hiroyasu, Sasayama Daichi, and Sakiyama Motoki. To Haga, with his fun personality, and sometimes unrelated speech to the topic (wuizzzz), but whom I feel the most sincerity as a person. To Sasayama, with his 'daddy' jokes, old taste, and complacent. Thank you for listening my never ending yelps and to introduced me to that Yamashita Tatsuro's songs. To Uncle Sakiyama, who always available with my sudden calls and play that interesting 136 tiles. In conclusion, the time that I spent in this laboratory was a delight and I really grateful for that.

I am especially thankful with my family with their support, love, and unrelentless comfort, my mother Masniari Situmorang, my father Mian Siahaan, and for my three sisters, Carina Siahaan, Sarah Siahaan, and Tasya Siahaan. Without their encouragement and prayers, this work would not have been possible.

Special thanks for every people that I cannot mentioned one by one with their help and support during my stay in Japan.

Finally, I thank my lord and Savior Jesus Christ who has given me strength and joy to preserve in this work. He has not only provided my needs but has redeemed me by his sacrifice on the cross.

Muroran, 8 February 2021

Andrey Stephan Siahaan

博士論文題目

高炉内ホールドアップとガス透過率の関係，並びに材料評価から得られる特殊鋼の安定生産に向けた充填層小型化モデルの研究

氏名　　：

ANDREY　STEPHAN SIAHAAN

論文内容の要旨

「高炉」や「転炉」は製鉄プロセスの要であり，高炉においては鉄の溶融と還元を同時に処理し，短時間に銑鉄を大量生産できる優れた装置である．しかし高炉で消費されるエネルギーは全プロセスの 70%であると言われ，また発生する CO2 の発生量も膨大であるなど大きな問題も発生している．一方，特殊合金鋼を生産する転炉でも，回収スクラップによるリサイクル率の大幅なアップや，スラグからの有用成分の効率的な回収など，より複雑なプロセス制御が要求されており，少量高品質化と省エネルギー化を狙ったプロセス革新は，激変する製鉄業界にあって期待度が高い．

高炉等の充填粒子内においては，微粒子によるガス流路の閉塞トラブル「bridge(棚吊り)」が最も多く，安定操業に大きな支障を来たしている．充填粒子間の空気の透過性と微粒子による閉塞過程については，従前より充填粒子と微粒子の粒径比が関与する可能性を示唆してきたが，その検証には膨大な実験を必要とした．本研究では，DEM-CFD(粒子－流体連成解析法)による三次元コンピューターシミュレーションを新たに導入し，閉塞の起点と予想されていた「粒径比 0.11 前後」についてケーススタディを徹底的に検証して，そのメカニズムを明らかにした．また空気流動と微粒子の落下現象がオリフィス部で拮抗する複雑な現象をシンプルな実験装置によりモデル化し，実験と数値シミュレーションが整合することも明らかにした．これより，閉塞の起因を粒子群の複雑な流動化の中から見出したことは大

きく，より確度の高いシミュレーション技術を進めることができ，小型炉のプロセス検討に向けて大きな前進に繋がったと言える．

一方，転炉では，最近注目度の高い「二相ステンレス鋼(SUS821L1)」の生産プロセスを取り上げ，その溶融段階での改良を最終材料の強度評価から提案する方法を試みた．二相ステンレス鋼は異なる性質の二相が同時に存在するため溶融段階での温度制御は複雑であり，更には一度スラグ化した酸化クロムを回収して再還元化する必要もあって，粒子やガス流の反応制御も難しい．本論文では材料強度の評価実験として準静的から衝撃の範囲までの引張試験を実施し，一例として低温領域(273K～233K)の準静的引張で，マルテンサイト変態による加工硬化挙動が顕著に発生することを捉えた．これより，新素材でも Ni 当量から材料物性を制御できる可能性を示唆した．

以上本論文は溶融炉における粒子挙動や流体の特徴的な流れを把握し，また特殊合金鋼の生産プロセスの処方箋を最終材料の特性から導くなど，前工程のプロセスオペレーションに関して新展開法を提供した功績は大きい．

ABSTRACT

"Blast furnaces" and "converters" are the key technology of the iron-making process. In blast furnaces, iron is melted and reduced at the same time, and it is an excellent device that can mass-produce pig iron in a short time. However, enormous amount of the energy consumed by the blast furnace about 70% of the total process, and generated CO_2 become major problems. Moreover, in the converters for special alloy production, proper control is required due to complicated process and significant increase in the recycling rate of recovered scrap and useful components from slag. Thus, process innovation of energy saving is highly expected in the rapidly changing steel industry.

Among the filled particles in a blast furnace, the most serious problem is "bridge", which is blocking the flow channel and hinder the gas permeability due to the fine particles accumulation that disturb the stable operation. From the previous study, the fine to packed bed particle size ratio is related to the start of the blockage. However, a huge amount of experiment are required.

In this study, three-dimensional computer simulation using DEM-CFD (Particle and Fluid Dynamics), already verified the previous study of “particle size ratio around 0.11" as the starting point of occlusion. Moreover, this study also modeled a phenomenon in which air flow and falling particles antagonize at the orifice by using a simple experimental device, where the experiment and numerical simulation are consistent. The blockage mechanism was understood even in the complicated fluidization of the particle swarm, which led to a great progress toward the process study of designing a small furnace.

Also, in the converter, this study took up the production process of "duplex stainless steel (SUS821L1)", which increase in demand recently. Duplex stainless

steel has two phases with different properties thus required complicated temperature control at the melting stage. Moreover, it is necessary to recover and reduce chromium oxide from the slag, which makes more difficult control.

In this study, a tensile test from quasi-static to impact range is carried out as an evaluation of material strength. As an example, work hardening behavior due to martensitic transformation is remarkable in quasi-static tensile in the low temperature region (273K to 233K), which suggests that the material properties may be able to control from Ni equivalents.

This paper provided a new development method for the process operation to understand the particle behavior and the gas flow characteristic in the melting furnace, and deriving the method of the production process of special alloy steel from the characteristics of the final material.

Table of Contents

List of Tables

List of Figures

CHAPTER I
RESEARCH BACKGROUND

CHAPTER I

1. Introduction

1.1. Research Background

The annual production of crude steel in Japan is about 100 million tons [1)], which is the largest production among artificial materials. Further said, this crude steel is the basic ingredient to produce derivative kind of special steels for wide range usages in society. The production of this kind of special steel cannot be separated from the production of iron. However, iron production involves enormous energy consumption and CO_2 emissions. In 20The CO_2 emissions of the Japanese steel industry in 2012 were 162,324 thousand tons, accounting for about 15% [2)] of the total CO_2 emissions and about 12% [3)] for energy consumption in Japan. About 70% of the energy consumption in the steel industry[4)] is consumed in the ironmaking process centered on the blast furnace. Furthermore, for the derivative product such as stainless steel, the converter is needed to mixed the alloy compound that necessary for the steelmaking. The ironmaking process is a production process that produces hot metal, that includes a sinter and coke production furnace and a hot air furnace that generates hot air. A large amount of CO_2 is generated by the reduction reaction in the blast furnace and the combustion reaction of carbon dioxide and carbon-containing gas in the sintering machine, coke oven, and hot air oven. Therefore, if the energy efficiency of the blast furnace is improved from the viewpoint of measures against global warming, it will be possible to greatly contribute to the reduction of CO_2 emissions, stabilize the production system for the derivative product such as special steel.

The blast furnace is a huge mobile layer type countercurrent reactor for producing pig iron. Figure 1.1, shows a schematic diagram of the blast furnace. The blast furnace is a vertical cylindrical container, which consists of a furnace opening, a shaft, a belly, a Bosch, and a hearth. Iron ore and coke are charged in layers from the

upper part of the blast furnace. Hot air of around 1000°C is blown from the hot air outlet called the tuyere at the bottom of the furnace. Since hot air has a high speed of 250 m / s or more at the outlet at the tip of the tuyere, a cavity called a raceway is created near the tuyere. In this area, coke burns while making a violent swirling motion to generate CO ($2C + O_2 = 2CO$), which is a reducing gas, and heat. The raw material inserted from the top of the furnace descends in the furnace, and during that time, the gas rising in the furnace promotes the temperature rise of the iron ore and the reduction of the iron ore by the reducing gas. In the belly part, the iron ore that has been heated and reduced partially starts to melt. In the high temperature region of 1200 ° C or higher, iron ores fuse with each other to form a fused layer with a low spatial ratio. The cohesive zone has a structure in which coke layers and coke layers that arranged alternately with the poor air permeability. Molten iron and slag that generated in the fusion zone dropped in the dropping zone below the fusion zone, and finally accumulate in the hearth at the bottom of the furnace, before discharged from the ironing port. On the other hand, CO-containing gas that can be used as energy in other processes is emitted from the top of the furnace [5)].

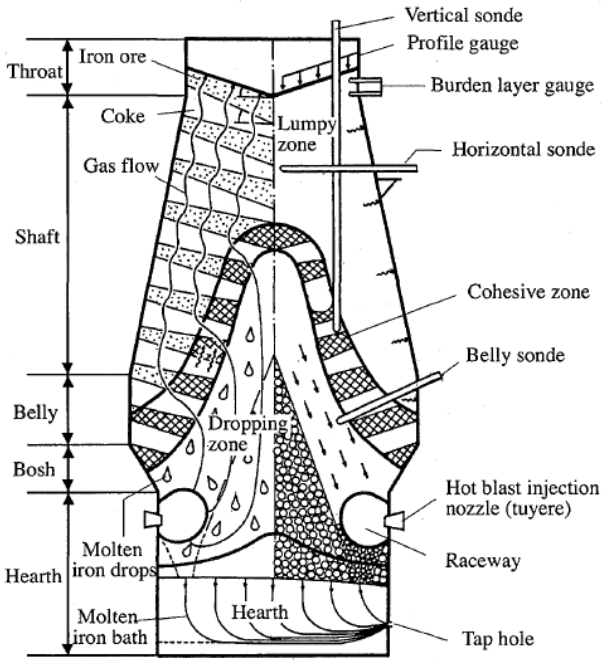

Fig. 1.1 Schematic diagram of blast furnace inside[7)]

As a CO_2 reduction method for blast furnaces, low-reducing agent ratio operations are being carried out to reduce the amount of coke used and the amount of carbon input to the blast furnace [5,6)]. Decreasing the amount of coke used can reduce not only the amount of CO_2 emitted from the blast furnace, but also the amount of CO_2 emitted from the coke oven since the amount of coke produced decreases. On the other hand, coke, which plays a role as a gas transportation route in the blast furnace, must have high mechanical strength, and for that reason, it is necessary to use coking coal, which has excellent calorific value and cohesiveness, instead of steaming coal. However, it already been known that the amount of coking coal produced is limited, and the price is on the rise[25)]. Therefore, it is an important issue to reduce the amount of coke produced from expensive coking coal to reduce the cost of blast furnace operation. In Japan, coke oven gas and heavy oil have been used as reducing agent since 1961[7)], but due to the soaring heavy oil price, the operation was shifted to all

coke operation in 1979 [8]. However, in all-coke operation, there is an urgent need to develop a technology that uses cheap raw materials and fuel from the viewpoint of operational stability and cost[9]. The application of pulverized coal injection technology has already been proven in the United States, the Soviet Union, and China. With the start of pulverized coal injection, research and development on improving pulverized coal combustibility was carried out. According to an experiment using an empty tower furnace, it was found that pulverized coal has poorer flammability than heavy oil and does not completely burn in the raceway. On the other hand, it was found that coal with high volatile content has higher flammability, and coal with smaller particle size has higher flammability[10]. With the pulverized coal injection technology, the coke ratio changed from 450 kg / t-p during heavy oil injection operation to 370 kg / t-p, and the cost could be reduced by low coke ratio operation [11]. Currently, in order to further reduce costs due to the rise in coal prices[12], high PCI (Pulverized Coal Injection) operations are being carried out, in which the amount of pulverized coal injected is increased by utilizing steam coal with abundant resource reserves[5,12,13]. However, as the amount of pulverized coal blown in increases, the amount of coke powder generated increases[14-17], and the air permeability of the blast furnace deteriorates[18,19].

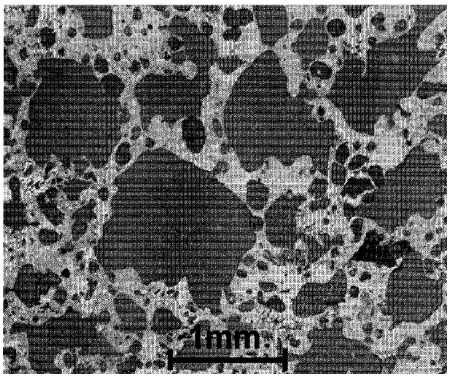

Fig. 1.2 Coke pore structure[20].

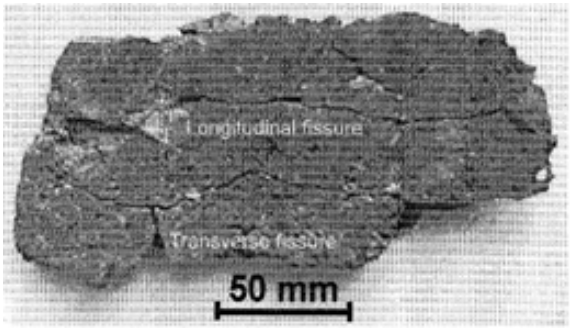

Fig. 1.3 Longitudinal cross section of a coke lump[20].

The type of coke charged into the blast furnace is carbonized coal, where the volatile components of the coal are removed during carbonization to make it porous. The part surrounding the pores is called the stomatal wall, and as shown in Fig. 1.2 [20], there are many smaller pores inside this stomatal wall as well. In addition, thermal stress is generated by the difference in the amount of shrinkage caused by the temperature distribution in the furnace during the carbonization process, and the strain caused by the thermal stress causes cracks inside the coke as shown in Fig. 1.4. When the temperature of coke is raised to 1000 ° C or higher in the blast furnace, CO_2 reacts with carbon of coke to generate CO, ($C + CO_2 \rightarrow 2CO$), which called as CO_2 gasification reaction. The gasification reaction reduces the stomatal wall of coke and reduces its strength [14-16]. On the other hand, the deteriorated part of the coke outer shell disappears due to the combustion reaction by O_2 in the raceway. However, due to the increase in the amount of pulverized coal blown in, oxygen during ventilation is used for combustion of carbon and hydrogen in the pulverized coal. Therefore, when a large amount of pulverized coal is injected, the combustion reaction in the raceway is suppressed, and a thick deteriorated layer is formed on the coke surface due to the reaction due to CO_2 gasification reaction [20]. Deteriorated coke destroys the deteriorated layer due to wear during descent, impact, and wear caused by turning in

the raceway. As a result, coke becomes finer and powdery in the lower part of the furnace and in the raceway [21-23]. The powder generated in the blast furnace circulates in the blast furnace filling layer along with the hot air and reducing the permeability of gas blown from the tuyere.

According to the survey results [18] of the in-core sediment in the actual furnace at the Nagoya 1 blast furnace, it was found that the dust was deposited in the area within a radius of 2 m in the center, observing the top of the layer. Most of the powder was coke, and it was presumed that it was generated in the lower part of the furnace because the surface was gasified. The particle size of coke powder was 3 mm or less about 15%, 1 mm or less was about 60%, and 0.5 mm or less was about 25%, by mass ratio. The terminal velocities of the deposited coke powder with a particle size of 0.5 mm and 1 mm are 1.4 m / s and 2.8 m / s, respectively, which are not largely different compared to the average actual gas flow velocity of 2 m / s at the furnace mouth. It was estimated that the central flow was considerably suppressed. From the above, it is presumed that the accumulation of powder in the furnace affects the air permeability of the blast furnace filling layer. Takahashi et al. conducted an experiment[24] mimicking the accumulation of powder coke and investigated the effect of powder accumulation on solid flow behavior. It was confirmed that the gas rising flow contracted to the part with low ventilation resistance without the powder coke layer due to the presence of the powder coke layer with high ventilation resistance. As long as the gas flow rate is constant, when the gas flow path contracts, the flow rate increases, resulting in high pressure loss. Therefore, the static pressure just below the coke layer increases, and the fluid drag of the coke layer increases, leading to shelf hanging and slipping, which destabilizes the descent of the container and the gas flow. Therefore, estimation of the behavior of powder particles in the furnace is very important for stable operation of the blast furnace. Therefore, in this study, we decided to deal with the blockage

phenomenon that is the cause of poor ventilation due to powder accumulation.

In regards of these matters, the production of steel, specifically for special grade steel such as duplex stainless steel is really dependence on the phenomena that occurred inside of the blast furnace. With the depletion of nickel, and integrated production of small quantity, high quality products using small blast furnace is highly expected in connection with energy saving and reducing the CO2 emission from the blast furnace, aimed at reducing the environmental burden. Thus, the problems that bridging the generated fine particle that create blockage the air flow path and destabilized the processes need to be measured and clarified immediately.

Numerous studies already been conducted to revealed the phenomena in cohesive zone, whether with experiments or numerical approaches using some models and assumptions to mimic the cohesive zone behavior or using direct observation. Regarding the control of cohesive zone, mainly three topic being struggled to discuss

1. Variation of bed structure
2. Control of softening
3. Rapid melting and rapid separation

Using experiment and numerical approaches by using the techniques of thermodynamics, metallurgy, thermos-physical properties, reaction kinetics, mechanics, thermal engineering, and fluid dynamic. The information thus will be used to improve the concepts of causes for cohesive zone would occur and by means to control it. These leads to improvements that reduce the cohesive zone thickness, maintain the instability and increase permeability inside the blast furnace.

As a study on powder behavior in a blast furnace, a study on solid-gas two-phase flow in a blast furnace packed bed has been reported. Yamaoka[26] conducted a cold experiment using a vertical cylindrical packed bed, examined the characteristics of solid-air two-phase flow in the packed bed, and derived a theoretical formula for

predicting the motion state and pressure loss of the powder, considered the blast furnace ventilation phenomenon. In a solid-gas two-phase flow, if the gas flow velocity is below the limit value, the pressure loss increases as the amount of powder retained increases. It was also shown that the critical value of the gas flow velocity depends on the powder supply rate, the powder particle size, and the packed particles. Shibata et al.[27] investigated the one-dimensional characteristics of the solid-gas two-phase flow in the packed bed using a cold model, constructed a dimensional mathematical model, and investigated the effect of the gas flow in the packed bed on the powder. The main cause of pressure loss is the interaction force between powder and packed particles in the high gas flow velocity range. The powder going upward in the low gas flow velocity region. It was also shown that the blockage phenomenon occurs when the hydraulically equivalent diameter formed by the powder and the packed particles becomes 6 times or less the diameter of the powder particles due to the increase in the amount of powder retained in the packed bed. Takahashi et al.[28] conducted a pulverized coal injection experiment using a vertical columnar packed bed. Based on the pressure loss and the ratio of the supply rate and discharge rate of fine powder, the blockage criterion inside the packed bed was judged. As a result, it was found that the ratio of fine powder to the packed particles is an important factor. In addition, assuming that the packed structure in the packed layer is composed of a cubic lattice and an orthorhombic lattice, clogging is likely to occur when the ratio of the average equivalent hydraulic diameter of the layer to the fine powder diameter is 5 times or less. Natsui et al.[29] conducted a numerical analysis of the powder moving in the packed bed and examined the deposition characteristics of the powder. As a result, it was found that particle clusters existed along the flow path. It was found that particles are not captured at the bottleneck when the powder particle size is sufficiently small, but when the powder particle size increases and reaches the threshold value, the powder

particles tend to form an arch structure between the packed particles. In addition, Fukuda et al.[30], aimed to elucidate the local blockage phenomenon that occurs in the packed bed, and it is expected that local blockage is likely to occur in the packed bed, which is a narrow part of the interparticle flow path in the packed bed. The behavior of particles passing through the gap between the three adjacent particles, which is the narrowest in the above, was simulated using the discrete element method (DEM). It was confirmed that the blockage originated from a small number of particles and acted as a stopper, preventing subsequent particles from passing through. Furthermore, it was confirmed that the larger the particle size, the higher the frequency of blockage, and the higher the powder supply rate, the higher the frequency of blockage. Honda et al.[31] conducted behavioral analysis and fluid analysis of powder particles by discrete element method (DEM) analysis for powder particles and fluids that pass between the narrowest adjacent three particles even in the narrow part of the interparticle flow path in the packed bed. Analysis was performed using a coupled method of DEM and computational fluid dynamic (CFD), where the flow characteristics of the two-phase flow of gas powder flowing through the packed bed in the blast furnace were investigated. It was shown that the influence of the contact force on the powder motion is small due to the upward gas flow is small, but the residence time on the orifice is long due to the action of the fluid resistance. In addition, the breakdown of the resistance force that affects the orifice passage time of powder particles is shown. Various studies have been conducted on the behavior of powder in the packed bed. However, the process leading to the clogging of powder particles has not been clarified in the examination of powder behavior on a microscale in the solid-gas two-phase flow in the packed bed. Therefore, in this study, the process of clogging of powder particles in the packed bed need to be investigated further.

On the other hand, in the converter process study, this study took up the

production process of "duplex stainless steel (SUS821L1)", which has been paid much attention recently, and tried a method to propose the improvement at the melting stage from the strength evaluation of the final material. Duplex stainless steel has two phases with different properties, so the temperature control at the melting stage is complicated, and more necessary to recover the reduce chromium oxide from once slagged, which makes the control more difficult.

Duplex stainless with high chromium as main alloying element is produced from high chromium pig iron and further will process in Basic oxygen steel making or electric furnace reactor in addition of alloying elements. With the expectation in the increasing demand of this type of steel, production of high chromium pig iron inside the blast furnace and further in the converter is needed. Clifford W. McCoy [31] stated that the control of permeability and particle size of the input chromium ore is urgent to reduce loss material and make the production process more stable. The process of high chromium pig iron is depicted in Fig. 1.4 below.

Duplex stainless is families of steel that consist of two-phase microstructures consisting of approximately austenite and ferrite in equal content, expecting the combination of good advantages of these two phases. From the previous study, it has already been observed that the physical properties of duplex steels are between those of austenitic and ferritic stainless steel. Moreover, they also proved to have significantly greater strength than the austenitic grades while exhibiting good ductility and toughness.

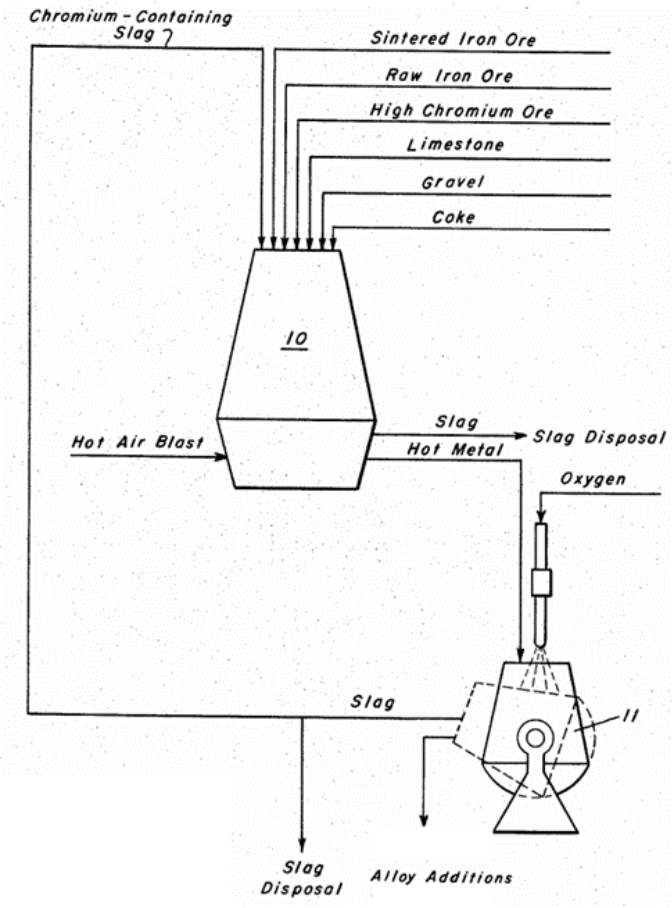

Fig. 1.4 Schematic diagram of high chromium pig iron

The mentioned duplex stainless steel family usually divide into three categories; lean, duplex, and super duplex stainless steel. The lean duplex stainless steel, obtained its name from the ‘lean’ composition of nickel content, about 1%-2%, which have developed further to reduce the cost, which is very important due to the price of Nickel element that had been increasing and fluctuate over years as depicted in Fig. 1.5. The nickel had been substituted by Manganese (Mn) and Nitrogen (N) as austenite stabilizer, to save the expensive element Ni. Despite the lack of Ni content, lean duplex stainless has good pitting corrosion and chloride stress corrosion resistance compared to the 300-series austenitic stainless steels. The resistance of stainless steel to corrosion is depends on alloy composition, which primarily affected by the composition of Cr, Mo, W, and N. The empirical relationship called Pitting

Resistance Equivalent Number (PREN) had been used to calculate the correlation between stainless steel compositions in weight % to its relative pitting corrosion resistance, which are given as follows:

$$PREN=Cr+3.3(Mo+0.5W) + 16N$$

Moreover, because of the higher strength, the weight to strength ratio is greater than the commonly used austenitic stainless steels which mean the cost to weight ratio will also reduce. These all advantages make the application of lean duplex stainless is deemed proportional for construction in chemistry, marine, power generation, and automobiles.

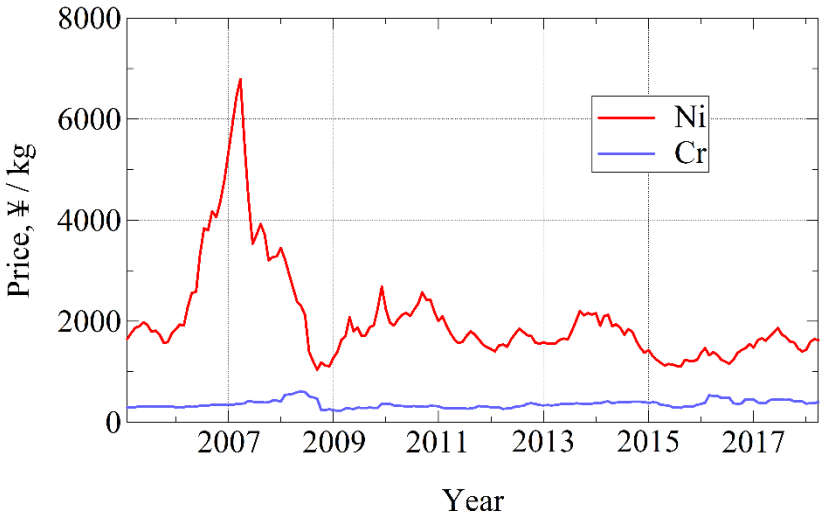

Fig.1.5 Price fluctuation of Nickel compare to Chromium as function of time (year)

From previous studies the transformation induced plasticity (TRIP) that occurred in metastable austenitic stainless steel already been reported. This TRIP effect is expected to increase the strength and ductility. Furthermore, more studies also reported that this TRIP effect is diminished in high strain rates due to adiabatic heating.

The adiabatic heating will increase the stabilization of austenite phase and suppressed the TRIP effect.

The stability of austenite phase usually measured by stacking fault energy (SFE). The SFE is mainly affected by alloy composition in the making of stainless steel, especially the nickel (Ni) content as austenite stabilizer. The stability of austenite phase is directly proportional with SFE, thus stainless steel with high SFE will have more stable austenite phase. This also explain the higher stability of AISI 316 (~50 mJ/m2) compare to AISI 304 (~18 mJ/m2). Apart from chemical, the SFE also increases with temperature increase, which corresponds to low metastibility of stainless steel in high strain rate due to adiabatic heating. From these facts, it can be conclude that the TRIP effect in metastable stainless steel is affected by strain rate and also temperature change.

Even though study on TRIP effect in austenitic grade stainless steel due to the coupling effect of strain rate and temperature change already well established, but the information for duplex stainless is still lack in comparison. Some studies already reported the mechanical behavior of lean duplex stainless due to the separate effect of temperature and strain rate

In this study, a tensile test from quasi-static to impact range is carried out as an evaluation experiment of material strength. As an example, work hardening behavior due to martensitic transformation is remarkable in quasi-static tension in the low temperature region (293K to 233K). This suggests that even this new material may be able to control the material properties from Ni equivalents.

As mentioned above, this paper provided a new development method for the process operation of the previous process, such as understanding the particle behavior and the characteristic flow of the fluid in the melting furnace, and deriving the prescription of the special alloy steel production process from the characteristics of the

final material.

1.2 The Outline

The outline of this dissertation is as follows.

1. In chapter one, brief explanation of duplex stainless steel from steelmaking and its utilization are explained, followed by the objectives of this research and the outline of the dissertation.
2. In chapter two, the effect of packing structure, blockage formation, and permeability criterion of fine particles due to the effect of gas flow, mimicking the blast furnace will be discussed.
3. In chapter three, more detailed analysis from microscopic perspective of the cohesive zone which change complexly and continuously due which reciprocally affected by passing behavior of fines particle will be presented.
4. In chapter four, the mechanical behavior, TRIP effect, and fracture analysis of lean duplex stainless due to the influence of temperature and strain rate will be reviewed.
5. In chapter six, will conclude and summarize the present work.

1.3 References

1) 日本鉄鋼連盟: world steel 銑鉄・粗鋼年間生産量・時系列表 2005~2014 年. (2015)

2)日本環境研究所: 日本国温室効果ガスインベントリ報告書. (2015)

3) Y. Ujisawa, K. Nakano, Y. Matsukura, K. Sunahara, S. Komatsu and T. Yamamoto: Tetsu-to-Hagané, 92 (2006), 1015.

4) M. Sato, T. Yamamoto and M. Sakurai: JFE GIHO, 32 (2012), 18.

5) 羽田野道春: 高炉製銑法, 地人書館, 東京 (1999), 49.

6) 日本鉄鋼協会: Research of Physical Limitation in Blast Furnace Operation with Low Reducing Agent Rates. (2006)

7) M. Naito, K. Kunitomo and S. Matsuzaki: Journal of the Japan Institute of Energy, 86 (2007), 748.

8) K. Hayase and H. Takahashi: KAWASAKI STEEL GIHO, 13 (1981), 551.

9) M. Naito: SHINNITTETSU GIHO, 384 (2006), 2.

10) T. Suzuki, R. Hirose, K. Morimoto and T. Abe: Transactions of the Japan Society of Mechanical Engineers. B, 50 (1984), 1067.

11) N. Takamatsu, K. Kurihara, A. Hatanaka, G. Saitoh and H. Kaku: SHINNITTETSU GIHO, 391 (2011), 79.

12) 資源エネルギー庁, エネルギー白書 2013.

13) 山口一良: 高炉を支えた操業技術と原燃料, 東北大学出版会, 仙台 (2001)

14) Y. Shigeno and Y. Omori: Tetsu-to-Hagané, 73 (1987), 1853.

15) K. Kanbara, T. Hagiwara, A. Shigemi, S. Kondo, Y. kanayama, K. Wakabayashi and N. Hiramoto: Tetsu-to-Hagané, 62 (1976), 535.

16) K. Kojima, T. Nisi, T. Yamaguchi, H. Nakama and S. Ida: Tetsu-to-Hagané, 62 (1976), 570.

17) K. Yamaguchi, T. Uno, T. Yamamoto, H. Ueno, N. Kon-no and S. Matsuzaki: Tetsu-to-Hagané, 82 (1996), 641.

18) M. Ichida, T. Nakayama, K. Tamura, H. Shiota, K. Araki and Y. Sugisaki: Tetsu-to-Hagané, 78 (1992), 1132.

19) H. Shimizu, K. Sato, M. Kojima, Y. Aminaga, F. Nakamura and Y. Iwanaga: Tetsu-to-Hagané, 72 (1986), 195.

20) T. Arima: Tetsu-to-Hagané, 92 (2006), 106 .

21) K. Yamaguchi and T. Ueno: J.Jpn. Inst. Energy, 78 (1999), 760.

22) K. Yamaguchi and T. Uno: Tetsu-to-Hagané, 85 (1999), 578.

23) K. Yamaguchi and T. Uno: Tetsu-to-Hagané, 86 (2000), 11.

24) H. Takahashi, H. Kawai, M. Kobayashi and T. Fukui: Tetsu-to-Hagané, 92 (2006), 996.

25) Y. Shigeno and Y. Xiao Wen: 国際文化研究科論集, (1994), 199.

26) H. Yamaoka: Tetsu-to-Hagané, 72 (1986), 403.

27) K. Shibata, M. Shimizu, R. Takahashi and J. Yagi: Tetsu-to-Hagané, 77 (1991), 236.

28) H. Takahashi, H. Kawai, T. Kondo and M. Sugawara: ISIJ Int., 51 (2011), 1608.

29) S. Natsui, S. Ueda, H. Nogami, J. Kano, R. Inoue and T. Ariyama: Chemical Engineering Science, 71 (2012), 274.

30)福田雅裕，粗粒子で構成されたオリフィスの粉体粒子通過挙動 DEM 解析，室蘭工業大学修士学位論文，（2014）

31)Clifford W. McCoy: United States Patent Office, US3336132A, (1967)

CHAPTER II

Numerical Approach on Permeation and Blockage of Fine Particles Transported by Updraft through a Packed Bed

SYNOPSIS

As a method for reducing CO_2 in blast furnaces, low-reducing agent ratio and large amount of pulverized coal is being carried out to reduce the amount of coke used and reduce the carbon input to the blast furnace and its operation cost. However, these operating methods increase the deposit amount of coke powder and unburned char generated in the blast furnace and decrease process efficiency. A three-dimensional numerical model is built and observed by the coupling system of DEM-CFD, performed to understand the principal factors that affected fine and gas permeability. Simulation is carried out in, where fine particles are injected simultaneously from the bottom of cylindrical packed bed, mimicking the experimental approach. The fine to packed diameter ration is given by $0.133 \leq Dp/dp \leq 0.162$. At a larger diameter ratio, fine particles tend to concentrate at the bottom of the packed bed. In the case of lower particle diameter ratio, updraft gas will easy to permeate along with fine particles because of the existing of large open flow channels relative to fine diameter. Furthermore, no significant change in fine fraction transported to the upper area due to the change of gas velocities. In this present study, the effect of continuous fine particles injection and its effect on gas flow can be observed, where the gas flow avoiding the heavily concentrated areas.

2.1. Introduction

In recent years, shifting trend in the iron making process, where the large supply of pulverized coal at tuyere directed at the low reducing agents rate [1]. This kind of operation is increasing in demand, however, it has the problem at agitated or unsteady behavior inside the blast furnace. Therefore, there is large growth demand in analyses about the fines deposited locally in iron making blast furnace and its influence on gas permeability inside that caused inhomogeneous flow [2].

Some experimental researches regarding the interactions between pressure drop and updraft gas inside the packed bed already been done. Hidaka et.al [3-6] performed investigations on the effect of inlet gas velocity, fine particles morphology, and packed bed model and the effect of these to static and dynamic holdup in the packed bed. Another experimental approach by Dong et al [7], conducted to understand the flow and accumulation behavior of powder in system like an ironmaking blast furnace. Similar to previous research, Dong et.al stated that fines accumulation behavior is affected by inlet gas velocity, fines mass flux. Moreover, the existence of impermeable blocks inside the packed bed, and packing model of fine particles was added as new parameters. Chen Jizhong et al [8] Pham et al [9] and Shibata et al [10] mainly focused in the investigation on the effect of powder mass flux and low gas velocity effect towards pressure drops inside the packed bed. It was found that pressure drop inside the packed bed will decrease with the decrease of gas velocity. However, further decrease will lead to the increase of pressure drop because of the rapid accumulation of fine particles. Takahashi et al [11] conducted a study on permeation and blockage of fine particles transported by updraft through the packed bed. This study mainly focused on the effect of fines to packed diameter ratio, updraft gas velocity, fines mass flux, and gas inlet velocities on clogging formation and gas permeability inside the packed bed. From this study, they proposed critical fines to packed diameter ratio of 0.11-0.12.

Studies regarding permeation and blockage behavior of fine flow characteristics inside the packed bed regarding the gas and fines habitual character are found to be exacting to inspect fines distribution because the inner part of packed bed is difficult to be observed directly. In recent years, advances in computing speed and power as well as improvements in programming have the way to open more understanding of modeling complex granular flow using discrete element method (DEM). This particulate system modeled as an assembly of singular discrete and interacting particles with its interactions towards gas flow using computational fluid dynamics (CFD). Some approaches on the method of DEM-CFD coupling is already been investigated. Chu and Yu [12], presented numerical study regarding complex particle-fluid flow using combined continuum and discrete method in various 3D systems such as pneumatic conveying bend, cyclone separator, and circulating fluidized bed. This numerical approach was able to capture key flow features that affected in the experimental approach of each system, such as axial solid segregation, shaped profile in the axial solid distributions, and annulus core flow structure that causes solid back mixing. Dong et al [13], developed mathematical model to describe the gas-powder two-phase flow in a packed bed. The calculated results show that the large difference in physical properties is the main factor responsible for the different flow behavior between gas and powder phases. Furthermore, similar to their experimental results [7], powder accumulation region also identified in low gas velocity. Xu. et al [14], and Matsuhashi et al [15], conducted simulation on the effect of the lateral gas inlet to bed transformations from fixed bed to fluidized bed and vice versa. Nogami et al [16] was able to identify that voidage takes more on permeability of the high temperature gas than coke diameter inside the blast furnace. Kikuchi et al [17] investigated wall effect, powder morphologies, and inlet gas velocity to voidage and blockage formation in packed bed of blast furnace. Natsui et al [18], using the DEM-CFD

approach to simulate the physical condition of previous research [11]. Natsui et al was able to show local blockage and cluster formation in the transition area between the test section bed and additional packed bed. However, because of time consuming calculation, the numerical model only lasts for 1.5 s in previously reported paper, where a large amount of fine particles is injected in one time to abridge the blockage formation behavior, thus the pressure distribution inside the bed between the numerical and experimental one cannot be compared.

The objective of this study is to clarify blockage formation and permeability criterion of fine particles due to the obstructing effect of updraft gas and fines to packed bed diameter ratio. Fine particles are injected continuously, with constant feed rate in regards to mimic the experimental conditions [11]. The numerical model is built and observed by coupling system of DEM-CFD. With the purposed model, it is possible to compare pressure distribution inside the packed bed due to resemblance conditions between experimental and numerical approaches. Moreover, some oddity in fine hold up also can be observed from this model of continuous feed rate and its relation with various velocities of updraft gas.

2.2. Governing equation and numerical method

In this study, gas-powder two-phase flow analysis was performed using fluid and powder analysis software “R-flow”. In this section, the analysis method of particles and fluid behaviors, also the method for coupling analysis of these two analyses method, will be explained.

2.2.1. Discrete Element Method (DEM) Analyses

The discrete element method (DEM) is a discrete assembly, where individual components satisfy the equation of motion and the transfer of force with other

components and obeys the law of action and reaction.

In the numerical analysis of dynamic behavior in moving and fluidized beds, powder particles flowing as a group of many particles while the particles move and collide with adjacent particles and walls. Based on Newton's second law of motion, equations of motion for translational and rotational motion of a particle are described as follows:

$$m_p = \frac{d\vec{v}_p}{dt} = \vec{F} + m\vec{g} \quad (1)$$

$$I_p \frac{d\omega_p}{dt} = r_p \vec{F} \quad (2)$$

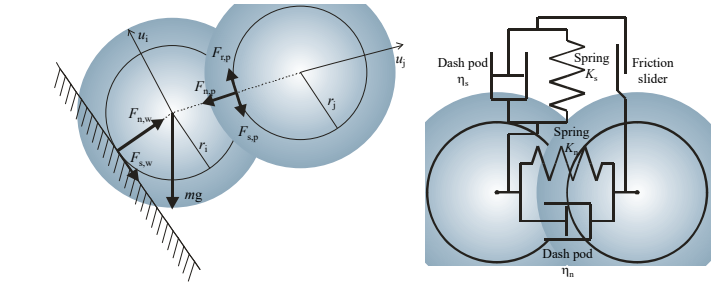

(a) Contact forces of particles i and j (b) Voigt Model.

Fig. 2.1 Analysis Model

Here, m_p is particle mass [kg], v_p is particle velocity [m.s^{-1}], t is time [s], F is external force which includes contact force and drag force [N], g is gravity [m.s^{-2}], Ip is particle moment of inertia [kg.m^2], ω_p is particle angular velocity [rad.s^{-1}], r_p is particle radius [m]. Focusing on one isolating pair of particle interaction of existing external force shown in **Fig. 2.1** (a). Particle movement is affected by the force and gravity due to the contact with the surrounding objects. The collision between particles is considered inelastic, which means kinetic energy is dissipated during the collision. The collision model is expressed by the Voigt model, consist of spring and dashpot shown in **Fig. 2.1** (b). The spring represents the repulsive forces when particles are in contact, and the dashpot represents subsided kinetic energy. To consider the friction between

particles and between particles and the wall, a friction slider is added to the model of rotational movement.

When a particle collides, a small deformation occurs, where a contact force corresponding to the amount of deformation and the rate of deformation is generated. The contact force acting between two particles in the Voigt model is described by the following equation, where *u* is the translational displacement of the particle [m], and ϕ is the rotational displacement [rad], expressed in equations below:

$$m_{\mathrm{i}} \frac{d^2 u_{\mathrm{i}}}{dt^2} + \eta \frac{du_{\mathrm{i}}}{dt} + K u_{\mathrm{i}} = 0 \tag{3}$$

$$I_{\mathrm{i}} \frac{d^2 \phi_{\mathrm{i}}}{dt^2} + \eta \frac{d\phi_{\mathrm{i}}}{dt} + K r^2 \phi = 0 \tag{4}$$

Here, *K* is the spring constant [N.m^{-1}] and η is damping coefficient [kg.s^{-1}]. As particle is in contact with another particle, Eqs. (3) and (4) corresponds to each contact point. The acceleration of the target particle calculated by integrating the contact forces at all the contact points and substituting them into Eqs. (1) and (2).

Since the contact force between particles acts in various directions, it is the combined force of the direction (normal direction n) perpendicular to the particle tangent plane and the direction of the particle tangent plane (shear direction s1, s2), where *F* is contact force [N], expressed by equation (5). The contact force is consist of normal force expressed by *F*n and shear force *F*s, expressed by Eqs. (6) and (7), respectively.

$$F = F_{\mathrm{n}} + F_{\mathrm{s}} \tag{5}$$

$$F_{\mathrm{n}} = -K_{\mathrm{n}} \Delta u_{\mathrm{n}} - \eta_{\mathrm{n}} \frac{\Delta u_{\mathrm{n}}}{\Delta t} \tag{6}$$

$$F_{\mathrm{s}} = \begin{pmatrix} F_{\mathrm{s1}} \\ F_{\mathrm{s2}} \end{pmatrix} = \begin{pmatrix} -K_{\mathrm{n}} \Delta u_{\mathrm{s1}} - \eta_{\mathrm{n}} \dfrac{\Delta u_{\mathrm{s1}}}{\Delta t} \\ -K_{\mathrm{n}} \Delta u_{\mathrm{s2}} - \eta_{\mathrm{n}} \dfrac{\Delta u_{\mathrm{s2}}}{\Delta t} \end{pmatrix} \tag{7}$$

2.2.2. DEM-CFD Couplings Analyses Method

The following momentum conservation law and continuity equation are used as coupling formula for fluid in gas-powder two-phase flow.

$$\alpha_f \rho_f \left(\frac{\partial V_f}{\partial t} + \left(V_f \cdot \nabla V_f \right) \right) = -\alpha_f \nabla p + \alpha_f \left(\rho_f - \rho E_{f0} \right) g + \alpha_f \alpha_p \beta \left(V_p - V_f \right) + \nabla \cdot \left(\alpha_f \mu_f \nabla V_f \right) \tag{8}$$

$$\frac{\partial \alpha_f}{\partial t} + \nabla \cdot \left(\alpha_f V_f \right) = 0 \tag{9}$$

The subscripts f and p indicate physical quantities of fluid and powder particles, where f represent the fluid part and p represent the particle part respectively, and $\alpha_f + \alpha_p = 1$. β represents the momentum exchange coefficient between the continuous phase and the dispersed phase. ρ_{f0} is the reference density to the pressure p and the deviation pressure from hydrostatic pressure [kg.m^{-3}], when the density ρ_f of the continuous phase is constant, noted as $\rho_{f0} = \rho_f$. For the drag coefficient, Ergun's drag model for solid particles is use as shown in Eqs. (10) to Eqs. (15).

$$\beta = \beta_1 \quad \left(\alpha_f \le 0.8 \right) \tag{10}$$

$$\beta = \beta_2 \quad \left(\alpha_f > 0.8 \right) \tag{11}$$

$$\beta_1 = \frac{150 \alpha_p \mu_f}{\left(\alpha_f d_p \right)^2} + \frac{1.75 \left| V_p - V_f \right| \rho_p}{\left(\alpha_f d_p \right)} \quad \left(\alpha_f \le 0.8 \right) \tag{12}$$

$$\beta_2 = \frac{0.75 C_D \rho_f \left| V_p - V_f \right|}{\left(d_p \alpha_f^{2.7} \right)} \quad \left(\alpha_f > 0.8 \right) \tag{13}$$

$$C_D = \max \left(\frac{16 \left(1 + 0.15 \mathrm{Re}^{0.687} \right)}{\mathrm{Re}_p}, 0.44 \right) \tag{14}$$

$$\mathrm{Re}_p = \frac{\rho_f \left| V_p - V_f \right| d_p}{\mu_f} \tag{15}$$

2.2.3. Numerical Conditions and Analyses

The calculation domain for the numerical model is set based on the experimental apparatus used in the literature [11], and it is shown in **Fig. 2.2** (a). The

domain consists of a conical diffuser bed which bottom diameter and height are of 40 and 51.96 mm, respectively, and a vertical circular column of which diameter and height are 100 and 530 mm, respectively. Beneath the column, a cone-shaped diffuser which is filled with glass beads of 12 mm is settled.

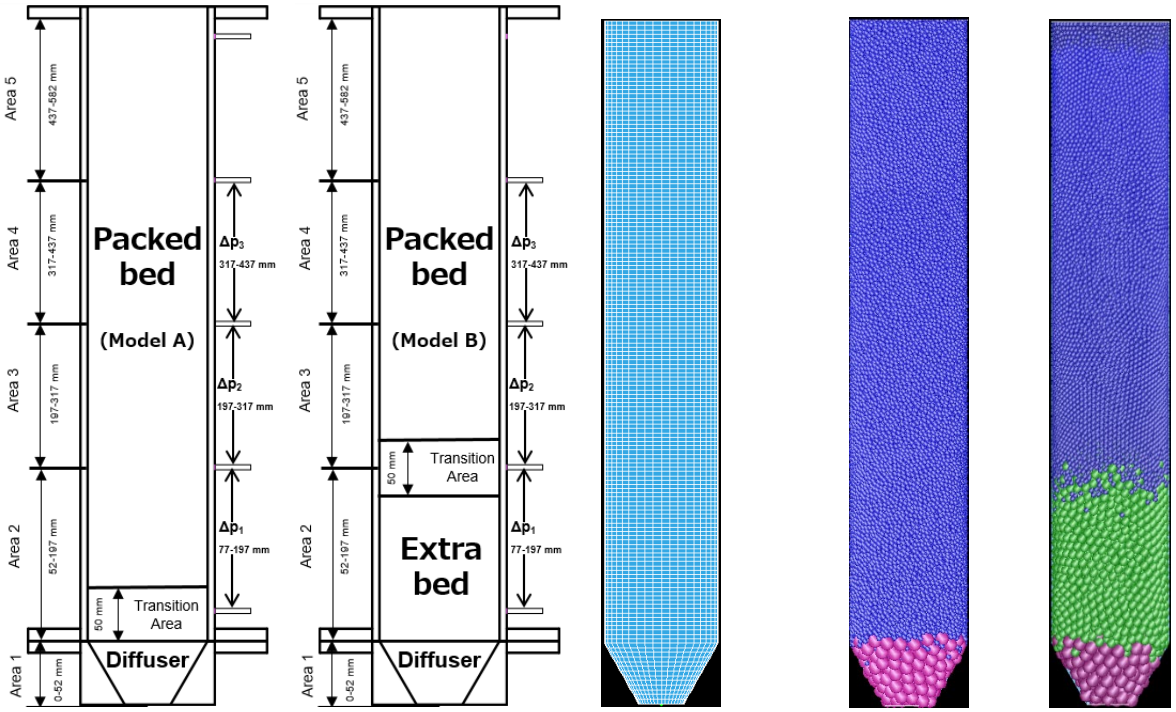

Fig. 2.2 (a) strain gauge position and area positions of each model (b) Calculation Domain (c) Model A (d) Model B

In the experiments, the column was filled with particle, and the gas-powder two phase flow is introduced from the bottom through the diffuser. The vertical pressure distribution was measured by the pressure sensors settled every 120 mm. The sections between sensors are designated as P1, P2 and P3 from the lower position and the pressure drops in these sections are expressed as Δp_1, Δp_2, and Δp_3, respectively. **Fig. 2.2** (b) shows the grid arrangement used in the numerical simulation. Two types of packed beds are formed according to the literature [11]. In model A, shown in **Fig. 2.2**

(c), the column is filled with only alumina particles while the diffuser bed exists at the bottom part. This top filled section is the test section. In model B, shown in **Fig. 2.2** (d), a packed bed of which height is 120 mm is formed with particles of 8 mm in diameter on the top of the diffuser bed, and this part is called the extra bed, hereinafter. Then the remaining part of the bed is filled with alumina particles and it is treated as the test section. In this paper, the bottom part of the alumina bed, with 50 mm in height is called the transition area. The powder behaviors in the transition area will be discussed later. After the packed bed is formed in the vertical column, the fine particles and gas are injected simultaneously from the bottom of the domain at constant rates for 30 seconds.

Table. 2.1 Calculation Conditions

	Alumina Beads [Dp]			Fine Particle[dp]	
Diameter [mm]	2.6	4.48	3.68	0.388	0.596
Density [kg.m^{-3}]	1500	1106	1732	1369	
Terminal Velocity [m.s^{-1}]	-			2.06	3.15
Mass Flux (m_f) [kg.m^{-2}s^{-1}]	-			0.059	0.064
Particle Diameter Ratio [-]	0.133; 0.149; 0.162				
Dynamic Friction Coefficient	0.7			1.0	
Rolling Friction Coefficient	0.7			0.7	
Young Modulus [GPa]	21			0.01	
Poisson ratio	0.24			0.21	
Time Step [s]	1 x 10^{-5}				
Fluid Density [kg.m^{-3}]	1.2				
Viscosity [Pa.s]	1.8 x 10^{-5}				
Gas Superficial Velocity (u_f) [m.s^{-1}]	0.88; 1.06; 1.24				
Number of Grids (h x r x θ)	150 x 12 x 42				
Total Simulation time [s]	30				

In the simulation, the packed beds of the alumina beads, extra bed, and diffuser are treated as fixed beds because the fluid drag and the contact force from the fine particles are small enough to move packed particles. Three combinations of the fine particles and the alumina particles are examined. In case 1, the fine particles with diameter of 0.388 mm are injected into packed bed model A, of alumina beads with diameter 2.6 mm. In this condition, the diameter ratio of the fine particles to the alumina beads (dp/Dp) is 0.149 [-]. The next two cases use model B and the fine particles with diameter 0.596 mm. In case 2, the alumina beads with diameter 4.48 mm (dp/Dp = 0.133) is used, and in case 3, the alumina beads of 3.68 mm (dp/Dp = 0.162) is used. For the first three cases, the updraft gas velocity of 0.88 m/s. The effect of updraft gas velocity will be discussed by using the same model as case 2 where the gas velocities are modified (u_f = 1.06 [m.s^{-1}] and u_f =1.24 [m.s^{-1}]), and later called as case 4 and case 5, respectively. The calculation conditions and the parameters for the numerical simulations are listed in **Table.1**.

For case 1 of packed bed model A, a constant mass of fines (dp = 0.388 [mm]; m_f = 0.059 [kg.m^{-2}s^{-1}]) is fed to the diffuser at every second. For case 2 and 3 (dp/Dp = 0.133 and dp/Dp = 0.162), of packed bed model B, a constant mass of fines (dp = 0.596 [mm]; m_f = 0.064 [kg.m^{-2}s^{-1}]) are also fed the diffuser continuosly at every second. Furthermore, using the same parameter as case 2, the change of updraft gas velocity (u_f = 1.06 [m.s^{-1}] and u_f = 1.24 [m.s^{-1}]) also will be discussed (cases 4 and 5). The gas-powder flow simulations are performed for 30.0 s of elapse of time and the powder feed rates are kept constant for this duration.

The conditions of this current study are determined based on the previous study with the same model of packed bed and flow rate[11]. As time lapses, fines hold up in the packed bed is increasing until the end of simulation time (t = 30 [s]). At this time, the total fines hold up for the case 1 (dp/Dp = 0.149 [-]) is 0.142 vol%, with the

total fine particles are 48630 [-], and for the cases 2 and 3 (dp/Dp = 0.133 and 0.162), the total fines hold up is 0.162 vol%, where the total fine particles is 14430 [-]. These values of fine particles hold ups are the average value of fine hold ups inside the packed bed and were obtained under the assumption that all fed fine particles stay in the packed bed. Indeed, these small amounts of fine hold up are quite smaller compare to the total volume of the packed bed, and cannot be applied to complete blockage. As a comparison, the simulation time and the total hold ups in this current study are much lower compared to each respective model of the experimental one. The total experimental time for each particle diameter ratio of 0.133, 0.149, and 0.162, are 3630, 255, and 927 seconds, with the total hold ups of 24.7, 2.2, and 6.2 vol%, respectively. However, due to continuous fines injection, it is expected to observe actual gas flow behavior and the initial stagnation of fine particles. Nevertheless, as the conditions of the previous study were recognized as experiment for the powder flow related to blast furnace[11], and for this current study the same conditions such as flow rate of fine particles, packed arrangement, and void fraction are applied, therefore conditions of this current study should be acceptable to be related to fine particle flow condition in the blast furnace. Moreover, the pressure drop in three sections of P1, P2, and P3 of the three cases obtained from the numerical analysis will be compared to measured result [11] as validation.

2.3. Results and Discussion

2.3.1. Numerical and Experimental Results Validation

In this section, the pressure drops in the three sections P1, P2, and P3 under the updraft gas velocity of 0.88 m.s^{-1} are compared. **Fig. 2.3** shows the comparison between measured and calculated pressure drops for the case 1 (packed bed model A, d_p= 0.388 [mm] and D_p= 2.60 [mm]). Fine particles are injected continuously from the bottom of packed bed by a diffuser, with a constant rate at 0.059 kg m^{-2} s^{-1}. Although

the measured pressure drops more fluctuate compared to the numerical results, the calculated pressure drops in the sections P2 and P3 show good agreement with the experimental ones. The numerical result for P1 is under predicted, however, it is considered that the average discrepancies about 50 Pa are still tolerable.

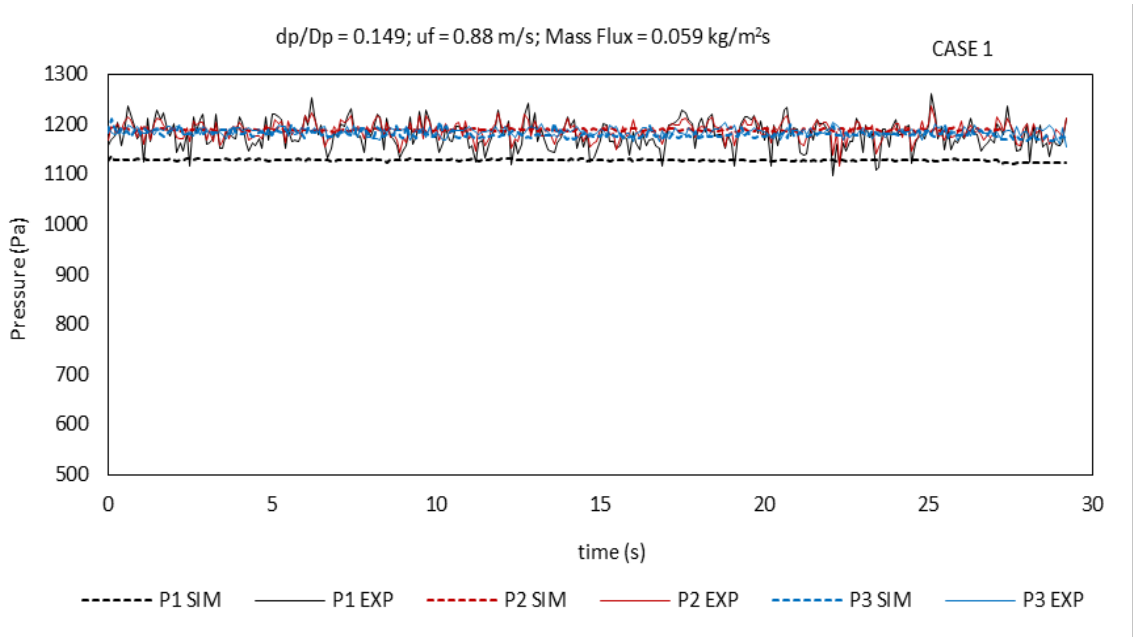

Fig. 2.3 Pressure Comparison; Experiment and Simulation *d*p/*D*p = 0.149 [-]

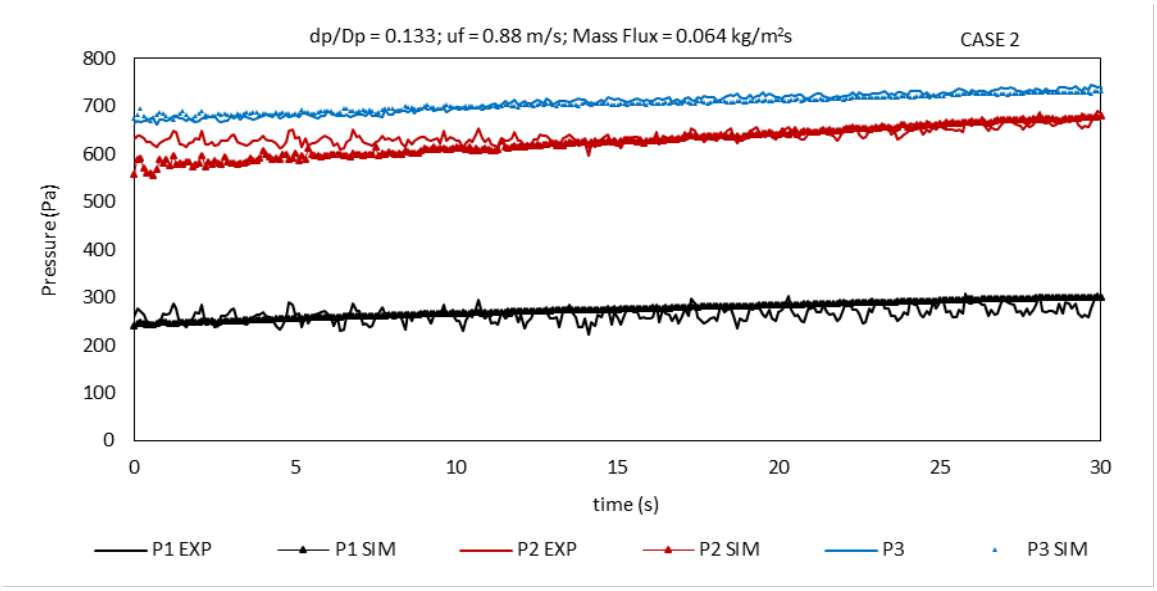

Fig. 2.4 Pressure Comparison; Experiment and Simulation dp/Dp = 0.133

Variation of the pressure drop in the case 2 (packed bed model B, d_p=0.596

[mm], D_p=4.48 [mm], the diameter ratio 0.133 [-]) is shown in **Fig. 2.4**. In this case, the mass flux of fine particles is 0.064 $kg.m^{-2}s^{-1}$. Similar to the previous case, the comparison between numerical and experimental results is displayed. Also, in this case, the measured pressure drops are more fluctuated compared to the simulation results. However, the average value is matched between the experimental and numerical results. Thus, there is a good agreement between numerical and experimental results in all sections P1, P2, and P3.

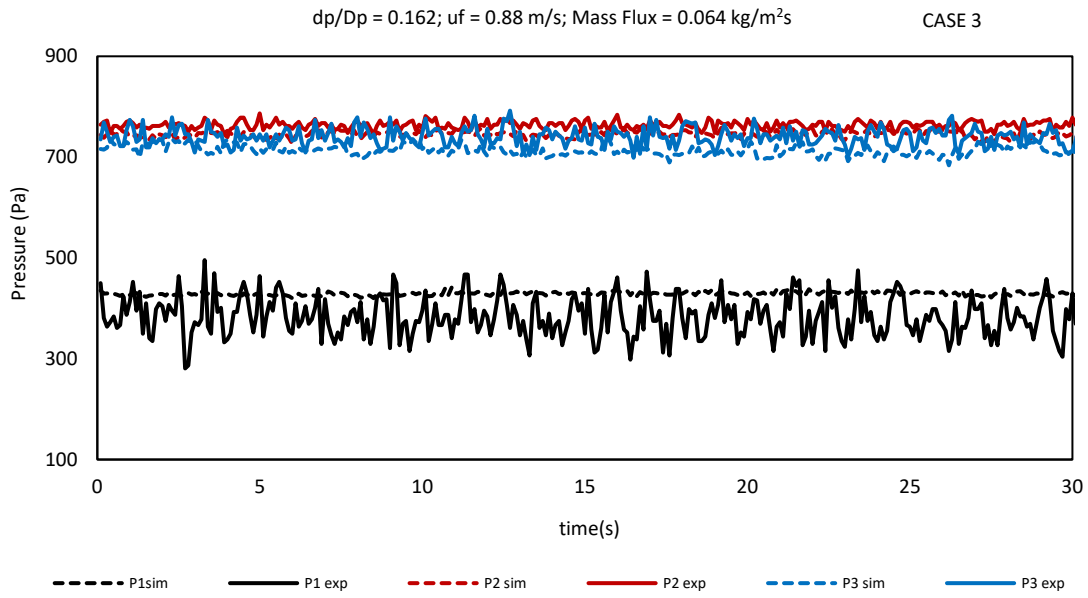

Fig. 2.5 Pressure Comparison; Experiment and Simulation dp/Dp = 0.162

Fig. 2.5 shows the variations of the pressure drops obtained by the numerical simulation and the experiments in the case 3 (packed bed model B, d_p=0.596 [mm], D_p=3.68 [mm], d_p/D_p = 0.162 [-]). Mass flux of injected fine particles is the same as the case 2. The pressure drops of numerical results are in good agreement with the experimental results. From the validation, it can be observed, there is no remarkable increase of pressure drop for each case. As aforementioned before, in this current

study total simulation time is 30 s, thus the pressure increase is generally not significant. For case 1, packed bed model A (without the extra bed of 8 mm), no remarkable differences in pressure distribution between P1 and P2 can be observed because the pressure gauge of P1 and P2 are located in the same packed bed with the diameter of 2.6 mm. Furthermore, no significant increase in pressure drop also occurred because, as the pressure tap of P1 is located in the middle part of the transition area, the fine particles are accumulated in the lower half of transition area, while the amount of accumulated fine particles in the upper half is relatively small, which merely affected the increase of pressure drop.

Case 2 and 3 are using packed bed model B (with extra-bed 8 mm). In this case, P1 is located at the extra bed with the diameter of 8 mm, while P2 is located in the packed bed with the diameter of 4.48 mm, therefore the pressure reading at P1 of these cases is lower compare to the pressure reading at P2 and P3. From Fig. 2.4, the pressure drop for section P1 not show significant increase. This phenomenon mainly occurred because most of the part of P1 located in the extra 8 mm bed, with only half of the transition area is included, which caused only slightly increase of pressure drop is legible in this section. More significant pressure drop can be observed in P2 section, which is located in the transition area and the bed with diameter of 4.48 mm, as the fine particles will penetrate from the transition area to the bed above.

2.3.2. The Effect of Fines to Coarse Particle Diameter Ratio (d_p/D_p)

The effect of diameter ratio (fines diameter to packed beads diameter (d_p/D_p) on the permeability of fine particles in the packed bed is discussed in this section. Three diameter ratios, namely 0.133, 0.149 and 0.162 [-], are set. The first case (d_p/D_p = 0.133 [-]) consists of alumina beads and fines of 4.48 mm and 0.596 mm. The second case (d_p/D_p = 0.149 [-]) consists of alumina beads and fines diameter of 2.60 and 0.388

mm. The last case (d_p/D_p = 0.162 [-]) is the case with beads and fines of 3.68 mm and 0.596 mm (they correspond cases 2,1, and 3 in the previous section). In these comparisons, the updraft gas velocity is set at 0.88 m.s^{-1} for all three cases. The fines mass flux for the first and third cases is 0.064 kg m^{-2} s^{-1} and 0.059 kg m^{-2} s^{-1} for the second case.

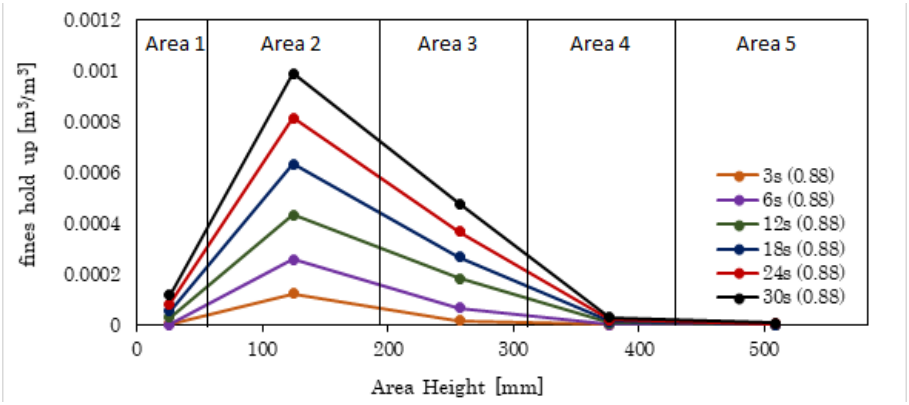

Fig. 2.6 Variation of fines hold up under d_p/D_p =0.133 [-] and U_f = 0.88 [m s^{-1}]

The variation of the vertical distribution of fine particles hold up with time under d_p/D_p = 0.133 [-] is shown in **Fig. 2.6**. The packed bed is divided into 5 areas as shown in **Fig. 2.1** (a) (0-52, 52-197, 197-317, 317-437 and 437-582 mm in height), called as area 1, 2, 3, 4, and 5, respectively. The fines hold up is defined as the volume of fine particles in the unit volume of packed bed in this paper. For packed bed model A, the transition area is located in area 2, on the top of diffusion bed or we called as area 1 (52-102 mm in height), and for packed bed model B, the transition area is located in between area 2 and 3 on top of the extra bed (172-222 mm in height). In this condition, the fine particles are continuously injected at a constant rate from the diffuser. In the beginning, the hold up in the area 2 increases, then the hold up in the area 3 start to increase. Till 30 s, the hold up in the area 2 continues to increases. The hold ups in the areas 2 and 3 reach about 0.099 and 0.048 vol%, respectively. The hold ups in the

upper parts increase with delay in order. This means that a part of the fine particles are stuck in the transition area and the remaining part flows to the upper part. It is considered that the vertical powder transfer and local sucking continue after this period, because the hold up distribution became uniform and the powder recovery ratio (the ratio particle flow-out rate from the top to the injection rate from the bottom) approached unity in the previous experimental study [11].

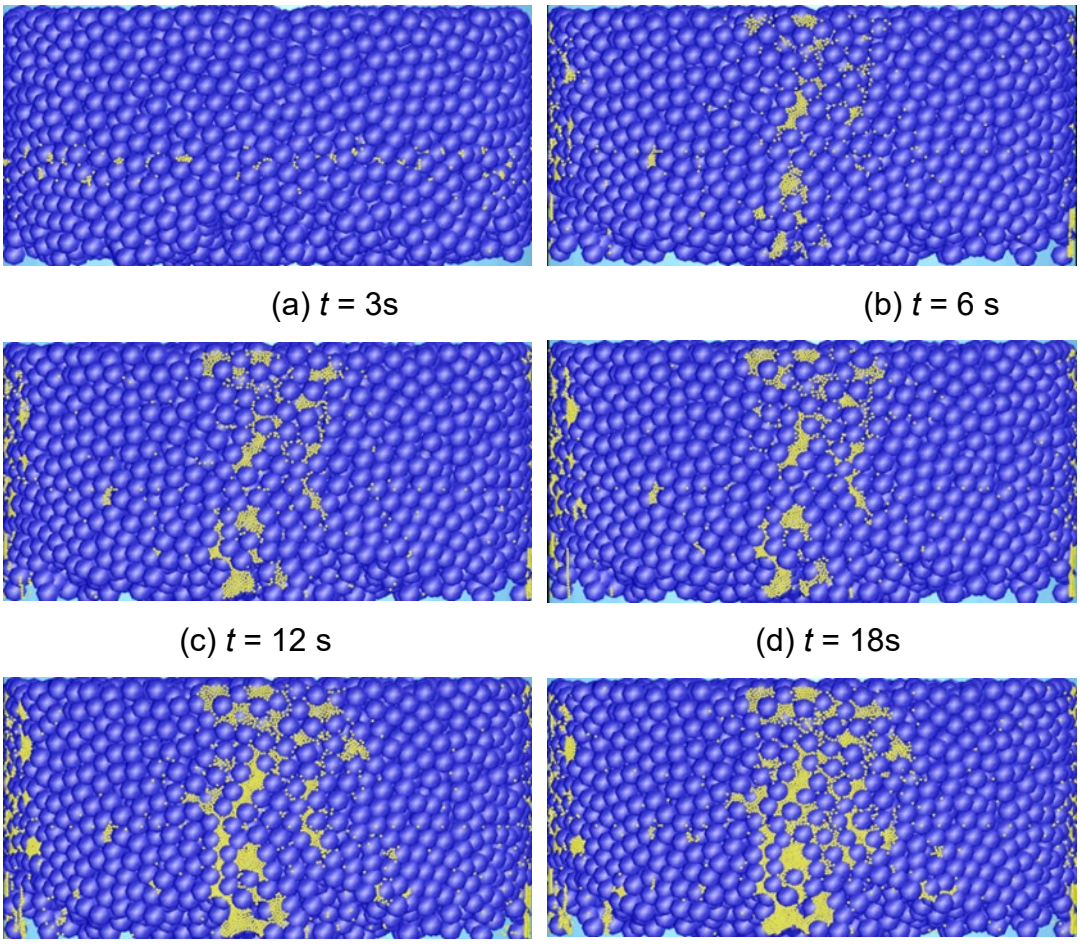

(a) t = 3s (b) t = 6 s

(c) t = 12 s (d) t = 18s

(e) t = 24 s (f) t = 30 s

Fig. 2.7 Fines hold up behavior under d_p/D_p = 0.133[-] condition.

Fig. 2.7 shows the snapshots of fines in the transition area of the packed bed under diameter ratio of 0.133 [-]. This figure was taken from the vertical cross section of the central area of the packed bed. At t = 3 [s], only a small amount of fine particles

can be seen in the middle height of the transition zone. At t = 6 [s], the fine particles reach to the upper area of the transition zone. In the following periods, the amount of the fine particles that are held in the packed bed gradually increases.

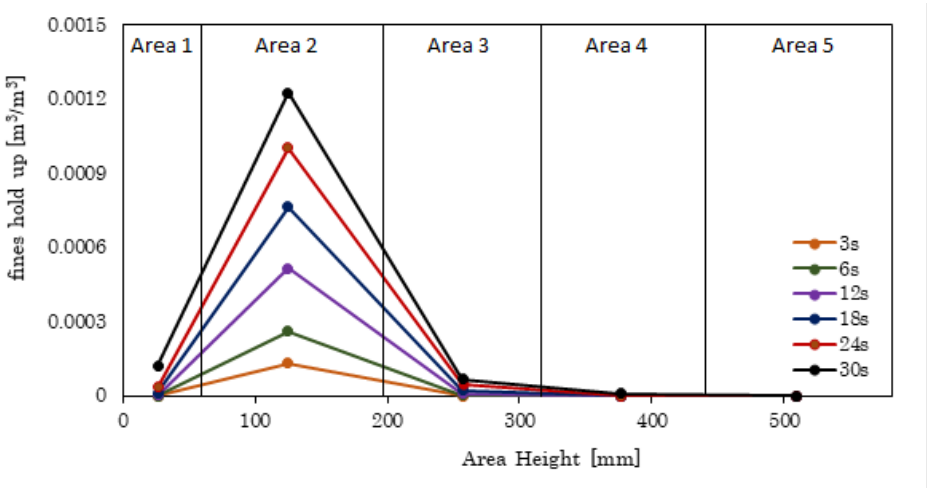

Fig. 2.8 Variation of fines hold up under d_p/D_p =0.149 [-] and U_f = 0.88 [m s^{-1}]

Fig. 2.8 shows the variation of vertical distribution of fine particles hold up with time under d_p/D_p = 0.149 [-]. Similar to the previous case, the fines hold up in the area 2 increases in the beginning. Although the hold up in the area 2 continues to increase, the hold up in the area 3 shows only a slight increase. Little hold up is observed in areas 4 and 5. The hold up in the area 2 reaches about 0.122 vol% that is higher than the previous case while the area 3 shows only about 0.0066 vol% at 30.0 s. This result indicates that most of the injected fine particles are trapped in the area 2 and only little particles can pass this area to the upper area. In the previous experimental study, a negligible amount of powder flowed out to the top of the packed bed under the same diameter ratio condition [11].

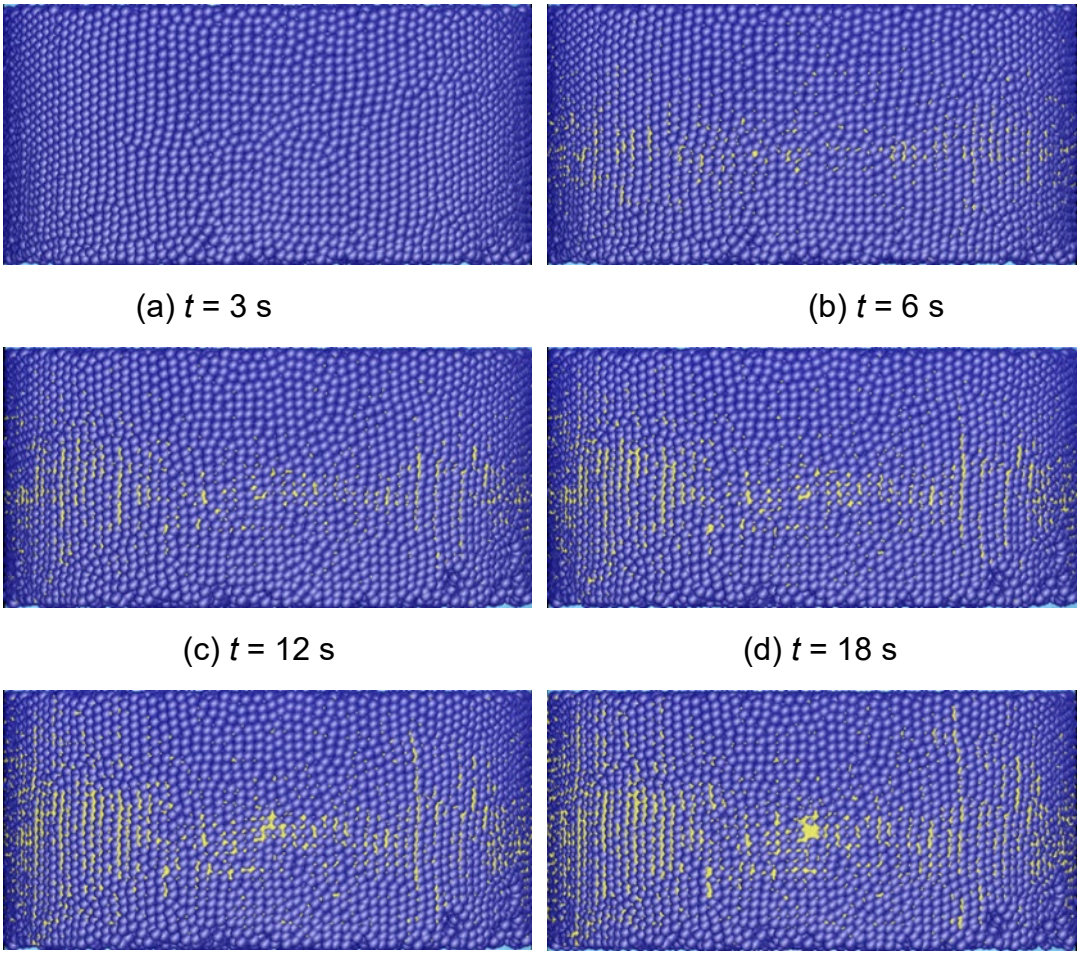

(a) t = 3 s (b) t = 6 s

(c) t = 12 s (d) t = 18 s

(e) t = 24 s (f) t = 30 s

Fig. 2.9 Fines hold up behavior under d_p/D_p = 0.149 [-] condition.

Fig. 2.9 shows the snapshots of fines hold up in the packed bed under d_p/D_p = 0.149 [-]. At t = 3 [s], a lot of small clusters are formed in the middle of the transition area. In each cluster, the fine particles lined vertically between the alumina beads in this packing structure. With time progresses, the number of clastters increases stuck and their shapes are elongated. At t = 30 [s], a few clusters reach the upper part of the transition area. This behavior means that most of fine particles are stuck in the first half of the transition area, and the latter half, the sucked particles increase and a small portion of the injected particles transported to the upper area, as shown in **Fig. 2.8**.

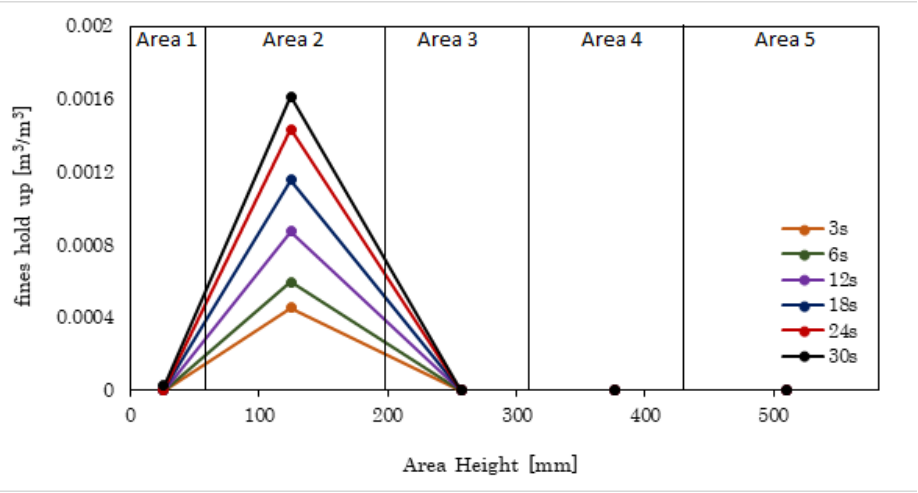

Fig. 2.10 Variation of fines hold up under d_p/D_p =0.162 [-] and U_f = 0.88 [m s^{-1}]

Fig. 2.10 shows the variation of the vertical distribution of fine particles hold up with time under d_p/D_p = 0.162 [-]. Similar to the d_p/D_p = 0.149 [-] case, the hold up in the area 2 mainly increases. Substantially no increase in the fines hold up also occurs in the upper areas. The hold up in the area 2 is about 0.162 vol% at 30.0 s.

Fig. 2.11 shows the snapshots of fines held up in the packed bed under d_p/D_p = 0.162 [-]. Similar to the previous case of dp/Dp = 0.149 [-], the injected particles are stuck in the transition area, especially in the bottom part of this area. Although the accumulation area expands with time progresses, it only reaches up to the middle height of the transition area. Therefore, the particles are unable to transport to the upper areas.

In the minimum and the maximum particle diameter ratio cases, namely d_p/D_p = 0.133 and 0.162 [-], the fine diameter, the mass flux, and the gas velocity are common. The fines behaviors, however, completely different. In the former, the fine particle can pass through the packed bed, while all the fine particles are accumulated in the bed in the latter case. Furthermore, the particles in d_p/D_p = 0.149 [-] case can penetrate up to the middle of the transition area while the particles in d_p/D_p = 0.162 [-] can reach to

only the bottom part of the bed, even some conditions are different. From these results, the diameter ratio has a great effect on the permeation of fine particles through the packed bed. This supports the conclusion of previous study [11] that the critical diameter ratio for blockage formation is 0.12 [-] while the fine particles pass through the bed under d_p/D_p = 0.133 [-] in this work. The difference could be the packing conditions in the experiments and the numerical simulation.

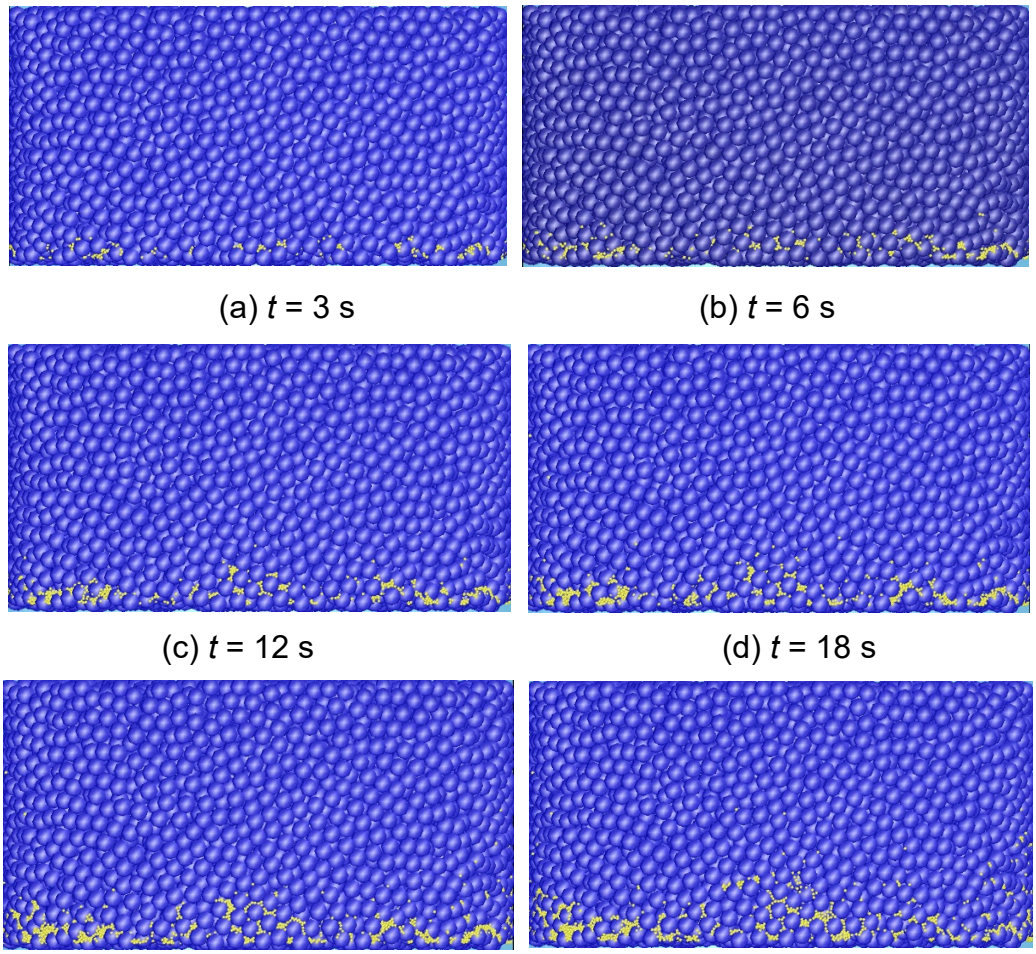

(a) t = 3 s (b) t = 6 s

(c) t = 12 s (d) t = 18 s

(e) t = 24 s (f) t = 30 s

Fig. 2.11 Fines hold up behavior under d_p/D_p = 0.162 [-] condition.

2.3.3. Effect of Gas Superficial Velocity

The effect of gas superficial velocity on the fine particle permeation behavior is discussed. The variations of fine particle hold up obtained under the gas superficial

velocity of 1.06 and 1.24 m s^{-1} are shown in **Figs. 2.12** and **2.13**. The diameter ratio is 0.133 [-], and the fines mass flux is 0.064 kg m^{-2} s^{-1}. Both cases show similar variations of the hold up to the result under the superficial gas velocity of 0.88 $m.s^{-1}$ shown in **Fig. 2.6**. It can be observed there are no significant change of fine particles hold ups for both cases (u_f = 1.06 $m.s^{-1}$ and 1.24 $m.s^{-1}$), compare to previous case (u_f = 0.88 [$m.s^{-1}$])

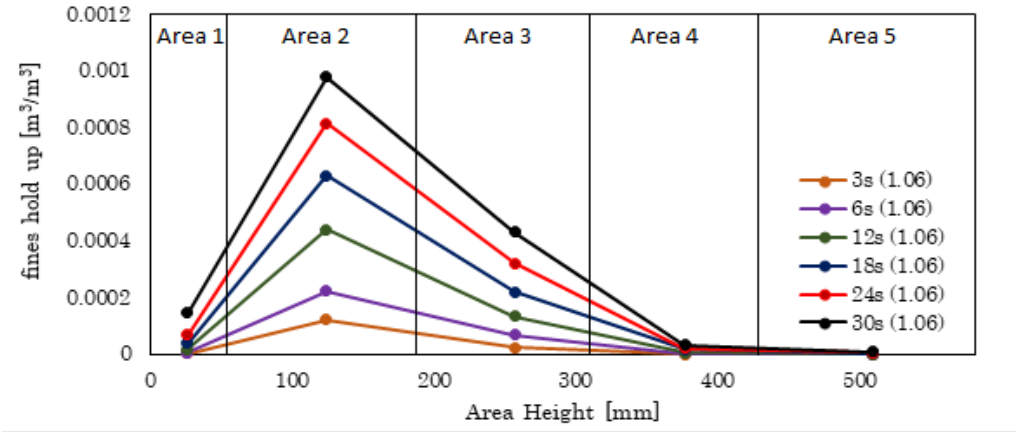

Fig. 12 Fines Hold Up; dp/Dp = 0.133; uf = 1.06 $m.s^{-1}$

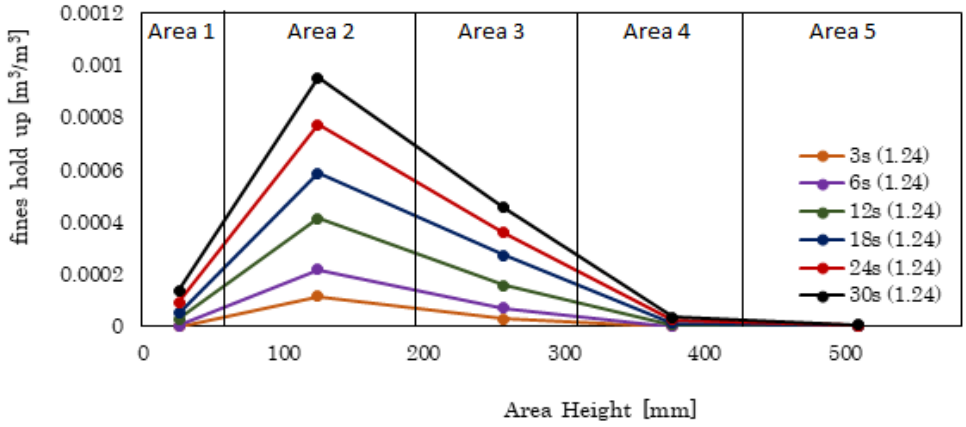

Fig. 2.13 Fines Hold Up; dp/Dp = 0.133; uf = 1.24$m.s^{-1}$

The variations of the fine powder hold up in areas 2, 3, 4 and 5 are shown in

Fig. 2.14. In the figure, the variations under the gas superficial velocities of 0.88, 1.06 and 1.24 m s^{-1} are displayed. The fines hold ups show similar monotonical increase regardless of the gas velocity and there are no significant differences among the three velocities can be observed. According to the previous study, the fraction of fines holdup decreases with the increase of gas velocity when the mass flux of fines is kept constant and hence, the pressure drop curve should have a tendency to approach the value of pure gas with increasing gas velocity [10]. This means with the increase of gas velocity, the fine particles will be easily transported to the upper area because of higher updraft driving force. However, this phenomenon is only consistent if the particle diameter ratio is small enough or the gap fine particle and flow channel aperture is big enough. Moreover, it should be noticed that in this section, the effect of gas superficial velocities are observed under *d*p/*D*p = 0.133 [-], where the particle diameter ratio already exceeds the critical diameter ratio of *d*p/*D*p = 0.12 [-] [11]. Thus it can be concluded that the change of gas superficial velocity becomes less significant when *d*p/*D*p already exceeds the critical diameter ratio.

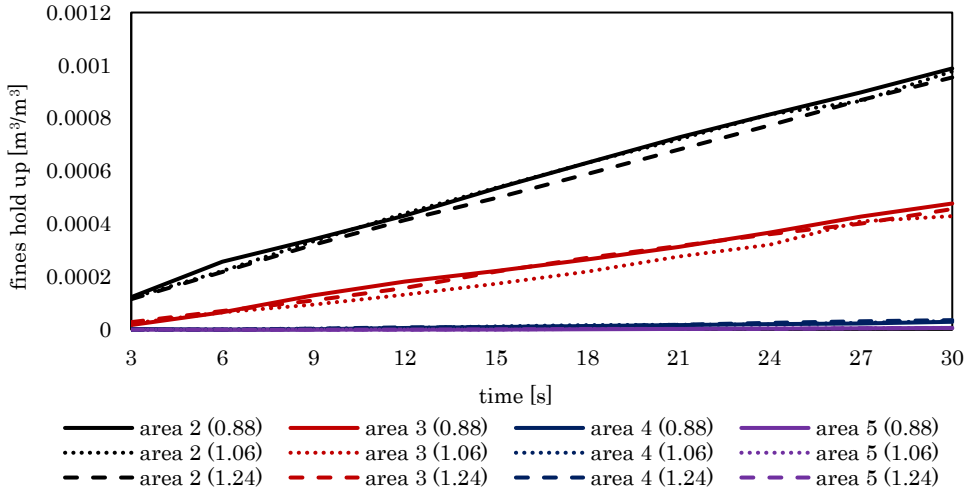

Fig. 2.14 Fines Hold Up of *d*p/*D*p = 0.133 [-] with various superficial gas velocities

2.3.4. Fraction of Local Blockage

In the previous paper by Natsui et.al [18], fine particles were injected in pulse-wise feeding, where the constant volume of fine particles was generated in the packed bed. Because of the constant volume of fine particles in their numerical approach, the gas flow becomes constant and uniform, where even heavily concentrated powder always received upward drag force and move upward little by little. Contrarily, in this present study, the actual behavior of gas flow is expected to be able to obtain because of continuous feeding. When the fine particles are injected continuously and going through the transition area, they will go together with the gas flow through the diffuser bed and extra bed. When the fine particles reached the bottom part of the transition area, with the gas flow they will avoid the heavily concentrated area or for instant, it will pass through the voids that exist within the transition area. Then, the voids in the transition area are eliminated and filled by the fine particles and change the gas flow patterns.

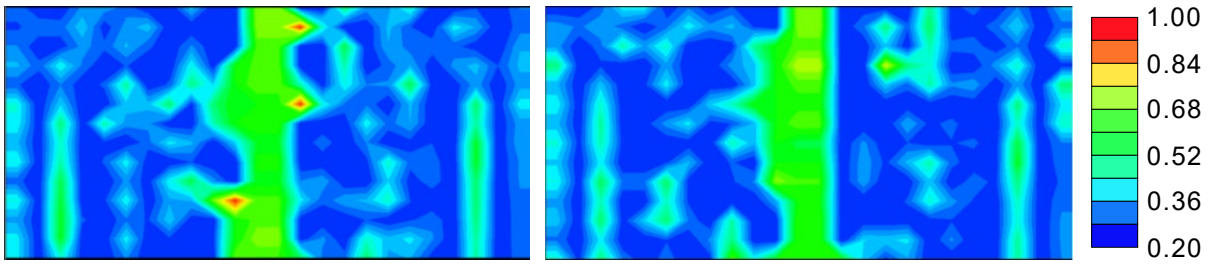

(a) Void fraction t = 0 s (b) void fraction t = 30 s

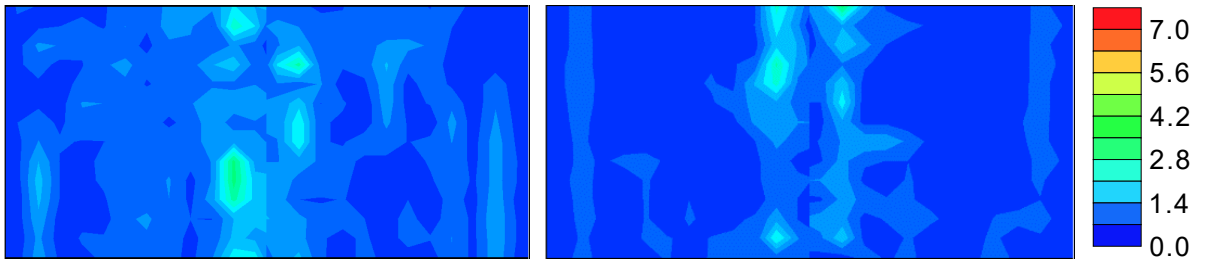

(c) absolute velocity t = 0 s (d) absolute velocity t = 30 s

Fig. 2.15 Void fraction and abs velocity distribution under dp/Dp = 0.133 [-] condition.

Fig. 2.15 shows the void fractions and the contour of absolute gas velocity (u_f = 0.88 m.s^{-1}) under dp/Dp = 0.133 [-] at t = 0 [s] and t = 30 [s], located in the transition area of packed bed model B. From **Fig. 2.15** (a) at t = 0 [s], it can be observed that the voids mainly exist in the middle section of the transition area, with several spots of high void concentration (red spots), can be observed. Some voids also scattered randomly and also connected around the transition area. As a comparison, **Fig. 2.15** (c) shows the contour of absolute velocity at t = 0 [s]. It can be seen that the gas flow pattern is following a similar pattern as voids fraction where the gas flow is mainly concentrated in the middle section of the transition area. Furthermore, high concentration gas flow also can be observed in the same location where the high void concentration (red spots) exists. Similar to void fractions that scattered and connected around the transition area, the gas flow also being scattered and connected in the same areas. In **Fig. 2.15** (b) at t = 30 [s], the high void concentrations are already eliminated and the scattered voids also become less connected, indicates the fine particles alreadyed filled the voids. From **Fig. 2.15** (d), the contour of absolute gas velocity at t = 30 [s] is also in a good agreement with the voids patterns. It shows that even though the gas flow is still concentrated in the middle section of the transition area, but it becomes less concentrated, similar to void patterns. This phenomenon indicates that gas flows avoiding the heavily concentrated area or become weak in highly concentrated area.

2.4. Conclusion

Numerical simulation of fines permeability inside the packed bed is already been done. In this simulation fine particles are injected continuously every second, mimicking the experimental approach by Takahashi et al [(11)]. The effect of particle diameter ratios and updraft gas velocities to fines permeability were analyzed. The following conclusions are as follows.

1. Comparison between numerical and experimental approaches showed a good agreement and high accuracy from the pressure distribution. Some differences mostly occurred because of the physical situation in the experimental conditions such as particle motion, sphericity, and pressure gauge reading that neglected in numerical approach.
2. The particle diameter ratio become the major cause for particle restrained in the transition area. Larger particle ratio resulted in higher particle hold up in area 2 while no significant increase of fines hold up in the upper area. Fine particles tend to concentrate at the bottom of the packed bed owing to an increase in their diameter ratio. From a broader scale point of view, the height of fine particles can penetrate vertically is changes according to the particle diameter ratio.
3. There are no significant change in fines fraction transported to upper area due to the change of gas velocity. This phenomenon more likely because the diameter ratio already exceeds the critical diamater ratio proposed by previous experimental study [11].
4. The change of void fraction actual pattern of gas flow can be obtained in this simulation. As the time lapsed, voids fraction are decreasing because being filled by fine particles. it also can be shown that the gas flow is avoiding the heavily concentrated area or become very weak in the low void fraction area.

2.5. References

1) Ministry of the Environment Japan: National Greenhouse Gas Inventory Report of Japan., (2013), 2.4, 3.2.

2) T. Ariyama, M. Sato: ISIJ Int., 46(2006), 1736.

3) N. Hidaka, J. Iyama, T. matsumoto, K. Kusakabe and S. Morooka: Powder Technology., 45(1998), 265.

4) N. Hidaka, J. Iyama, T. Matsumoto, K. Kusakabe and S. Morooka: Korean J. Chem Eng., 16(1999), 852.

5) N. Hidaka, J. Iyama, T. Matsumoto, K. Kusakabe and S. Morooka: Journal Chemical Engineering of Japan., 32(1999), 197.

6) N. Hidaka, J. Iyama, T. Matsumoto, K. Kusakabe and S. Morooka: Journal Chemical Engineering of Japan., 33(2000), 152.

7) X.F. Dong, D. Pinson, S.J. Zhang, A.B. Yu and P. Zulli: Powder Technology., 149(2004), 1.

8) C. Jizhong, T. Akiyama, H. Nogami and J. Yagi: ISIJ Int., 34(1994), 133.

9) T.S. Pham, D. Pinson, A.B. Yu and P. Zulli: Chemical Engineering Science., 54(1999), 5339.

10) S. Koichiro, M. Shimizu, S. Inaba, R. Takahashi and J. Yagi: ISIJ Int., 31(1991), 434.

11) H. Takahashi, H. Kawai, T. Kondo and M. Sugawara: ISIJ Int., 51(2011), 1608.

12) K.W. Chu and A.B. Yu: Powder Technology., 179(2008), 104.

13) X.F. Dong, D. Pinson, S.J. Zhang, A.B. Yu and P. Zulli: Powder Technology., 149(2004), 10.

14) B.H. Xu, A.B. Yu, S.J. Chew and P. Zulli: Powder Technology., 109(2000), 13.

15) S. Matsuhashi, H. Kurosawa, S. Natsui, T. Kon, S. Ueda, R. Inoue, T. Ariyama: ISIJ Int., 52(2012), 1990.

16) H. Nogami, P.R. Austin, J. Yagi and K. Yamaguchi: ISIJ Int., 44(2004), 500.

17) S. Kikuchi, T. Kon, S. Ueda, S. Natsui, R. Inoue and T. Ariyama: ISIJ Int., 55(2015), 1313.

18) S. Natsui, S. Ueda, H. Nogami, J. Kano, R. Inoue and T. Ariyama: Chemical Engineering Science., 71(2012), 274.

CHAPTER III

Numerical Simulation on Phenomena of Fine Particles Passing through an Orifice under Gas Flow Condition

CHAPTER 3

Numerical Simulation on Phenomena of Fine Particles Passing through an Orifice under Gas Flow Condition

Synopsis

Under low reducing agent rate and high pulverized-coal injection rate operations, coke powder and unburnt char are generated in the blast furnace. These powders flow through the packed bed inside the furnace entrained by the gas flow. The powders accumulation in packed bed will deteriorate gas and liquid permeability and creates an unstable situation inside the blast furnace. Thus, it is important to quantitatively evaluate the accumulation rate on a distribution channel of coke powders. In this study, the behavior of the powder particles passing through the orifice formed by three coarse particles that osculate one another and compound in an equilateral triangle was numerically analyzed using the DEM-CFD. The results revealed the effect of drag force on the powder motion passing through the orifice. Moreover, the effect of the position of the powder passing through the orifice to pressure drop fluctuation inside the triangular prism is also analyzed.

3.1. Introduction

Every year, Japan steelmaking industries produce about 100 million tones pig iron which consumes 12% of Japan's total energy consumption. Moreover, this steelmaking process also contributes about 15% of the total CO_2 emissions[1)]. On average, 70% of the primary energy input to the integrated steelworks is used for the ironmaking process, thus the design of a high-efficiency blast furnace with an aim for the reduction of CO_2 emission and energy consumption is in high demand[2,3)].

As a method for reducing CO_2 in blast furnaces, a low-reducing agent ratio operation is being carried out to reduce the amount of coke used and reduce the carbon input to the blast furnace. At the same time, in order to reduce the cost of blast furnace operation, a large amount of pulverized coal is injected into the furnace using inexpensive pulverized coal as an auxiliary reducing agent. However, these operating methods increase the amount of coke powder and unburned char generated in the blast furnace. The generated powder flows through the packed bed in the blast furnace as a solid-gas two-phase flow, which affects the ventilation and liquid permeability in the blast furnace. It is important to quantitatively evaluate the distribution route of the generated powder in the blast furnace and the accumulation rate on that route because excessive accumulation of powder in the packed bed may cause operational malfunctions such as hanging and slips.

As the method for blockage prevention is very important in blast furnace operation, some studies regarding the inspections, experimental approaches, and numerical approaches already been done in the past years. For inspection approaches, Puttinger et al [3,4,5)] discussed the detection method for blockages inside the blast furnace and its relation to blast flow rate. Their works were divided into three series; classification of blockage events, signal processing of hot blast pressure data, and visual detection based on tuyere camera images. Takahashi et al [6,7)], and Dong et al

[8], conducted some experiment using macroscopic approach to obtain the blockage behavior of fine particles inside the packed bed in basic level experiments. Takahashi et al, then proposed a critical ratio of fine to coarse diameter greater than 0.12 for the blockage to occur. Various numerical approaches also had been done to predict the behavior of ore particles inside the blast furnace using DEM or DEM-CFD coupling analysis. Fukuda et al [9] and Luo et al [10], used Discrete Element Method (DEM) to analyze the powder behavior in static flow inside the equilateral triangle system where number of fine particles are dropped simultaneously towards the orifice formed by the arrangement of three equilateral coarse particles. Zaki et al [11], predicted granular mass discharge rate through different orifice shapes of the same opening area at flat bottomed cylindrical silo. Ariyama et al [12] and Zhou et al [13] were discussed the development model of the fine particle inside the blast furnace using DEM model, which contains the key phenomena including percolation velocity, residence time distribution, longitudinal and transverse dispersion, of cohesive fine particles in a packed bed. However, for a system like a blast furnace where the gas flow is strongly affected the fine particle arrangements and porosity distribution, the coupling analysis between DEM and Computational Fluid Dynamic (CFD) for gas flow is needed. Natsui et al [14,15] Kurosawa et al [16], Matsuhashi et al [17], Kawai et al [18], Mahmoodi et al [19], Ishii et al [20], and Kikuchi et al [21] summarized the coupling analysis of DEM-CFD inside the fluidized bed in macroscopic level. It can be noticed that the previous studies of numerical analyses mainly focused on DEM-CFD coupling analysis in macroscopic level, while for microscopic level the analysis were mostly focused focused on DEM approach, on the interactions of fine to coarse particle through their morphology characteristics and cohesive behavior. However, since DEM information is Lagragian analysis and CFD is Eulerian analysis, it is also become important to investigate the accuracy of DEM-CFD model in microscopic level, and compare it to experimental set

up.

In this research, microscopic behavior analysis has been performed to show the passing behavior of fine particles through the narrowest possible gap inside the packed bed or we call as an orifice. The interaction between gas flow and the existence of fine particles also been observed, where the fine particle affecting the characteristic of gas flow such as pressure drop fluctuations, while gas flow also affecting the passing behavior of the fine particle. Furthermore, two-phase flow gas-solid behavior leading to the initial clogging process at the microscopic level will also be observed using multiple fine particle dropping in the triangular prism model of the packed bed.

3.2. Numerical Approach

3.2.1. Analysis of solid-gas two phase flow

The moving particles are tracked using discrete element method (DEM), in which each element is numerically analyzed on the condition where each particle is adequate the equation of motion and the force transfer of Newton's third law of action and reaction. Powder particles flowing as a group consisting of a large number of particles in a moving bed or a fluidized bed move while repeating collision and friction with neighboring particles and walls. The equations of motion for the translational and rotational motions of a particle receiving a force from its surroundings are described as follows, based on Newton's second law of motion given by the following equations (1) and (2).

$$m_i \frac{d\vec{v}_i}{dt} = \sum_j^N \vec{F}_{n,j} + m_i \vec{g} + \vec{F}_D \quad (1)$$

$$I_i \frac{d\vec{\omega}_i}{dt} = \sum_j^N r_i \vec{F}_{s,j} - M_r \quad (2)$$

Where m is particle mass [kg], v is particle velocity [m s^{-1}], t is time [s], g is gravity [m s^{-2}], and I is the moment of inertia of the particle [kg m^2], ω is the particle angular velocity [rad s^{-1}], and r is the particle radius [m]. The motion of the particle of interest is affected by force and gravity due to contact with surrounding objects. Fn, Fs, F_D and M_r are inter-particle contact forces in the normal direction [N], contact forces in the tangential direction [N], drag force [N], and rotational resistivity [N m]. Subscripts i and j each determine the particle of interest and the particles that come into contact with this particles, respectively.

The normal direction and tangential direction are defined as the direction of the line that passes through the center of two interconnected particles, and the direction that is perpendicular to this line. Contact forces in the normal and tangential directions can be given by the following equations (3) and (4). The u and □ are the small displacements ([m] and [rad]) in normal and tangential direction because of the contact. K is spring constant [N m^{-1}], and □□is damping constant [kg s^{-1}]. Under slip condition, the tangential contact force is given by the following equation (5). The rotational motion resistance force is given by following equation (6) and incorporated in equation (2), where □ and r_c are rotational friction coefficient [-] and radius of contact circle [m].

$$F_{\mathrm{n}} = \eta_{\mathrm{n}} \frac{du}{dt} + K_{\mathrm{n}} u = 0 \tag{3}$$

$$F_{\mathrm{s}} = \eta_{\mathrm{s}} r_i \frac{d\phi}{dt} + K_{\mathrm{s}} r_i \phi = 0 \tag{4}$$

$$F_{\mathrm{s}} = \mu_{\mathrm{f}} F_{\mathrm{n}} \tag{5}$$

$$M_{\mathrm{r}} = \frac{3}{8} \alpha r_{\mathrm{c}} F_{\mathrm{n}} \tag{6}$$

In this study, gas-powder two-phase flow analysis was performed using thermal fluid and powder analysis software R-FLOW. The governing equations for the gas flow

are the momentum conservation law (Navier-Stokes equation), Eq. (7) and the mass conservation law (continuity equation), Eq. (8).

$$\rho_{\mathrm{d}} \frac{dV_{\mathrm{d}}}{dt} = (\rho_{\mathrm{d}} - \rho_{\mathrm{c}})\boldsymbol{g} + \varepsilon_{\mathrm{c}}\beta(V_{\mathrm{c}} - V_{\mathrm{d}}) - \nabla p + \boldsymbol{F}_{\mathrm{p}} \quad (7).$$

$$\frac{\partial}{\partial t}(\varepsilon_c \rho_c) + \nabla.(\varepsilon_c \rho_c V_c) = 0 \quad (8).$$

Here, the flow velocity is V [m s^{-1}], density is ρ [kg m^{-3}], and F_{p} is force that applied to particles other than fluid [N]. The sufficives c and d are physical quantities related to the gas flow as continuous phase and the powder particles as dispersed phase, respectively. ε_{c} and ($\varepsilon_{\mathrm{d}} = 1 - \varepsilon_{\mathrm{c}}$) are the volume fractions of the continuous and disperse phases, and β is the coefficient of momentum exchange between the continuous and the disperse phases .

The Gidaspow drag model [23] is adopted as the gas-powder interaction force in the two-phase flow analysis. The Gidaspow model is the combination between two drag model, which consist of the Ergun model [22] which is use for the low void fraction region ($\varepsilon_{\mathrm{c}} \leqq 0.8$), and Wen-Yu model for high void fraction region ($\varepsilon_{\mathrm{c}} > 0.8$) [24], as shown in equations (9) and (10). Here d_{p} is particle diameter [m]. The drag coefficient C_{D} is given as the function of Reynolds number as written in equation (11).

$$\beta = 150\frac{\varepsilon_d \mu_c}{\left(\varepsilon_c d_p\right)^2} + 1.75\frac{\rho_d \left|V_d - V_c\right|}{\left(\varepsilon_c d_p\right)} \quad (9)$$

$$\beta = 0.75\frac{C_D \rho_c \left|V_d - V_c\right|}{\left(\varepsilon_c^{2.7} d_p\right)} \quad (10)$$

$$C_D = \begin{pmatrix} \frac{24\left(1+0.15Re_{\mathrm{p}}^{0.687}\right)}{Re_{\mathrm{p}}} & (Re_{\mathrm{p}} \leqq 1000) \\ 0.44 & (Re_{\mathrm{p}} > 1000) \end{pmatrix} \quad (11)$$

3.2.2. Calculation conditions and Setup

In this simulation, the narrowest part of the flow path in the spherical packed bed is being discussed. It is obvious that the arrangement of the actual packed bed inside the blast furnace is more likely irregularly shaped and randomly packed, which sets complex flow paths among the packed material. However, it is considered that the possible narrowest gap in the packed bed is the opening of three coarse particles that osculate with one another and compound in an equilateral triangle. In this paper the gap will be called as an orifice hereinafter. As mentioned, the packed particles are placed horizontally, and form a small aperture or orifice in the middle by nudging each other. The powder particles are dropped onto the orifice by gravity, and the trajectories of the particles are numerically tracked. The calculation domain is set as a vertical triangular prism, of which the cross section is an equilateral triangle comprised of orifice particles in the center, as shown in **Fig. 3.1**. This study is focused on the passing behavior of powder particles onto the orifice and its interactions with gas flow blown from the bottom of the packed bed.

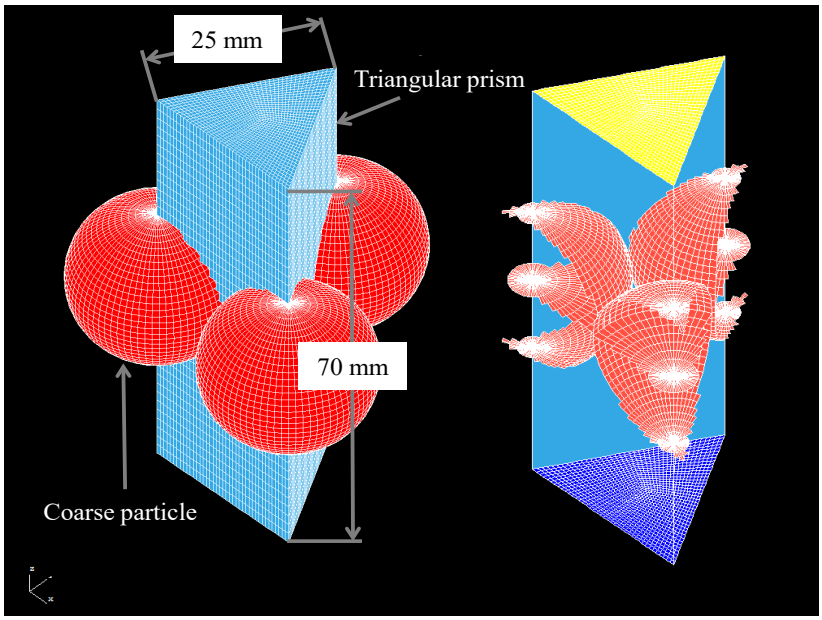

Fig. 3.1 Analysis model.

In this study, the packed powder that creates the orifice and the sides of the prism is treated as a solid wall. As the scale of the model, the packed particle diameter is 25 mm, the vertical triangular prism height is 70 mm, and the fine particle diameter is 2.5 mm. In this simulation, prism walls are treated as a non-slip wall. The analysis conditions are shown in **Table 3.1**. The input particles were set to 1 or 30 particles and the gas inflow velocity is 1.0 m s^{-1}. For this analysis, friction coefficient is 0.2 [-] and spring constant is 100 [N m^{-1}]. Before discussing the gas-solid flow characteristic inside the triangular prism, initial investigation using experimental and numerical approaches will be performed in the next section to determine the basic value of the coefficient of restitution and comparing the passing time of fine particle using numerical and experimental approach.

Table 3.1 Numerical Analysis Condition

Diameter of coarse particle	25.0	[mm]
Diameter of fine particle	2.5	[mm]
Particles Number	1 or 30	[-]
Fine to Coarse Particle Diameter Ratio	0.1	[-]
Friction Coefficient	0.2	[-]
Spring Constant	100	[N m^{-1}]
Gas-blowing velocity	0 or 1.0	[m s^{-1}]

3.3. Results and Discussions

3.3.1. Determination of the Coefficient of Restitution

The validation process for numerical analysis is taken in two steps. The first step is to measure the passing time of fine particle through the orifice, continuing with the

second step to determine the coefficient restitution using experimental apparatus to be applied in numerical analysis. The first step of validation is performed as follows. A schematic diagram of the experimental apparatus is shown in **Fig. 3.2 (a)**. The measuring device consists of a positioning device for setting the position of dropped fine particles into a triangular flow path. Consisting of three beads particles that osculates with one and another and compound in an equilateral triangle with orifice in the middle, an optical sensor that detects the inflow and outflow of particles, and data logger that records the signal from the sensor.

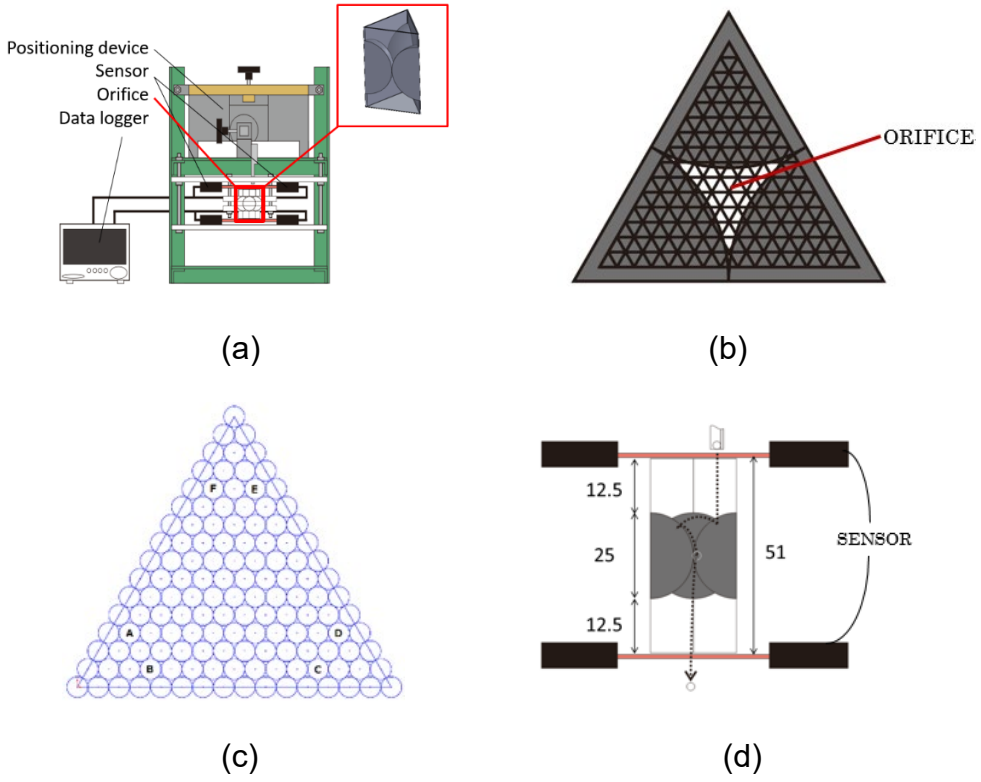

Fig 3.2. (a) Experimental Apparatus for Passing Time (b) Orifice Position (c) Particle Dropped Positions (d) Schematic for Calculate Passing Time.

The transit time is defined by the time difference between the signals of the upper and lower sensors. The horizontal cross section of the triangular prism was set

so that the inside is divided to 136 points as shown in **Fig. 3.2 (b)**, and the center of the particle was at the vertex of the triangle. From these 136 points, 6 points are selected and then named as point A (4.167; 4.333), B (5.83; 1.44), C (19.167; 1.44), D (20.835; 4.33), E (14.167; 15.877), and F (10.835; 15,877), where the coordinate of the nearest vertex to point A is (0.0; 0.0), (unit: mm), shown in **Fig. 3.2 (c)**. The distance between the laser sheets from the optical sensors is 51 mm and the length of the channel is 50 mm, as shown in **Fig. 3.2 (d)**. Three measurements are made per one point, and the average value of transit time is taken from every dropped position. The passing time from this experimental approach will be shown in **Table 3.3**.

Table 3.2 Experimental Condition

Diameter of powder particle *d*p [mm]	2.5
Diameter of coarse particle *D*p [mm]	25
Diameter ratio (*d*p/*D*p) [-]	0.1
Falling Height [mm]	60
Frame rate [fps]	1000

The second step is performed to determine coefficient restitution to be used in numerical analysis. This second step is performed as follows. A schematic diagram of experimental apparatus is shown in **Fig. 3.3 (a)**. A fine glass spherical particle of which the diameter is 2.5 mm was dropped from above of which the height is 60 mm, onto the coarse spherical particle with the diameter of 25 mm. The particle trajectory was recorded by high speed camera, and the velocity of the glass spheres before and after the collision was determined using image analysis software. **Table 3.2** shows the experimental conditions.

The coefficient of restitution was calculated from the ratio of velocity of the glass sphere after and before the collision. **Fig 3.3 (b)** shows the coefficient of restitution obtained by the experiment, where the average value is 0.92 [-].

Table. 3.3. Analysis result at coefficient of restitution 0.92 [-]

	Coefficient of restitution 0.92 [-]	Experiment results*
Position A	0.40 [s]	0.33 [s]
Position B	0.49 [s]	0.43 [s]
Position C	0.34 [s]	0.36 [s]
Position D	0.32 [s]	0.44 [s]
Position E	0.48 [s]	0.41 [s]
Position F	0.43 [s]	0.42 [s]
Average	0.41 [s]	0.40 [s]

This obtained coefficient restitution is used for numerical analysis, mimicking the experimental model as mentioned in step one, **Fig. 3.2**. In numerical analysis, the glass bead is dropped from 6 coordinate positions; A, B, C, D, E, and F, similar to the coordinates of the experimental model. The comparison between the numerical analysis and the experimental result for the coefficient restitution of 0.92 [-] are shown in **Table 3.3**. For the simulation results, even though the transit time of positions B and E are larger than the other input positions, the average transit time of the numerical analysis with a coefficient of restitution of 0.92 [-] is 0.41 s, which is close to the experimental results. The difference in result may occurred because some errors during experiment such as the precision of dropping location and shape distortion of both fine and coarse particle. However, because the average value between the

numerical and experimental result are close, the numerical approach is reliable to be used for the next model. For the next analysis, the fine particle dropping position is set at point F, where the experimental and numerical result are the closest. The coefficient of restitution is set to 0.95 [-] with the aim to extend the retention time of fine particle above the orifice, while the friction coefficient and spring constant are remain the same as mentioned in Table 1.

3.3.2. Velocity and Pressure Profile

The analysis result of the fluid for single phase flow through the orifice of coarse particles will be discussed in this section. **Figs. 3.4** and 3.**5** show the variation of flow fields after the gas is introduced from the bottom of the triangular prism. The side and the height of the triangular prism are 25 mm and 70 mm, the particle diameter is 25 mm, and the coarse particle center locates at the height of 35 mm. Updraft gas is introduced uniformly from the bottom at 1 m s^{-1}. The plane shows in these figures are located in 8.66 mm from the side face. **Fig. 3.4** shows the variation of the velocity field. Although the air is uniformly introduced from the bottom, the gas flow concentrates at the orifice aperture at t = 0.04 [s]. With this concentration of flow, a gas plume is formed and its velocity increases rapidly in this region and the downstream region. The maximum velocity reaches about 13 m s^{-1}, where the sudden increase of upward gas velocity is caused mainly because the area ratio between the aperture to the prism area is about 0.093 [-] or approximately 1:12. **Fig. 3.5** shows the variations of the pressure field. The pressure field rapidly decreases during the process of passing through the orifice, inverse to the velocity profile. The velocity profile and pressure distribution inside the system are changed immediately after the fluid is introduced at short intervals, but reach a steady state in about 0.2 s under no fine particle condition.

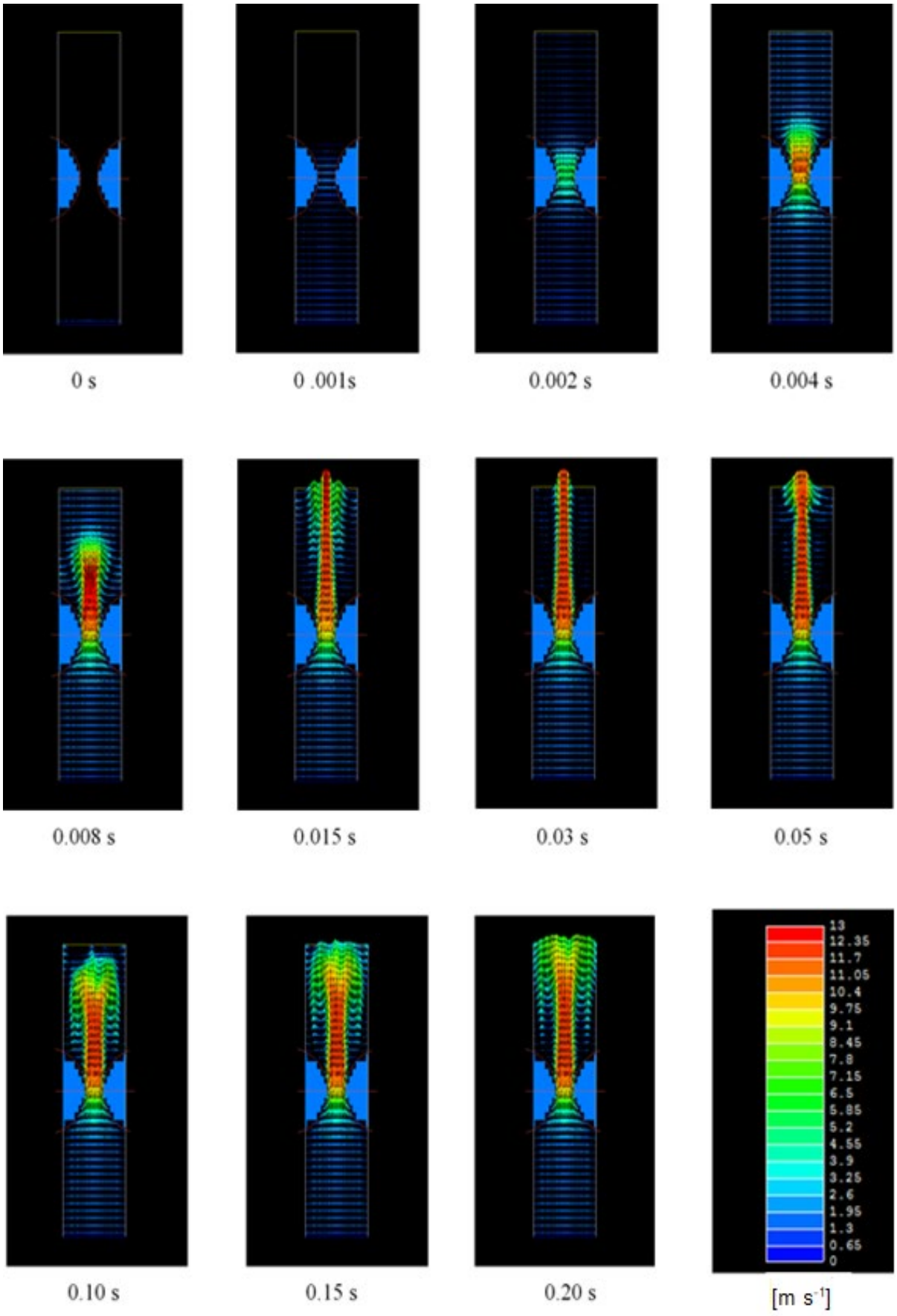

Fig. 3.4 Time Variation of Flow Velocity.

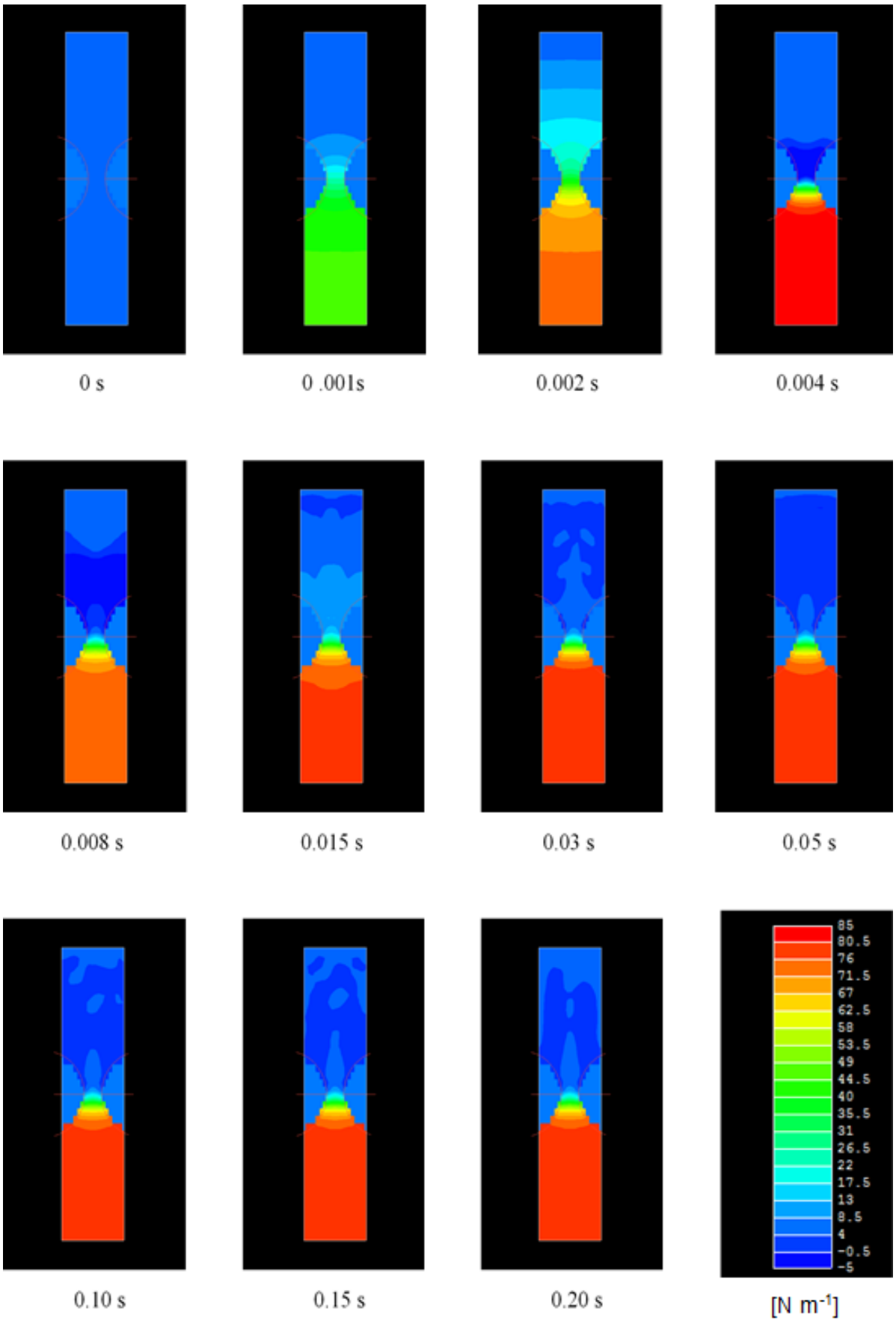

Fig. 3.5 Time variation of pressure distribution.

3.3.3. Passing Behavior of Single Particle

Fig. 3.6 shows the trajectories of a single particle inside the prism through the coarse particle orifice, with and without upward gas flow. The particle drop position is located at point F. On the trajectories, the cross marks are plotted every 0.002 s. In both cases, the fine particle initially falls onto the right-front coarse particle. It bounces and collides with the prism walls and coarse particles several times then it comes into the region just above the aperture opening. In this region, the fine particle collides many times with coarse particles and finally passes the aperture. In these figures, remarkable differences can be seen in two regions. One is above the aperture and the other is beneath the coarse particles. In the former, horizontal motion is enhanced under the upward gas flow condition. In the latter, the fine particle trajectory is almost straight downward under no gas flow condition compared to the under upward gas flow condition.

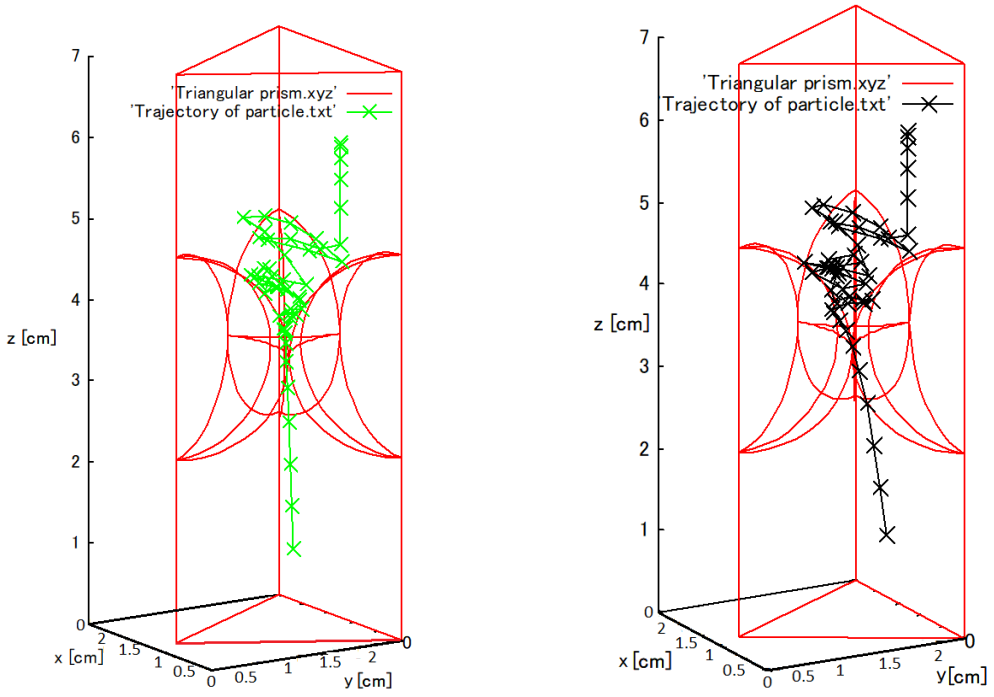

(a) (b)

Fig. 3.6 Particle Trajectory (a) stationary fluid (b) gas flow of 1 m s^{-1}.

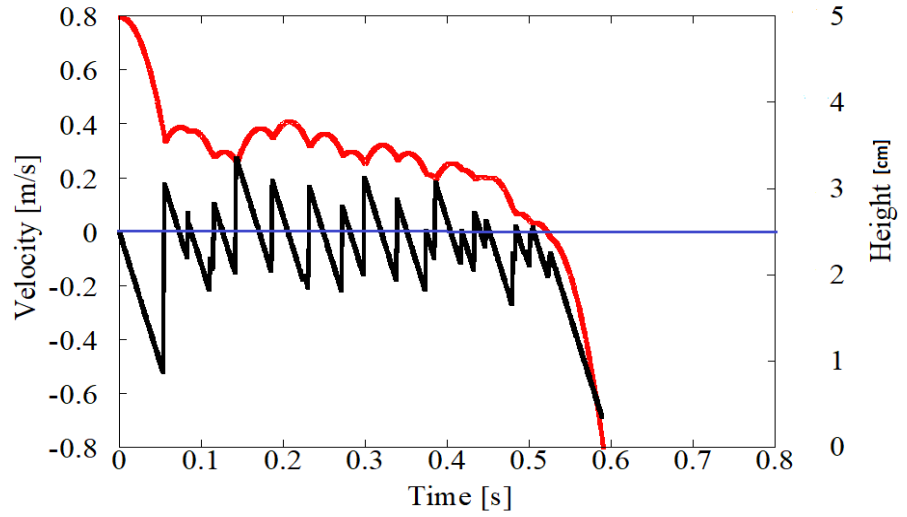

(a)

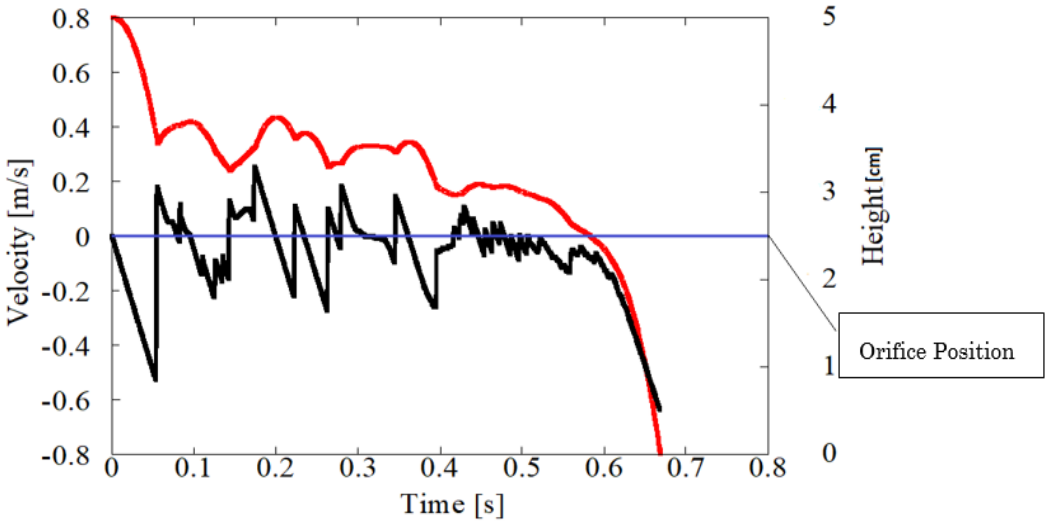

(b)

Fig. 3.7 Velocity and Height of Powder in (a) static fluid (b) gas flow 1 m s^{-1}.

Fig. 3.7 compares the variations of the velocity and the height of powder particles with and without upward gas flow. In these figures, the red and black lines represent the height position and velocity of fine particles, respectively. In static fluid, the velocity of fine particles shows linear jagged changes. This profile indicates that the downward acceleration and sudden velocity change due to the collision occurs alternately. The downward acceleration is mainly affected by gravitational acceleration with less drag resistance from static gas. Contrarily, the effect of the drag force is

significant under upward gas flow conditions. In **Fig. 3.6 (b)**, the velocity profile of dropping fine particles is curved around t =0.09, 0.15, 0.3, and 0.40 s. especially around 0.1 and 0.4 s, the upward acceleration occurs. During the time when the particle stays in the aperture region, the chance of contact between fine and coarse particles increases. Under the upward gas flow conditions, numerous fine-coarse particle collisions occur from 0.40 and 0.62 s. It is considered due to the strong upward gas flow in the aperture region, because the fine particle velocity fluctuates around 0 m s^{-1}. As a result, the residence times of the fine particles in the orifice are 0.59 s for static fluid and become longer for upward flowing conditions, about 0.67 s.

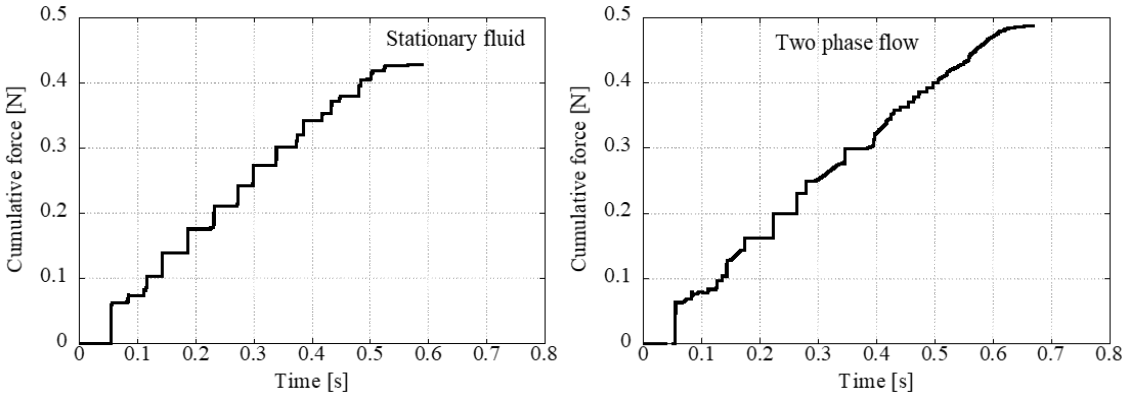

(a) (b)

Fig. 3.8 Cumulative Contact Force (a) Static Fluid (b) Gas Flow 1 m s^{-1}.

The cumulative contact force is shown in **Fig. 3.8**. In the case of static fluid, the cumulative contact force is lower compared to the case of upward gas flow of 1.0 m s^{-1}. These two results indicate that more contact occurred between fine to coarse particles in the case with upward gas flow compared to the static fluid case. For both cases we can see that cumulative contact force increases, where in the case of static flow, it is noticeable that the accumulated contact force occurs in stepwise configuration. In the case of upward gas flow, the change of cumulative contact force

to time passage occurs in much smaller stepwise configuration passed between t = 0.42 to t = 0.6 [s], compared to the prior case. In the later case, this phenomenon occurred when the powder entered the area near the orifice which was strongly affected by the high-speed airflow concentrated at the aperture area, and rapidly bounced back and forward amongst the coarse particles before finally entering the orifice.

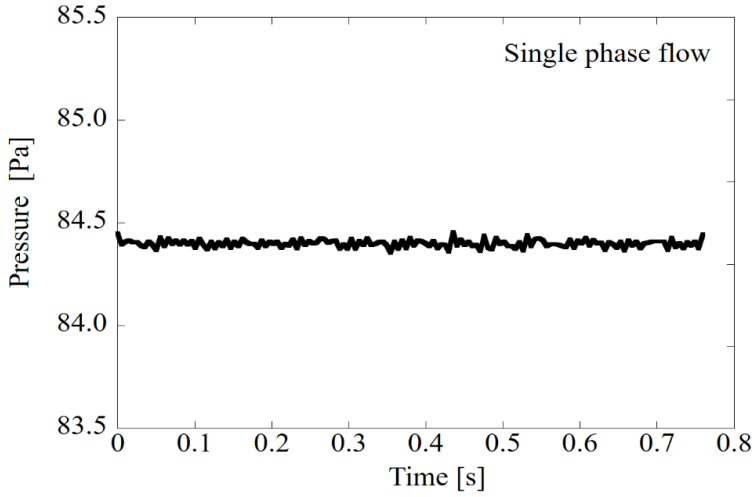

(a)

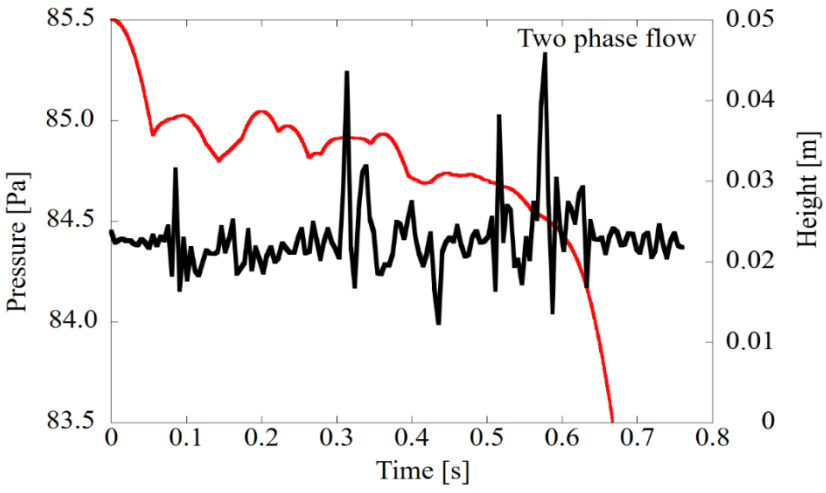

(b)

Fig. 3.9 Pressure loss in triangular prism (a) Single Phase Flow (b) Two Phase Flow.

Fig. 3.9 shows the variations of pressure drops inside the prism in upward flow with time. **Fig. 3.8 (a)** is the single phase flow without dropping fine particles and **Fig. 3.8 (b)** is the two phase flow case with single fine particle dropping. The pressure drop in this figure was defined by the difference between average pressures in the cross-sectional areas at the bottom and the top of triangular prisms. Under the single phase flow, the pressure drop is almost constant at 84.4 Pa and it can be treated as a steady system. In the case of two-phase flow, the pressure drop starts to fluctuate from t = 0.09 [s] and continues till t = 0.65 [s]. Fairly large pressure fluctuation can be divided into 4 periods, occurring around 0.09, 0.32, 0.40, and from 0.50 to 0.62 s. In the last period, the fine particle stays in the orifice region and blocks the major area of the orifice aperture, and generates a large pressure drop. The fine particle continues to move as indicated in **Fig. 3.6 (b)** and cause large fluctuations, where during this period fine particles going back and forth among coarse particles before finally passing through the orifice. These fluctuations mainly occur because the orifice area becomes narrower during fine penetration which causes a temporary increase in fluid resistance and energy loss.

In the first three periods, judging from fine particle trajectories, the pressure fluctuations occurred when the fine particle went across the upward gas plume formed above the aperture as shown in **Fig. 3.4**. Thus the duration of the fluctuations are shorter compare to the last period. After the initial collision, at t = 0.07 [s], the particle passes the gas plume at 0.09 s, and after that collides with coarse particles and passes again at t = 0.32 [s] and t = 0.4 [s]. This also can be observed from the moment where the velocity profile curves, as shown in **Fig. 3.7 (b)**, at the same time when the pressure inside the triangular prism fluctuated at t = 0.09, 0.32 and 0.40 s.

After 0.65 s, fluctuation continued for a while after the particle passed the orifice and positioned at the area just below the orifice before finally falling into the

bottom of the triangular prism. Judging from this fact, it can conclude that the collision between fine and coarse particles itself does not affect the fluctuations of pressure drop, but after the collision the fine particle sometimes will pass the gas plume and block the aperture area of the orifice, causing the pressure inside the system to fluctuate.

3.3.4. Passing Behavior of Multiple Particles

To demonstrate the passing behavior of multiple fine particles, 30 fine particles are dropped on to the orifice at the same time. The geometry of the system is the same as the previous section, but 20 mm of additional height is added on the upper section of the prism above the orifice. The fine particles are dispatched pseudo-randomly. The motions of 30 particles are tracked under the static fluid and upward gas flow (1.0 m s^{-1}) conditions.

Arch like Structure

Fig. 3.10 shows the visualization of 30 fine particles dropped in an equilateral triangle system with an upward gas flow of 1 m s^{-1}. From the visualizations, it can be observed that fine particles do not immediately pass through the orifice, but first form an arch-like structure as shown in **Fig. 3.10 (h)** around the orifice aperture. The arch-like structure is blocked configuration of fine particles that form concave surface of the clogged dome. This arch-like structure occurred around t = 0.2 [s] to t = 0.3 [s] as depicted in **Fig. 3.10 (b)** and **(c)**, and will gradually break down because of the unstable condition between fine to fine and fine to coarse particles due to the existence of the upward gas flow. The upward gas flow causes the particles to budge all the time, which results in loose friction between particles, and makes it difficult to maintain the arch-like structure. Finally, the arch-like structure will completely collapse as shown in **Fig. 3.10 (d)**, where fine particles gradually pass through the orifice. From the observation of this phenomenon, we can deduce that the presence of the upward gas flow will

obstruct the emergence of blockages because of the arch-like structure become unstable due to loose friction between the particles. Another reason that complete blockage does not occur is because the diameter ratio between fine to coarse particles is less than the critical value of the diameter ratio proposed by Takahashi et al. [7] of 0.12 [-], where in this current study the diameter ratio is 0.1 [-].

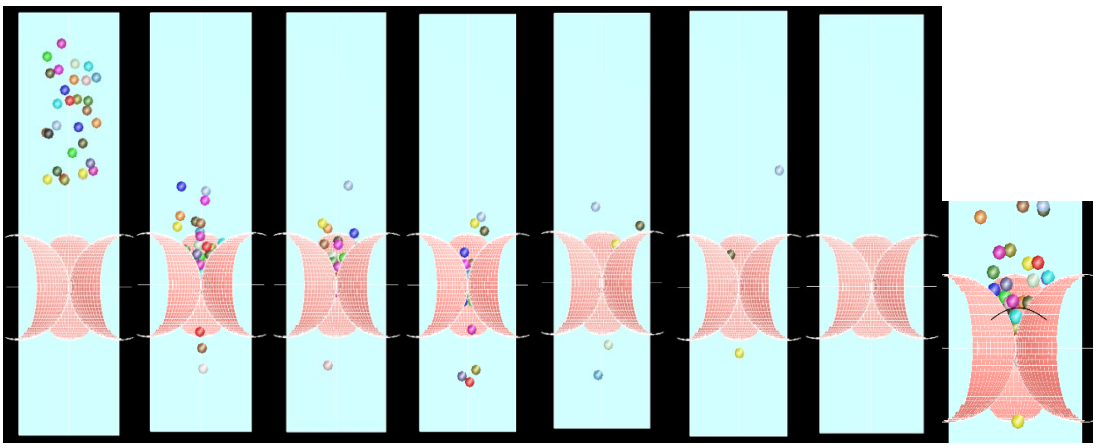

(a) (b) (c) (d) (e) (g) (f) (h)

Fig. 3.10 Powders Positions inside the bed at (a) initial condition (b) 0.2 s (c) 0.3 s (d) 0.4 s (e) 0.5 s (f) 0.740 s (g) 0.940 s (h) arch like structure at t = 0.15 [s].

Fig. 3.11 shows the pressure drop inside the vertical triangular prism of multiple fine particles. Compared to the previous case with a single occurrence of dropping particles, pressure fluctuations already occurred since the beginning of the dropping process. In the case of single particles dropping, the possibilities of fine particles to collide and bounce to the area above the aperture is less compared to the case of multiple fine particles. This is because fine particles already preclude above the aperture since the beginning of the dropping process. In this case, fine particles congregated and collided back and forth and resulted in fluctuating changes in the area of the aperture above the orifice and caused the pressure drop to oscillate since the

beginning of the dropping process. In the case of multiple fine particles, the average pressure drop also becomes higher, mainly because of the additional height above the orifice, where the vacuum area occurred in the upper section of the vertical triangular prism.

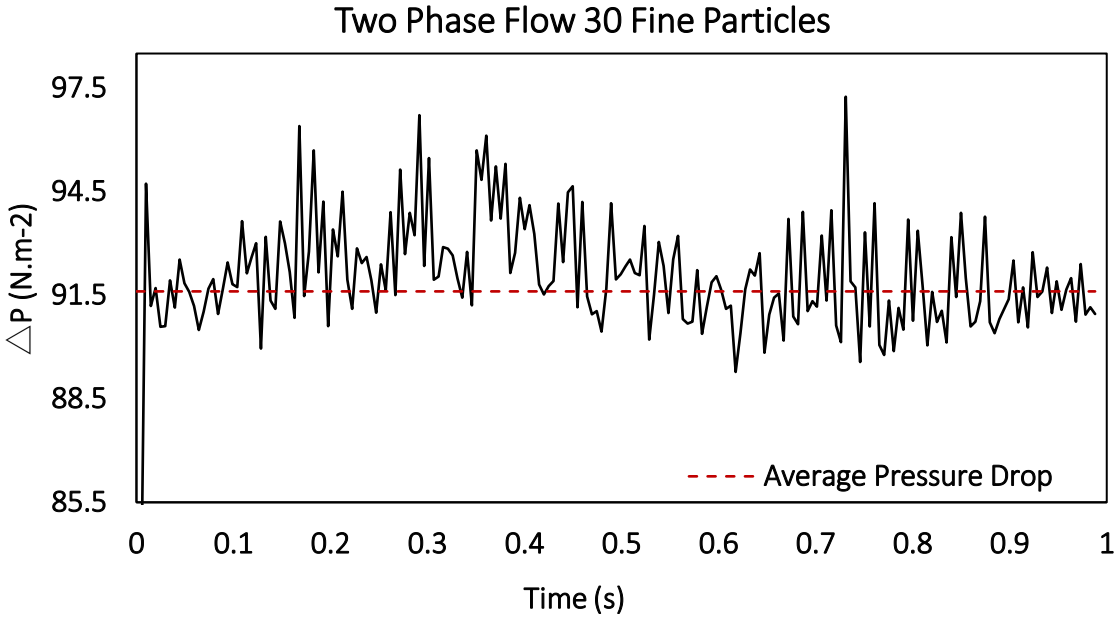

Fig. 3.11 Pressure loss in triangular prism of 30 fine particles dropped.

Figs. 3.12 and **3.13** show the number of particles in the stationary fluid, and in upward gas flow, respectively. In this simulation, particle count exists in the range between 80 mm at the highest and 10 mm at the lowest. From these two figures, it can be observed that the passing time for fine particles in static flow is shorter compared to the case of updraft gas flow. In both cases, a sudden increase of contact force occurred at t = 0.1 [s], where at this time, the initial collision between coarse particles and fine particles occurred. After the initial collision, contact force is suddenly increased again in the second collision at t = 0.15 [s], where fine particles bounced after the initial collision and collided with the coarse particles again. Finally, following the second

collision, the contact force smoothly decreased without significant fluctuation.

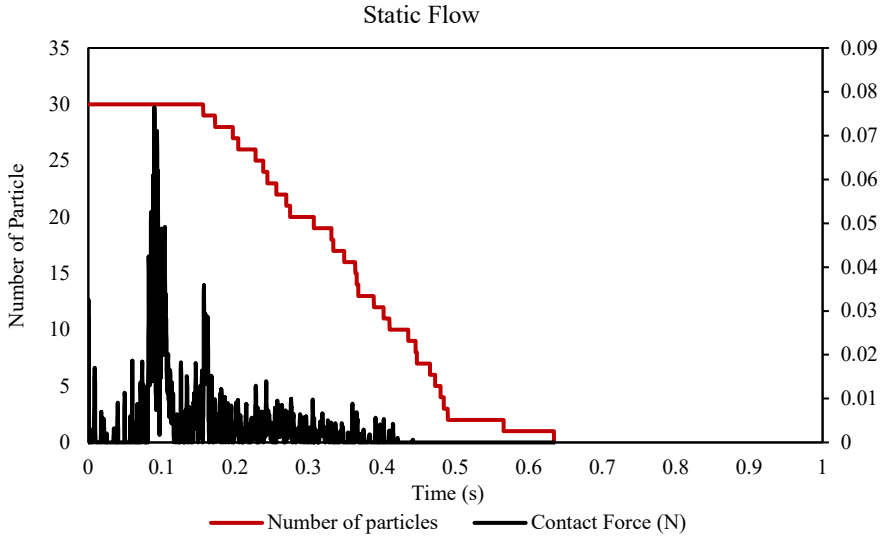

Fig. 3.12 Number of Particles and Contact Force in Time Passage for Static Flow.

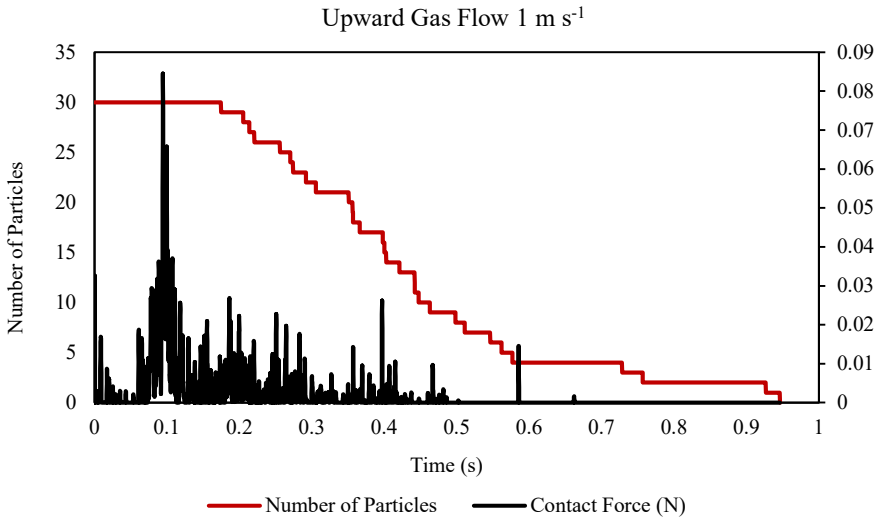

Fig. 3.13 Number of Particles and Contact Force in Time Passage for Upward Gas Flow.

Gradual decreasing of contact force in the case of stationary fluid also can be clarified with the number of particles inside the triangular prism, where the number of particles are decreased smoothly with time changes. This means it is relatively easy

for fine particles to pass through the orifice, resulting in less collision among particles as the time goes on. In the case with updraft gas flow, after the sudden increase of contact force at the initial collision similar to the previous case, the contact force also decreases but in more fluctuated way.

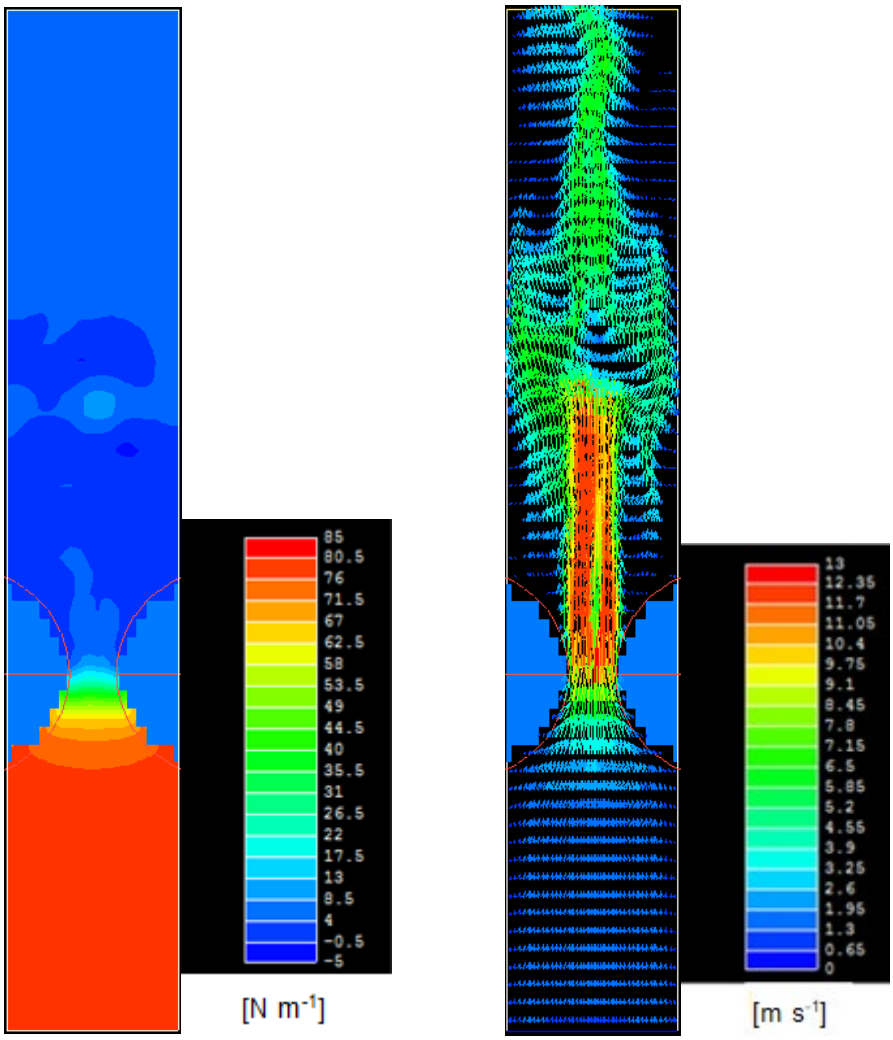

(a) (b)

Fig. 3.14 (a) Pressure Distribution and (b) Velocity Profile, of Multiple Fine Particles at t = 0.1 [s].

Fig. 3.14 (a) and **(b)** shows the pressure distribution and the velocity profile inside of triangular prism at t = 0.1 [s] and gas velocity of 1 m s^{-1} with the case of

multiple fine particles, respectively. From the pressure distribution depicted in Fig. 14 (a) it can be observed some local pressure drop or low pressure spotted above the orifice area, because the existence of fine particle straiten the aperture of orifice area. Furthermore, for the velocity profile depicted in Fig. 14 (b), fluctuation in gas plume can also be observed, mainly because the presence of fine particles narrowing the aperture of the orifice area. The effect of the drag force is significant under upward gas flow conditions to make it difficult for fine particles to pass through the orifice. The existence of updraft gas, makes the fine particles floating and restrained in the area above the orifice aperture and makes the fine particles unstable. This resulted in more collisions occurring before passing the orifice, compared to the case of stationary fluid. These statements can be clarified by observing the number of particles inside the triangular prism that decreased in a stepwise manner which resulted in a longer time passage for fine particles to pass through the orifice.

3.4 Conclusion

This study performed some analysis of powder motion passing through the orifice consisting of the coarse particles. For single and multiple particle dropping it is discovered that residence time of fine particles above the aperture is longer when the upward gas flow is being injected. This longer residence time occurred because the upward gas drag force obstructed the fine particle path to pass through the orifice. In the case with singe particle dropping, the existence of fine particles did not necessarily influence pressure drop fluctuation. Pressure fluctuations inside the packed bed are largely affected when the particles stay in the main channel of the gas flow located in the aperture area above the orifice. However, when the fine particle is outside the aperture area, the pressure drop fluctuations are not significant. Pressure drop fluctuations also occurred when fine particle passing the orifice region and block the

major area of the orifice aperture and caused the area to become narrower. This phenomena caused a temporary increase in fluid resistance and energy loss. Remarkable fluctuations of the pressure drop occurred in the case of multiple particle dropping, since the beginning of the dropping process of fine particles. This phenomenon occurred because the possibilities of fine particle bounce and obstructing the aperture area above the orifice is higher due to the existence of larger amount of particles.

3.5 References

1) Ministry of the Environment Japan: National Greenhouse Gas Inventory Report of Japan.,(2013), 2.4, 3.2.

2) T. Ariyama and M. Sato: *ISIJ Int*., **46**(2006), 1736.

3) S. Puttinger and H. Stocker: *ISIJ Int Advance Publication*., (2018), 530

4) S. Puttinger and H. Stocker: *ISIJ Int Advance Publication*., (2018), 531

5) S Puttinger and H. Stocker: *ISIJ Int*., **59**(2019), 481

6) H. Takahashi, H. Kawai, M. Kobayashi and T. Fukui: *ISIJ Int*., 92(2006), 996.

7) H. Takahashi, H. Kawai, M. Kobayashi and T. Fukui: *ISIJ Int*., **45**(2005), 1386.

8) X.F. Dong, D. Pinson, S.J. Zhang, A.B. Yu and P. Zulli: *Powder Tech*., **149**(2004), 1.

9) M. Fukuda, J. Suzuki, H. Kawai and H. Nogami: *ISIJ Int*., **55**(2015), 1291.

10) Z.G. Luo, H. Zhou, T. Zhang, Y. You, L.J. Zhang, Z.S. Zou and Y.S. Shen: *Powder Tech*., **314**(2017), 102.

11) M. Zaki and M. S. Siraj: Powder Tech., **354**(2019), 641

12) T. Ariyama, S. Natsui, T. Kon, S. Ueda, S. Kikuchi and H. Nogami: *ISIJ Int*., **54**(2014), 1457.

13) H. Zhou, S. Wu, M. Kou, Z. Luo, Z. Zou, Y. Shen: *ISIJ Int*., **58**(2018), 43

14) S. Natsui, S. Ueda, H. Nogami, J. Kano, R. Inoue and T. Ariyama: *ISIJ Int*., **51**(2011), 51.

15) S. Natsui, T. Kikuchi and R.O. Suzuki: *Metallurgical and Materials Transaction B*., **45**(2014), 2395.

16) H. Kurosawa, S. Matsuhashi, S. Natsui, T. Kon, S. Ueda, R. Inoue and T. Ariyama: *ISIJ Int*., **52**(2012), 1010.

17) S. Matsuhashi, H. Kurosawa, S. Natsui, T. Kon, S. Ueda, R. Inoue and T. Ariyama: *ISIJ Int*., **52**(2012), 1990.

18) H. Kawai and H. Takahashi: *ISIJ Int*., **44**(2004), 1140.

19) B. Mahmoodi, S. H. Hosseini, G. Ahmadi: *Particuology*., **43**(2019), 171.

20) J. Ishii, R. Murai, I. Sumi, Y Yongxiang, R. Boom: *ISIJ Int*., **57**(2017), 1531

21) S. Kikuchi, T. Kon, S. Ueda, S. Natsui, R. Inoue and T. Ariyama: *ISIJ Int*., **55**(2015), 1313.

22) S. Ergun: *Chem Eng Prog*., **48**(1952), 89.

23) D. Gidaspow: Multiphase Flow and Fluidization: Continuum and Kinetic Theory Descriptions, Academic Press, New York, (1994), 467.

24) C. Y. Wen and Y. H. Yu: *Chem Eng Prog Symp*., **62**(1966), 100.

CHAPTER IV

Tensile Properties and Fracture Morphology Analysis on Lean Duplex Stainless SUS821L1 at Various Temperatures during Quasi-Static and Impact Tensile

Synopsis

Deformation and behavior of duplex stainless SUS821L1 under quasi-static (0.0167/s) and impact (~350/s) loading has been studied by using a universal testing machine and split Hopkinson tensile bar at temperature ranges of 293 K to 233K. From 293 K to 253 K, the flow stress in impact tensile is higher than the quasi-static, shows positive strain rate sensitivity. However, the strain rate sensitivity is diminished at 233 K mainly because the martensitic transformation becomes dominant, and narrow the gap of flow stress between quasi-static and impact tensile. Furthermore, positive temperature sensitivity that occurred at 293 K and 273 K turns into negative at temperature 253 K at impact tensile. he toughness of SUS821L1 by means of specific energy absorption (SEA) and ECO-index are observed. At 293 K, the difference in toughness between quasi-static and impact tensile is not profound which are 0.28 J/m3 and 0.25 J/m3. However, at low temperatures, the difference is widened because of the loss of ductility at a high strain rate. From the fractography analysis, finer and deeper dimples can be observed at quasi-static, show the behavior of ductile material. Meanwhile, at impact tensile shallower dimples can be seen, and uneven in size distribution can be seen. In addition, quantitative analysis revealed a directly proportional relation between average dimple size with elongation and dimple number density with ultimate strength. Compare to the experimental results, the modified Johnson-Cook model was performed considering the coupling effect between temperature and strain rate. At quasi-static the proposed model does not fit with the experiment due to the martensitic transformation. At impact tensile the modified Johnson-Cook model showing a good agreement with the experiment.

4.1 Introduction

In recent years, there are shifting trends of commonly used single-phase austenitic stainless steel, into duplex stainless steel which consists of austenite-ferrite phases in a rough ratio of 1:1 (1). The duplex stainless steel can be classified into three major types which are standard, super, and lean duplex stainless steel. The lean duplex stainless steel has some advantages, intending to lower the initial and instability cost by reducing the dependency of expensive alloy elements such as nickel and substitute it with cheaper austenite stabilizer such as Nitrogen (N) and Manganese (Mn) during the manufacturing process [1]. For comparison, the commonly used austenitic grade stainless steel such as SUS 304 has a nickel content around 8 to 10%, while for lean duplex stainless around 1% to 2%. Moreover, the addition of inexpensive austenite stabilizers will upgrade the resistance to pitting corrosion and also increase the potent solid solution which increases the mechanical properties, despite the leaner composition of Ni.

Studies on the transformation induced plasticity (TRIP) effect on the improvement of mechanical properties of stainless steel already been done widely. The main study usually focused on the effect of strain rate [2-13], from quasi-static to high deformation rate. Another researches discussed the effect of temperature change to martensitic transformation [14-21]. Also, some studies regarding the coupling effect of temperature and strain rate to martensitic transformation already have been observed [22-25], but still rarer than the previous two. Huh.et.al [2], had been studying the dynamic flow stress of TRIP-type steel sheets for auto-body at intermediate strain rates, and found that work hardening rates of the steel sheets are insensitive with strain rate variations. Tsuchida.et.al, studied the separate effect of temperature and strain rate on metastable austenitic [14] and lean duplex stainless steel [15], also reported that the effect of temperature change has a more influence on flow stress transformations during quasi-static tensile experiment below the room temperature than the effect of

strain rate change at room temperature. More studies also show that secondary hardening occurs after the material being deformed at high strain levels, resulting from the transformation of the austenite phase into the martensite phase [16-21], at quasi-static strain rate and low temperature. However, this phenomenon of secondary hardening seems to disappear during high strain rate tensile, due to the suppression of martensitic transformation [22]. These phenomenon linked with the lower fraction of martensite formed during the dynamic test, which attributed to the higher stability of austenite, and so less effective TRIP effect, due to the higher temperature reached in the dynamically deformed sample because of the adiabatic heating [23]. Moreover, because of the behavior of dynamic tensile which being held in a brief time, the heat generated in the fracture area cannot fully be dissipated to the surrounding [24].

One of the utilization of stainless steel is to be applied in the automotive industries. The main requirement of steel used in automotive is the ability to withstand deformation from a crash. The high energy absorption capacity is required for the use in the production of high-performance structural parts in automobiles with superior crash performance and lightweight structural reinforcement. Some analyses that can be used to describe the performance of steels can be obtained using combining the strength and elongation of the material. Analyses such as strain rate and temperature sensitivity are used to test the material susceptibility, due to the change of strain rate and temperature [22-25, 26-28]. Furthermore, the ability of the material to withstand impact during a crash can be observed by the rate of energy absorption that can be restrained by the material before necking start to occur which can be expressed by specific energy absorption (SEA). Meanwhile, the ECO-index is also being used to describe the overall performance of material which is expressed from the product of ultimate tensile strength and uniform elongation. Some researchers already reported some notable value of ECO-index of some steels. Such as the ECO-index of AHSS

steel that not much changed when the strain rate transform from quasi-static to impact that limited to 0.2 mJ/m^2 [29]. Considering all the facts above, it becomes important to observe the crash-worthiness of lean duplex stainless using the aforementioned analyses. The tensile test at high strain rates usually been conducted with the split Hopkinson bar method. This method mainly can be divided into two categories, compression and tension bar methods. While more studies on stainless steel flow stress behavior in the dynamic tensile region using split Hopkinson pressure bar method (SHPB) [10,22-23, 30], the studies on stainless steel flow stress behavior using split Hopkinson tensile bar method (SHTB) is still lack, even more with the coupling temperature due to the complex geometry of SHTB. Thus, it becomes a challenge to develop a system where the coupling effect between temperature change and high strain rate can be performed. Moreover, for mechanical design, the requirement of the tensile behavior of the material is more desirable compare to the compression.

The characteristic material deformation behaviors can be observed from its fracture surface, which possessed the culmination from the continuation of deformation processes. Thus, the analysis of the fracture surface of stainless steel to reveal its correlation with the deformation features and fracture mechanism becomes worth noted. It has already been reported that the rate of martensitic transformation will affect the fracture surface of stainless steel due to its strengthening behavior. Thus, with a high rate of martensitic transformation, the appearance of finer dimples increased [15-18], thus it means bigger and shallower dimples expected to occur in higher strain rate due to austenite stability [3-10] Characteristics of the fracture morphology in various steels already been studied by some researches [31-43]. Regarding the Hall-Patch law Linear proportional relation between dimple size and the uniform elongation have been reported [32-34], another study reported a linear correlation between the dimple density and the strength of the material, while another study reported a reversely

proportional relation between fracture elongation and dimple size [35-36]. These uncertainties make the study on the relation of fracture morphologies and mechanical properties of stainless steel need to elucidate, let alone at lean duplex stainless that still lacks in observation.

There are two main categories of constitutive models proposed to explain the deformation behavior of materials, a physical-based model and a phenomenology-based model. The first category describes the material flow stress according to the deformation mechanism [44-47]. Another group explains flow stress according to empirical observations [48-50]. The Johnson-Cook (J-C), based phenomenological models is widely used because of its simple form and requires less effort to estimate material constants. However, from a metallurgical point of view, the original J-C model lacks the ability to predict the deformation mechanisms of complex mechanisms, such as the coupling effect between temperature and strain rates. To overcome this shortcoming. Thus, it becomes a huge demand to modify the original J-C to increase its susceptibility for a specific strain rate and temperature range.

In this current research, the coupling effect of strain rate transformation from quasi-static to dynamic at various temperatures on the strain hardening characteristics of duplex stainless SUS821L1 will be observed. Uniaxial tensile tests at different rates during quasi-static (0.0167/s) and dynamic (~350/s) and various temperatures (293 K, 273 K, 253 K, and 233 K) were performed to elucidate the mechanical behavior of SUS821L1 under different strain rates and temperatures. The self-designed cooling chamber is coupled with the SHTB system for impact tensile at low temperatures. Furthermore, because of the high demand for cheaper and sustainable material substitution in automobiles, it becomes adequate to observe the ability of SUS821L1 to withstand the crash. The overall performance of the material will be observed by using the SEA and ECO-index. Moreover, the effect of strain rate and temperature

were also being carried to investigate their correlation with fracture morphologies of SUS821L1. Qualitative and quantitative observations on dimple characteristics in regards to SUS821L1 mechanical properties are carried for all specimens at different strain rates and temperatures. In the end, a modified Johnson-Cook (J-C) material model will be applied to predict the appropriate flow stress model of SUS821L1 under the coupled effect of strain, strain rate, and temperature.

4.2 Materials and Method

4.2.1 Specimen for quasi-static and impact tensile tests.

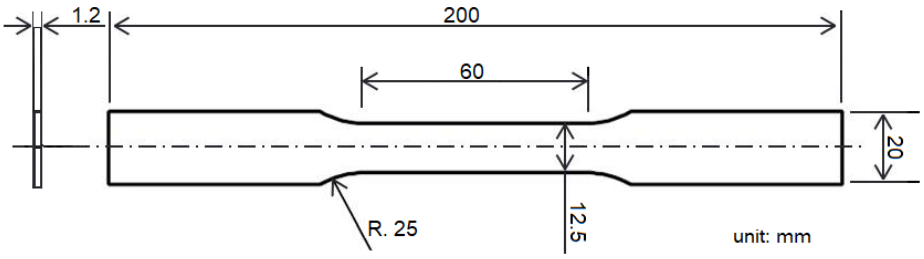

(a)

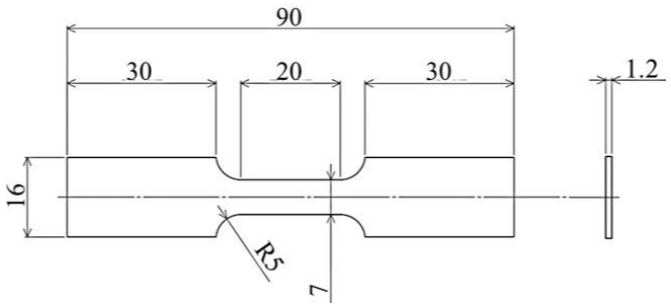

(b)

Fig. 4.1 dimensions of (a) quasi-static and (b) impact tensile specimen

Table 4.1 chemical composition (wt.%) of SUS821L1 stainless steel

C	Si	Mn	P	S	Ni	Cr	Mo	Cu	N	Fe
0.019	0.31	3.21	0.024	0	2.16	20.86	0.29	0.102	0.16	Bal.

In this current research, lean duplex stainless plates SUS821L1 were used,

supplied from Nippon Steel & Sumikin Stainless Steel Corporation. The chemical compositions of the SUS821L1 are listed in Table 4.1. The quasi-static and impact specimens for the tensile test are shown in Fig. 4.1 (a) and (b), respectively. For quasi-static tensile test specimen, the gauge length is 60 mm, a width of 12.5 mm, and a thickness of 1.2 mm. For impact tensile test specimen, the gauge length is 20 mm, a width of 7 mm, and a thickness of 1.2 mm, where the test piece was installed by attaching the flat specimen to cylinder jig attachment, as illustrated in Fig. 4.2.

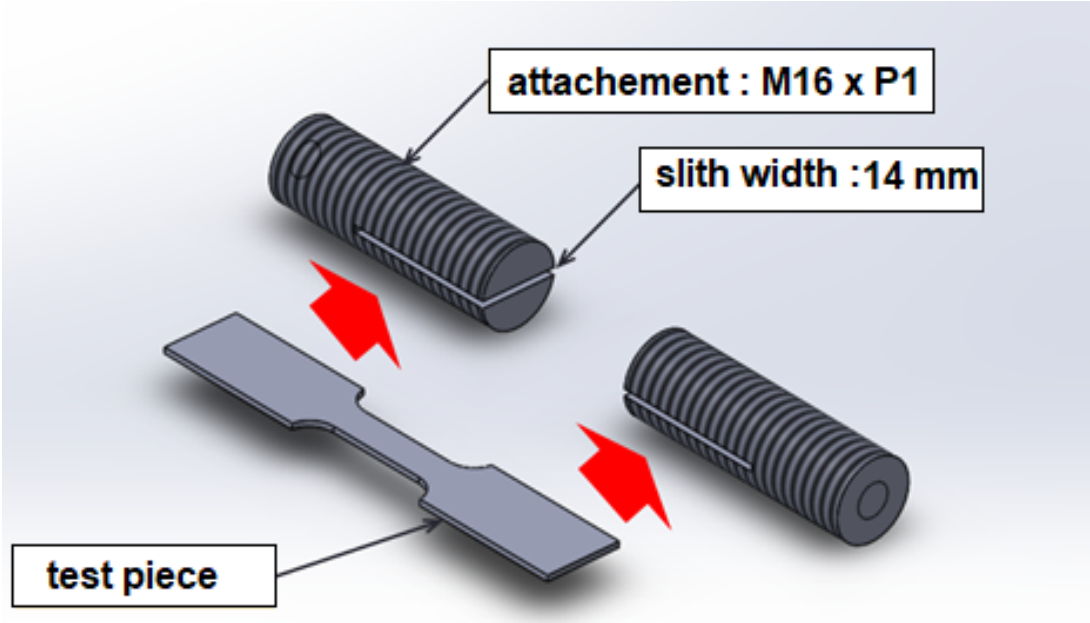

Fig. 4.2 Mount mechanism of flat plate specimen for impact tensile test

4.2.2 Quasi-static Tensile Test

Quasi-static tensile tests were carried out by the INSTRON 5586 material testing machine with 300kN maximum load capacity, equipped with a chamber used for cooling and heating as depicted in Fig. 4.3 (a), fitted with 25 mm gauge length extensometer INSTRON 2630 at deformation rates of 1 $mm.min^{-1}$ (0.0167/s), as shown in Fig. 4.3 (b). In this research, four temperature conditions of 293 K, 273 K, 253 K, and 233 K were performed to observe the effect of temperature change on the

mechanical properties of SUS821L1 at the quasi-static tensile condition. Nitrogen gas is used as a coolant to the lowered temperature inside the chamber. To monitor the surface temperature of the specimen, the external thermocouples were attached to the specimen. Experiments are carried out after the specimen already reached the desired temperature and the temperature is steady. The surface temperature of the specimen is kept constant throughout the tensile test

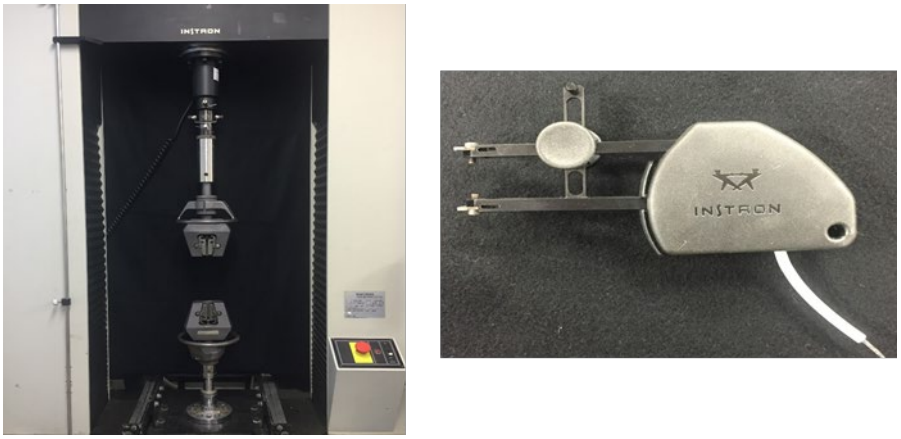

(a) (b)

Fig. 4.3 (a) Material testing machine INSTRON5586 and (b) Extensometer INSTRON2630

4.2.3 Impact Tensile Test

The impact tensile tests, were performed by the vertical type of split Hopkinson tension bar apparatus, as shown in Fig. 4.4 (a). The input and output bars are made of SUS304 stainless steel with the same dimensions, where the diameter is 25 mm and the length is 4000 mm. the bar Young modulus is 194 GPa, the mass density is 7760 $kg.m^{-3}$, and the velocity of the elastic wave is 5020 $m.s^{-1}$. The steel bar striker (STS370), which outside diameter is 42.7 mm with a thickness of 3.5 mm and 2000 mm in length, was dropped from the height of 6 m. In this case, the impact velocity of the striker is

about 10.85 $m.s^{-1}$. Two semiconductor strain gauges (KYOWA, KSP-2-120-E4), were attached axisimetrically at three locations to capture the stress waves propagated in the input and output bars. The signals from the strain gauges were passing through the bridge boxes and amplifiers (KYOWA, CDV-700A), and finally recorded by a digital oscilloscope with sampling time every 1 μs. The schematic diagram of the impact tensile stress measurement system is shown in Fig. 4.4 (b).

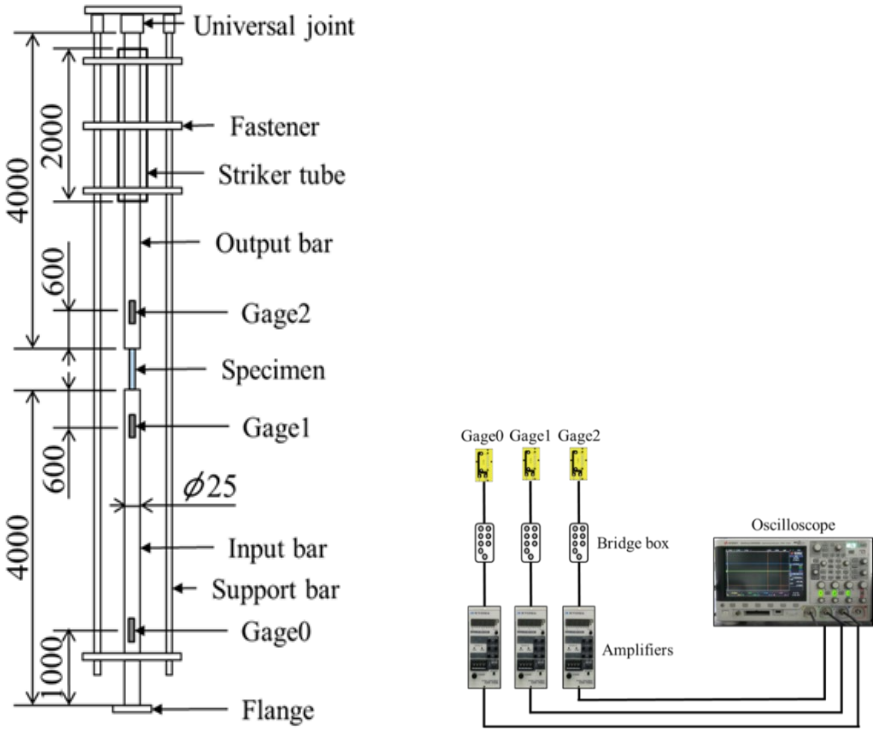

(a) (b)

Fig. 4.4 (a) Split Hopkinson Tensile Bar Method (b) Measurement system of impact stress

The specimen strain rate has been formulated based on one-dimensional assumptions, where the specimen expands freely along the radial direction and there is no friction between the specimen and the bar when the axial deformation occurs. Furthermore, the inertia effect is also being neglected while the specimen deformation

is assumed uniform along the axial direction. The stress and strain of the specimen are the same as those at the rear surface of the specimen. This stress uniformity of the specimen results in the force equilibrium between the ends of the bars, which are in contact with the specimen.

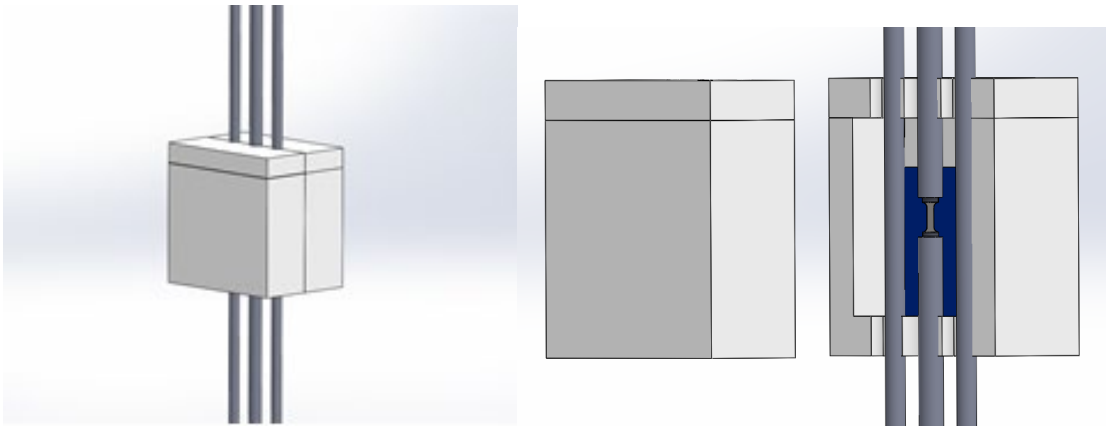

Fig. 4.5 Schematic diagram of cooling process during impact tensile test

Similar to the quasi-static tensile test, four temperature conditions of 293 K, 273 K, 253 K, and 233 K are also performed in the impact tensile test. The schematic diagram of the cooling process of the specimen is shown in Figure 4.5. The mechanisms are as follows, the Styrofoam was used as the material for the cooling chamber, which covers the specimen and its surrounding by making holes for the input, output, and support bars to pass through. The connection between the other half is formed to follow the shape of the bars, to tightly seal the chamber during the cooling process. Dry ice was used as the coolant for the specimen, where it set not to touch the specimen during the cooling process. The chamber was divided in half, so it can be separated quickly and the striker could be dropped as soon as the constant desirable temperature recorded by the thermocouples is reached.

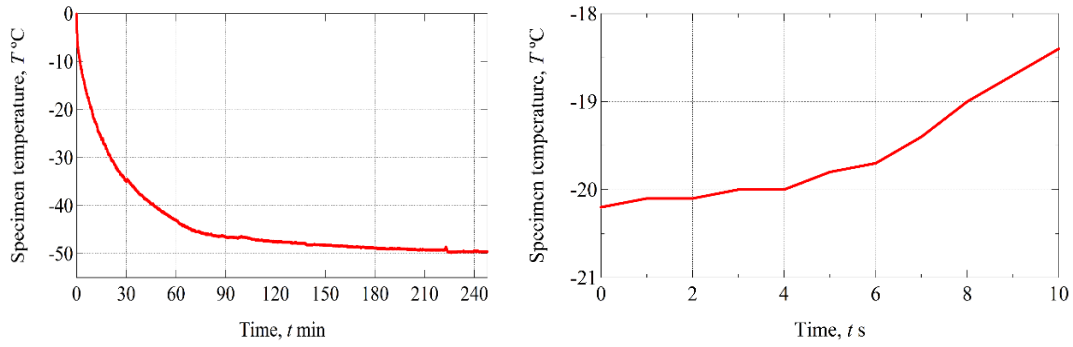

(a) (b)

Fig. 4.6 (a) Preliminary test for cooling experiment (b) Temperature change of test specimen after cooling chamber being removed

As preliminary testing, a cooling experiment of the test piece was conducted using this constant temperature bath. Figure 4.6 (b) shows the temperature of the test piece for each hour. At this time, the temperature of the test piece was measured using a thermocouple (MF-O-K). From the test results, it was confirmed that by using dry ice, the temperature of the test piece could be lowered about 223 K. As aforementioned before, the lowest temperature set for this study is 233 K. Even though the cooling chamber need to be taken out during impact tensile experiment, but the temperature change during this process is considered to be neglected because the impact tensile experiment is held in a short time, less than 1 s. As a verification, the temperature change in the specimen after the cooling chamber being removed is shown in Fig. 4.6 (b). From this figure, it can be noticed that that temperature only slight changes in the first 4 s. Thus, the cooling method proposed in this study is considered adequate to perform during the impact tensile test. Furthermore, for quasi-static and impact tensile test, at least two specimens are used of each temperature parameter, to ensure data reliability.

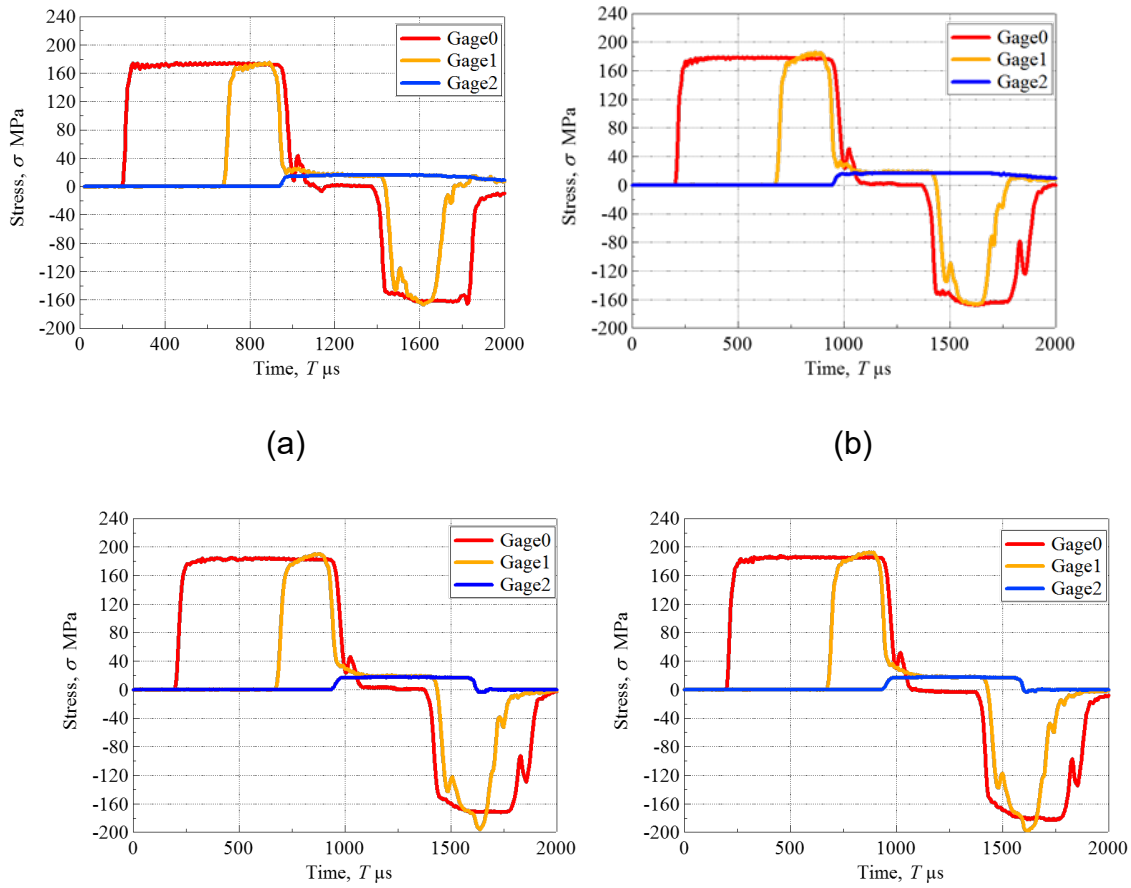

Fig. 4.7 Stress values over time measured with at each strain gauge at various temperatures; (a) 293 K, (b) 273 K, (c) 253 K, and (d) 233 K, respectively

Fig. 4.7 (a), (b), (c), (d), are shown the change of impact stress with time, which propagated through input and output bars, recorded by strain gauge recorded by strain gauges 0, 1, and 2 at temperature 293 K, 273 K, 253 K, and 233 K, respectively. The recorded stress values at each test temperature were used to calculate the engineering stress and strain of SUS821L1, as shown in eq (1) to eq (4). Here, ρ is the density of the input and output bar (kg m^{-3}), c is the stress propagation velocity (m s^{-1}), l is the length of the input and output bar (m), σ_I, σ_T, and, σ_R are incident, transmission, and reflection stress wave (MPa), and A and A_o are the cross-sectional areas of the input and output bar and the specimen, respectively. As the striker dropped from the height

of 6 m and collided with the flange at the bottom of the split Hopkinson bar, the incident stress (σ_I), will be generated and recorded at gauge 0 and gauge 1. This incident stress will then propagates through the input bar unto the specimen. A portion of the incident stress will be propagated through the specimen as a transmission stress wave (σ_T) and recorded at gauge 2. Some waves that cannot be transmitted will be reflected as reflection stress wave (σ_R) at the interface with the specimen. The average strain rate in the plastic region is calculated using eq (4), where *t* is the time of each designated strain (s), from this equation it was found that the strain rate generated during the impact tensile test was approximately 350 s^{-1}. Stress propagation recorded at strain gauge 0, 1, and 2, of each temperature conditions, are depicted in Fig. 4.7, below.

$$\varepsilon = \frac{1}{\rho c l}\int (\sigma_I + \sigma_R - \sigma_T)dt \quad (1)$$

$$\dot{\varepsilon} = \frac{1}{\rho c l}\,(\sigma_I + \sigma_R - \sigma_T) \quad (2)$$

$$\sigma = \frac{A}{2A_0}\,(\sigma_I - \sigma_R + \sigma_T) \quad (3)$$

$$\dot{\bar{\varepsilon}}_p = \frac{\varepsilon_{0.15} - \varepsilon_{0.1}}{t_{0.15} - t_{0.1}} \quad (4)$$

4.2.4 Fracture Morphology Analysis by Scanning Electron Microscope

The morphology of fracture surface, such as microstructure dimple transformation of SUS821L1 from quasi-static to impact strain rate at various temperatures were observed using JEOL JSM-6510 scanning electron microscope (SEM). An operating voltage of 15 kV is used to observe the tensile fracture surface throughout. The magnification of 2000 times was deemed appropriate to record the representative fracture features for all cases. The average dimple size and dimple number density for each case then will be examined quantitatively using image software ImageJ.

Furthermore, the relation between mechanical properties transformation of SUS821L1 due to the strain rate and temperature change with its fracture morphology characteristics will be performed qualitatively and quantitatively.

4.3 Result and Discussion

4.3.1 Tensile Properties of SUS821L1 during Quasi-Static and Impact Strain Rates at Various Temperatures

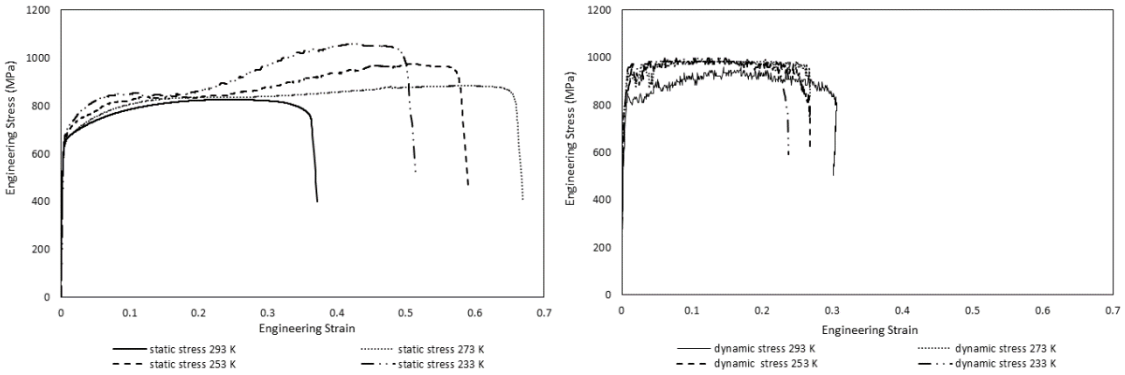

(a) (b)

Fig. 4.8. Engineering stress and stress diagram of (a) quasi-static and (b) impact SUS821L1 with various temperatures.

The engineering stress-strain diagram of quasi-static and impact tensile test of SUS821L1 at various temperatures are shown in Fig. 4.8 (a) and (b), respectively. At quasi-static and impact tensile, the flow stress increasing with strain increase until the necking point, and gradually decrease with further strain increase. At quasi-static tensile, the total elongation of SUS821L1 is increasing when temperature lowered from 293 K to 273 K, but gradually decrease with further temperature decrease. During impact tensile test at T = 293 K, SUS821L1 still exhibits the behavior of ductile steel, which can be observed from a fair amount of elongation after goes beyond the ultimate

strength point. However, with temperature decrease, the SUS821L1 stress and strain characteristic during impact tensile show the ductile-to-brittle behavior. These phenomena can be observed from the decreasing of the total elongation of SUS821L1. Moreover, while the flow stress increase with strain increasing, the increasing rate is more moderate compare to the quasi-static tensile case. Other than that, there is no significant difference between the ultimate tensile strength and the breaking point of SUS821L1, which is almost flat and the failure occurs without any noticeable or prior change in elongation.

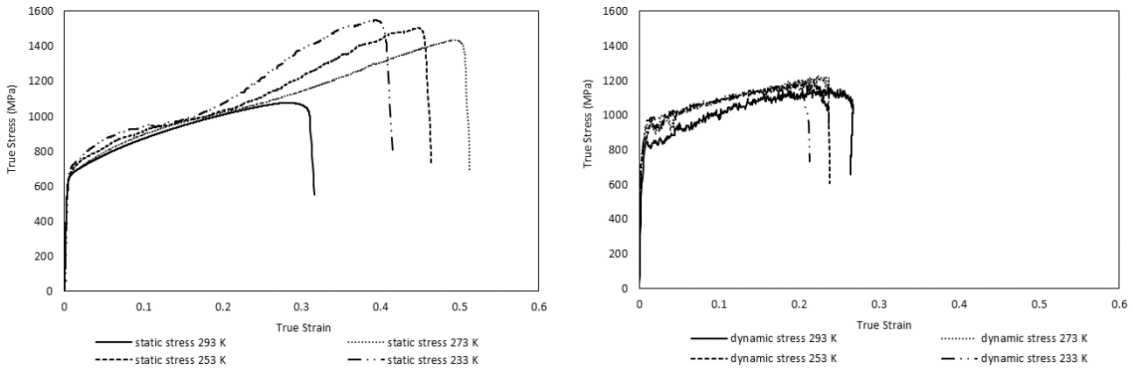

(a) (b)

Fig. 4.9. True stress and stress diagram of (a) quasi-static and (b) impact SUS821L1 with various temperatures.

Figure 4.9 shows the (a) quasi-static and (b) impact true stress-strain diagrams of SUS821L1 at various temperatures. During quasi-static tensile in the form of the true stress-strain diagram, the TRIP effect can be observed at temperatures lower than 293 K, from significant increases of flow stress after a previously steady increase of flow stress until approximately strain level 0.15. According to Vercruysse et al [24], the portion of restrained austenite that stable at room temperature transforms into martensite at lower temperatures. In this state, more friction occurred in regards to

strain-induced martensite which improves the tension resistance by either hindering the crack propagation or reducing the crack growth rate thus increase the flow stress [17]. It can be seen that the influence of TRIP on increasing the flow stress becomes more profound when temperature decrease due to a more unstable state of the austenite phase being transformed into the martensite phase. During impact tensile at various temperatures, the TRIP effect cannot be observed. The suppression of the TRIP effect mainly because of the lower fraction of martensite formed during impact tensile which attributed to the higher stability of retained austenite due to adiabatic heating [4, 6, 8-9]. Moreover, due to the characteristic of impact tensile experiments that occurred in a short amount of time, the heat generated by plastic work in the sample's fracture area cannot be dissipated to the environment thoroughly [3].

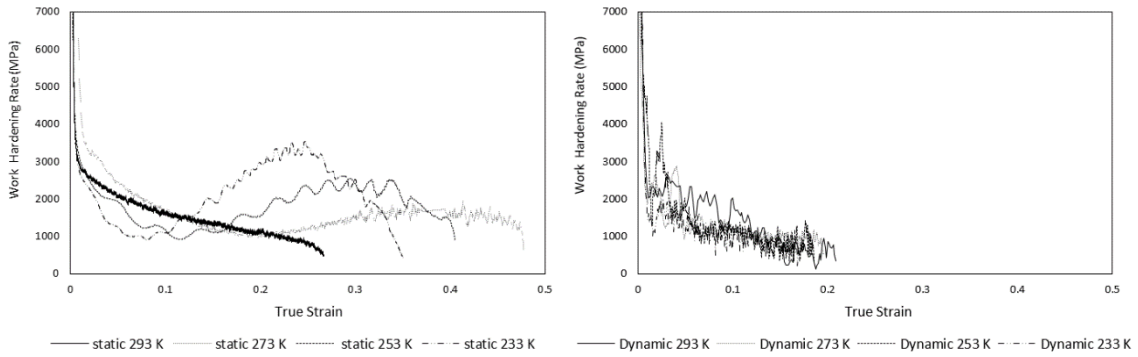

(a) (b)

Fig. 4.10. Work hardening rate as a function of true strain diagram of (a) quasi-static and (b) impact SUS821L1 with various temperatures.

Figure 4.10 shows the work hardening rate of (a) quasi-static and (b) impact tensile at various temperatures as the function of true strain. During quasi-static tensile, the variation of strain hardening is different and strongly affected by temperature change. Initially, work hardening of stainless steel is characterized by a sharp drop at

the beginning of the tensile test until the onset of plastic deformation as the mark of first inflection and then decreases steadily as the deformation increase until the fracture point. During the quasi-static in all temperatures, the first marked inflection is occurred approximately at strain 0.05, with the work hardening rate above 3000 MPa. At 293 K, the strain hardening rate decreases steadily with the increasing true strain, thereafter no worth notice transformation as the work hardening rate shows a general drop until the fracture level of about 1000 MPa. On the contrary, at lower temperatures, after the hardening rate steadily decreases, the second inflection appeared, signifies the onset of martensitic transformation [6]. The transient deformation at low temperatures might occur because of the back stress hardening due to the deformation in lower temperatures that results from different phases over the strain regime corresponding to the elastic-plastic transition stage, thus enhanced the work hardening rate and the flow stress of SUS821L1. From Fig. 4.10 (a), it is also obvious that the inflection point is become lower, emerged faster, and the peak of secondary hardening becomes higher at lower temperatures indicating the TRIP effect at quasi-static tensile is strongly affected by temperature change.

As depicted in Fig. 4.10 (b), at impact tensile the first inflection occurred approximately at strain 0.05 with the work hardening rate of about 4000 MPa at every temperature parameter. After the first inflection, the work hardening is decreased regardless of the fluctuation. However, as the true strain continues to increase the second inflection point cannot be seen even with further temperature decrease indicating the suppression of TRIP at the high strain rate. During quasi-static tensile at temperatures lower than 293 K, the deformation continued as the strain increase and the mechanism changed into a competition between dislocation slip and martensitic transformation. While at quasi-static tensile there is sufficient time for the martensitic transformation to occur, the same does not happen at impact tensile because the

process lasted at a very short time which makes there is not enough time for the martensitic transformation to take place.

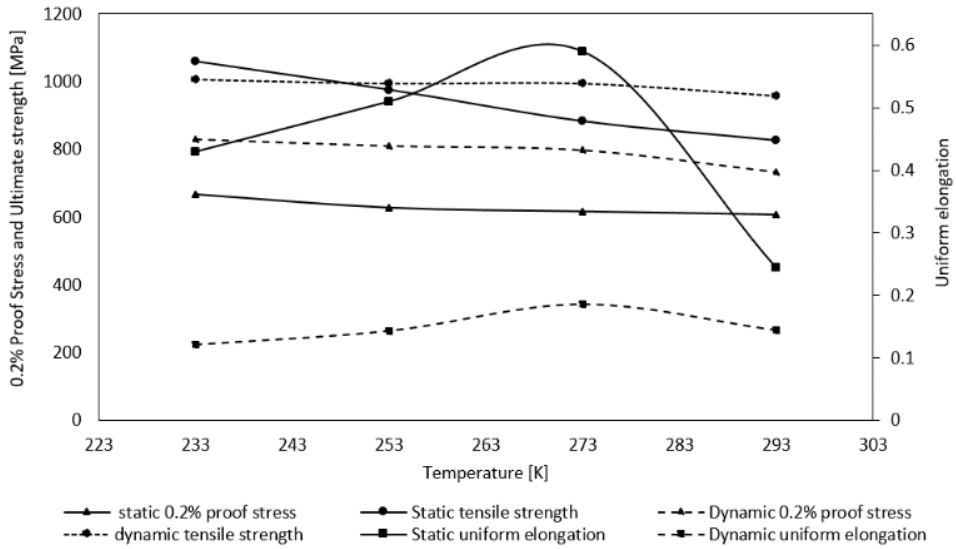

Fig. 4.11. Mechanical properties as a function of temperature of quasi-static and impact SUS821L1

Figure 4.11 concludes the yield strength (0.2% proof stress), ultimate tensile strength, and uniform elongation of quasi-static and impact tensile tests as the function of temperature. The yield strength of SUS821L1 is increasing with temperature decrease both for quasi-static and impact tensile tests. At impact tensile, the yield strength of SUS821L1 is higher compare to the quasi-static. At low strain level, the amount of martensitic transformation is low [4], thus only slight changes in yield strength at quasi-static. Meanwhile at impact tensile, to maintain the higher imposed strain rate, the dislocation velocity needs to be simultaneously increased flow stress [3-13], which results in more profound increases in flow stress. The ultimate strength of SUS821L1 at quasi-static tensile is lower compare to impact tensile from 293 K to 253 K. As temperature decrease, the flow stress of SUS821L1 is constantly increasing both for quasi-static and impact tensile. However, the change rate of flow stress over

temperature during quasi-static tensile is more dominant compare to the impact, because the TRIP becomes more profound as temperature decreases and strain increases. More martensitic transformation at low temperatures will increase the tension resistance, due to the mixture of austenite-ferrite and martensite phases are much harder to slipped compare to the ferrite-austenite phases, which might the reason for the ultimate tensile strength of quasi-static tensile is higher than impact tensile at 233 K.

At quasi-static tensile, the uniform elongation of SUS821L1 significantly increased (about 58%) as temperature decreased from 293 K to 273 K. This mainly because of the increasing martensite phase at low temperature will efficiently delay the onset of necking and increase the elongation [14-24]. Thereafter, the uniform elongation steadily decreases with further temperature decrease. As the temperature continues to decrease, the martensitic transformation is more easily formed which increases the flow stress of SUS821L1 while the ductility is decreasing.

As aforementioned before, sudden abridgment in elongation can be observed when the strain rate transformed from quasi-static to impact tensile, shows the ductile-to-brittle transition. This transition becomes obvious at 273 K, while the longest elongation occurred during quasi-static tensile, the abrupt elongation's abridgment occurred during impact tensile of the same temperature. Furthermore, from Fig. 4.8 (b) the characteristic features stress-strain diagram of brittle steel can be observed, where the flow stress only increases slightly and almost flat from the onset of plastic deformation until the ultimate tensile strength at the temperature lower than 293 K, which shows a huge gap between the uniform elongations of SUS821L1 at impact tensile compare to the quasi-static tensile test.

4.3.2 Strain Rate and Temperature Sensitivity of SUS821L1

Material sensitivity defined the sensitivity response of materials behavior especially the flow stress due to the change of strain rate (strain rate sensitivity) and temperature (temperature sensitivity). The strain rate and temperature sensitivities can be defined as the following equations (5) and (6), respectively.

$$\mathrm{m} = \left(\frac{\delta \ln \sigma}{\delta \ln \dot{\varepsilon}}\right)_{T,\varepsilon} \quad (5)$$

$$\mathrm{n} = \left(\frac{\delta \sigma}{\delta \mathrm{T}}\right)_{\dot{\varepsilon},\varepsilon} \quad (6)$$

Where *m, n, σ,ε,ε̇,* and *T* are strain rate sensitivity, temperature sensitivity, true stress, true strain, strain rate, and temperature, respectively. Figure 4.12 shows the (a) strength revolution as a function of strain rate, (b) strain rate sensitivity as temperature function, (c) strength revolution as temperature function, and (d) temperature sensitivity at quasi-static and impact tensile tests of SUS821L1 as a function of testing temperature at true strain 0.05 and 0.2.

The selection aimed to capture the strength revolution of each strain during the deformation of pure austenite-ferrite phases and the mixed phases between austenite-ferrite and transformed martensite. The positive value of flow stress revolution with the change of strain rate at strain 0.05 and 0.2, both for quasi-static and impact tensile tests can be observed in Fig. 4.12 (a). However, with further observation, it can be seen that higher strain rate sensitivity occurred at the low strain rate (0.05), while lower strain rate sensitivity at high strain level (0.2), with temperature decrease. These phenomena occurred because of the increase in flow stress due to the TRIP effect that dominant at high strain level during quasi-static will narrowing the difference of flow stress between the quasi-static and impact tensile. For ease of comparison, Fig. 4.12

(b) shows the strain rate sensitivity as the function of temperature is decreasing with strain increase. In each strain level, the strain rate sensitivities increases as temperature decrease from 293 K to 273 K and decreased slightly from 273 K to 253 K. From 253 K to 233 K, a steeper decrease in strain rate sensitivity can be observed. At impact tensile at temperatures lower than 273 K, the uniform strain has occurred before the strain level 0.2. Thus, the flow stress already declines towards the fracture point at the selected strain level and results in lower strain rate sensitivity. The same phenomena have also been reported in austenitic stainless steel [22-23], which shows the difference in flow stress between quasi-static and impact tensile tests of the same strain level is diminishing with temperature decrease and even reached negative value with further temperature decrease.

Fig 4.12 (c) shows the transformation of flow stress at strain 0.05 and 0.2 as temperature change at quasi-static and impact tensile. At quasi-static, flow stress change only slightly at strain 0.05 because the amount of martensitic transformation is small at low strain levels. This phenomenon also corresponds with quasi-static yield strength's that only changed for about 10 MPa, when temperature decrease from 293 K to 273 K. At strain 0.2, the change of flow stress is not profound from 293 K until 253 K might be because at the selected strain (0.2) the TRIP effect is still beginning to start, and the change in flow stress more profound in higher strain level. However, at 233 K as the TRIP effect occurred at a lower strain level, a more profound change can be observed. At impact tensile test, the flow stress transformation increases profoundly from 293 K to 273 K at strain level 0.05 and 0.2, which indicates positive temperature sensitivity. However, at 253 K, while flow stress still slightly increase at strain level 0.05, the flow stress is decreasing at strain level 0.2. During impact tensile at strain level 0.2 the flow stress already passed the uniform elongation and undergoes necking mechanism until fracture point. As depicted in Fig. 4.12 (d) temperature sensitivity of

SUS821L1 at quasi-static and impact tensile at strain 0.05 and 0.2 are shown as the function of temperature. The temperature sensitivity at impact tensile when temperature decrease from 293 K to 273 K is much higher compare to the quasi-static tensile, shows strong temperature sensitivity. However, at temperatures lower than 273 K the temperature sensitivity almost turns into zero at strain level 0.05 and even turns into negative value at strain level 0.2, shows the diminishing strong temperature sensitivity. While the temperature sensitivity continues to increase with temperature decrease at quasi-static tensile. Similar phenomena also had been reported by Lee et al [22, 25], Jia et al [23], and Vercruysse et al [24], which shows diminishing in stress differences between various temperatures at high strain rate.

The phenomena of the diminishing temperature sensitivity can be associated with the thermally activated dislocation motion theory [23, 49]. The decomposition of the total flow stress can be divide into two types, internal stress (U) and effective stress (E). The two halves each illustrate the strain hardening effect and the thermal activation process. At various temperatures and strain rates, the value U is mostly steady. On contrary, E is strongly influenced by the strain rate and temperature. During the quasi-static tensile test at various temperatures, the effective stress remains constant and increases significantly at low temperatures. Thus, the flow stress increase with temperature decrease. At impact tensile, the effective stress increases continuously because the coupling effect of strain rate and temperature, which resulted in smaller temperature differences of flow stress between temperatures, indicates the decline of temperature sensitivity at impact tensile test, while the temperature sensitivity at quasi-static tensile is steadily increasing with temperature decrease.

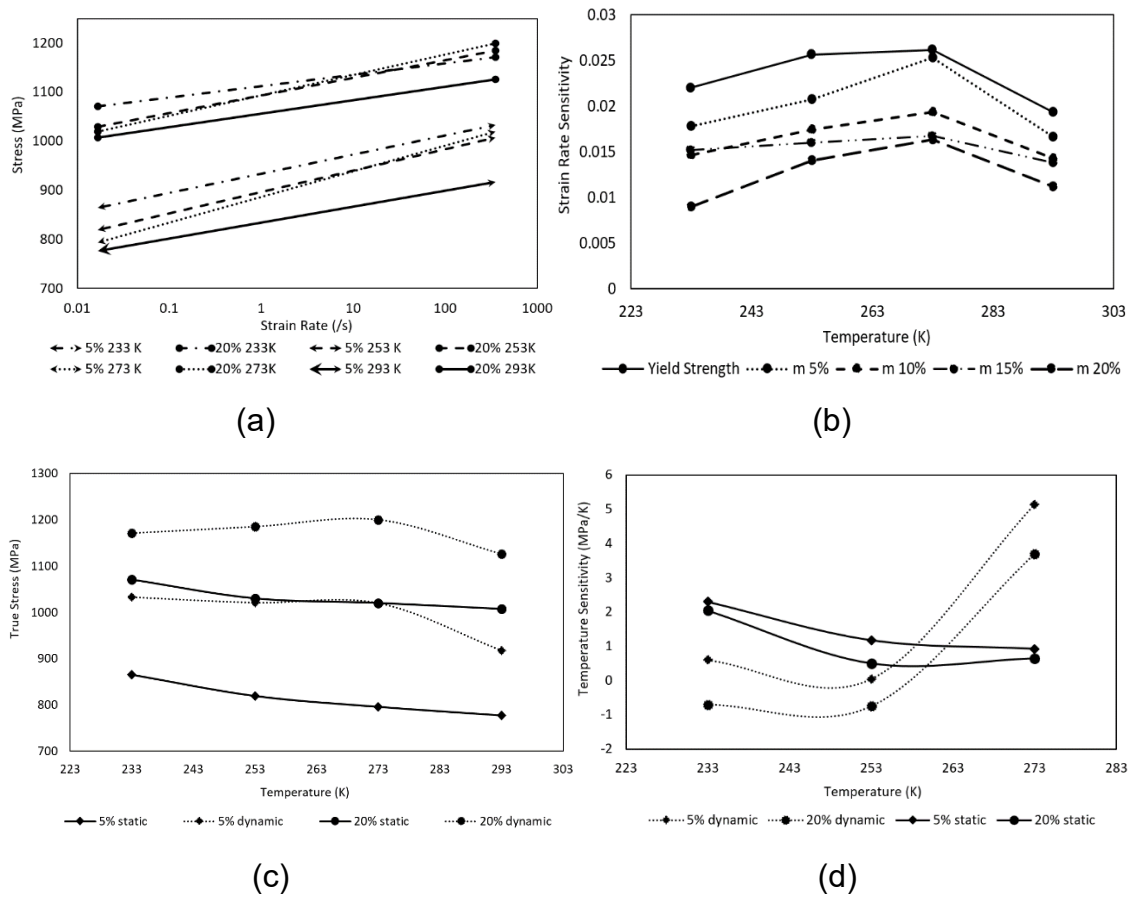

Fig. 4.12 (a) Flow stress revolution as a function of strain rate at various true strains and temperatures, (b) Strain rate sensitivity of SUS821L1 as the function of temperature, (c) Flow stress revolution of quasi-static and impact tensile tests as a function of temperature at strain of 0.05 and 0.2, (d) Temperature sensitivity of quasi-static and impact tensile tests as a function of temperature at strain of 0.05 and 0.2.

4.3.3 Specific energy Absorption Analysis

Important properties that characterize the crash behavior of materials is the specific energy absorption (SEA), described as the deformation energy per unit volume of material, which can be defined by integrating the area under the stress and strain curve stated in equation (7).

$$W_s = \int \sigma_e d\varepsilon_e \quad (7)$$

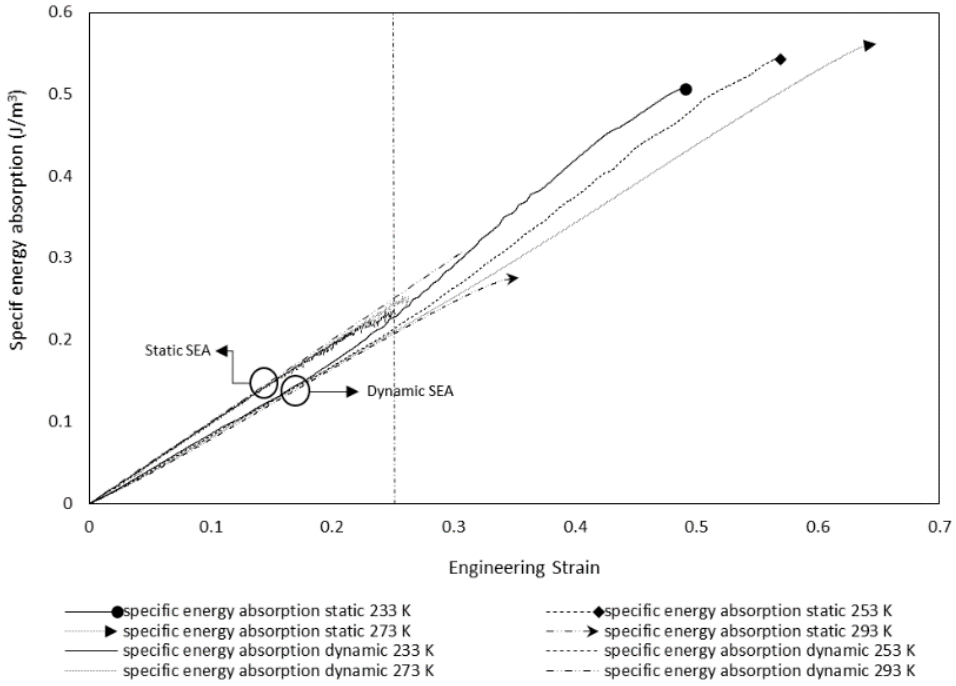

Fig. 4.13 SEA as a function of engineering strain at various strain rates and temperatures.

Fig. 4.13 shows the revolution of the SEA as the function of the engineering strain at various strain levels and temperatures until the fracture of SUS821L1 takes place for quasi-static and impact tensile tests. In Fig. 4.14, the total performance of the SUS821L1 or usually called the ECO-index is determined as the energy absorption of materials before necking occurred. Moreover, it had been common knowledge that parts subjected to crash loading are designed to never been deformed until failure, which makes it reasonable to compare the SEA of SUS821L1 at more strain levels. Thus, the SEA of four strain levels at 0.05, 0.1, 0.15, and 0.20 are shown as a comparison. Also, with this method the adiabatic heating effect and also statistical error arising in estimating the elongation values can be avoided. As depicted in Fig. 4.13, the SEA until failure of the quasi-static tensile is higher compare to the impact tensile,

which is mainly affected by the elongation of SUS821L1 that much longer during quasi-static compare to the impact tensile test. Nevertheless, until the strain of 0.2, the SEA during impact tensile at all temperature tests are collectively higher compare to the quasi-static one.

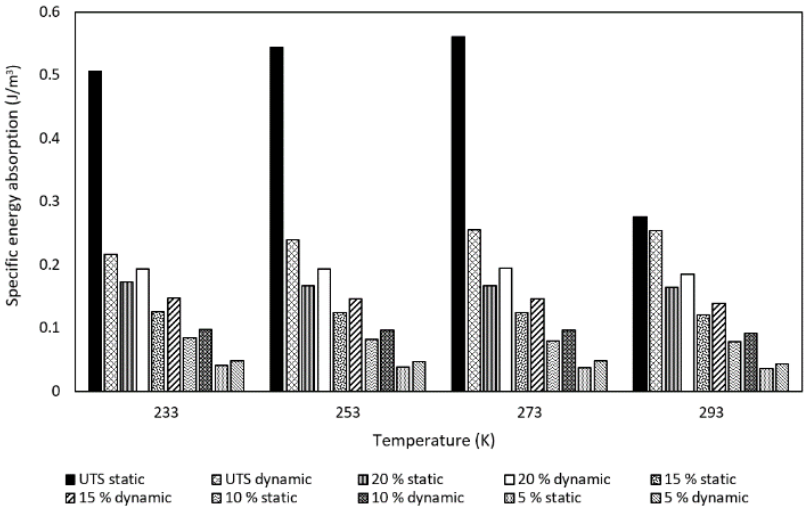

Fig. 4.14 SEA and ECO-index of SUS 821L1 during quasi-static and impact tensile tests at various engineering strains as a function of temperature.

In Fig. 4.14, for both quasi-static and impact tensile tests the SEA at selected strain levels are increasing as temperature decrease, due to the higher flow stress at low temperature. Meanwhile, it can be observed that the SUS821L1 can absorb more energy during impact compare to quasi-static tensile up to the strain 0.2 at all temperatures. This phenomenon had been observed in section 3.2, which shows positive strain sensitivity of SUS821L1 as depicted in Fig. 4.12 (a). At 293 K, the ECO-index between quasi-static and impact tensile are almost similar. There are two main reasons, first; regardless of the longer elongation at quasi-static tensile, the difference is not too significant, and second, higher flow stress compensates the elongation abridgment during impact tensile test. At a quasi-static tensile test, as temperature

decrease from 293 K to 273 K, the elongation of SUS821L1 is extended, where the highest elongation is achieved at 273 K and after that steadily decrease as temperature decrease. Similarly, the revolution of ECO-index also proportional to the elongation revolution, where an incisive increase in ECO-index occurred from 293 K to 273 K. Following the pattern of elongation revolution, the highest ECO-index occurred at 273 K and steadily decrease as temperature decrease.

At impact tensile stress, the difference of ECO-index due to the temperature change is not profound. At impact tensile test, even though, the ultimate tensile strength is higher at a lower temperature, but the difference is not significant due to the low temperature sensitivity from 273 K to 233 K at high strain rate as being observed in section 3.2. Moreover, the elongation is also decreasing with temperature decrease which also proportional to the revolution of ECO-index. At 293 K the ECO index during quasi-static and impact tensile tests are approximately 0.28 J/m^3 and 0.25 J/m^3, which accounted for the diminishing of ECO-index for about 8%. However, at a temperature lower than 293 K, the ECO-index of SUS821L1 during quasi-static and impact tensile tests have a huge difference, approximately 0.53 J/m^3 and 0.24 J/m^3, which accounted for the 55% less energy absorbance at impact tensile. The same condition also goes for the temperature test at 253 K and 233 K, where the ECO-index is decreasing for about 55% from quasi-static to impact tensile.

Compare to the previous studies, of AHSS steel which can only absorb energy about 0.2 J/m^3 [26] for quasi-static and impact tensile and TWIP steel which energy absorption decreased significantly from 0.55 J/m^3 to 0.35 J/m^3 from quasi-static to high strain rate tensile at room temperature [27], it can be concluded that SUS821L1 can be a good candidate to be used for automotive application due to no significant change of the amount of energy it can absorb during the crash, especially at room temperature. Furthermore, the energy-absorbing ability of SUS821L1 during impact tensile also not

much changed even with further temperature decrease. It can be concluded that the toughness of SUS821L1 is mainly is proportional to the total elongation, which can be seen from the diminishing value of ECO-index in high strain rates.

4.3.4 Fractography Analysis of SUS821L1

The characteristic material deformation behaviors can be observed from its fracture surface, which possessed the culmination from the continuation of deformation processes. Thus, the analysis of the fracture surface of SUS821L1 to reveal its correlation with the deformation features and fracture mechanism becomes worth noted. Scanning Electron Microscope (SEM) JEOL JSM-6510 with an operating voltage of 15 kV is used to observe the tensile fracture surface throughout. The magnification of 2000 times was deemed appropriate to reveal the fracture surface of SUS821L1 of quasi-static (0.0167/s) and impact (~350/s) tensile specimen at each parameter temperature of 293 K, 273 K, 253 K, and 233 K.

Fig. 4.15 shows the tensile fracture morphology of SUS821L1, at a quasi-static strain rate and different temperatures (293K, 273 K, 253 K, and 233 K). The fractographic images revealed a ductile profile at all studied deformation temperatures. The mechanism of ductile fracture is related to the nucleation, growth, and coalescence of the microvoids. Void nucleation occurs by decohesion of the austenite-martensite interfaces or localized deformation of the martensite phase. At 293 K, more even dimple distribution with the characteristics of large round dimples surrounded by smaller micro dimples. As temperature decreased, at 273 K the dimples become more uneven in size, the large dimples become deeper, and the increase of finer dimples located inside the large dimples due to the increasing of martensitic transformation acting as void nucleation sites. At 273 K, the network of finer dimples is steadily strengthened due to the intemperance of the martensite phase generated in the

austenite matrix at lower temperatures. Moreover, the appearance of more fine dimples at 273 K will improve the tension resistance by either hindering the crack propagation or reducing the crack growth rate. Lesser total elongation at 293 K might correspond to the lesser resistance due to more homogenous phases between ferrite-austenite and lack martensitic transformation because of a more stable austenite phase at high temperature. For the fracture surface at 273 K, deeper dimples exist compare to the fracture surface at different temperature parameters. In lower temperature than 273 K, the existence of big and the depth of the dimples are steadily decreasing with more appearance of smaller dimples due to the strengthening mechanism of martensitic transformation.

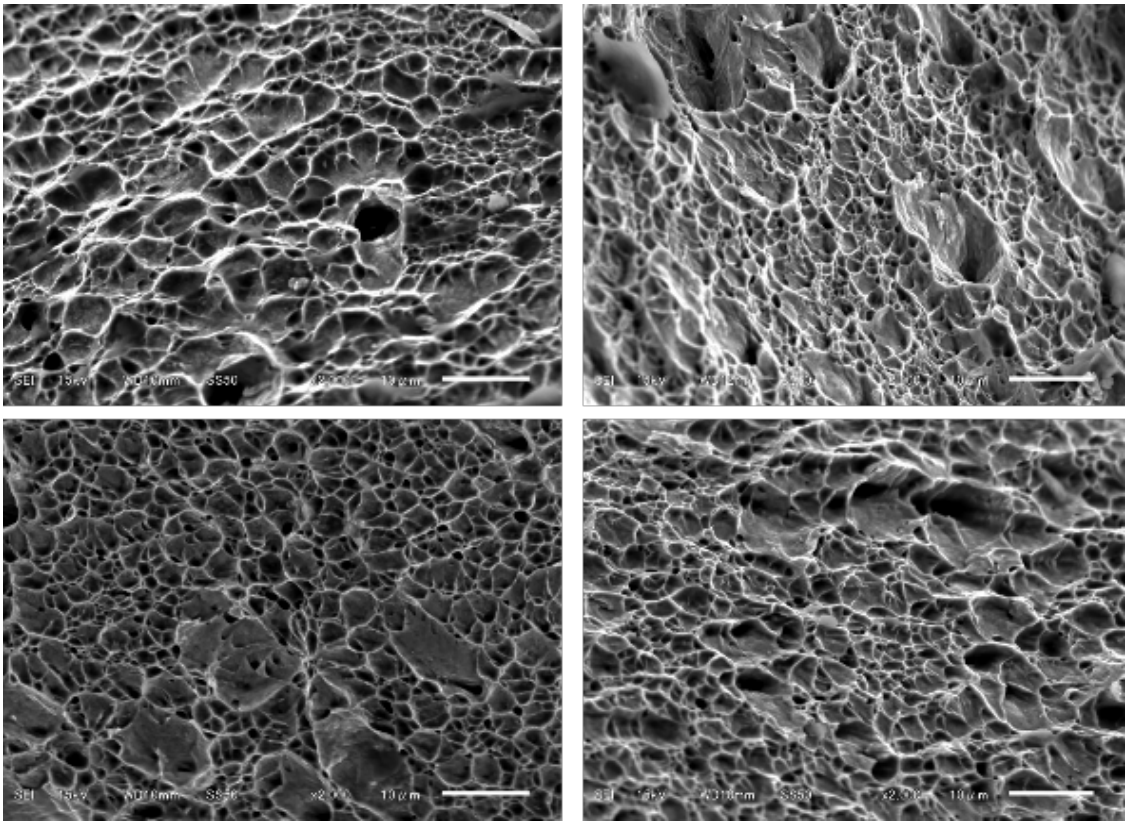

Fig. 4.15 Fractography of SUS821L1 during quasi-static strain rate at various temperature 293 K, 273 K, 253 K, and 233 K, repectively

These phenomena of the appearance of big and deep dimple correspond to the mechanical properties characteristics of SUS821L1 during quasi-static tensile. At 293 K, SUS821L1 has the shortest elongation and the lowest ultimate strength compare to other temperatures. Averagely, bigger dimple size corresponds to lower tensile strength and shallower dimple corresponds to a lower total elongation compare to other temperature parameters. The elastic behavior of a material can be seen from the existence of deep dimples in the fracture surface. Therefore, the longest elongation that occurred at 273 K is also corresponding with the existence of the deepest dimples that occurred at this temperature. Even though the deep big dimples exist at 273 K, but much finer dimples surround the big dimples also appeared, that can mean averagely smaller dimple size and higher dimple number density compare to 293 K. This result is corresponding with higher flow stress at 273 K compared to 293 K.

From Qualitative observation, the average dimple size is decreasing when the temperature continues to decrease passed the 273 K, while the dimple number density is increasing. Furthermore, the existence of big dimples is also decreasing followed by the decrease in their depth. Due to temperature decrease, the austenite phase becomes more unstable and transforms into the martensite phase. This transformation will eventually strengthen the network between the small dimples and steadily replace the existence of big and deep dimples. These phenomena are getting along with the strength of SUS821L1, where the flow stress is increasing with temperature decrease. At 273 K the martensitic transformation makes the relation between martensite-austenite-ferrite phases cause more accumulation of dislocations in the austenite phase which results in the elongation increase [17]. However, when the temperature continues to decrease the more ductile austenite phase is being replaced by more brittle but higher in the strength martensite phase, which will increase the formation of the small and finer dimple, while the existence of the big and deep dimple will cease

to exist.

The decrease of average dimple size is related to the increase in grain boundaries, which can be obstacles preventing dislocation motion with the formation of dislocation pile-up [33], followed by decreasing in ductility [34-35]. This also corresponds with the energy absorption of SUS821L1 which shows the largest capacity at 273 K compared to lower temperature parameters. These phenomena agreed with the elongation of SUS821L1. After passed 273 K the total elongation is continued to decrease at 253 K and 233 K, while the flow stress steadily increases.

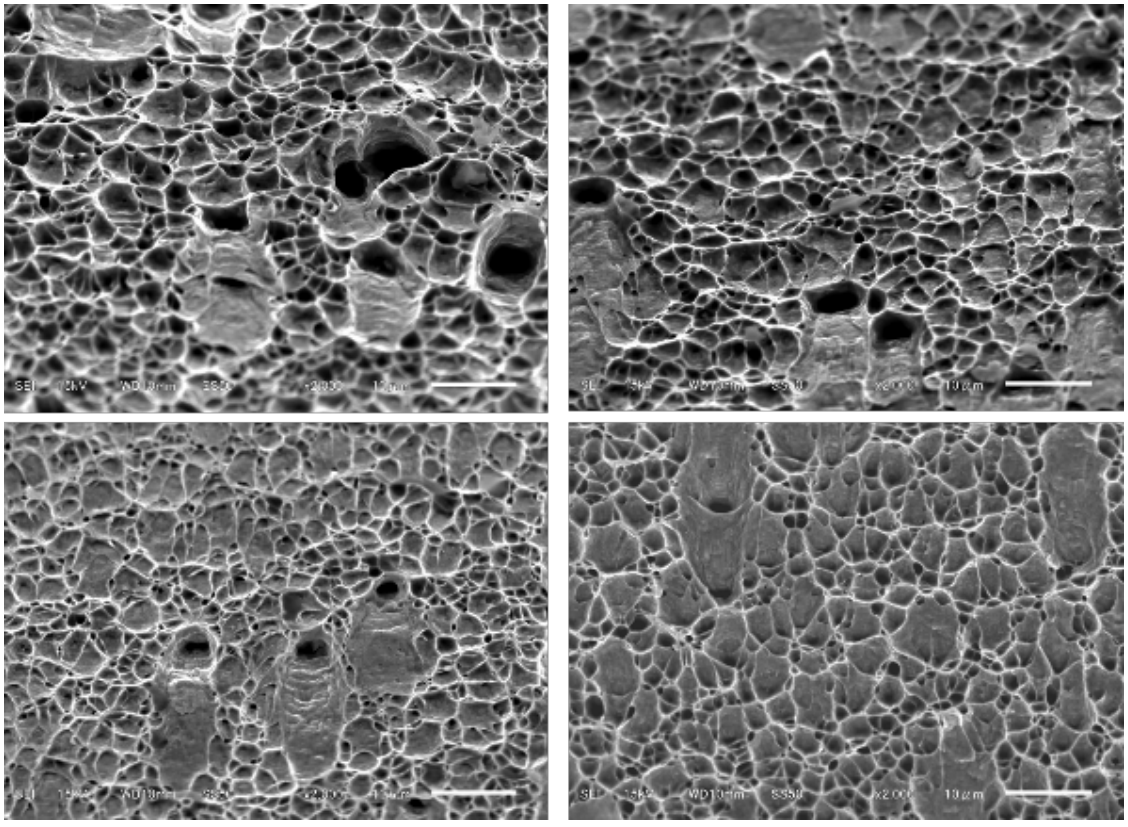

Fig. 4.16 Fractography of SUS821L1 during impact strain rate at various temperature (a) 293 K, (b) 273 K, (c) 253 K, and (d) 233 K, repectively

Fig. 4.16, shows the fracture morphologies of SUS821L1 during impact tensile at 293 K, 273 K, 253 K, and 233 K, respectively. Similar to the fracture surfaces during

quasi-static, the fracture surfaces at impact tensile consist of the formation of big dimples surrounded by much smaller dimples. Even though the formation of dimples is almost the same compare to the quasi-static, but the dimples are shallower. This phenomenon might occur because the high loading speed becomes so fast that the rotation of the crystal surface along the loading force was not sufficient, which blocked the growth and extension of slip [9]. Thus, in this state, the total elongation of SUS821L1 reduced compare to the quasi-static stage. Moreover, a reduction in elongation can be seen from the significant deformation behavior of martensite near tensile fracture due to adiabatic heating. At lower temperatures, the grain slip becomes more difficult due to the strengthening mechanism. The evidence can be seen from finer dimples that occurred when the temperature continues to decrease, which corresponds with the increasing flow rate and the decreasing elongation. The increasing flow stress at impact tensile can be described as the work of the dislocation activity during the process of plastic deformation. While the initial dislocation density and configuration are constant, the increasing strain rate will eventually increase the flow stress to maintain the increasing dislocation velocity [3].

At lower temperature, dislocation in the deformed microstructure is being strengthened, means the rate of dislocation annihilation is lower than to dislocation generation. Moreover, at lower temperatures, the density and rate of multiplication of the dislocation in the deformed microstructure will increase, which means higher resistance to plastic flow and more brittle behavior. With the coupling with a high strain rate, the flow behavior will be determined by mutual support between the enhanced dislocation multiplication and thermal hardening. The enhanced dislocation multiplication and decrease in temperatures will eventually increase the resistance towards plastic flow and more brittle behavior. The increase in flow stress after first yielding continued due to the generation of dislocations and interaction among

themselves with various types of microstructural barriers during plastic deformation. Thus, the flow stress becomes higher while the elongation becomes shortened during impact tensile when the temperature continues to decrease. The aforementioned phenomena can be noticed in the microstructure of fracture surfaces of SUS821L1 during impact strain rate. The result of dislocation multiplication also can be seen from the existence of small and shallow dimples throughout the fracture surface, which correspond to brittle behavior in the material.

Fig. 4.17 shows the quantitative correlation between mechanical properties of SUS821L1 and its fracture morphologies during quasi-static and impact tensile at various temperatures obtained by image processing. Figure 4.17 (a) shows the correlation between dimple number density and average dimple size with total elongation of SUS821L1 during quasi-static as temperature function. With the exception at 293 K, the total elongation is directly proportional with the dimple number density, and inversely proportional with the average dimple size, with the function of temperature. At 293 K austenite phase is more stable compare to other temperature parameters. The lack amount of martensite content compare to other temperatures, will make small dimples steadily replaced by larger dimples, which cause the density of finer dimples to decrease.

Furthermore, the lack of existence of martensite-austenite-ferrite interaction reduces the total elongation despite more austenite being retained. The largest average dimple diameter can be seen at 273 K, in line with the largest average dimple diameter that occurred at this stage. When temperature continues to decrease, the average dimple diameter is decreasing due to more martensite being transformed, which corresponds with the diminishing size of the average dimple diameter. Figure 4.17 (b) shows the correlation between dimple number density and average dimple size with total elongation as the function of temperature. Compare to the quasi-static

stage in Fig. 4.17 (a), a clearer relation among these three parameters can be observed during impact. With minor interaction among martensite-austenite-ferrite phases, a more proportional correlation can be observed between fracture morphologies and their correlation with mechanical properties.

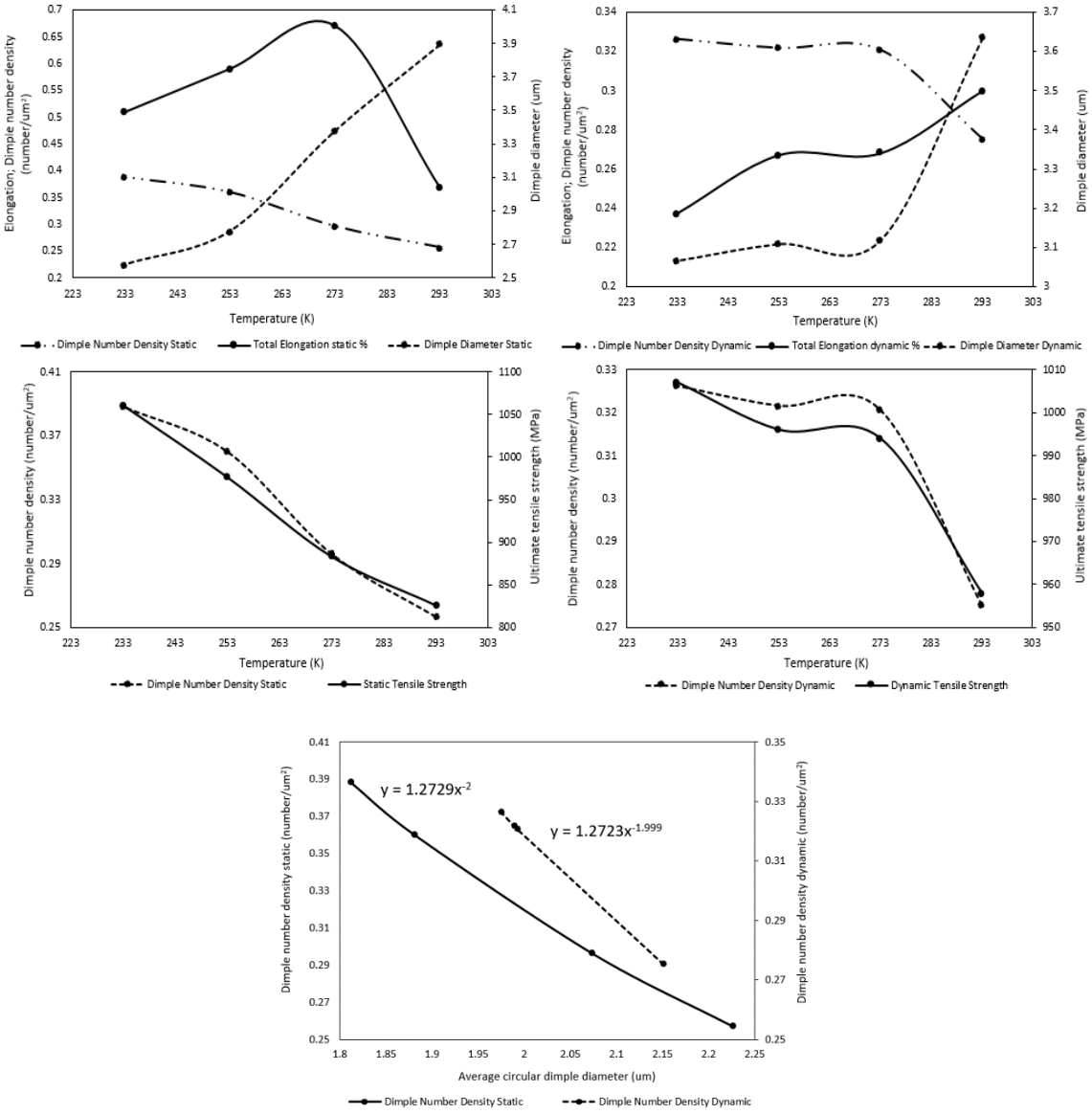

Fig. 4.17 Summary of fracture morphologies and its correlation with mechanical properties of SUS821L1

The correlation between dimple number density and ultimate tensile strength can be observed in Fig. 4.17 (c) and (d) for quasi-static and impact tensile, respectively. For both strain rates, the directly proportional relation can be observed, however, more linear correlation can be observed during quasi-static, which shows higher temperature sensitivity compared to the impact tensile, as stated in section 3.2. At quasi-static, the reduced mobility of dislocation and TRIP due to low temperature seems more profound to enhance the flow stress compare to the effect of low temperature in high strain rate, while for the later, the enhanced flow stress occurred due to multiplication dislocation and strengthened mechanism due to the effect of temperature decrease. It was already stated that the amount of martensitic transformation is small at a lower strain level. This phenomenon corresponds with the revolution of yield strength at impact tensile which more profound compare to quasi-static, as the yield strength at impact tensile is being enhanced by two mechanisms, which are dislocation multiplication due to the high strain rate and strengthening mechanism due to the low temperature. Thus, it can be observed that the increasing level of yield stress from 293 K to 233 K during impact tensile more profound compare to the quasi-static, which are 96 MPa and 60 MPa, respectively. As strain continues to elevate, the transformation mechanism from austenite to martensite phase take place at quasi-static which cause the flow stress during this condition will eventually surpass the flow stress of impact tensile at a temperature lower than 253 K. Thus, it also can be noted that the change of ultimate tensile strength during quasi-static is higher compare to the impact tensile, which are 234 MPa and 49 MPa, respectively. As aforementioned before, with the increasing amount of martensitic transformation at a lower temperature, the network of small dimples will be strengthened, thus the density of dimple number will eventually increase, which corresponds with the increasing ultimate tensile strength.

Fig. 4.17 (e) shows the both for quasi-static and high strain rate, the average

dimple diameter decreases with a simultaneous increase in dimple density, as temperature function. Furthermore, in regards to the proposed correlation formula, the revolution of dimple number density and average dimple diameter with temperature function is proportional between the quasi-static and impact tensile.

4.4 Fitting Analysis with Original J-C Constitiutive Model

The metallic material behaviors with the coupling effect of strain, strain rate, and temperatures can be described by the Jhonson-Cook model under the condition of plastic deformation. This method has been applying widely by previous studies to predict materials' flow behavior due to its simple form and less complication to estimate the material constant

The parameter *A, B, n, C,* and *m* are original J-C parameters, which are yield stress, strain hardening constant, strain hardening coefficient, strengthening coefficient, and thermal softening coefficient, respectively. These constants then will be use to be fitted based on this following equation 8, and the value of each parameters are obtained and shown in table 4.2.

$$\sigma = (A + B\varepsilon^{n})\left(1 + C\ln\left(\frac{\dot{\varepsilon}}{\dot{\varepsilon}_0}\right)\right)\left(1 - \left(\frac{\mathrm{T}-\mathrm{T}_0}{\mathrm{T}_\mathrm{m}-\mathrm{T}_0}\right)^{m}\right) \quad (8)$$

Table 4.2. Original Jhonson-Cook Parameters

J-C Variant	*A*	*B*	*n*	*C*	*m*
Value	609	1008.5	0.5787	0.012822	3.9

Figure 4.18 (a) and (b) shows the fitting results of flow stress between experimental and original JC for quasi-static and impact tensile at various temperature,

respectively. Due to respect to strain rates and temperature, the J-C model showing poor fit compared to the experimental results, especially in the yielding point of impact tensile. With the decreasing temperature in the high strain rate, the JC model cannot predict the increase in flow stress of the coupling effect. Furthermore, the negative temperature sensitivity at high strain level at impact tensile. At quasi-static tensile, the J-C model seems to be fit with the flow stress of the experimental result, especially at 293 K. At low temperature, the J-C model is fitted with the experimental results until approximately strain level 0.1, since the amount of martensitic transformation is small at low strain stage. However, the J-C model seems off high strain level where the TRIP effect takes a more important role in the work hardening mechanism and martensite pre-dominantly determines the increase in flow stress and ductility due to its high fraction. It needs to be noted that the J-C model is based on empirical observation and does not have any physical background. Thus the TRIP effect that occurred at quasi-static at low temperatures during plastic deformation cannot be predicted using the J-C model. However, due to the application of steel never means to deformed until failure, the making of the stress flow model is still deemed important. In the original J-C model, each component is not separately calibrated whereas the well-established methodology for the fitting of each J-C parameter is needed.

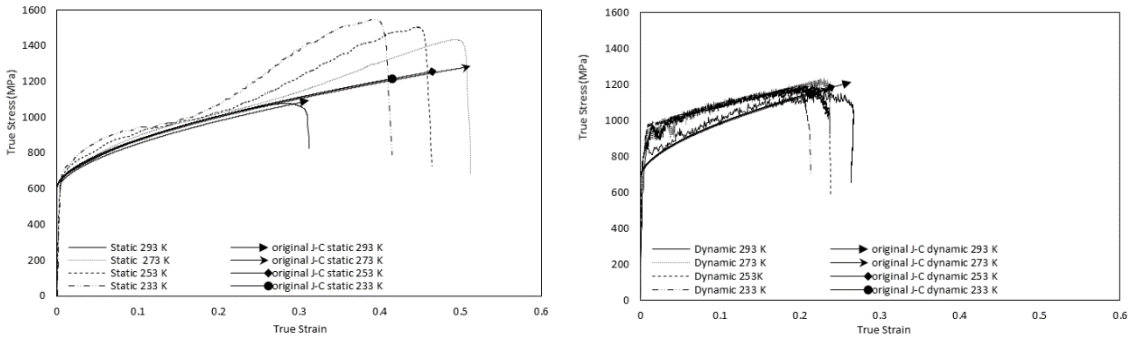

(a) (b)

Fig. 4.18 Flow stress curves fitted with original J-C model of (a) quasi-static and (b) impact tensile at various temperatures.

4.5 Modified J-C model

Adopting the modified J-C model developed by Devotta et al [49], the first line of strain hardening behavior of the original J-C constitutive model become polynomial function, where the effect of temperature and strain rate are included in first line of J-C strain hardening model as shown in eq. 9 to eq. 12.

$$\sigma = (A_i + B_i \varepsilon^{n_i}) \left(1 + C \ \ln\left(\frac{\dot{\varepsilon}}{\dot{\varepsilon}_0}\right)\right) \left(1 - \left(\frac{\mathrm{T}-\mathrm{T}_0}{\mathrm{T}_\mathrm{m}-\mathrm{T}_0}\right)^m\right) \quad (9)$$

$$A_i = A_0 + A_1 \ln\left(\frac{\dot{\varepsilon}}{\dot{\varepsilon}_0}\right) + A_2 \mathrm{T}^* + A_3 \left[\ln\left(\frac{\dot{\varepsilon}}{\dot{\varepsilon}_0}\right) \mathrm{T}^*\right] \quad (10)$$

$$B_i = B_0 + B_1 \ln\left(\frac{\dot{\varepsilon}}{\dot{\varepsilon}_0}\right) + B_2 \mathrm{T}^* + B_3 \left[\ln\left(\frac{\dot{\varepsilon}}{\dot{\varepsilon}_0}\right) \mathrm{T}^*\right] \quad (11)$$

$$n_i = n_0 + n_1 \ln\left(\frac{\dot{\varepsilon}}{\dot{\varepsilon}_0}\right) + n_2 \mathrm{T}^* + n_3 \left[\ln\left(\frac{\dot{\varepsilon}}{\dot{\varepsilon}_0}\right) \mathrm{T}^*\right] \quad (12)$$

The original J-C model's parameters *A, B*, and *n* being constant, thus unable to predict the influence of temperature and strain effect. In modified J-C, the value of *A, B,* and *n* has been modeled to able to capture the flow stress variations due to the coupling effect of strain rate and temperature.

The value of *C,* and *m* is similar to the original J-C model, however, the value of *A, B*, and *n* are captured from each test condition. This method will provide the value of *A, B, n* of each test condition which will lead to 8 sets of J-C strain hardening, fitted with the natural logarithmic function of each parameter with the homologous temperature and strain rate. From eq. 10 to eq. 12, the first line concludes the initial value of each *A, B*, and *n* parameters with no regard for strain rate and temperature. The second line sum up the influence of strain rate with no regards for temperature change, the third line of the equations based on work hardening only in regards to temperature change, and the fourth line sums up the coupling effect between strain rate and temperature change. The value of each parameter is shown in table 4.3.

Table 4.3. Parameter *A, B*, and *n* as polynomial function

Index	*A*	*B*	*n*
0	661.1	1474.5	0.7483
1	1452	-8231.3	-3.9106
2	18.147	-81.86	-0.383
3	-77.86	1224.04	0.74

Fig. 4.19 (a) and (b) shows the fitted curves of true stress and strain diagram with the modified J-C model during quasi-static and impact tensile, respectively. It can be seen that the modified J-C model can predict more accurate the coupling effect between strain rate and temperature change compared to the original J-C model. At quasi-static tensile, the modified J-C model can capture the increasing flow stress due to the thermal strengthening of low temperature at the low strain level. However, in a high strain level where the flow stress is predominantly affected by martensitic

transformation, the effect of secondary hardening can not be predicted. As aforesaid before, the nature of the J-C model only can predict the phenomenological or empirical observation and not based on a physical-based model. Fig 4.19 (b), shows the fitting relation between the modified J-C model and experimental results at various temperatures during impact tensile. The increasing flow stress due to dislocation pile-up and strengthening mechanism by the coupling effect between high strain rate and low temperature can be captured more accurately using this modified J-C model. Moreover, this modified J-C model also able to capture the flow stress of SUS821L1 at a high strain level.

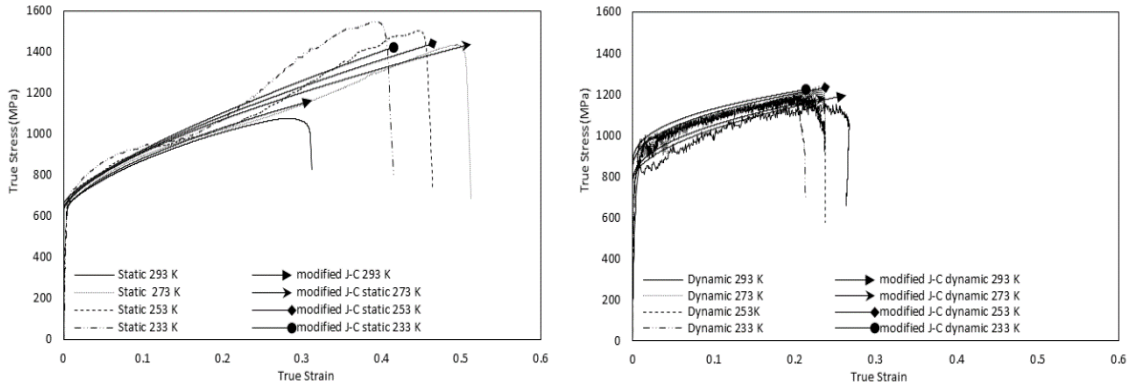

(a) (b)

Fig. 4.19. Modified J-C model compare to true stress-strain curves during (a) quasi-static and (b) impact tensile at various temperatures.

As a comparison, Fig. 4.20 (a) and (b) shows the comparison of relative error between the original and modified J-C model at quasi-static and impact tensile, respectively. The modified J-C model has a lower relative error value compare to the original one.

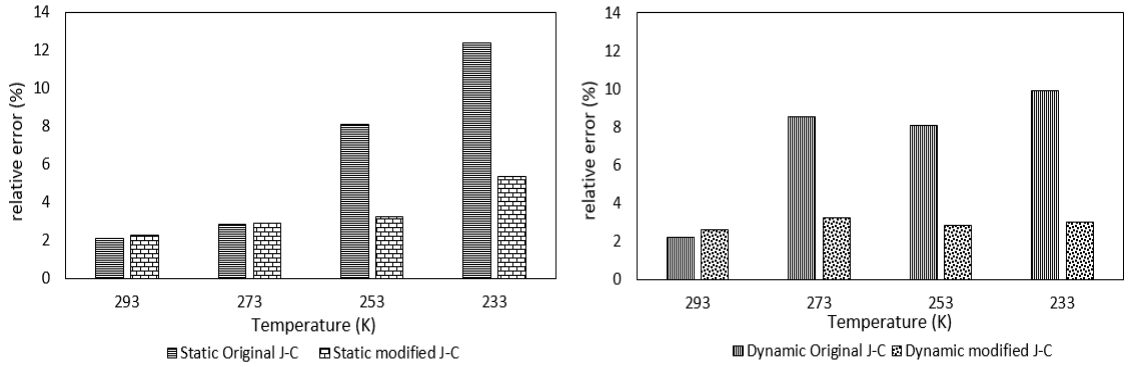

(a) (b)

Fig. 4.20 Relative error comparison between original and modified J-C model during (a) quasi-static and (b) impact tensile at various temperatures.

In the quasi-static tensile, even though the modified J-C model has a lower relative error compared to the original, the error value is increasing with temperature decrease. This phenomenon because the J-C model cannot be used to predict the martensitic transformation that increases with temperature . However, at impact tensile, the relative error is approximately steady which shows the TRIP effect being suppressed during impact as the effect of adiabatic heating that occurred in the fracture area.

4.6 Conclusion.

The tensile behavior of SUS821L1 at various temperatures and strain rates were investigated in the present study. The main findings are summarized as follows:

1. The flow stress of SUS821L1 is increasing due to the respect of low temperature at quasi-static and impact tensile, but the increasing trend of flow stress is more profound at quasi-static, especially in high strain level. These phenomena mainly due to the martensitic transformation that occurred at quasi-static, while the effect being hindered during impact due to the adiabatic heating at the fracture area of the

specimen.

2. The deformation behavior is dominated by the competition between dislocation glide and martensitic transformation. Both temperature and strain rate have a significant effect on the two mechanics. Which is shown from strain rate and temperature sensitivity. The strain rate sensitivity shows a positive value for each temperature change until the strain level of 0.2. Furthermore, the temperature sensitivity also reaches a negative value start at 253 K during impact tensile mostly because the SUS821L1 already passed the uniform elongation after exceeds the strain level of 0.2.

3. The toughness of SUS821L1 is reduced at impact, corresponds to reduce in ductility in this condition. Nevertheless, SUS821L1 is still deemed as an excellent candidate for crash absorber material. As a comparison, this material absorbs more energy during impact tensile compare to the quasi-static until the strain level of 0.2. As aforementioned in section 3.3, the application of material is usually never designed to exceeds its proof stress.

4. Finer, deeper, and more homogenous dimples can be observed at quasi-static tensile can be seen as the effect of martensitic transformation which strengthens the network among small dimple, while the interaction between martensite-austenite-ferrite phases increases dimple depth which related to ductile behavior in this state. At impact tensile, SUS821L1 shows ductile to brittle transformation during high strain rate shown from more irregular and shallow dimples corresponds to the abridgment of total elongation. The quantitative observation on fracture morphologies shows a directly proportional correlation between average dimple size and total elongation and inversely proportional with ultimate tensile strength. A positive correlation also can be observed from dimple number density and ultimate tensile strength both for quasi-static and impact tensile. In addition, the correlation between dimple number density and

average dimple size corresponds with both quasi-static and impact tensile condition.

5. The modified J-C constitutive model is more reliable to capture the coupling effect of strain rate and temperature at the beginning of plastic deformation. However, as the TRIP will play a dominant role in the high strain level, the J-C modified model cannot predict the flow stress at quasi-static. At impact, the modified J-C model successfully predicts the flow stress, mainly because the TRIP effect is not shown during this condition even with further lowered temperature. As a comparison, while the relative error at quasi-static keeps increasing with temperature decrease, these are not the case for impact tensile.

4.7 References

1. Takayuki Oshima, Yasuhiro Habara, Kotaro Kuroda. Efforts to save nickel in austenitic stainless steel. ISIJ Int 2007;47:359-364.
2. Hoon Huh, Seok Bong Kim, Jung Han Song, Ji Ho Lim. Dynamic tensile characteristics of TRIP-type and DP-type steel sheets for an auto-body. Int J Mech Sci 2008;50:918-931.
3. Jaeyeong Park, Min Cheol Jo, Hyeok Jae Jeong, Seok SU Sohn, Jae Hyun Kwak, Hyoung Seop Kim, Sunghak Lee. Interpretation of dynamic tensile behavior by austenite stability in ferrite-austenite duplex laightweight steels. Sci Rep 2017;7:15726.
4. Xifeng Li, Jun Chen, Liyan Ye, Wei Ding, Pengchao Song. Influence of strain rate in tensile charcteristics of SUS304 metastable austenitic stainless steel. Acta Metall Sin (Engl Lett) 2013;26:657-662.
5. Arpan Das, Soumitra Tarafder. Experimental investigation on martensitic transformation and fracture morphologies of austenitic stainless steel. Int J Plast. 2009;25:2222-2247.
6. Jeom Yong Choi, Jeeun lee, keunho Lee, Ji Yeon Koh, Jae Hyung Cho. Heung Nam Han, Kyung Tae Park. Effects of strain rate on tensile properties of TRIP aided duplex stainless steel. Mater Sci Eng A 2016;666:280-287.
7. Woei Shyan Lee, Chi Feng Lin. The morphologies and characteristics of impact induced martensite in 304L stainless steel. Scr Mater 2000;43:777-782.
8. S Oliver, T B Jones, G Fourlaris. Dual phase versus TRIP strip steels: Microstructural changes as a consequence of quasi-static and dynamic tensile testing. Mater Charac 2007;58:390-400.
9. Shengchi Li, Yonglin Kang, Guoming Zhu, Shuang Kuang. Effects of strain rates on mechanical properties and fracture mechanism of DP780 dual phase steel. J Mater

Eng Perform. 2015;24:2426-2434.

10. Woei Shyan lee, Chi Feng Lin. Comparative study of the impact response and microstructure of 304L stainless steel with and without prestrain. Metall Mater Trans A 2002;33:2801.
11. Juho Talonen, Pertti Nenonen, Gersom Pape, Hannu Hanninen. Effect of strain rate on strain induced y-a-martensite transformation and mechanical properties of austenitic stainless steels. Metall Mater Trans A 2005;36:421.
12. Noriyuki Tsuchida, Satoshi Okura, Takaaki Tanaka, Yuki Toji. High speed tensile deformation behavior of 1 GPa-grade TRIP-aided multi-phase steels. ISIJ Int 2018;58:978-986.
13. Zan Li Thomas Viosin, Joseph T McKeown, Jianchao Ye, Tom Braun, Chandrika Kamath, Wayne E King, Y Morris Wang. Tensile Properties, strain rate sensitivity, and activation volume of additively manufactured 316L stainless steel. Int J Plast 2019;120:395-410.
14. Noriyuki Tsuchida, Yuko Yamaguchi, Yoshiki Morimoto, Tomoyuki Tonan, Yoshinori Takagi, Rintaro Ueji. Effects of temperature and strain rate on TRIP effect in SUS301L metatstable austenitic stainless steel. ISIJ Int 2013;53:1881-1887.
15. Noriyuki Tsuchida, Taiji Kawahata, Eiichiro Ishimaru, Akihiko Takahashi. Effect of temperature and strain rate on tensile properties of a lean duplex stainless. ISIJ Int 2014;54:1971-1977.
16. Chengsi Zheng, Chunjiao Liu, Minghaou Ren, Heng Jiang, Longfei Li. Microstructure and mechanical behavior of an AISI 304 austenitic stainless steel prepared by cold-or cryogenic-rolling and annealing. Mater Sci Eng A 2018;724:260-268.
17. Heping Liu, Bin Liu, Peikang Bai, Huer Sun, Dazhou Li, Fenger Sun, Naiming Lin. Martensitic transformation and fractography analysis of lean duplex stainless steel

during low temperature tension deformation. Mater Charact 2015;107:262-269.

18. Chengsi Zheng, Wangwei Yu. Effect of low temperature on mechanical behavior for an AISI 304 austenitic stainless steel. Mater Sci Eng A 2018;710:359-365.
19. V G Gavriljuk, W Theisen, v V Sirosh, E V Polshin, A Kortmann, G S Mogilny, Yu N Petrov, Ye V Tarushin. Low-temperature martensitic transformation in tool steels in relation to their deep cryogenic treatement. Act Mater 2013;61:1705-1715.
20. Guilherme Correa Soares, Mariana Carla Mendes Rodrigues, Leandro de Arruda Santos. Influence of temperature on mechanical properties, fracture morphology and strain hardening behavior of a 304 stainless steel. Mater Res 2017;20:141-151.
21. T S Byun, N Hashimoto, K Farrell. Temperature dependence of strain hardening and plastic instability behaviors in austenitic stainless steels. Acta Mater 2004;52:3889-3899.
22. Woei Shyan Lee, Chi Feng Lin, Tao Hsing Chen, Wen Zhen Luo. High temperature deformation and fracture behavior of 316L stainless steel under high strain rate loading. J Nucl Mater. 2012;420:226-234.
23. B Jia, A Rusinek, R Pesci, S Bahi, R Bernier. Thermo-viscoplastic behavior of 304 austenitic stainless steel at various strain rates and temperatures: Testing, modeling and validation. Int J Mech Sci 2020;170:105356.
24. Florian Vercruysse, Carola Celada Casero, bernd M Linke, Patricia Verlysen, Roumen H Petrov. Temperature dependence of the static and dynamic behavior in quenching and partitioning processed low-Si steel. Metals 2020;10:509.
25. Woei Shyan Lee, Tao hsing Chen, Chi Feng Lin, Zong Yun Li. Effect of strain rate and temperature on shear properties and fracture characteristics of 316L stainless steel. Mater Trans 2012;53:469-476.
26. Manjunatha Madivala, Wolfgang Bleck. Strain rate dependent mechanical properties of TWIP steel. JOM-US 2019;71:1291-1303.

27. Wei Wang, Yan Ma, Muxin Yang, Ping Jiang, Fuping Yuan, Xiaolei Wu. Strain rate effect on tensile behavior for a high specific strength steel: from quasi-static to intermediate strain rates. Metals 2018;8:11.
28. S Lou, D O Northwood. Effect of strain aging on the strength coefficient and strain-hardening exponent of construction-grade steels. J materl Eng Perf 1994;3:344-349.
29. H Nahme, E Lach, A Tarrant. Mechanical properties under high dynamic loading and microstructure evaluation of TiB_2 particle-reinforced stainless steel. J Mater Sci 2009;44:463-468.
30. Valentin Davaze, Nicolas Vallino, Sylvia Feld-Payet, Bertrand Langrand. Plastic and fracture behavior of dual phase steel under quasi-static and dynamic loadings. Eng Fract Mech 2020;235:107165.
31. A J Cooper. W J Brayshaw, A H Sherry. Tensile fracture behavior if 316L austenitic stainless steel manufactured by hot isostatic pressing. Metall Mater Trans A 2018;49:1579.
32. O A Hilders, M Ramos, N D Pena, L Saenz. Fractal geometry of fracture surfaces of duplex stainless steel. J Mater Sci 2016;41:5739-5742.
33. Wenbo Qin, Jiansheng Li, Yaoyao Liu, Jiajie Kang, Lina Zhu, Dengfeng Shu, Peng Peng, Dingshun She, Dezhong Meng, Yusheng Li. Effect of grain size on tensile property and fracture morphology of 316L stainless steel. Mater Lett 2019;254:116-119.
34. Arpan Das, Soumitra Tarafder. Geometry of dimples and its correlation with mechanical properties in austenitic stainless steel. Script Mater 2008;59:1014-1017.
35. Arpan Das. Martensite-void interaction. Script Mater 2013;68:514-517.
36. M A Beltran-Zuniga, J L Gonzalez Velasquez, D I Rivaz-Lopez, F Hernandes Santiago, H J Dorantes-Rosales, V M Lopez Hirata. Determination if fracture

toughness in short transverse direction of low carbon steel pipes by compact-tension specimen completed by welded attachments. Eng Fract Mech 2109;222:106711.

37. Jeffrey W Sowards, Chris N McCowan, Elizabeth S Drexler. Interpretation and significance of reverse chevron-shaped markings on fracture surfaces of API X100 pipeline steels. Mater Sci Eng A 2012;551:140-148.
38. C Defaisse, M Maziere, L Marcin, J Besson. Ductile fracture of an ultra-high strength steel under low to moderate stress triaxiality. Eng Fract Mech 2018;194:301-318.
39. Takahiro Kaneko, Motomichi Koyama, Tomoya Fujisawa, Kaneaki Tsuzaki. Combined Multi-scale analyses on strain /damage/microstructure in steel: example of damage evolution associated with e-martensitic transformation. ISIJ Int 2016;56:2037-2046.
40. Bing Wang, Xinran Xiao, Viktor P Astakhov, Zhanqiang Liu. A quantitative analysis of the transition of fracture mechanism of Ti6Al4V over a wide range of stress triaxiality and strain rate. Eng Fract Mech 2020;231:107020.
41. Liangyun Lan Yiting Zhang, Xiangwei Kong. Dynamic fracture behavior of low carbon bainitic steel after different welding thermal cycles. Eng Fract Mech 2019;220:106653.
42. H S Arora, A Ayyagari, J Saini, K Selvam, S Riyadh, M Pole, H S Grewell S Mukherjee. High tensile ductility and strength in dual-phase bimodal steel through stationary friction stir processing. Sci Rep 2019;9:1972.
43. Kyung Jun Lee, Ming Sung Chun, Myung Hyun Kim, Jae Myung lee. A new constitutive model of austenitic stainless steel for cryogenic applications. Comput Mater Sci 2009;46:1152-1162.
44. J A Rodriguez Martinez, A Rusinek, J R Klepaczko, R B Pecherski. Extension of R-

K constitutive relation to phase transformation phenomena. Mater Des 2009;30:2513-2520.

45. Seong Won Yoo, Chi Seung lee, Woong Sup Park, Myung Hyun Kim, Jae Myung Lee. Temperature and strain rate dependent constitutive model of TRIP steels. Comput Mater Sci 2011;50:2014-2027.
46. Huabing Li, WeichaoJiao, hao Feng, Xinxu Li, Zhouhuo Jiang, Guoping Li, Lixin Wang, Guangwei Fan, Peide Han. Metals 2016;6:223.
47. Pierre Simon, Yael Demarty, Alexis Rusinek, George Z Voyiadjis. Material behavior description for a large range of strain rates from low to high temperatures: application to high strength steel. Metals 2018;8:795.
48. Mohanraj Murugesan, Dong Won Jung. Johnson Cook material and failure model parameters estimation of AISI-1045 medium carbon steel for metal forming applications. Materials 2019;12:609.
49. Ashwin Moris Devotta, P V Sivaprasad, Tomas Beno, Mahdi Eynian, Kjell Hjertig, Martin Magnevall, Mikael Lundblad. A modified Johnson-Cook model for ferritic-pearlitic steel in dynamic strain aging regime. Metals 2019;9:528.

CHAPTER 5

SUMMARY

I. The non-moving packed bed model was used to mimic and study any factor that affect the inhomogeneous or dispersed phenomena such as the instability and permeability of the fine particles transported by updraft inside the blast furnace by means the numerical approach using DEM-CFD. The alumina spheres were used for packing particles of the bed and coke are used as the fine particles transported, mimicking the fine element for steel making process such as chromium and coarse particle. The following results are obtained. (1) A principal factor controlling the blockage is a particle diameter ratio, defined by the particle diameter of fine divided by that of packing particle. (2) The superficial gas velocity is not a primary factor for the blockage to occur. If the generated powder inside the blast furnace already large enough compare to the flow channel, increasing the gas blown from the tuyere will not increase the permeability of the generated fines, mainly because the diameter ratio already exceeds the critical diameter ratio proposed by Takahashi et.al (0.12). (3) The numerical value by means the pressure drop distribution is in fairly good agreement with the experimental result. (4). With continuous injection of fine particle it is possible to observed the complex movement of fine particles together with the gas flow, where the gas flow is avoiding the highly concentrated area that filled with the fine particles as the time progress.

II. The interaction among gas, coarse particle, and fine powder inside the blast furnace filling layer, such as alloying element and pulverized coal for steel making process have a very complicated behavior, moreover if observed in

micros scale point of view. Even the scale of obstruction is micro, but it is expected that the same phenomena are generated in various spot and finally will be accumulated, thus reduce the stability of the blast furnace. While most studies that already conducted by some researches are in macro scale, the study on this kind of interaction in micro scale is still lack. Analysis on the narrowest filling layer inside the blast furnace by using adjacent three spheres of the inter-particle flow path in the packed bed, where the possibility of blockage to occur was conducted. Gas-powder in an orifice composed of spherical coarse particles using a hybrid analysis method that combines the discrete element method (DEM) for powder particles and computational fluid dynamic (CFD) for the fluids that pass through the interstices of the particles. The following results were obtained. The airflow that flows in from the bottom of the equilateral triangle region at a uniform velocity causes the flow velocity to rise sharply at the narrowest part of the orifice, while also in the contrary increase the pressure drop inside the system and affects the motion and prolonged the passage time of the powder particles due to the fluid resistance. For multiple fine particles case, Remarkable fluctuations of the pressure drop occurred since the beginning of the dropping process of fine particles. This phenomenon occurred because the possibilities of fine particle bounce and obstructing the aperture area above the orifice is higher due to the existence of larger amounts of particles.

III. The flow stress of SUS821L1 at various temperatures (293 K, 273 K, 253 K, 233 K) coupling with quasi-static and impact tensile already being performed. It was found that the strain rate sensitivity at 293 K is higher compare to the other test temperatures, shows the declining strain rate sensitivity in low temperature.

At quasi-static the transformation induced plasticity (TRIP) effect take a major role in flow stress while being hindered at impact tensile due to the adiabatic heating, as already reported by various researches. The temperature sensitivity shows a positive value in quasi-static tensile and the gradient of sensitivity is increasing with temperature increases. Meanwhile, at impact tensile the temperature sensitivity is higher compare to the quasi-static when the temperature lowered from 293 K to 273 K but, continue to decrease with further temperature decrease and even reached negative value, corresponds with thermally activated dislocation motion theory that already been reported in previous studies. From the fractography analysis, the large, round, and deep dimple can be observed during quasi-static tensile. Qualitatively, the deepest dimples surrounded by much more finer dimples occurred at 273 K, which corresponds with the longest elongation at this case. After that the big dimple seems to shrink and the depth also decrease with further temperature decrease. This kind of phenomena corresponds with the increasing flow stress and the decreasing of the elongation. At impact tensile, the dimple shape become irregular and shallower. With temperature decrease the dimple become shallower. This indicates the martensitic phase that generated at low temperature become rupture and collapse into the ferritic phase. This kind of occurrence can explain the phenomena of sudden elongation abridgement of SUS821L1 when the strain rate transforms from quasi-static to impact tensile, and further decreases in elongation when temperature continue to decrease.

APPENDIX

SOURCE CODE

Case 1 dp/Dp = 0.133 Uf = 0.88 m/s

```
# version 2015.05.14_tmp
# Reading Session=I:¥andrey¥particle¥4 phase diff K¥pre.his
menu:    point/generate;
pmenu: total no. = 5,
          coord = 1, component = 0, 0, 0,
          coord = 1, component = 0, 0.02, 0,
          coord = 1, component = 0, 0.05, 0.05196,
          coord = 1, component = 0, 0.05, 0.58196,
          coord = 1, component = 0, 0, 0.58196;
max no. (p,l,s,v,b):       5,       0,       0,       0,       0;;

menu:    point/generate;
pmenu: total no. = 1,
          coord = 1, component = 0, 0, 0.05196;
max no. (p,l,s,v,b):       6,       0,       0,       0,       0;;

menu:    line/generate/line;
click: total no. = 4,
          no. of point = 2, point = 1, 2,
          no. of point = 2, point = 2, 3,
          no. of point = 2, point = 3, 6,
          no. of point = 2, point = 6, 1;
max no. (p,l,s,v,b):       6,       4,       0,       0,       0;;

menu:    line/generate/line;
click: total no. = 3,
          no. of point = 2, point = 3, 4,
          no. of point = 2, point = 4, 5,
          no. of point = 2, point = 5, 6;
max no. (p,l,s,v,b):       6,       7,       0,       0,       0;;

menu:    surface/generate/manual;
click: no. of line = 4, line = 6, 5, 7, 3;
max no. (p,l,s,v,b):       6,       7,       1,       0,       0;;
```

menu: surface/generate/manual;
click: no. of line = 4, line = 3, 2, 1, 4;
max no. (p,l,s,v,b): 6, 7, 2, 0, 0;;

menu: surface/copy/rotate;
click: total no. of surface = 0;
pmenu: select = trajectory/on, center point = 0, 0, 0, axis vector = 0, 0, 1,
angle = 360, height = 0,
no. of copies = 1;
max no. (p,l,s,v,b): 6, 13, 9, 2, 0;;

menu: line/grid(cont)/on single line;
click: total no. = 1, line = 8;
pmenu: select = division ratio copy / on, num = 42, start = 1, end = 1;
max no. (p,l,s,v,b): 6, 13, 9, 2, 0;;

menu: line/grid(cont)/on single line;
click: total no. = 1, line = 6;
pmenu: select = division ratio copy / on, num = 12, start = 1, end = 1;
max no. (p,l,s,v,b): 6, 13, 9, 2, 0;;

menu: line/grid(cont)/on single line;
click: total no. = 1, line = 7;
pmenu: select = division ratio copy / on, num = 145, start = 1, end = 1;
max no. (p,l,s,v,b): 6, 13, 9, 2, 0;;

menu: line/grid(end)/on single line;
click: total no. = 1, line = 4;
pmenu: select = division ratio copy / on, num = 132, start = 1, end = 1;
max no. (p,l,s,v,b): 6, 13, 9, 2, 0;;

menu: line/grid/on single line;
click: total no. = 1, line = 2;
pmenu: select = division ratio copy / on, num = 13, start = 1, end = 1;
max no. (p,l,s,v,b): 6, 13, 9, 2, 0;;

menu: block/generate/auto;
click: total no. = 1, total no. of volume = 0;

```
max no. (p,l,s,v,b):       6,     13,       9,       2,       1;;

menu:    block/set ibctyp;
click: total no. = 1, block = 1, index = 4;
pmenu: value = 4;
max no. (p,l,s,v,b):       6,     13,       9,       2,       1;;

menu:    block/set ibctyp;
click: total no. = 1, block = 1, index = 5;
pmenu: value = 3;
max no. (p,l,s,v,b):       6,     13,       9,       2,       1;;

menu:    block/set ibctyp;
click: total no. = 1, block = 1, index = 3;
pmenu: value = 9;
max no. (p,l,s,v,b):       6,     13,       9,       2,       1;;

menu:    physical variable/set value/flow velocity;
click: total no. = 1, block = 1,
          no. of mesh_range = 1, mesh range = 0,-1,0,-1,-1,-1;
pmenu: select = velocity(x), value = 0, 0, 2.38;
max no. (p,l,s,v,b):       6,     13,       9,       2,       1;;

menu:    physical variable/set value/flow velocity;
click: total no. = 1, block = 1,
          no. of mesh_range = 1, mesh range = 0,-1,0,-1,-1,-1;
pmenu: select = velocity(x), value = 0, 0, 6.6;
max no. (p,l,s,v,b):       6,     13,       9,       2,       1;;

menu:    physical variable/set value/in cell;
click: total no. = 1, block = 1,
          no. of mesh_range = 1, mesh range = 1,-1,1,-1,1,-1;
pmenu: select = alpha, no = 1, value = 0.8;
max no. (p,l,s,v,b):       6,     13,       9,       2,       1;;

menu:    physical variable/set value/flow velocity;
click: total no. = 1, block = 1,
          no. of mesh_range = 1, mesh range = 0,-1,0,-1,-1,-1;
```

```
pmenu: select = velocity(x), value = 0, 0, 1.7;
max no. (p,l,s,v,b):       6,      13,       9,       2,       1;;

menu:    physical variable/set value/in cell;
click: total no. = 1, block = 1,
          no. of mesh_range = 1, mesh range = 1,-1,1,-1,1,-1;
pmenu: select = alpha, no = 1, value = 0.2;
max no. (p,l,s,v,b):       6,      13,       9,       2,       1;;

menu:    physical variable/set value/in cell;
click: total no. = 1, block = 1,
          no. of mesh_range = 1, mesh range = 1,-1,1,-1,1,-1;
pmenu: select = alpha, no = 1, value = 0;
max no. (p,l,s,v,b):       6,      13,       9,       2,       1;;

menu:    physical variable/set value/flow velocity;
click: total no. = 1, block = 1,
          no. of mesh_range = 1, mesh range = 0,-1,0,-1,-1,-1;
pmenu: select = velocity(x), value = 0, 0, 0;
max no. (p,l,s,v,b):       6,      13,       9,       2,       1;;

menu:    physical variable/set value/flow velocity;
click: total no. = 1, block = 1,
          no. of mesh_range = 1, mesh range = 0,-1,0,-1,-1,-1;
pmenu: select = velocity(x), value = 0, 0, 6.6;
max no. (p,l,s,v,b):       6,      13,       9,       2,       1;;

menu:    parameter/particle/generate;
pmenu: kmark = 1, density = 0, diameter = 0,
          coord = 1, start = -0.044,-0.044,0, end = 0.044,0.044,0.025,
          number = 5,5,5;
max no. (p,l,s,v,b):       6,      13,       9,       2,       1;;

menu:    parameter/particle/generate;
pmenu: kmark = 2, density = 0, diameter = 0,
          coord = 1, start = -0.046,-0.046,0.025, end = 0.046,0.046,0.145,
          number = 12,12,15;
max no. (p,l,s,v,b):       6,      13,       9,       2,       1;;
```

```
menu:    parameter/particle/generate;
pmenu: kmark = 3, density = 0, diameter = 0,
          coord = 1, start = -0.0478,-0.0478,0.145, end = 0.0478,0.0478,0.5,
          number = 40,40,80;
max no. (p,l,s,v,b):       6,      13,       9,       2,       1;;

menu:    parameter/particle/generate;
pmenu: kmark = 4, density = 0, diameter = 0,
          coord = 1, start = -0.049806,0.049806,0.145, end = 0.049806,0.049806,
          0.5, number = 39,1,915;
max no. (p,l,s,v,b):       6,      13,       9,       2,       1;;

menu:    parameter/particle/generate;
pmenu: kmark = 1, density = 0, diameter = 0,
          coord = 1, start = -0.044,-0.044,0, end = 0.044,0.044,0.019,
          number = 6,6,6;
max no. (p,l,s,v,b):       6,      13,       9,       2,       1;;

menu:    parameter/particle/generate;
pmenu: kmark = 2, density = 0, diameter = 0,
          coord = 1, start = -0.046,-0.046,0.023, end = 0.046,0.046,0.141,
          number = 16,16,16;
max no. (p,l,s,v,b):       6,      13,       9,       2,       1;;

menu:    parameter/particle/generate;
pmenu: kmark = 3, density = 0, diameter = 0,
          coord = 1, start = -0.0478,-0.0478,0.1432, end = 0.0478,0.0478,0.5,
          number = 40,40,81;
max no. (p,l,s,v,b):       6,      13,       9,       2,       1;;

menu:    parameter/particle/generate;
pmenu: kmark = 4, density = 0, diameter = 0,
          coord = 1, start = -0.049806,-0.049806,0.49, end = 0.049806,0.049806,
          0.5, number = 453,453,10;
max no. (p,l,s,v,b):       6,      13,       9,       2,       1;;

menu:    parameter/particle/generate;
```

```
pmenu: kmark = 2, density = 0, diameter = 0,
        coord = 1, start = -0.046,-0.046,0.3, end = 0.046,0.046,0.5,
        number = 16,16,1;
max no. (p,l,s,v,b):      6,     13,      9,      2,      1;;

menu:   physical variable/set value/flow velocity;
click: total no. = 1, block = 1,
        no. of mesh_range = 1, mesh range = 0,-1,0,-1,0,-1;
pmenu: select = velocity(x), value = 0, 0, 0;
max no. (p,l,s,v,b):      6,     13,      9,      2,      1;;

menu:   parameter/acceleration;
pmenu: g = 0, 0, -9.806, bf = 0, 0, 0, rotate0 = 0, rot_p = 0, 0, 0,
        rot_v = 0, 0, 1;
max no. (p,l,s,v,b):      6,     13,      9,      2,      1;;

menu:   parameter/particle/generate;
pmenu: kmark = 0, density = 0, diameter = 0,
        coord = 1, start = -0.042,-0.042,0.3, end = 0.042,0.042,0.42,
        number = 15,15,15;
max no. (p,l,s,v,b):      6,     13,      9,      2,      1;;

menu:   parameter/particle/generate;
pmenu: kmark = 2, density = 0, diameter = 0,
        coord = 1, start = -0.046,-0.046,0.3, end = 0.046,0.046,0.3,
        number = 15,15,1;
max no. (p,l,s,v,b):      6,     13,      9,      2,      1;;

menu:   parameter/particle/generate;
pmenu: kmark = 3, density = 0, diameter = 0,
        coord = 1, start = -0.047,-0.047,0.55, end = 0.047,0.047,0.56,
        number = 24,24,2;
max no. (p,l,s,v,b):      6,     13,      9,      2,      1;;

menu:   parameter/particle/delete;
max no. (p,l,s,v,b):      6,     13,      9,      2,      1;;

menu:   physical variable/set value/flow velocity;
```

```
click: total no. = 1, block = 1,
        no. of mesh_range = 1, mesh range = 0,0,0,-1,0,-1;
pmenu: select = velocity(x), value = 0, 0, -5;
max no. (p,l,s,v,b):      6,     13,      9,      2,      1;;

menu:   physical variable/set value/flow velocity;
click: total no. = 1, block = 1,
        no. of mesh_range = 1, mesh range = 0,-1,0,-1,0,-1;
pmenu: select = velocity(x), value = 0, 0, 0;
max no. (p,l,s,v,b):      6,     13,      9,      2,      1;;

menu:   physical variable/set value/flow velocity;
click: total no. = 1, block = 1,
        no. of mesh_range = 1, mesh range = 0,-1,0,-1,-1,-1;
pmenu: select = velocity(x), value = 0, 0, 0.88;
max no. (p,l,s,v,b):      6,     13,      9,      2,      1;;

menu:   physical variable/set value/flow velocity;
click: total no. = 1, block = 1,
        no. of mesh_range = 1, mesh range = 0,-1,0,-1,0,-1;
pmenu: select = velocity(x), value = 0, 0, 0;
max no. (p,l,s,v,b):      6,     13,      9,      2,      1;;

menu:   physical variable/set value/flow velocity;
click: total no. = 1, block = 1,
        no. of mesh_range = 1, mesh range = 0,-1,0,-1,-1,-1;
pmenu: select = velocity(x), value = 0, 0, 0.88;
max no. (p,l,s,v,b):      6,     13,      9,      2,      1;;

menu:   parameter/particle/generate;
pmenu: kmark = 4, density = 0, diameter = 0,
        coord = 1, start = -0.0496,-0.0496,0.17196, end = 0.0496,0.0496,
        0.17196, number = 25,25,1;
max no. (p,l,s,v,b):      6,     13,      9,      2,      1;;

menu:   physical variable/set value/flow velocity;
click: total no. = 1, block = 1,
        no. of mesh_range = 1, mesh range = 0,-1,0,-1,0,-1;
```

```
pmenu: select = velocity(x), value = 0, 0, 0;
max no. (p,l,s,v,b):       6,      13,       9,       2,       1;;

menu:    physical variable/set value/flow velocity;
click: total no. = 1, block = 1,
          no. of mesh_range = 1, mesh range = 0,-1,0,-1,-1,-1;
pmenu: select = velocity(x), value = 0, 0, 6.6;
max no. (p,l,s,v,b):       6,      13,       9,       2,       1;;

menu:    physical variable/set value/flow velocity;
click: total no. = 1, block = 1,
          no. of mesh_range = 1, mesh range = 0,-1,0,-1,0,-1;
pmenu: select = velocity(x), value = 0, 0, 0;
max no. (p,l,s,v,b):       6,      13,       9,       2,       1;;

menu:    physical variable/set value/flow velocity;
click: total no. = 1, block = 1,
          no. of mesh_range = 1, mesh range = 0,-1,0,-1,-1,-1;
pmenu: select = velocity(x), value = 0, 0, 0.88;
max no. (p,l,s,v,b):       6,      13,       9,       2,       1;;

menu:    parameter/property;
pmenu: density = 1.2, sigma = 0;
max no. (p,l,s,v,b):       6,      13,       9,       2,       1;;

menu:    parameter/viscosity;
pmenu: viscosity = 1.8e-005, newton = 0, nvistemp = 0, uplowvis = 1e+020, 0,
          1e+020, 0, 1e+020, -273;
max no. (p,l,s,v,b):       6,      13,       9,       2,       1;;

menu:    physical variable/set value/flow velocity;
click: total no. = 1, block = 1,
          no. of mesh_range = 1, mesh range = 0,-1,0,-1,0,-1;
pmenu: select = velocity(x), value = 0, 0, 0;
max no. (p,l,s,v,b):       6,      13,       9,       2,       1;;

menu:    physical variable/set value/flow velocity;
click: total no. = 1, block = 1,
```

```
        no. of mesh_range = 1, mesh range = 0,-1,0,-1,-1,-1;
pmenu: select = velocity(x), value = 0, 0, 0.88;
max no. (p,l,s,v,b):      6,     13,      9,      2,      1;;

menu:   parameter/multi-phase flow;
pmenu: nphase = 4, idrift = 0, isdgsl = 0, iresta = 1, dtalph = 0,
        alpha(min) = 0, rgsl = 0.012, rhogsl = 7850, visco = 0, sftension = 0,
        vterm0 = 0, stokes = 3, nonstokes = 1.5, speh = 0, therco = 0,
        degx = 0, degy = 0, degz = 0, overx = 0, overy = 0, overz = 0,
        rgsl = 0.008, rhogsl = 7850, visco = 0, sftension = 0, vterm0 = 0,
        stokes = 3, nonstokes = 1.5, speh = 0, therco = 0, degx = 0, degy = 0,
        degz = 0, overx = 0, overy = 0, overz = 0, rgsl = 0.00448,
        rhogsl = 1106, visco = 0, sftension = 0, vterm0 = 0, stokes = 3,
        nonstokes = 1.5, speh = 0, therco = 0, degx = 0, degy = 0, degz = 0,
        overx = 0, overy = 0, overz = 0, rgsl = 0.000596, rhogsl = 1369,
        visco = 0, sftension = 0, vterm0 = 3.15, stokes = 3, nonstokes = 1.5,
        speh = 0, therco = 0, degx = 0, degy = 0, degz = 0, overx = 0,
        overy = 0, overz = 0;
max no. (p,l,s,v,b):      6,     13,      9,      2,      1;;

# End of Read Session=I:¥andrey¥particle¥4 phase diff K¥pre.his
menu:   parameter/control;
pmenu: title = , nousr = 0, istead = 0, iturb = 0, nmax = -1, tmax = 300,
        elapsed time(max) = 0, dt = 0.0001, couran = 0, irest = 1, iveloc = 1,
        istokes = 0, imvgrd = 1, imvgsc = 1;
max no. (p,l,s,v,b):      6,     13,      9,      2,      1;;

menu:   parameter/io;
pmenu: nintpo = 0, tintpo = 0.1, nowpost = 0, iwstrs = 0, iwchtr = 0,
        iwpost = 0, iwmean = 0, itypos = 0, nfview = 0, nintre = 0,
        iwrest = 0, ityres = 0, npower = 0, nforce = 0, iprint = 0,
        pre.file = pre.txt, restart.file = restart.bin;
max no. (p,l,s,v,b):      6,     13,      9,      2,      1;;

menu:   parameter/particle/control;
pmenu: nintpg = 0, tintpg = 1, nptscal = 0, irestp = 1, iturbp = 0,
        nptclmax = 0, nptgmax = 0, rclenwpt = 0, nptcompt = 0, plencopt = 0,
        ireversp = 0, nwphis = 1, nwptcl = 5, ityptcl = 1, nopts_wr = 1,
```

nopte_wr = -1, noptd_wr = 1, nwptwall = 0;
max no. (p,l,s,v,b): 6, 13, 9, 2, 1;;

menu: parameter/dem/basic settings;
pmenu: idem = 1, idemrot = 0, idemiof = -1, sprcn = 4000, sprct = 0,
rescn = 0.5, resct = -1, fricc = 0.7, friccw = 0.7, rsrohnrp = 0,
ndtfdem = 1, rdpdem = 1, rdpcont = 1, chtrpp = 0, chtrpw = 0,
chtrpf = -1, idemcoh = 0;
max no. (p,l,s,v,b): 6, 13, 9, 2, 1;;

Case 2 dp/Dp = 0.149 Uf = 0.88 m/s (no additional bed)

version 2015.05.14_tmp
Reading Session=I:¥andrey¥particle¥2.6; 0.388¥新しいフォルダー¥normalizing¥flow inlet¥fines charging¥pre.his
menu: point/generate;
pmenu: total no. = 5,
coord = 1, component = 0, 0, 0,
coord = 1, component = 0, 0.02, 0,
coord = 1, component = 0, 0.05, 0.05196,
coord = 1, component = 0, 0.05, 0.58196,
coord = 1, component = 0, 0, 0.58196;
max no. (p,l,s,v,b): 5, 0, 0, 0, 0;;

menu: point/generate;
pmenu: total no. = 1,
coord = 1, component = 0, 0, 0.05196;
max no. (p,l,s,v,b): 6, 0, 0, 0, 0;;

menu: line/generate/line;
click: total no. = 4,
no. of point = 2, point = 1, 2,
no. of point = 2, point = 2, 3,
no. of point = 2, point = 3, 6,
no. of point = 2, point = 6, 1;
max no. (p,l,s,v,b): 6, 4, 0, 0, 0;;

menu: line/generate/line;
click: total no. = 3,
no. of point = 2, point = 3, 4,
no. of point = 2, point = 4, 5,
no. of point = 2, point = 5, 6;
max no. (p,l,s,v,b): 6, 7, 0, 0, 0;;

menu: surface/generate/manual;
click: no. of line = 4, line = 6, 5, 7, 3;
max no. (p,l,s,v,b): 6, 7, 1, 0, 0;;

menu: surface/generate/manual;
click: no. of line = 4, line = 3, 2, 1, 4;
max no. (p,l,s,v,b): 6, 7, 2, 0, 0;;

menu: surface/copy/rotate;
click: total no. of surface = 0;
pmenu: select = trajectory/on, center point = 0, 0, 0, axis vector = 0, 0, 1,
angle = 360, height = 0,
no. of copies = 1;
max no. (p,l,s,v,b): 6, 13, 9, 2, 0;;

menu: line/grid(cont)/on single line;
click: total no. = 1, line = 8;
pmenu: select = division ratio copy / on, num = 42, start = 1, end = 1;
max no. (p,l,s,v,b): 6, 13, 9, 2, 0;;

menu: line/grid(cont)/on single line;
click: total no. = 1, line = 6;
pmenu: select = division ratio copy / on, num = 12, start = 1, end = 1;

max no. (p,l,s,v,b): 6, 13, 9, 2, 0;;

menu: line/grid(cont)/on single line;
click: total no. = 1, line = 7;
pmenu: select = division ratio copy / on, num = 145, start = 1, end = 1;
max no. (p,l,s,v,b): 6, 13, 9, 2, 0;;

menu: line/grid(end)/on single line;
click: total no. = 1, line = 4;
pmenu: select = division ratio copy / on, num = 132, start = 1, end = 1;
max no. (p,l,s,v,b): 6, 13, 9, 2, 0;;

menu: line/grid/on single line;
click: total no. = 1, line = 2;
pmenu: select = division ratio copy / on, num = 13, start = 1, end = 1;
max no. (p,l,s,v,b): 6, 13, 9, 2, 0;;

menu: block/generate/auto;
click: total no. = 1, total no. of volume = 0;
max no. (p,l,s,v,b): 6, 13, 9, 2, 1;;

menu: block/set ibctyp;
click: total no. = 1, block = 1, index = 4;
pmenu: value = 4;
max no. (p,l,s,v,b): 6, 13, 9, 2, 1;;

menu: block/set ibctyp;
click: total no. = 1, block = 1, index = 5;
pmenu: value = 3;
max no. (p,l,s,v,b): 6, 13, 9, 2, 1;;

menu: block/set ibctyp;
click: total no. = 1, block = 1, index = 3;
pmenu: value = 9;
max no. (p,l,s,v,b): 6, 13, 9, 2, 1;;

menu: physical variable/set value/flow velocity;
click: total no. = 1, block = 1,

no. of mesh_range = 1, mesh range = 0,-1,0,-1,-1,-1;
pmenu: select = velocity(x), value = 0, 0, 2.38;
max no. (p,l,s,v,b): 6, 13, 9, 2, 1;;

menu: physical variable/set value/flow velocity;
click: total no. = 1, block = 1,
no. of mesh_range = 1, mesh range = 0,-1,0,-1,-1,-1;
pmenu: select = velocity(x), value = 0, 0, 6.6;
max no. (p,l,s,v,b): 6, 13, 9, 2, 1;;

menu: physical variable/set value/in cell;
click: total no. = 1, block = 1,
no. of mesh_range = 1, mesh range = 1,-1,1,-1,1,-1;
pmenu: select = alpha, no = 1, value = 0.8;
max no. (p,l,s,v,b): 6, 13, 9, 2, 1;;

menu: physical variable/set value/flow velocity;
click: total no. = 1, block = 1,
no. of mesh_range = 1, mesh range = 0,-1,0,-1,-1,-1;
pmenu: select = velocity(x), value = 0, 0, 1.7;
max no. (p,l,s,v,b): 6, 13, 9, 2, 1;;

menu: physical variable/set value/in cell;
click: total no. = 1, block = 1,
no. of mesh_range = 1, mesh range = 1,-1,1,-1,1,-1;
pmenu: select = alpha, no = 1, value = 0.2;
max no. (p,l,s,v,b): 6, 13, 9, 2, 1;;

menu: physical variable/set value/in cell;
click: total no. = 1, block = 1,
no. of mesh_range = 1, mesh range = 1,-1,1,-1,1,-1;
pmenu: select = alpha, no = 1, value = 0;
max no. (p,l,s,v,b): 6, 13, 9, 2, 1;;

menu: physical variable/set value/flow velocity;
click: total no. = 1, block = 1,
no. of mesh_range = 1, mesh range = 0,-1,0,-1,-1,-1;
pmenu: select = velocity(x), value = 0, 0, 0;

```
max no. (p,l,s,v,b):       6,      13,       9,       2,       1;;

menu:    physical variable/set value/flow velocity;
click: total no. = 1, block = 1,
          no. of mesh_range = 1, mesh range = 0,-1,0,-1,-1,-1;
pmenu: select = velocity(x), value = 0, 0, 6.6;
max no. (p,l,s,v,b):       6,      13,       9,       2,       1;;

menu:    parameter/particle/generate;
pmenu: kmark = 1, density = 0, diameter = 0,
          coord = 1, start = -0.044,-0.044,0, end = 0.044,0.044,0.025,
          number = 5,5,5;
max no. (p,l,s,v,b):       6,      13,       9,       2,       1;;

menu:    parameter/particle/generate;
pmenu: kmark = 2, density = 0, diameter = 0,
          coord = 1, start = -0.046,-0.046,0.025, end = 0.046,0.046,0.145,
          number = 12,12,15;
max no. (p,l,s,v,b):       6,      13,       9,       2,       1;;

menu:    parameter/particle/generate;
pmenu: kmark = 3, density = 0, diameter = 0,
          coord = 1, start = -0.0478,-0.0478,0.145, end = 0.0478,0.0478,0.5,
          number = 40,40,80;
max no. (p,l,s,v,b):       6,      13,       9,       2,       1;;

menu:    parameter/particle/generate;
pmenu: kmark = 4, density = 0, diameter = 0,
          coord = 1, start = -0.049806,0.049806,0.145, end = 0.049806,0.049806,
          0.5, number = 39,1,915;
max no. (p,l,s,v,b):       6,      13,       9,       2,       1;;

menu:    parameter/particle/generate;
pmenu: kmark = 1, density = 0, diameter = 0,
          coord = 1, start = -0.044,-0.044,0, end = 0.044,0.044,0.019,
          number = 6,6,6;
max no. (p,l,s,v,b):       6,      13,       9,       2,       1;;
```

menu: parameter/particle/generate;
pmenu: kmark = 2, density = 0, diameter = 0,
coord = 1, start = -0.046,-0.046,0.023, end = 0.046,0.046,0.141,
number = 16,16,16;
max no. (p,l,s,v,b): 6, 13, 9, 2, 1;;

menu: parameter/particle/generate;
pmenu: kmark = 3, density = 0, diameter = 0,
coord = 1, start = -0.0478,-0.0478,0.1432, end = 0.0478,0.0478,0.5,
number = 40,40,81;
max no. (p,l,s,v,b): 6, 13, 9, 2, 1;;

menu: parameter/particle/generate;
pmenu: kmark = 4, density = 0, diameter = 0,
coord = 1, start = -0.049806,-0.049806,0.49, end = 0.049806,0.049806,
0.5, number = 453,453,10;
max no. (p,l,s,v,b): 6, 13, 9, 2, 1;;

menu: parameter/particle/generate;
pmenu: kmark = 2, density = 0, diameter = 0,
coord = 1, start = -0.046,-0.046,0.3, end = 0.046,0.046,0.5,
number = 16,16,1;
max no. (p,l,s,v,b): 6, 13, 9, 2, 1;;

menu: physical variable/set value/flow velocity;
click: total no. = 1, block = 1,
no. of mesh_range = 1, mesh range = 0,-1,0,-1,0,-1;
pmenu: select = velocity(x), value = 0, 0, 0;
max no. (p,l,s,v,b): 6, 13, 9, 2, 1;;

menu: parameter/property;
pmenu: density = 1.2, sigma = 0;
max no. (p,l,s,v,b): 6, 13, 9, 2, 1;;

menu: parameter/acceleration;
pmenu: g = 0, 0, -9.806, bf = 0, 0, 0, rotate0 = 0, rot_p = 0, 0, 0,
rot_v = 0, 0, 1;
max no. (p,l,s,v,b): 6, 13, 9, 2, 1;;

```
menu:    parameter/viscosity;
pmenu: viscosity = 1.8e-005, newton = 0, nvistemp = 0, uplowvis = 1e+020, 0,
          1e+020, 0, 1e+020, -273;
max no. (p,l,s,v,b):       6,     13,       9,       2,       1;;

menu:    parameter/particle/generate;
pmenu: kmark = 0, density = 0, diameter = 0,
          coord = 1, start = -0.042,-0.042,0.3, end = 0.042,0.042,0.42,
          number = 15,15,15;
max no. (p,l,s,v,b):       6,     13,       9,       2,       1;;

menu:    parameter/particle/generate;
pmenu: kmark = 2, density = 0, diameter = 0,
          coord = 1, start = -0.046,-0.046,0.3, end = 0.046,0.046,0.3,
          number = 15,15,1;
max no. (p,l,s,v,b):       6,     13,       9,       2,       1;;

menu:    parameter/particle/generate;
pmenu: kmark = 3, density = 0, diameter = 0,
          coord = 1, start = -0.047,-0.047,0.55, end = 0.047,0.047,0.56,
          number = 24,24,2;
max no. (p,l,s,v,b):       6,     13,       9,       2,       1;;

menu:    parameter/particle/generate;
pmenu: kmark = 3, density = 0, diameter = 0,
          coord = 1, start = -0.048,-0.048,0.55, end = 0.048,0.048,0.5526,
          number = 40,40,2;
max no. (p,l,s,v,b):       6,     13,       9,       2,       1;;

menu:    parameter/particle/delete;
max no. (p,l,s,v,b):       6,     13,       9,       2,       1;;

menu:    physical variable/set value/flow velocity;
click: total no. = 1, block = 1,
          no. of mesh_range = 1, mesh range = 0,-1,0,-1,-1,-1;
pmenu: select = velocity(x), value = 0, 0, 0.88;
max no. (p,l,s,v,b):       6,     13,       9,       2,       1;;
```

End of Read Session=I:¥andrey¥particle¥2.6; 0.388¥新しいフォルダー¥normalizing¥flow inlet¥fines charging¥pre.his
menu: parameter/multi-phase flow;
pmenu: nphase = 4, idrift = 0, isdgsl = 0, iresta = 1, dtalph = 0,
alpha(min) = 0, rgsl = 0.012, rhogsl = 7850, visco = 0, sftension = 0,
vterm0 = 0, stokes = 3, nonstokes = 1.5, speh = 0, therco = 0,
degx = 0, degy = 0, degz = 0, overx = 0, overy = 0, overz = 0,
rgsl = 0.008, rhogsl = 7850, visco = 0, sftension = 0, vterm0 = 0,
stokes = 3, nonstokes = 1.5, speh = 0, therco = 0, degx = 0, degy = 0,
degz = 0, overx = 0, overy = 0, overz = 0, rgsl = 0.0026,
rhogsl = 1500, visco = 0, sftension = 0, vterm0 = 0, stokes = 3,
nonstokes = 1.5, speh = 0, therco = 0, degx = 0, degy = 0, degz = 0,
overx = 0, overy = 0, overz = 0, rgsl = 0.000388, rhogsl = 1369,
visco = 0, sftension = 0, vterm0 = 2.06, stokes = 3, nonstokes = 1.5,
speh = 0, therco = 0, degx = 0, degy = 0, degz = 0, overx = 0,
overy = 0, overz = 0;
max no. (p,l,s,v,b): 6, 13, 9, 2, 1;;

menu: parameter/dem/basic settings;
pmenu: idem = 1, idemrot = 0, idemiof = -1, sprcn = 4000, sprct = 0,
rescn = 0.5, resct = -1, fricc = 0.7, friccw = 0.7, rsrohnrp = 0,
ndtfdem = 1, rdpdem = 1, rdpcont = 1, chtrpp = 0, chtrpw = 0,
chtrpf = -1, idemcoh = 0;
max no. (p,l,s,v,b): 6, 13, 9, 2, 1;;

menu: parameter/particle/generate;
pmenu: kmark = 4, density = 0, diameter = 0,
coord = 1, start = -0.0498,-0.0498,0.17196, end = 0.0498,0.0498,
0.17196, number = 45,45,1;
max no. (p,l,s,v,b): 6, 13, 9, 2, 1;;

menu: parameter/particle/control;
pmenu: nintpg = 0, tintpg = 1, nptscal = 0, irestp = 1, iturbp = 0,
nptclmax = 0, nptgmax = 0, rclenwpt = 0, nptcompt = 0, plencopt = 0,
ireversp = 0, nwphis = 1, nwptcl = 5, ityptcl = 1, nopts_wr = 1,
nopte_wr = -1, noptd_wr = 1, nwptwall = 0;
max no. (p,l,s,v,b): 6, 13, 9, 2, 1;;

menu: parameter/control;
pmenu: title = , nousr = 0, istead = 0, iturb = 0, nmax = -1, tmax = 200,
        elapsed time(max) = 0, dt = 0.0001, couran = 0, irest = 1, iveloc = 1,
        istokes = 0, imvgrd = 1, imvgsc = 1;
max no. (p,l,s,v,b): 6, 13, 9, 2, 1;;

menu: parameter/io;
pmenu: nintpo = 0, tintpo = 0.1, nowpost = 0, iwstrs = 0, iwchtr = 0,
        iwpost = 0, iwmean = 0, itypos = 0, nfview = 0, nintre = 0,
        iwrest = 0, ityres = 0, npower = 0, nforce = 0, iprint = 0,
        pre.file = pre.txt, restart.file = restart.bin;
max no. (p,l,s,v,b): 6, 13, 9, 2, 1;;

Case 3 dp/Dp = 0.162 Uf = 0.88 m/s

version 2015.05.14_tmp
Reading Session=I:¥andrey¥particle¥3.68¥next 3.68¥0.596 charging¥new¥新しいフォルダー¥pre.his
menu: point/generate;
pmenu: total no. = 5,
        coord = 1, component = 0, 0, 0,
        coord = 1, component = 0, 0.02, 0,
        coord = 1, component = 0, 0.05, 0.05196,
        coord = 1, component = 0, 0.05, 0.58196,
        coord = 1, component = 0, 0, 0.58196;
max no. (p,l,s,v,b): 5, 0, 0, 0, 0;;

menu: point/generate;
pmenu: total no. = 1,
        coord = 1, component = 0, 0, 0.05196;
max no. (p,l,s,v,b): 6, 0, 0, 0, 0;;

menu: line/generate/line;
click: total no. = 4,
        no. of point = 2, point = 1, 2,

```
        no. of point = 2, point = 2, 3,
        no. of point = 2, point = 3, 6,
        no. of point = 2, point = 6, 1;
max no. (p,l,s,v,b):      6,      4,      0,      0,      0;;

menu:   line/generate/line;
click: total no. = 3,
        no. of point = 2, point = 3, 4,
        no. of point = 2, point = 4, 5,
        no. of point = 2, point = 5, 6;
max no. (p,l,s,v,b):      6,      7,      0,      0,      0;;

menu:   surface/generate/manual;
click: no. of line = 4, line = 6, 5, 7, 3;
max no. (p,l,s,v,b):      6,      7,      1,      0,      0;;

menu:   surface/generate/manual;
click: no. of line = 4, line = 3, 2, 1, 4;
max no. (p,l,s,v,b):      6,      7,      2,      0,      0;;

menu:   surface/copy/rotate;
click: total no. of surface = 0;
pmenu: select = trajectory/on, center point = 0, 0, 0, axis vector = 0, 0, 1,
        angle = 360, height = 0,
        no. of copies = 1;
max no. (p,l,s,v,b):      6,     13,      9,      2,      0;;

menu:   line/grid(cont)/on single line;
click: total no. = 1, line = 8;
pmenu: select = division ratio copy / on, num = 42, start = 1, end = 1;
max no. (p,l,s,v,b):      6,     13,      9,      2,      0;;

menu:   line/grid(cont)/on single line;
click: total no. = 1, line = 6;
pmenu: select = division ratio copy / on, num = 12, start = 1, end = 1;
max no. (p,l,s,v,b):      6,     13,      9,      2,      0;;

menu:   line/grid(cont)/on single line;
```

```
click: total no. = 1, line = 7;
pmenu: select = division ratio copy / on, num = 145, start = 1, end = 1;
max no. (p,l,s,v,b):       6,     13,       9,       2,       0;;

menu:    line/grid(end)/on single line;
click: total no. = 1, line = 4;
pmenu: select = division ratio copy / on, num = 132, start = 1, end = 1;
max no. (p,l,s,v,b):       6,     13,       9,       2,       0;;

menu:    line/grid/on single line;
click: total no. = 1, line = 2;
pmenu: select = division ratio copy / on, num = 13, start = 1, end = 1;
max no. (p,l,s,v,b):       6,     13,       9,       2,       0;;

menu:    block/generate/auto;
click: total no. = 1, total no. of volume = 0;
max no. (p,l,s,v,b):       6,     13,       9,       2,       1;;

menu:    block/set ibctyp;
click: total no. = 1, block = 1, index = 4;
pmenu: value = 4;
max no. (p,l,s,v,b):       6,     13,       9,       2,       1;;

menu:    block/set ibctyp;
click: total no. = 1, block = 1, index = 5;
pmenu: value = 3;
max no. (p,l,s,v,b):       6,     13,       9,       2,       1;;

menu:    block/set ibctyp;
click: total no. = 1, block = 1, index = 3;
pmenu: value = 9;
max no. (p,l,s,v,b):       6,     13,       9,       2,       1;;

menu:    physical variable/set value/flow velocity;
click: total no. = 1, block = 1,
          no. of mesh_range = 1, mesh range = 0,-1,0,-1,-1,-1;
pmenu: select = velocity(x), value = 0, 0, 2.38;
max no. (p,l,s,v,b):       6,     13,       9,       2,       1;;
```

menu: physical variable/set value/flow velocity;
click: total no. = 1, block = 1,
        no. of mesh_range = 1, mesh range = 0,-1,0,-1,-1,-1;
pmenu: select = velocity(x), value = 0, 0, 6.6;
max no. (p,l,s,v,b): 6, 13, 9, 2, 1;;

menu: physical variable/set value/in cell;
click: total no. = 1, block = 1,
        no. of mesh_range = 1, mesh range = 1,-1,1,-1,1,-1;
pmenu: select = alpha, no = 1, value = 0.8;
max no. (p,l,s,v,b): 6, 13, 9, 2, 1;;

menu: physical variable/set value/flow velocity;
click: total no. = 1, block = 1,
        no. of mesh_range = 1, mesh range = 0,-1,0,-1,-1,-1;
pmenu: select = velocity(x), value = 0, 0, 1.7;
max no. (p,l,s,v,b): 6, 13, 9, 2, 1;;

menu: physical variable/set value/in cell;
click: total no. = 1, block = 1,
        no. of mesh_range = 1, mesh range = 1,-1,1,-1,1,-1;
pmenu: select = alpha, no = 1, value = 0.2;
max no. (p,l,s,v,b): 6, 13, 9, 2, 1;;

menu: physical variable/set value/in cell;
click: total no. = 1, block = 1,
        no. of mesh_range = 1, mesh range = 1,-1,1,-1,1,-1;
pmenu: select = alpha, no = 1, value = 0;
max no. (p,l,s,v,b): 6, 13, 9, 2, 1;;

menu: physical variable/set value/flow velocity;
click: total no. = 1, block = 1,
        no. of mesh_range = 1, mesh range = 0,-1,0,-1,-1,-1;
pmenu: select = velocity(x), value = 0, 0, 0;
max no. (p,l,s,v,b): 6, 13, 9, 2, 1;;

menu: physical variable/set value/flow velocity;

```
click: total no. = 1, block = 1,
        no. of mesh_range = 1, mesh range = 0,-1,0,-1,-1,-1;
pmenu: select = velocity(x), value = 0, 0, 6.6;
max no. (p,l,s,v,b):      6,     13,      9,      2,      1;;

menu:   parameter/particle/generate;
pmenu: kmark = 1, density = 0, diameter = 0,
        coord = 1, start = -0.044,-0.044,0, end = 0.044,0.044,0.025,
        number = 5,5,5;
max no. (p,l,s,v,b):      6,     13,      9,      2,      1;;

menu:   parameter/particle/generate;
pmenu: kmark = 2, density = 0, diameter = 0,
        coord = 1, start = -0.046,-0.046,0.025, end = 0.046,0.046,0.145,
        number = 12,12,15;
max no. (p,l,s,v,b):      6,     13,      9,      2,      1;;

menu:   parameter/particle/generate;
pmenu: kmark = 3, density = 0, diameter = 0,
        coord = 1, start = -0.0478,-0.0478,0.145, end = 0.0478,0.0478,0.5,
        number = 40,40,80;
max no. (p,l,s,v,b):      6,     13,      9,      2,      1;;

menu:   parameter/particle/generate;
pmenu: kmark = 4, density = 0, diameter = 0,
        coord = 1, start = -0.049806,0.049806,0.145, end = 0.049806,0.049806,
        0.5, number = 39,1,915;
max no. (p,l,s,v,b):      6,     13,      9,      2,      1;;

menu:   parameter/particle/generate;
pmenu: kmark = 1, density = 0, diameter = 0,
        coord = 1, start = -0.044,-0.044,0, end = 0.044,0.044,0.019,
        number = 6,6,6;
max no. (p,l,s,v,b):      6,     13,      9,      2,      1;;

menu:   parameter/particle/generate;
pmenu: kmark = 2, density = 0, diameter = 0,
        coord = 1, start = -0.046,-0.046,0.023, end = 0.046,0.046,0.141,
```

number = 16,16,16;
max no. (p,l,s,v,b): 6, 13, 9, 2, 1;;

menu: parameter/particle/generate;
pmenu: kmark = 3, density = 0, diameter = 0,
coord = 1, start = -0.0478,-0.0478,0.1432, end = 0.0478,0.0478,0.5,
number = 40,40,81;
max no. (p,l,s,v,b): 6, 13, 9, 2, 1;;

menu: parameter/particle/generate;
pmenu: kmark = 4, density = 0, diameter = 0,
coord = 1, start = -0.049806,-0.049806,0.49, end = 0.049806,0.049806,
0.5, number = 453,453,10;
max no. (p,l,s,v,b): 6, 13, 9, 2, 1;;

menu: parameter/particle/generate;
pmenu: kmark = 2, density = 0, diameter = 0,
coord = 1, start = -0.046,-0.046,0.3, end = 0.046,0.046,0.5,
number = 16,16,1;
max no. (p,l,s,v,b): 6, 13, 9, 2, 1;;

menu: physical variable/set value/flow velocity;
click: total no. = 1, block = 1,
no. of mesh_range = 1, mesh range = 0,-1,0,-1,0,-1;
pmenu: select = velocity(x), value = 0, 0, 0;
max no. (p,l,s,v,b): 6, 13, 9, 2, 1;;

menu: parameter/property;
pmenu: density = 1.2, sigma = 0;
max no. (p,l,s,v,b): 6, 13, 9, 2, 1;;

menu: parameter/acceleration;
pmenu: g = 0, 0, -9.806, bf = 0, 0, 0, rotate0 = 0, rot_p = 0, 0, 0,
rot_v = 0, 0, 1;
max no. (p,l,s,v,b): 6, 13, 9, 2, 1;;

menu: parameter/viscosity;
pmenu: viscosity = 1.8e-005, newton = 0, nvistemp = 0, uplowvis = 1e+020, 0,

```
        1e+020, 0, 1e+020, -273;
max no. (p,l,s,v,b):      6,     13,      9,      2,      1;;

menu:   parameter/particle/generate;
pmenu: kmark = 0, density = 0, diameter = 0,
        coord = 1, start = -0.042,-0.042,0.3, end = 0.042,0.042,0.42,
        number = 15,15,15;
max no. (p,l,s,v,b):      6,     13,      9,      2,      1;;

menu:   parameter/particle/generate;
pmenu: kmark = 2, density = 0, diameter = 0,
        coord = 1, start = -0.046,-0.046,0.3, end = 0.046,0.046,0.3,
        number = 15,15,1;
max no. (p,l,s,v,b):      6,     13,      9,      2,      1;;

menu:   parameter/particle/generate;
pmenu: kmark = 3, density = 0, diameter = 0,
        coord = 1, start = -0.047,-0.047,0.55, end = 0.047,0.047,0.56,
        number = 24,24,2;
max no. (p,l,s,v,b):      6,     13,      9,      2,      1;;

menu:   parameter/particle/delete;
max no. (p,l,s,v,b):      6,     13,      9,      2,      1;;

menu:   parameter/particle/generate;
pmenu: kmark = 4, density = 0, diameter = 0,
        coord = 1, start = -0.0496,-0.0496,0.17196, end = 0.0496,0.0496,
        0.17196, number = 25,25,1;
max no. (p,l,s,v,b):      6,     13,      9,      2,      1;;

menu:   physical variable/set value/flow velocity;
click: total no. = 1, block = 1,
        no. of mesh_range = 1, mesh range = 0,-1,0,-1,-1,-1;
pmenu: select = velocity(x), value = 0, 0, 0.88;
max no. (p,l,s,v,b):      6,     13,      9,      2,      1;;

menu:   parameter/io;
pmenu: nintpo = 0, tintpo = 0.1, nowpost = 0, iwstrs = 0, iwchtr = 0,
```

iwpost = 0, iwmean = 0, itypos = 0, nfview = 0, nintre = 0,
iwrest = 0, ityres = 0, npower = 0, nforce = 0, iprint = 0,
pre.file = pre.txt, restart.file = restart.bin;
max no. (p,l,s,v,b): 6, 13, 9, 2, 1;;

menu: parameter/multi-phase flow;
pmenu: nphase = 4, idrift = 0, isdgsl = 0, iresta = 1, dtalph = 0,
alpha(min) = 0, rgsl = 0.012, rhogsl = 7850, visco = 0, sftension = 0,
vterm0 = 0, stokes = 3, nonstokes = 1.5, speh = 0, therco = 0,
degx = 0, degy = 0, degz = 0, overx = 0, overy = 0, overz = 0,
rgsl = 0.008, rhogsl = 7850, visco = 0, sftension = 0, vterm0 = 0,
stokes = 3, nonstokes = 1.5, speh = 0, therco = 0, degx = 0, degy = 0,
degz = 0, overx = 0, overy = 0, overz = 0, rgsl = 0.00368,
rhogsl = 1732, visco = 0, sftension = 0, vterm0 = 0, stokes = 3,
nonstokes = 1.5, speh = 0, therco = 0, degx = 0, degy = 0, degz = 0,
overx = 0, overy = 0, overz = 0, rgsl = 0.000596, rhogsl = 1369,
visco = 0, sftension = 0, vterm0 = 3.15, stokes = 3, nonstokes = 1.5,
speh = 0, therco = 0, degx = 0, degy = 0, degz = 0, overx = 0,
overy = 0, overz = 0;
max no. (p,l,s,v,b): 6, 13, 9, 2, 1;;

menu: parameter/particle/control;
pmenu: nintpg = 0, tintpg = 1, nptscal = 0, irestp = 1, iturbp = 0,
nptclmax = 0, nptgmax = 0, rclenwpt = 0, nptcompt = 0, plencopt = 0,
ireversp = 0, nwphis = 1, nwptcl = 5, ityptcl = 1, nopts_wr = 1,
nopte_wr = -1, noptd_wr = 1, nwptwall = 0;
max no. (p,l,s,v,b): 6, 13, 9, 2, 1;;

End of Read Session=I:¥andrey¥particle¥3.68¥next 3.68¥0.596 charging¥new¥新しいフォルダー¥pre.his
menu: parameter/dem/basic settings;
pmenu: idem = 1, idemrot = 0, idemiof = -1, sprcn = 2000, sprct = 0,
rescn = 0.5, resct = -1, fricc = 0.7, friccw = 0.7, rsrohnrp = 0,
ndtfdem = 1, rdpdem = 1, rdpcont = 1, chtrpp = 0, chtrpw = 0,
chtrpf = -1, idemcoh = 0;
max no. (p,l,s,v,b): 6, 13, 9, 2, 1;;

menu: parameter/control;

pmenu: title = , nousr = 0, istead = 0, iturb = 0, nmax = -1, tmax = 300,
elapsed time(max) = 0, dt = 0.0001, couran = 0, irest = 1, iveloc = 1,
istokes = 0, imvgrd = 1, imvgsc = 1;
max no. (p,l,s,v,b): 6, 13, 9, 2, 1;;

Case 4 dp/Dp = 0.133 Uf = 1.06 m/s

version 2015.05.14_tmp
Reading Session=I:¥andrey¥particle¥4 phase uf= 1.06¥pre.his
menu: point/generate;
pmenu: total no. = 5,
coord = 1, component = 0, 0, 0,
coord = 1, component = 0, 0.02, 0,
coord = 1, component = 0, 0.05, 0.05196,
coord = 1, component = 0, 0.05, 0.58196,
coord = 1, component = 0, 0, 0.58196;
max no. (p,l,s,v,b): 5, 0, 0, 0, 0;;

menu: point/generate;
pmenu: total no. = 1,
coord = 1, component = 0, 0, 0.05196;
max no. (p,l,s,v,b): 6, 0, 0, 0, 0;;

menu: line/generate/line;
click: total no. = 4,
no. of point = 2, point = 1, 2,
no. of point = 2, point = 2, 3,
no. of point = 2, point = 3, 6,
no. of point = 2, point = 6, 1;
max no. (p,l,s,v,b): 6, 4, 0, 0, 0;;

menu: line/generate/line;
click: total no. = 3,
no. of point = 2, point = 3, 4,
no. of point = 2, point = 4, 5,
no. of point = 2, point = 5, 6;
max no. (p,l,s,v,b): 6, 7, 0, 0, 0;;

menu: surface/generate/manual;
click: no. of line = 4, line = 6, 5, 7, 3;
max no. (p,l,s,v,b): 6, 7, 1, 0, 0;;

menu: surface/generate/manual;
click: no. of line = 4, line = 3, 2, 1, 4;
max no. (p,l,s,v,b): 6, 7, 2, 0, 0;;

menu: surface/copy/rotate;
click: total no. of surface = 0;
pmenu: select = trajectory/on, center point = 0, 0, 0, axis vector = 0, 0, 1,
angle = 360, height = 0,
no. of copies = 1;
max no. (p,l,s,v,b): 6, 13, 9, 2, 0;;

menu: line/grid(cont)/on single line;
click: total no. = 1, line = 8;
pmenu: select = division ratio copy / on, num = 42, start = 1, end = 1;
max no. (p,l,s,v,b): 6, 13, 9, 2, 0;;

menu: line/grid(cont)/on single line;
click: total no. = 1, line = 6;
pmenu: select = division ratio copy / on, num = 12, start = 1, end = 1;
max no. (p,l,s,v,b): 6, 13, 9, 2, 0;;

menu: line/grid(cont)/on single line;
click: total no. = 1, line = 7;
pmenu: select = division ratio copy / on, num = 145, start = 1, end = 1;
max no. (p,l,s,v,b): 6, 13, 9, 2, 0;;

menu: line/grid(end)/on single line;
click: total no. = 1, line = 4;
pmenu: select = division ratio copy / on, num = 132, start = 1, end = 1;
max no. (p,l,s,v,b): 6, 13, 9, 2, 0;;

menu: line/grid/on single line;
click: total no. = 1, line = 2;

```
pmenu: select = division ratio copy / on, num = 13, start = 1, end = 1;
max no. (p,l,s,v,b):       6,     13,       9,       2,       0;;

menu:    block/generate/auto;
click: total no. = 1, total no. of volume = 0;
max no. (p,l,s,v,b):       6,     13,       9,       2,       1;;

menu:    block/set ibctyp;
click: total no. = 1, block = 1, index = 4;
pmenu: value = 4;
max no. (p,l,s,v,b):       6,     13,       9,       2,       1;;

menu:    block/set ibctyp;
click: total no. = 1, block = 1, index = 5;
pmenu: value = 3;
max no. (p,l,s,v,b):       6,     13,       9,       2,       1;;

menu:    block/set ibctyp;
click: total no. = 1, block = 1, index = 3;
pmenu: value = 9;
max no. (p,l,s,v,b):       6,     13,       9,       2,       1;;

menu:    physical variable/set value/flow velocity;
click: total no. = 1, block = 1,
          no. of mesh_range = 1, mesh range = 0,-1,0,-1,-1,-1;
pmenu: select = velocity(x), value = 0, 0, 2.38;
max no. (p,l,s,v,b):       6,     13,       9,       2,       1;;

menu:    physical variable/set value/flow velocity;
click: total no. = 1, block = 1,
          no. of mesh_range = 1, mesh range = 0,-1,0,-1,-1,-1;
pmenu: select = velocity(x), value = 0, 0, 6.6;
max no. (p,l,s,v,b):       6,     13,       9,       2,       1;;

menu:    physical variable/set value/in cell;
click: total no. = 1, block = 1,
          no. of mesh_range = 1, mesh range = 1,-1,1,-1,1,-1;
pmenu: select = alpha, no = 1, value = 0.8;
```

```
max no. (p,l,s,v,b):       6,     13,       9,       2,       1;;

menu:    physical variable/set value/flow velocity;
click: total no. = 1, block = 1,
          no. of mesh_range = 1, mesh range = 0,-1,0,-1,-1,-1;
pmenu: select = velocity(x), value = 0, 0, 1.7;
max no. (p,l,s,v,b):       6,     13,       9,       2,       1;;

menu:    physical variable/set value/in cell;
click: total no. = 1, block = 1,
          no. of mesh_range = 1, mesh range = 1,-1,1,-1,1,-1;
pmenu: select = alpha, no = 1, value = 0.2;
max no. (p,l,s,v,b):       6,     13,       9,       2,       1;;

menu:    physical variable/set value/in cell;
click: total no. = 1, block = 1,
          no. of mesh_range = 1, mesh range = 1,-1,1,-1,1,-1;
pmenu: select = alpha, no = 1, value = 0;
max no. (p,l,s,v,b):       6,     13,       9,       2,       1;;

menu:    physical variable/set value/flow velocity;
click: total no. = 1, block = 1,
          no. of mesh_range = 1, mesh range = 0,-1,0,-1,-1,-1;
pmenu: select = velocity(x), value = 0, 0, 0;
max no. (p,l,s,v,b):       6,     13,       9,       2,       1;;

menu:    physical variable/set value/flow velocity;
click: total no. = 1, block = 1,
          no. of mesh_range = 1, mesh range = 0,-1,0,-1,-1,-1;
pmenu: select = velocity(x), value = 0, 0, 6.6;
max no. (p,l,s,v,b):       6,     13,       9,       2,       1;;

menu:    parameter/particle/generate;
pmenu: kmark = 1, density = 0, diameter = 0,
          coord = 1, start = -0.044,-0.044,0, end = 0.044,0.044,0.025,
          number = 5,5,5;
max no. (p,l,s,v,b):       6,     13,       9,       2,       1;;
```

menu: parameter/particle/generate;
pmenu: kmark = 2, density = 0, diameter = 0,
coord = 1, start = -0.046,-0.046,0.025, end = 0.046,0.046,0.145,
number = 12,12,15;
max no. (p,l,s,v,b): 6, 13, 9, 2, 1;;

menu: parameter/particle/generate;
pmenu: kmark = 3, density = 0, diameter = 0,
coord = 1, start = -0.0478,-0.0478,0.145, end = 0.0478,0.0478,0.5,
number = 40,40,80;
max no. (p,l,s,v,b): 6, 13, 9, 2, 1;;

menu: parameter/particle/generate;
pmenu: kmark = 4, density = 0, diameter = 0,
coord = 1, start = -0.049806,0.049806,0.145, end = 0.049806,0.049806,
0.5, number = 39,1,915;
max no. (p,l,s,v,b): 6, 13, 9, 2, 1;;

menu: parameter/particle/generate;
pmenu: kmark = 1, density = 0, diameter = 0,
coord = 1, start = -0.044,-0.044,0, end = 0.044,0.044,0.019,
number = 6,6,6;
max no. (p,l,s,v,b): 6, 13, 9, 2, 1;;

menu: parameter/particle/generate;
pmenu: kmark = 2, density = 0, diameter = 0,
coord = 1, start = -0.046,-0.046,0.023, end = 0.046,0.046,0.141,
number = 16,16,16;
max no. (p,l,s,v,b): 6, 13, 9, 2, 1;;

menu: parameter/particle/generate;
pmenu: kmark = 3, density = 0, diameter = 0,
coord = 1, start = -0.0478,-0.0478,0.1432, end = 0.0478,0.0478,0.5,
number = 40,40,81;
max no. (p,l,s,v,b): 6, 13, 9, 2, 1;;

menu: parameter/particle/generate;
pmenu: kmark = 4, density = 0, diameter = 0,

coord = 1, start = -0.049806,-0.049806,0.49, end = 0.049806,0.049806,
0.5, number = 453,453,10;
max no. (p,l,s,v,b): 6, 13, 9, 2, 1;;

menu: parameter/particle/generate;
pmenu: kmark = 2, density = 0, diameter = 0,
coord = 1, start = -0.046,-0.046,0.3, end = 0.046,0.046,0.5,
number = 16,16,1;
max no. (p,l,s,v,b): 6, 13, 9, 2, 1;;

menu: physical variable/set value/flow velocity;
click: total no. = 1, block = 1,
no. of mesh_range = 1, mesh range = 0,-1,0,-1,0,-1;
pmenu: select = velocity(x), value = 0, 0, 0;
max no. (p,l,s,v,b): 6, 13, 9, 2, 1;;

menu: parameter/acceleration;
pmenu: g = 0, 0, -9.806, bf = 0, 0, 0, rotate0 = 0, rot_p = 0, 0, 0,
rot_v = 0, 0, 1;
max no. (p,l,s,v,b): 6, 13, 9, 2, 1;;

menu: parameter/particle/generate;
pmenu: kmark = 0, density = 0, diameter = 0,
coord = 1, start = -0.042,-0.042,0.3, end = 0.042,0.042,0.42,
number = 15,15,15;
max no. (p,l,s,v,b): 6, 13, 9, 2, 1;;

menu: parameter/particle/generate;
pmenu: kmark = 2, density = 0, diameter = 0,
coord = 1, start = -0.046,-0.046,0.3, end = 0.046,0.046,0.3,
number = 15,15,1;
max no. (p,l,s,v,b): 6, 13, 9, 2, 1;;

menu: parameter/particle/generate;
pmenu: kmark = 3, density = 0, diameter = 0,
coord = 1, start = -0.047,-0.047,0.55, end = 0.047,0.047,0.56,
number = 24,24,2;
max no. (p,l,s,v,b): 6, 13, 9, 2, 1;;

menu: parameter/particle/delete;
max no. (p,l,s,v,b): 6, 13, 9, 2, 1;;

menu: physical variable/set value/flow velocity;
click: total no. = 1, block = 1,
  no. of mesh_range = 1, mesh range = 0,0,0,-1,0,-1;
pmenu: select = velocity(x), value = 0, 0, -5;
max no. (p,l,s,v,b): 6, 13, 9, 2, 1;;

menu: physical variable/set value/flow velocity;
click: total no. = 1, block = 1,
  no. of mesh_range = 1, mesh range = 0,-1,0,-1,0,-1;
pmenu: select = velocity(x), value = 0, 0, 0;
max no. (p,l,s,v,b): 6, 13, 9, 2, 1;;

menu: physical variable/set value/flow velocity;
click: total no. = 1, block = 1,
  no. of mesh_range = 1, mesh range = 0,-1,0,-1,-1,-1;
pmenu: select = velocity(x), value = 0, 0, 0.88;
max no. (p,l,s,v,b): 6, 13, 9, 2, 1;;

menu: physical variable/set value/flow velocity;
click: total no. = 1, block = 1,
  no. of mesh_range = 1, mesh range = 0,-1,0,-1,0,-1;
pmenu: select = velocity(x), value = 0, 0, 0;
max no. (p,l,s,v,b): 6, 13, 9, 2, 1;;

menu: physical variable/set value/flow velocity;
click: total no. = 1, block = 1,
  no. of mesh_range = 1, mesh range = 0,-1,0,-1,-1,-1;
pmenu: select = velocity(x), value = 0, 0, 0.88;
max no. (p,l,s,v,b): 6, 13, 9, 2, 1;;

menu: parameter/particle/generate;
pmenu: kmark = 4, density = 0, diameter = 0,
  coord = 1, start = -0.0496,-0.0496,0.17196, end = 0.0496,0.0496,
  0.17196, number = 25,25,1;

max no. (p,l,s,v,b): 6, 13, 9, 2, 1;;

menu: physical variable/set value/flow velocity;
click: total no. = 1, block = 1,
  no. of mesh_range = 1, mesh range = 0,-1,0,-1,0,-1;
pmenu: select = velocity(x), value = 0, 0, 0;
max no. (p,l,s,v,b): 6, 13, 9, 2, 1;;

menu: physical variable/set value/flow velocity;
click: total no. = 1, block = 1,
  no. of mesh_range = 1, mesh range = 0,-1,0,-1,-1,-1;
pmenu: select = velocity(x), value = 0, 0, 6.6;
max no. (p,l,s,v,b): 6, 13, 9, 2, 1;;

menu: physical variable/set value/flow velocity;
click: total no. = 1, block = 1,
  no. of mesh_range = 1, mesh range = 0,-1,0,-1,0,-1;
pmenu: select = velocity(x), value = 0, 0, 0;
max no. (p,l,s,v,b): 6, 13, 9, 2, 1;;

menu: physical variable/set value/flow velocity;
click: total no. = 1, block = 1,
  no. of mesh_range = 1, mesh range = 0,-1,0,-1,-1,-1;
pmenu: select = velocity(x), value = 0, 0, 0.88;
max no. (p,l,s,v,b): 6, 13, 9, 2, 1;;

menu: parameter/property;
pmenu: density = 1.2, sigma = 0;
max no. (p,l,s,v,b): 6, 13, 9, 2, 1;;

menu: parameter/viscosity;
pmenu: viscosity = 1.8e-005, newton = 0, nvistemp = 0, uplowvis = 1e+020, 0,
  1e+020, 0, 1e+020, -273;
max no. (p,l,s,v,b): 6, 13, 9, 2, 1;;

menu: physical variable/set value/flow velocity;
click: total no. = 1, block = 1,
  no. of mesh_range = 1, mesh range = 0,-1,0,-1,0,-1;

```
pmenu: select = velocity(x), value = 0, 0, 0;
max no. (p,l,s,v,b):       6,      13,       9,       2,       1;;

menu:    physical variable/set value/flow velocity;
click: total no. = 1, block = 1,
          no. of mesh_range = 1, mesh range = 0,-1,0,-1,-1,-1;
pmenu: select = velocity(x), value = 0, 0, 0.88;
max no. (p,l,s,v,b):       6,      13,       9,       2,       1;;

menu:    physical variable/set value/flow velocity;
click: total no. = 1, block = 1,
          no. of mesh_range = 1, mesh range = 0,-1,0,-1,-1,-1;
pmenu: select = velocity(x), value = 0, 0, 0;
max no. (p,l,s,v,b):       6,      13,       9,       2,       1;;

menu:    physical variable/set value/flow velocity;
click: total no. = 1, block = 1,
          no. of mesh_range = 1, mesh range = 0,-1,0,-1,-1,-1;
pmenu: select = velocity(x), value = 0, 0, 1.24;
max no. (p,l,s,v,b):       6,      13,       9,       2,       1;;

menu:    parameter/multi-phase flow;
pmenu: nphase = 4, idrift = 0, isdgsl = 0, iresta = 1, dtalph = 0,
          alpha(min) = 0, rgsl = 0.012, rhogsl = 7850, visco = 0, sftension = 0,
          vterm0 = 0, stokes = 3, nonstokes = 1.5, speh = 0, therco = 0,
          degx = 0, degy = 0, degz = 0, overx = 0, overy = 0, overz = 0,
          rgsl = 0.008, rhogsl = 7850, visco = 0, sftension = 0, vterm0 = 0,
          stokes = 3, nonstokes = 1.5, speh = 0, therco = 0, degx = 0, degy = 0,
          degz = 0, overx = 0, overy = 0, overz = 0, rgsl = 0.00448,
          rhogsl = 1106, visco = 0, sftension = 0, vterm0 = 0, stokes = 3,
          nonstokes = 1.5, speh = 0, therco = 0, degx = 0, degy = 0, degz = 0,
          overx = 0, overy = 0, overz = 0, rgsl = 0.000596, rhogsl = 1369,
          visco = 0, sftension = 0, vterm0 = 3.15, stokes = 3, nonstokes = 1.5,
          speh = 0, therco = 0, degx = 0, degy = 0, degz = 0, overx = 0,
          overy = 0, overz = 0;
max no. (p,l,s,v,b):       6,      13,       9,       2,       1;;

menu:    parameter/io;
```

```
pmenu: nintpo = 0, tintpo = 0.1, nowpost = 0, iwstrs = 0, iwchtr = 0,
        iwpost = 0, iwmean = 0, itypos = 0, nfview = 0, nintre = 0,
        iwrest = 0, ityres = 0, npower = 0, nforce = 0, iprint = 0,
        pre.file = pre.txt, restart.file = restart.bin;
max no. (p,l,s,v,b):      6,     13,      9,      2,      1;;

menu:   parameter/dem/basic settings;
pmenu: idem = 1, idemrot = 0, idemiof = -1, sprcn = 4000, sprct = 0,
        rescn = 0.5, resct = -1, fricc = 0.7, friccw = 0.7, rsrohnrp = 0,
        ndtfdem = 1, rdpdem = 1, rdpcont = 1, chtrpp = 0, chtrpw = 0,
        chtrpf = -1, idemcoh = 0;
max no. (p,l,s,v,b):      6,     13,      9,      2,      1;;

# End of Read Session=I:¥andrey¥particle¥4 phase uf= 1.06¥pre.his
menu:   physical variable/set value/flow velocity;
click: total no. = 1, block = 1,
        no. of mesh_range = 1, mesh range = 0,-1,0,-1,-1,-1;
pmenu: select = velocity(x), value = 0, 0, 0;
max no. (p,l,s,v,b):      6,     13,      9,      2,      1;;

menu:   physical variable/set value/flow velocity;
click: total no. = 1, block = 1,
        no. of mesh_range = 1, mesh range = 0,-1,0,-1,-1,-1;
pmenu: select = velocity(x), value = 0, 0, 1.06;
max no. (p,l,s,v,b):      6,     13,      9,      2,      1;;

menu:   parameter/particle/control;
pmenu: nintpg = 0, tintpg = 1, nptscal = 0, irestp = 1, iturbp = 0,
        nptclmax = 0, nptgmax = 0, rclenwpt = 0, nptcompt = 0, plencopt = 0,
        ireversp = 0, nwphis = 1, nwptcl = 5, ityptcl = 1, nopts_wr = 1,
        nopte_wr = -1, noptd_wr = 1, nwptwall = 0;
max no. (p,l,s,v,b):      6,     13,      9,      2,      1;;

menu:   parameter/control;
pmenu: title = , nousr = 0, istead = 0, iturb = 0, nmax = -1, tmax = 300,
        elapsed time(max) = 0, dt = 0.0001, couran = 0, irest = 1, iveloc = 1,
        istokes = 0, imvgrd = 1, imvgsc = 1;
max no. (p,l,s,v,b):      6,     13,      9,      2,      1;;
```

Case 5 dp/Dp = 0.133 Uf = 1.24 m/s

```
# version 2015.05.14_tmp
# Reading Session=I:¥andrey¥particle¥4 phase    uf= 1.24¥pre.his
menu:    point/generate;
pmenu: total no. = 5,
          coord = 1, component = 0, 0, 0,
          coord = 1, component = 0, 0.02, 0,
          coord = 1, component = 0, 0.05, 0.05196,
          coord = 1, component = 0, 0.05, 0.58196,
          coord = 1, component = 0, 0, 0.58196;
max no. (p,l,s,v,b):       5,       0,       0,       0,       0;;

menu:    point/generate;
pmenu: total no. = 1,
          coord = 1, component = 0, 0, 0.05196;
max no. (p,l,s,v,b):       6,       0,       0,       0,       0;;

menu:    line/generate/line;
click: total no. = 4,
          no. of point = 2, point = 1, 2,
          no. of point = 2, point = 2, 3,
          no. of point = 2, point = 3, 6,
          no. of point = 2, point = 6, 1;
max no. (p,l,s,v,b):       6,       4,       0,       0,       0;;

menu:    line/generate/line;
click: total no. = 3,
          no. of point = 2, point = 3, 4,
          no. of point = 2, point = 4, 5,
          no. of point = 2, point = 5, 6;
max no. (p,l,s,v,b):       6,       7,       0,       0,       0;;

menu:    surface/generate/manual;
click: no. of line = 4, line = 6, 5, 7, 3;
```

```
max no. (p,l,s,v,b):      6,      7,      1,      0,      0;;

menu:    surface/generate/manual;
click: no. of line = 4, line = 3, 2, 1, 4;
max no. (p,l,s,v,b):      6,      7,      2,      0,      0;;

menu:    surface/copy/rotate;
click: total no. of surface = 0;
pmenu: select = trajectory/on, center point = 0, 0, 0, axis vector = 0, 0, 1,
          angle = 360, height = 0,
          no. of copies = 1;
max no. (p,l,s,v,b):      6,     13,      9,      2,      0;;

menu:    line/grid(cont)/on single line;
click: total no. = 1, line = 8;
pmenu: select = division ratio copy / on, num = 42, start = 1, end = 1;
max no. (p,l,s,v,b):      6,     13,      9,      2,      0;;

menu:    line/grid(cont)/on single line;
click: total no. = 1, line = 6;
pmenu: select = division ratio copy / on, num = 12, start = 1, end = 1;
max no. (p,l,s,v,b):      6,     13,      9,      2,      0;;

menu:    line/grid(cont)/on single line;
click: total no. = 1, line = 7;
pmenu: select = division ratio copy / on, num = 145, start = 1, end = 1;
max no. (p,l,s,v,b):      6,     13,      9,      2,      0;;

menu:    line/grid(end)/on single line;
click: total no. = 1, line = 4;
pmenu: select = division ratio copy / on, num = 132, start = 1, end = 1;
max no. (p,l,s,v,b):      6,     13,      9,      2,      0;;

menu:    line/grid/on single line;
click: total no. = 1, line = 2;
pmenu: select = division ratio copy / on, num = 13, start = 1, end = 1;
max no. (p,l,s,v,b):      6,     13,      9,      2,      0;;
```

menu: block/generate/auto;
click: total no. = 1, total no. of volume = 0;
max no. (p,l,s,v,b): 6, 13, 9, 2, 1;;

menu: block/set ibctyp;
click: total no. = 1, block = 1, index = 4;
pmenu: value = 4;
max no. (p,l,s,v,b): 6, 13, 9, 2, 1;;

menu: block/set ibctyp;
click: total no. = 1, block = 1, index = 5;
pmenu: value = 3;
max no. (p,l,s,v,b): 6, 13, 9, 2, 1;;

menu: block/set ibctyp;
click: total no. = 1, block = 1, index = 3;
pmenu: value = 9;
max no. (p,l,s,v,b): 6, 13, 9, 2, 1;;

menu: physical variable/set value/flow velocity;
click: total no. = 1, block = 1,
    no. of mesh_range = 1, mesh range = 0,-1,0,-1,-1,-1;
pmenu: select = velocity(x), value = 0, 0, 2.38;
max no. (p,l,s,v,b): 6, 13, 9, 2, 1;;

menu: physical variable/set value/flow velocity;
click: total no. = 1, block = 1,
    no. of mesh_range = 1, mesh range = 0,-1,0,-1,-1,-1;
pmenu: select = velocity(x), value = 0, 0, 6.6;
max no. (p,l,s,v,b): 6, 13, 9, 2, 1;;

menu: physical variable/set value/in cell;
click: total no. = 1, block = 1,
    no. of mesh_range = 1, mesh range = 1,-1,1,-1,1,-1;
pmenu: select = alpha, no = 1, value = 0.8;
max no. (p,l,s,v,b): 6, 13, 9, 2, 1;;

menu: physical variable/set value/flow velocity;

```
click: total no. = 1, block = 1,
        no. of mesh_range = 1, mesh range = 0,-1,0,-1,-1,-1;
pmenu: select = velocity(x), value = 0, 0, 1.7;
max no. (p,l,s,v,b):      6,     13,      9,      2,      1;;

menu:   physical variable/set value/in cell;
click: total no. = 1, block = 1,
        no. of mesh_range = 1, mesh range = 1,-1,1,-1,1,-1;
pmenu: select = alpha, no = 1, value = 0.2;
max no. (p,l,s,v,b):      6,     13,      9,      2,      1;;

menu:   physical variable/set value/in cell;
click: total no. = 1, block = 1,
        no. of mesh_range = 1, mesh range = 1,-1,1,-1,1,-1;
pmenu: select = alpha, no = 1, value = 0;
max no. (p,l,s,v,b):      6,     13,      9,      2,      1;;

menu:   physical variable/set value/flow velocity;
click: total no. = 1, block = 1,
        no. of mesh_range = 1, mesh range = 0,-1,0,-1,-1,-1;
pmenu: select = velocity(x), value = 0, 0, 0;
max no. (p,l,s,v,b):      6,     13,      9,      2,      1;;

menu:   physical variable/set value/flow velocity;
click: total no. = 1, block = 1,
        no. of mesh_range = 1, mesh range = 0,-1,0,-1,-1,-1;
pmenu: select = velocity(x), value = 0, 0, 6.6;
max no. (p,l,s,v,b):      6,     13,      9,      2,      1;;

menu:   parameter/particle/generate;
pmenu: kmark = 1, density = 0, diameter = 0,
        coord = 1, start = -0.044,-0.044,0, end = 0.044,0.044,0.025,
        number = 5,5,5;
max no. (p,l,s,v,b):      6,     13,      9,      2,      1;;

menu:   parameter/particle/generate;
pmenu: kmark = 2, density = 0, diameter = 0,
        coord = 1, start = -0.046,-0.046,0.025, end = 0.046,0.046,0.145,
```

number = 12,12,15;
max no. (p,l,s,v,b): 6, 13, 9, 2, 1;;

menu: parameter/particle/generate;
pmenu: kmark = 3, density = 0, diameter = 0,
coord = 1, start = -0.0478,-0.0478,0.145, end = 0.0478,0.0478,0.5,
number = 40,40,80;
max no. (p,l,s,v,b): 6, 13, 9, 2, 1;;

menu: parameter/particle/generate;
pmenu: kmark = 4, density = 0, diameter = 0,
coord = 1, start = -0.049806,0.049806,0.145, end = 0.049806,0.049806,
0.5, number = 39,1,915;
max no. (p,l,s,v,b): 6, 13, 9, 2, 1;;

menu: parameter/particle/generate;
pmenu: kmark = 1, density = 0, diameter = 0,
coord = 1, start = -0.044,-0.044,0, end = 0.044,0.044,0.019,
number = 6,6,6;
max no. (p,l,s,v,b): 6, 13, 9, 2, 1;;

menu: parameter/particle/generate;
pmenu: kmark = 2, density = 0, diameter = 0,
coord = 1, start = -0.046,-0.046,0.023, end = 0.046,0.046,0.141,
number = 16,16,16;
max no. (p,l,s,v,b): 6, 13, 9, 2, 1;;

menu: parameter/particle/generate;
pmenu: kmark = 3, density = 0, diameter = 0,
coord = 1, start = -0.0478,-0.0478,0.1432, end = 0.0478,0.0478,0.5,
number = 40,40,81;
max no. (p,l,s,v,b): 6, 13, 9, 2, 1;;

menu: parameter/particle/generate;
pmenu: kmark = 4, density = 0, diameter = 0,
coord = 1, start = -0.049806,-0.049806,0.49, end = 0.049806,0.049806,
0.5, number = 453,453,10;
max no. (p,l,s,v,b): 6, 13, 9, 2, 1;;

menu: parameter/particle/generate;
pmenu: kmark = 2, density = 0, diameter = 0,
        coord = 1, start = -0.046,-0.046,0.3, end = 0.046,0.046,0.5,
        number = 16,16,1;
max no. (p,l,s,v,b): 6, 13, 9, 2, 1;;

menu: physical variable/set value/flow velocity;
click: total no. = 1, block = 1,
        no. of mesh_range = 1, mesh range = 0,-1,0,-1,0,-1;
pmenu: select = velocity(x), value = 0, 0, 0;
max no. (p,l,s,v,b): 6, 13, 9, 2, 1;;

menu: parameter/acceleration;
pmenu: g = 0, 0, -9.806, bf = 0, 0, 0, rotate0 = 0, rot_p = 0, 0, 0,
        rot_v = 0, 0, 1;
max no. (p,l,s,v,b): 6, 13, 9, 2, 1;;

menu: parameter/particle/generate;
pmenu: kmark = 0, density = 0, diameter = 0,
        coord = 1, start = -0.042,-0.042,0.3, end = 0.042,0.042,0.42,
        number = 15,15,15;
max no. (p,l,s,v,b): 6, 13, 9, 2, 1;;

menu: parameter/particle/generate;
pmenu: kmark = 2, density = 0, diameter = 0,
        coord = 1, start = -0.046,-0.046,0.3, end = 0.046,0.046,0.3,
        number = 15,15,1;
max no. (p,l,s,v,b): 6, 13, 9, 2, 1;;

menu: parameter/particle/generate;
pmenu: kmark = 3, density = 0, diameter = 0,
        coord = 1, start = -0.047,-0.047,0.55, end = 0.047,0.047,0.56,
        number = 24,24,2;
max no. (p,l,s,v,b): 6, 13, 9, 2, 1;;

menu: parameter/particle/delete;
max no. (p,l,s,v,b): 6, 13, 9, 2, 1;;

menu: physical variable/set value/flow velocity;
click: total no. = 1, block = 1,
        no. of mesh_range = 1, mesh range = 0,0,0,-1,0,-1;
pmenu: select = velocity(x), value = 0, 0, -5;
max no. (p,l,s,v,b): 6, 13, 9, 2, 1;;

menu: physical variable/set value/flow velocity;
click: total no. = 1, block = 1,
        no. of mesh_range = 1, mesh range = 0,-1,0,-1,0,-1;
pmenu: select = velocity(x), value = 0, 0, 0;
max no. (p,l,s,v,b): 6, 13, 9, 2, 1;;

menu: physical variable/set value/flow velocity;
click: total no. = 1, block = 1,
        no. of mesh_range = 1, mesh range = 0,-1,0,-1,-1,-1;
pmenu: select = velocity(x), value = 0, 0, 0.88;
max no. (p,l,s,v,b): 6, 13, 9, 2, 1;;

menu: physical variable/set value/flow velocity;
click: total no. = 1, block = 1,
        no. of mesh_range = 1, mesh range = 0,-1,0,-1,0,-1;
pmenu: select = velocity(x), value = 0, 0, 0;
max no. (p,l,s,v,b): 6, 13, 9, 2, 1;;

menu: physical variable/set value/flow velocity;
click: total no. = 1, block = 1,
        no. of mesh_range = 1, mesh range = 0,-1,0,-1,-1,-1;
pmenu: select = velocity(x), value = 0, 0, 0.88;
max no. (p,l,s,v,b): 6, 13, 9, 2, 1;;

menu: parameter/particle/generate;
pmenu: kmark = 4, density = 0, diameter = 0,
        coord = 1, start = -0.0496,-0.0496,0.17196, end = 0.0496,0.0496,
        0.17196, number = 25,25,1;
max no. (p,l,s,v,b): 6, 13, 9, 2, 1;;

menu: physical variable/set value/flow velocity;

click: total no. = 1, block = 1,
no. of mesh_range = 1, mesh range = 0,-1,0,-1,0,-1;
pmenu: select = velocity(x), value = 0, 0, 0;
max no. (p,l,s,v,b): 6, 13, 9, 2, 1;;

menu: physical variable/set value/flow velocity;
click: total no. = 1, block = 1,
no. of mesh_range = 1, mesh range = 0,-1,0,-1,-1,-1;
pmenu: select = velocity(x), value = 0, 0, 6.6;
max no. (p,l,s,v,b): 6, 13, 9, 2, 1;;

menu: physical variable/set value/flow velocity;
click: total no. = 1, block = 1,
no. of mesh_range = 1, mesh range = 0,-1,0,-1,0,-1;
pmenu: select = velocity(x), value = 0, 0, 0;
max no. (p,l,s,v,b): 6, 13, 9, 2, 1;;

menu: physical variable/set value/flow velocity;
click: total no. = 1, block = 1,
no. of mesh_range = 1, mesh range = 0,-1,0,-1,-1,-1;
pmenu: select = velocity(x), value = 0, 0, 0.88;
max no. (p,l,s,v,b): 6, 13, 9, 2, 1;;

menu: parameter/property;
pmenu: density = 1.2, sigma = 0;
max no. (p,l,s,v,b): 6, 13, 9, 2, 1;;

menu: parameter/viscosity;
pmenu: viscosity = 1.8e-005, newton = 0, nvistemp = 0, uplowvis = 1e+020, 0,
1e+020, 0, 1e+020, -273;
max no. (p,l,s,v,b): 6, 13, 9, 2, 1;;

menu: physical variable/set value/flow velocity;
click: total no. = 1, block = 1,
no. of mesh_range = 1, mesh range = 0,-1,0,-1,0,-1;
pmenu: select = velocity(x), value = 0, 0, 0;
max no. (p,l,s,v,b): 6, 13, 9, 2, 1;;

menu: physical variable/set value/flow velocity;
click: total no. = 1, block = 1,
        no. of mesh_range = 1, mesh range = 0,-1,0,-1,-1,-1;
pmenu: select = velocity(x), value = 0, 0, 0.88;
max no. (p,l,s,v,b): 6, 13, 9, 2, 1;;

menu: physical variable/set value/flow velocity;
click: total no. = 1, block = 1,
        no. of mesh_range = 1, mesh range = 0,-1,0,-1,-1,-1;
pmenu: select = velocity(x), value = 0, 0, 0;
max no. (p,l,s,v,b): 6, 13, 9, 2, 1;;

menu: physical variable/set value/flow velocity;
click: total no. = 1, block = 1,
        no. of mesh_range = 1, mesh range = 0,-1,0,-1,-1,-1;
pmenu: select = velocity(x), value = 0, 0, 1.24;
max no. (p,l,s,v,b): 6, 13, 9, 2, 1;;

menu: parameter/dem/basic settings;
pmenu: idem = 1, idemrot = 0, idemiof = -1, sprcn = 4000, sprct = 0,
        rescn = 0.5, resct = -1, fricc = 0.7, friccw = 0.7, rsrohnrp = 0,
        ndtfdem = 1, rdpdem = 1, rdpcont = 1, chtrpp = 0, chtrpw = 0,
        chtrpf = -1, idemcoh = 0;
max no. (p,l,s,v,b): 6, 13, 9, 2, 1;;

End of Read Session=I:¥andrey¥particle¥4 phase uf= 1.24¥pre.his
menu: parameter/multi-phase flow;
pmenu: nphase = 4, idrift = 0, isdgsl = 0, iresta = 1, dtalph = 0,
        alpha(min) = 0, rgsl = 0.012, rhogsl = 7850, visco = 0, sftension = 0,
        vterm0 = 0, stokes = 3, nonstokes = 1.5, speh = 0, therco = 0,
        degx = 0, degy = 0, degz = 0, overx = 0, overy = 0, overz = 0,
        rgsl = 0.008, rhogsl = 7850, visco = 0, sftension = 0, vterm0 = 0,
        stokes = 3, nonstokes = 1.5, speh = 0, therco = 0, degx = 0, degy = 0,
        degz = 0, overx = 0, overy = 0, overz = 0, rgsl = 0.00448,
        rhogsl = 1106, visco = 0, sftension = 0, vterm0 = 0, stokes = 3,
        nonstokes = 1.5, speh = 0, therco = 0, degx = 0, degy = 0, degz = 0,
        overx = 0, overy = 0, overz = 0, rgsl = 0.000596, rhogsl = 1369,
        visco = 0, sftension = 0, vterm0 = 3.15, stokes = 3, nonstokes = 1.5,

```
        speh = 0, therco = 0, degx = 0, degy = 0, degz = 0, overx = 0,
        overy = 0, overz = 0;
max no. (p,l,s,v,b):      6,     13,       9,       2,       1;;

menu:   parameter/control;
pmenu: title = , nousr = 0, istead = 0, iturb = 0, nmax = -1, tmax = 300,
        elapsed time(max) = 0, dt = 0.0001, couran = 0, irest = 1, iveloc = 1,
        istokes = 0, imvgrd = 1, imvgsc = 1;
max no. (p,l,s,v,b):      6,     13,       9,       2,       1;;

menu:   parameter/io;
pmenu: nintpo = 0, tintpo = 0.1, nowpost = 0, iwstrs = 0, iwchtr = 0,
        iwpost = 0, iwmean = 0, itypos = 0, nfview = 0, nintre = 0,
        iwrest = 0, ityres = 0, npower = 0, nforce = 0, iprint = 0,
        pre.file = pre.txt, restart.file = restart.bin;
max no. (p,l,s,v,b):      6,     13,       9,       2,       1;;

menu:   parameter/particle/control;
pmenu: nintpg = 0, tintpg = 1, nptscal = 0, irestp = 1, iturbp = 0,
        nptclmax = 0, nptgmax = 0, rclenwpt = 0, nptcompt = 0, plencopt = 0,
        ireversp = 0, nwphis = 1, nwptcl = 5, ityptcl = 1, nopts_wr = 1,
        nopte_wr = -1, noptd_wr = 1, nwptwall = 0;
max no. (p,l,s,v,b):      6,     13,       9,       2,       1;;
```

SOURCE CODE FOR ORIFICE MODEL

```
# version 2015.05.14_tmp
# Reading Session=I:¥andrey¥particle¥re-create yoshino¥100 particle 10^-6¥restart¥pre.his
menu:    point/generate;
pmenu: total no. = 1,
          coord = 1, component = 0, 0, 0;
max no. (p,l,s,v,b):       1,       0,       0,       0,       0;;

menu:    point/copy/parallel;
click: total no. of point = 0;
pmenu: select = trajectory/on, vector = 0.00129326, 0, 0,
          no. of copies = 1;
max no. (p,l,s,v,b):       2,       1,       0,       0,       0;;

menu:    point/modify/rotate;
click: total no. = 0;
pmenu: center point = 0, 0, 0, axis vector = 0, 0, 1, angle = 60, height = 0;
max no. (p,l,s,v,b):       2,       1,       0,       0,       0;;
```

```
menu:    point/copy/parallel;
click: total no. of point = 1, point = 1;
pmenu: select = trajectory/off, vector = 0.00258653, 0, 0,
          no. of copies = 1;
max no. (p,l,s,v,b):       3,       1,       0,       0,       0;;

menu:    line/generate/line;
click: total no. = 1,
          no. of point = 2, point = 3, 2;
max no. (p,l,s,v,b):       3,       2,       0,       0,       0;;

menu:    line/copy/mirror;
click: total no. of line = 0;
pmenu: select = trajectory/off, point on plane = 0, 0, 0,
          plane normal vector = 0, 1, 0;
max no. (p,l,s,v,b):       4,       4,       0,       0,       0;;

menu:    surface/generate/auto;
click: total no. = 1,
          no. of line = 4, line = 1, 2, 3, 4;
max no. (p,l,s,v,b):       4,       4,       1,       0,       0;;

menu:    line/grid/on single line;
click: total no. = 2, line = 2, 4;
pmenu: select = division ratio copy / on, num = 20, start = 1, end = 1;
max no. (p,l,s,v,b):       4,       4,       1,       0,       0;;

menu:    surface/copy/parallel;
click: total no. of surface = 0;
pmenu: select = trajectory/on, vector = 0, 0, 0.00896,
          no. of copies = 1;
max no. (p,l,s,v,b):       8,      12,       6,       1,       0;;

menu:    line/grid/on single line;
click: total no. = 1, line = 12;
pmenu: select = division ratio copy / on, num = 40, start = 1, end = 1;
max no. (p,l,s,v,b):       8,      12,       6,       1,       0;;
```

```
menu:    volume/modify/rotate;
click: total no. = 0;
pmenu: center point = 0, 0, 0, axis vector = 0, 0, 1, angle = -30,
          height = 0;
max no. (p,l,s,v,b):       8,     12,       6,       1,       0;;

menu:    block/generate/auto;
click: total no. = 1, total no. of volume = 0;
max no. (p,l,s,v,b):       8,     12,       6,       1,       1;;

menu:    block/copy/rotate;
click: total no. of block = 0;
pmenu: center point = 0, 0, 0, axis vector = 0, 0, 1, angle = 120,
          height = 0,
          no. of copies = 2;
max no. (p,l,s,v,b):     14,     25,     15,       3,       3;;

menu:    parameter/change scale;
pmenu: scale = 5.58036, direction = 0;
max no. (p,l,s,v,b):     14,     25,     15,       3,       3;;

menu:    file/read history file start;
pmenu: C:¥rflow¥DEM 解析¥オリフィスモデル - 25.0 - コピー¥wall.his;
max no. (p,l,s,v,b):     14,     25,     15,       3,       3;;

menu:    point/generate;
pmenu: total no. = 1,
          coord = 1, component = 0, 0, 0;
max no. (p,l,s,v,b):     15,     25,     15,       3,       3;;

menu:    point/copy/parallel;
click: total no. of point = 0;
pmenu: select = trajectory/on, vector = 0.00224, 0, 0,
          no. of copies = 1;
max no. (p,l,s,v,b):     16,     26,     15,       3,       3;;

menu:    line/copy/rotate;
```

```
click: total no. of line = 0;
pmenu: select = trajectory/on, center point = 0, 0, 0, axis vector = 0, 1, 0,
        angle = 90, height = 0,
        no. of copies = 1;
max no. (p,l,s,v,b):    17,    29,    16,      3,      3;;

menu:   surface/copy/rotate;
click: total no. of surface = 0;
pmenu: select = trajectory/on, center point = 0, 0, 0, axis vector = 0, 0, 1,
        angle = 360, height = 0,
        no. of copies = 1;
max no. (p,l,s,v,b):    17,    31,    20,      4,      3;;

menu:   line/grid(cont)/on single line;
click: total no. = 1, line = 27;
pmenu: select = division ratio copy / on, num = 8, start = 1, end = 1;
max no. (p,l,s,v,b):    17,    31,    20,      4,      3;;

menu:   line/grid(cont)/on single line;
click: total no. = 1, line = 29;
pmenu: select = division ratio copy / on, num = 20, start = 1, end = 1;
max no. (p,l,s,v,b):    17,    31,    20,      4,      3;;

menu:   line/grid(end)/on single line;
click: total no. = 1, line = 30;
pmenu: select = division ratio copy / on, num = 80, start = 1, end = 1;
max no. (p,l,s,v,b):    17,    31,    20,      4,      3;;

menu:   volume/copy/mirror;
click: total no. of volume = 0;
pmenu: point on plane = 0, 0, 0, plane normal vector = 0, 0, 1;
max no. (p,l,s,v,b):    18,    34,    23,      5,      3;;

menu:   volume/set body/wall element;
click: total no. of volume = 0;
max no. (p,l,s,v,b):    18,    34,    23,      5,      3;;

menu:   volume/modify/parallel;
```

click: total no. = 0;
pmenu: vector = 0.00224, -0.00129326, 0.00448;
max no. (p,l,s,v,b): 18, 34, 23, 5, 3;;

menu: volume/copy/rotate;
click: total no. of volume = 0;
pmenu: center point = 0, 0, 0, axis vector = 0, 0, 1, angle = 120,
       height = 0,
       no. of copies = 2;
max no. (p,l,s,v,b): 26, 52, 39, 9, 3;;

menu: parameter/change scale;
pmenu: scale = 5.58036, direction = 0;
max no. (p,l,s,v,b): 26, 52, 39, 9, 3;;

menu: file/read history file end;
max no. (p,l,s,v,b): 26, 52, 39, 9, 3;;

menu: block/set ibctyp;
click: total no. = 4, block = 1, index = 1, 0, 2, 4;
pmenu: value = 3, 1, 1, 1;
max no. (p,l,s,v,b): 26, 52, 39, 9, 3;;

menu: block/set ibctyp;
click: total no. = 3, block = 1, index = 0, 2, 4;
pmenu: value = 4, 0, 0;
max no. (p,l,s,v,b): 26, 52, 39, 9, 3;;

menu: block/set ibctyp;
click: total no. = 4, block = 2, index = 1, 0, 4, 2;
pmenu: value = 3, 4, 0, 0;
max no. (p,l,s,v,b): 26, 52, 39, 9, 3;;

menu: block/set ibctyp;
click: total no. = 4, block = 3, index = 1, 0, 4, 2;
pmenu: value = 3, 4, 0, 0;
max no. (p,l,s,v,b): 26, 52, 39, 9, 3;;

menu: block/set ibctyp;
click: total no. = 2, block = 1, index = 1, 0;
pmenu: value = 4, 3;
max no. (p,l,s,v,b): 26, 52, 39, 9, 3;;

menu: block/set ibctyp;
click: total no. = 2, block = 2, index = 1, 0;
pmenu: value = 4, 3;
max no. (p,l,s,v,b): 26, 52, 39, 9, 3;;

menu: block/set ibctyp;
click: total no. = 2, block = 3, index = 1, 0;
pmenu: value = 4, 3;
max no. (p,l,s,v,b): 26, 52, 39, 9, 3;;

menu: physical variable/set value/flow velocity;
click: total no. = 1, block = 1,
    no. of mesh_range = 1, mesh range = 0,-1,0,0,0,-1;
pmenu: select = velocity(x), value = 0, 0, 1;
max no. (p,l,s,v,b): 26, 52, 39, 9, 3;;

menu: physical variable/set value/flow velocity;
click: total no. = 1, block = 2,
    no. of mesh_range = 1, mesh range = 0,-1,0,0,0,-1;
pmenu: select = velocity(x), value = 0, 0, 1;
max no. (p,l,s,v,b): 26, 52, 39, 9, 3;;

menu: physical variable/set value/flow velocity;
click: total no. = 1, block = 3,
    no. of mesh_range = 1, mesh range = 0,-1,0,0,0,-1;
pmenu: select = velocity(x), value = 0, 0, 1;
max no. (p,l,s,v,b): 26, 52, 39, 9, 3;;

menu: physical variable/set value/flow velocity;
click: total no. = 3, block = 1, block = 2, block = 3;
pmenu: select = velocity(x), value = 0, 0, 0;
max no. (p,l,s,v,b): 26, 52, 39, 9, 3;;

```
menu:    physical variable/set value/flow velocity;
click: total no. = 3, block = 1, block = 2, block = 3;
pmenu: select = velocity(x), value = 0, 0, 1;
max no. (p,l,s,v,b):     26,     52,     39,       9,       3;;

menu:    surface/modify/parallel;
click: total no. = 3, surface = 13, 2, 8;
pmenu: vector = 0, 0, 0.01;
max no. (p,l,s,v,b):     26,     52,     39,       9,       3;;

menu:    surface/modify/parallel;
click: total no. = 3, surface = 12, 1, 7;
pmenu: vector = 0, 0, -0.01;
max no. (p,l,s,v,b):     26,     52,     39,       9,       3;;

menu:    physical variable/set value/flow velocity;
click: total no. = 1, block = 1,
          no. of mesh_range = 1, mesh range = 0,-1,0,0,0,-1;
pmenu: select = velocity(x), value = 0, 0, 1;
max no. (p,l,s,v,b):     26,     52,     39,       9,       3;;

menu:    physical variable/set value/flow velocity;
click: total no. = 1, block = 2,
          no. of mesh_range = 1, mesh range = 0,-1,0,0,0,-1;
pmenu: select = velocity(x), value = 0, 0, 1;
max no. (p,l,s,v,b):     26,     52,     39,       9,       3;;

menu:    physical variable/set value/flow velocity;
click: total no. = 1, block = 3,
          no. of mesh_range = 1, mesh range = 0,-1,0,0,0,-1;
pmenu: select = velocity(x), value = 0, 0, 1;
max no. (p,l,s,v,b):     26,     52,     39,       9,       3;;

menu:    physical variable/set value/flow velocity;
click: total no. = 3, block = 1, block = 2, block = 3;
pmenu: select = velocity(x), value = 0, 0, 0;
max no. (p,l,s,v,b):     26,     52,     39,       9,       3;;
```

```
menu:    physical variable/set value/flow velocity;
click: total no. = 1, block = 1,
          no. of mesh_range = 1, mesh range = 0,-1,0,0,0,-1;
pmenu: select = velocity(x), value = 0, 0, 1;
max no. (p,l,s,v,b):     26,     52,     39,       9,       3;;

menu:    physical variable/set value/flow velocity;
click: total no. = 1, block = 2,
          no. of mesh_range = 1, mesh range = 0,-1,0,0,0,-1;
pmenu: select = velocity(x), value = 0, 0, 1;
max no. (p,l,s,v,b):     26,     52,     39,       9,       3;;

menu:    physical variable/set value/flow velocity;
click: total no. = 1, block = 3,
          no. of mesh_range = 1, mesh range = 0,-1,0,0,0,-1;
pmenu: select = velocity(x), value = 0, 0, 1;
max no. (p,l,s,v,b):     26,     52,     39,       9,       3;;

menu:    block/set ibctyp;
click: total no. = 1, block = 1, index = 1;
pmenu: value = 4;
max no. (p,l,s,v,b):     26,     52,     39,       9,       3;;

menu:    physical variable/set value/flow velocity;
click: total no. = 1, block = 1,
          no. of mesh_range = 1, mesh range = 0,-1,0,-1,0,-1;
pmenu: select = velocity(x), value = 0, 0, 0;
max no. (p,l,s,v,b):     26,     52,     39,       9,       3;;

menu:    physical variable/set value/flow velocity;
click: total no. = 1, block = 2,
          no. of mesh_range = 1, mesh range = 0,-1,0,0,0,-1;
pmenu: select = velocity(x), value = 0, 0, 0;
max no. (p,l,s,v,b):     26,     52,     39,       9,       3;;

menu:    physical variable/set value/flow velocity;
click: total no. = 1, block = 3,
          no. of mesh_range = 1, mesh range = 0,-1,0,0,0,-1;
```

```
pmenu: select = velocity(x), value = 0, 0, 0;
max no. (p,l,s,v,b):     26,     52,     39,       9,       3;;

menu:    parameter/particle/generate;
pmenu: kmark = 1, density = 0, diameter = 0,
          coord = 1, start = 0.0066,-0.00103923,0.05, end = 0,0,0, number = 1,1,
          1;
max no. (p,l,s,v,b):     26,     52,     39,       9,       3;;

menu:    physical variable/set value/flow velocity;
click: total no. = 1, block = 1,
          no. of mesh_range = 1, mesh range = 0,-1,0,0,0,-1;
pmenu: select = velocity(x), value = 0, 0, 1;
max no. (p,l,s,v,b):     26,     52,     39,       9,       3;;

menu:    physical variable/set value/flow velocity;
click: total no. = 1, block = 2,
          no. of mesh_range = 1, mesh range = 0,-1,0,0,0,-1;
pmenu: select = velocity(x), value = 0, 0, 1;
max no. (p,l,s,v,b):     26,     52,     39,       9,       3;;

menu:    physical variable/set value/flow velocity;
click: total no. = 1, block = 3,
          no. of mesh_range = 1, mesh range = 0,-1,0,0,0,-1;
pmenu: select = velocity(x), value = 0, 0, 1;
max no. (p,l,s,v,b):     26,     52,     39,       9,       3;;

menu:    parameter/scheme;
pmenu: ismac = 0, ischv = 0, ischke = 0, ischt = 0, ischc = 0, ischa = 0,
          isor = 0;
max no. (p,l,s,v,b):     26,     52,     39,       9,       3;;

menu:    parameter/coordinate;
pmenu: no. of block = 3, block = 1, block = 2, block = 3, rotatg = 0,
          rotatg = 0, rotatg = 0, xrotax = 0, xrotax = 0, xrotax = 0,
          yrotax = 0, yrotax = 0, yrotax = 0, zrotax = 0, zrotax = 0,
          zrotax = 0, xaxs = 0, xaxs = 0, xaxs = 0, yaxs = 0, yaxs = 0,
          yaxs = 0, zaxs = 1, zaxs = 1, zaxs = 1, idefgr = 0, idefgr = 0,
```

idefgr = 0, nsymme = 0, nsymme = 0, nsymme = 0;
max no. (p,l,s,v,b): 26, 52, 39, 9, 3;;

menu: parameter/boundary condition/ibctyp;
pmenu: no. of block = 3, block = 1, block = 2, block = 3, ibctyp = 0,1,1,0,3,
4,0, ibctyp = 1,0,0,1,3,4,0, ibctyp = 1,0,1,0,3,4,0, nbsmin = 0,0,0,0,
0,0,0, nbsmin = 0,0,0,0,0,0,0, nbsmin = 0,0,0,0,0,0,0, nbsmax = 0,0,0,
0,0,0,0, nbsmax = 0,0,0,0,0,0,0, nbsmax = 0,0,0,0,0,0,0, nbperi = 0,0,
0,0,0,0, nbperi = 0,0,0,0,0,0, nbperi = 0,0,0,0,0,0, isetbc = 0,0,0,0,
0,0,0, isetbc = 0,0,0,0,0,0,0, isetbc = 0,0,0,0,0,0,0;
max no. (p,l,s,v,b): 26, 52, 39, 9, 3;;

menu: parameter/flow velocity;
pmenu: vinflx = 0, iporous = 0, icircl = 0;
max no. (p,l,s,v,b): 26, 52, 39, 9, 3;;

menu: parameter/wall friction;
pmenu: iwalfric = 0;
max no. (p,l,s,v,b): 26, 52, 39, 9, 3;;

menu: parameter/wall element file;
pmenu: number of files = 1, file names =
wall-element.txt;
max no. (p,l,s,v,b): 26, 52, 39, 9, 3;;

menu: parameter/particle/generate;
pmenu: kmark = 0, density = 0, diameter = 0,
coord = 1, start = 0,0,0, end = 0,0,0, number = 1,1,1;
max no. (p,l,s,v,b): 26, 52, 39, 9, 3;;

menu: parameter/particle/generate;
pmenu: kmark = 0, density = 0, diameter = 0,
coord = 1, start = -0.005,-0.00311769,0.05, end = 0,0,0, number = 1,1,
1;
max no. (p,l,s,v,b): 26, 52, 39, 9, 3;;

menu: parameter/particle/generate;
pmenu: kmark = 0, density = 0, diameter = 0,

coord = 1, start = -0.005,-0.00311769,0.05, end = 0,0,0, number = 1,1,
1;
max no. (p,l,s,v,b): 26, 52, 39, 9, 3;;

menu: physical variable/set value/flow velocity;
click: total no. = 1, block = 1,
no. of mesh_range = 1, mesh range = 0,-1,0,0,0,-1;
pmenu: select = velocity(x), value = 0, 0, 1;
max no. (p,l,s,v,b): 26, 52, 39, 9, 3;;

menu: physical variable/set value/flow velocity;
click: total no. = 1, block = 3,
no. of mesh_range = 1, mesh range = 13,13,0,0,11,11;
pmenu: select = velocity(x), value = 0, 0, 1;
max no. (p,l,s,v,b): 26, 52, 39, 9, 3;;

menu: physical variable/set value/flow velocity;
click: total no. = 1, block = 2,
no. of mesh_range = 1, mesh range = 0,-1,0,0,0,-1;
pmenu: select = velocity(x), value = 0, 0, 1;
max no. (p,l,s,v,b): 26, 52, 39, 9, 3;;

menu: physical variable/set value/flow velocity;
click: total no. = 1, block = 1,
no. of mesh_range = 1, mesh range = 0,1,0,0,0,1;
pmenu: select = velocity(x), value = 0, 0, 1;
max no. (p,l,s,v,b): 26, 52, 39, 9, 3;;

menu: physical variable/set value/flow velocity;
click: total no. = 1, block = 3,
no. of mesh_range = 1, mesh range = 0,-1,0,0,0,-1;
pmenu: select = velocity(x), value = 0, 0, 1;
max no. (p,l,s,v,b): 26, 52, 39, 9, 3;;

menu: physical variable/set value/flow velocity;
click: total no. = 1, block = 2,
no. of mesh_range = 1, mesh range = 0,-1,0,0,0,-1;
pmenu: select = velocity(x), value = 0, 0, 1;

max no. (p,l,s,v,b): 26, 52, 39, 9, 3;;

menu: parameter/particle/append;
pmenu: nmark = 3;
pmenu: coord = 1, xmark = -0.00185, ymark = -0.00342, zmark = 0.061945,
kmark = 0, density = 2450, markdiameter = 0.0025, coord = 1,
xmark = 0.000816, ymark = 0.005154, zmark = 0.063209, kmark = 0,
density = 2450, markdiameter = 0.0025, coord = 1, xmark = 0.00236,
ymark = -0.00119, zmark = 0.061248, kmark = 0, density = 2450,
markdiameter = 0.0025;
max no. (p,l,s,v,b): 26, 52, 39, 9, 3;;

menu: parameter/particle/append;
pmenu: nmark = 3;
pmenu: coord = 1, xmark = 0.003479, ymark = -0.00135, zmark = 0.066256,
kmark = 0, density = 2450, markdiameter = 0.0025, coord = 1,
xmark = -0.00132, ymark = 0.000256, zmark = 0.068042, kmark = 0,
density = 2450, markdiameter = 0.0025, coord = 1, xmark = -0.00285,
ymark = -0.00508, zmark = 0.069304, kmark = 0, density = 2450,
markdiameter = 0.0025;
max no. (p,l,s,v,b): 26, 52, 39, 9, 3;;

menu: parameter/particle/append;
pmenu: nmark = 3;
pmenu: coord = 1, xmark = 0.00126, ymark = -0.00593, zmark = 0.063792,
kmark = 0, density = 2450, markdiameter = 0.0025, coord = 1,
xmark = 0.004484, ymark = -0.00497, zmark = 0.066314, kmark = 0,
density = 2450, markdiameter = 0.0025, coord = 1, xmark = -0.00472,
ymark = 0.003795, zmark = 0.062903, kmark = 0, density = 2450,
markdiameter = 0.0025;
max no. (p,l,s,v,b): 26, 52, 39, 9, 3;;

menu: parameter/particle/append;
pmenu: nmark = 3;
pmenu: coord = 1, xmark = -0.00107, ymark = -0.00154, zmark = 0.066353,
kmark = 0, density = 2450, markdiameter = 0.0025, coord = 1,
xmark = -0.00506, ymark = -0.00604, zmark = 0.061638, kmark = 0,
density = 2450, markdiameter = 0.0025, coord = 1, xmark = 0.001518,

ymark = 0.004025, zmark = 0.061226, kmark = 0, density = 2450,
markdiameter = 0.0025;
max no. (p,l,s,v,b): 26, 52, 39, 9, 3;;

menu: parameter/particle/append;
pmenu: nmark = 3;
pmenu: coord = 1, xmark = 0.00431, ymark = -0.00116, zmark = 0.06881,
kmark = 0, density = 2450, markdiameter = 0.0025, coord = 1,
xmark = -0.00308, ymark = 0.004573, zmark = 0.061245, kmark = 0,
density = 2450, markdiameter = 0.0025, coord = 1, xmark = 0.003467,
ymark = 0.001702, zmark = 0.065339, kmark = 0, density = 2450,
markdiameter = 0.0025;
max no. (p,l,s,v,b): 26, 52, 39, 9, 3;;

menu: parameter/particle/append;
pmenu: nmark = 3;
pmenu: coord = 1, xmark = 0.005328, ymark = -0.00373, zmark = 0.068695,
kmark = 0, density = 2450, markdiameter = 0.0025, coord = 1,
xmark = -0.00293, ymark = 0.007384, zmark = 0.061296, kmark = 0,
density = 2450, markdiameter = 0.0025, coord = 1, xmark = 0.006822,
ymark = 0.000256, zmark = 0.06325, kmark = 0, density = 2450,
markdiameter = 0.0025;
max no. (p,l,s,v,b): 26, 52, 39, 9, 3;;

menu: parameter/particle/append;
pmenu: nmark = 3;
pmenu: coord = 1, xmark = -0.00256, ymark = -0.00068, zmark = 0.061239,
kmark = 0, density = 2450, markdiameter = 0.0025, coord = 1,
xmark = 0.004767, ymark = 0.003803, zmark = 0.061364, kmark = 0,
density = 2450, markdiameter = 0.0025, coord = 1, xmark = 0.006021,
ymark = 0.001559, zmark = 0.061332, kmark = 0, density = 2450,
markdiameter = 0.0025;
max no. (p,l,s,v,b): 26, 52, 39, 9, 3;;

menu: parameter/particle/append;
pmenu: nmark = 3;
pmenu: coord = 1, xmark = -0.00541, ymark = 0.001583, zmark = 0.069769,
kmark = 0, density = 2450, markdiameter = 0.0025, coord = 1,

xmark = -0.00103, ymark = 0.000636, zmark = 0.063182, kmark = 0,
density = 2450, markdiameter = 0.0025, coord = 1, xmark = -0.00535,
ymark = -0.00547, zmark = 0.066263, kmark = 0, density = 2450,
markdiameter = 0.0025;
max no. (p,l,s,v,b): 26, 52, 39, 9, 3;;

menu: parameter/particle/append;
pmenu: nmark = 3;
pmenu: coord = 1, xmark = 0.000198, ymark = -0.00592, zmark = 0.061253,
kmark = 0, density = 2450, markdiameter = 0.0025, coord = 1,
xmark = 0.004868, ymark = -0.00095, zmark = 0.061288, kmark = 0,
density = 2450, markdiameter = 0.0025, coord = 1, xmark = 0.006841,
ymark = -0.00439, zmark = 0.062505, kmark = 0, density = 2450,
markdiameter = 0.0025;
max no. (p,l,s,v,b): 26, 52, 39, 9, 3;;

menu: parameter/particle/append;
pmenu: nmark = 3;
pmenu: coord = 1, xmark = -0.00069, ymark = 0.005251, zmark = 0.061253,
kmark = 0, density = 2450, markdiameter = 0.0025, coord = 1,
xmark = -0.00567, ymark = 0.001489, zmark = 0.061454, kmark = 0,
density = 2450, markdiameter = 0.0025, coord = 1, xmark = 0.00342,
ymark = 0.001351, zmark = 0.061279, kmark = 0, density = 2450,
markdiameter = 0.0025;
max no. (p,l,s,v,b): 26, 52, 39, 9, 3;;

menu: parameter/particle/append;
pmenu: nmark = 3;
pmenu: coord = 1, xmark = 0.002038, ymark = -0.00246, zmark = 0.06951,
kmark = 0, density = 2450, markdiameter = 0.0025, coord = 1,
xmark = 0.005871, ymark = -0.00014, zmark = 0.065522, kmark = 0,
density = 2450, markdiameter = 0.0025, coord = 1, xmark = -0.00182,
ymark = 0.005647, zmark = 0.0655, kmark = 0, density = 2450,
markdiameter = 0.0025;
max no. (p,l,s,v,b): 26, 52, 39, 9, 3;;

menu: parameter/particle/append;
pmenu: nmark = 3;

```
pmenu: coord = 1, xmark = -0.00614, ymark = 0.000179, zmark = 0.065744,
        kmark = 0, density = 2450, markdiameter = 0.0025, coord = 1,
        xmark = 0.001449, ymark = 0.003271, zmark = 0.068057, kmark = 0,
        density = 2450, markdiameter = 0.0025, coord = 1, xmark = 0.003215,
        ymark = 0.003234, zmark = 0.063274, kmark = 0, density = 2450,
        markdiameter = 0.0025;
max no. (p,l,s,v,b):     26,     52,     39,       9,       3;;

menu:    parameter/particle/append;
pmenu: nmark = 3;
pmenu: coord = 1, xmark = 0.004132, ymark = 0.00019, zmark = 0.063365,
        kmark = 0, density = 2450, markdiameter = 0.0025, coord = 1,
        xmark = -0.00465, ymark = 0.00375, zmark = 0.065458, kmark = 0,
        density = 2450, markdiameter = 0.0025, coord = 1, xmark = -0.00648,
        ymark = -0.00305, zmark = 0.066965, kmark = 0, density = 2450,
        markdiameter = 0.0025;
max no. (p,l,s,v,b):     26,     52,     39,       9,       3;;

menu:    parameter/particle/append;
pmenu: nmark = 3;
pmenu: coord = 1, xmark = 0.001468, ymark = 0.000101, zmark = 0.063516,
        kmark = 0, density = 2450, markdiameter = 0.0025, coord = 1,
        xmark = 0.000669, ymark = -0.00481, zmark = 0.066145, kmark = 0,
        density = 2450, markdiameter = 0.0025, coord = 1, xmark = -0.00568,
        ymark = -0.00165, zmark = 0.061382, kmark = 0, density = 2450,
        markdiameter = 0.0025;
max no. (p,l,s,v,b):     26,     52,     39,       9,       3;;

menu:    parameter/particle/append;
pmenu: nmark = 3;
pmenu: coord = 1, xmark = -0.00147, ymark = -0.0053, zmark = 0.063675,
        kmark = 0, density = 2450, markdiameter = 0.0025, coord = 1,
        xmark = 0.0031, ymark = -0.00594, zmark = 0.061583, kmark = 0,
        density = 2450, markdiameter = 0.0025, coord = 1, xmark = 0.000969,
        ymark = 0.007377, zmark = 0.06427, kmark = 0, density = 2450,
        markdiameter = 0.0025;
max no. (p,l,s,v,b):     26,     52,     39,       9,       3;;
```

menu: parameter/particle/append;
pmenu: nmark = 3;
pmenu: coord = 1, xmark = 0.003501, ymark = 0.005844, zmark = 0.063021,
kmark = 0, density = 2450, markdiameter = 0.0025, coord = 1,
xmark = 0.002168, ymark = 0.00603, zmark = 0.065982, kmark = 0,
density = 2450, markdiameter = 0.0025, coord = 1, xmark = -0.00964,
ymark = -0.00532, zmark = 0.06672, kmark = 0, density = 2450,
markdiameter = 0.0025;
max no. (p,l,s,v,b): 26, 52, 39, 9, 3;;

menu: parameter/particle/append;
pmenu: nmark = 3;
pmenu: coord = 1, xmark = 0.003052, ymark = -0.00286, zmark = 0.063698,
kmark = 0, density = 2450, markdiameter = 0.0025, coord = 1,
xmark = -0.00356, ymark = -0.00055, zmark = 0.063665, kmark = 0,
density = 2450, markdiameter = 0.0025, coord = 1, xmark = -0.0004,
ymark = 0.00101, zmark = 0.065608, kmark = 0, density = 2450,
markdiameter = 0.0025;
max no. (p,l,s,v,b): 26, 52, 39, 9, 3;;

menu: parameter/particle/append;
pmenu: nmark = 3;
pmenu: coord = 1, xmark = -0.0021, ymark = 0.003228, zmark = 0.067182,
kmark = 0, density = 2450, markdiameter = 0.0025, coord = 1,
xmark = 0.000492, ymark = 0.000895, zmark = 0.061222, kmark = 0,
density = 2450, markdiameter = 0.0025, coord = 1, xmark = -0.003,
ymark = 0.001477, zmark = 0.065655, kmark = 0, density = 2450,
markdiameter = 0.0025;
max no. (p,l,s,v,b): 26, 52, 39, 9, 3;;

menu: parameter/particle/append;
pmenu: nmark = 3;
pmenu: coord = 1, xmark = 0.00097, ymark = -0.00077, zmark = 0.067487,
kmark = 0, density = 2450, markdiameter = 0.0025, coord = 1,
xmark = -0.00263, ymark = 0.001808, zmark = 0.069441, kmark = 0,
density = 2450, markdiameter = 0.0025, coord = 1, xmark = 0.002264,
ymark = -0.00559, zmark = 0.068277, kmark = 0, density = 2450,
markdiameter = 0.0025;

```
max no. (p,l,s,v,b):     26,     52,     39,       9,       3;;

menu:    parameter/particle/append;
pmenu: nmark = 3;
pmenu: coord = 1, xmark = 0.000983, ymark = 0.003201, zmark = 0.0652,
          kmark = 0, density = 2450, markdiameter = 0.0025, coord = 1,
          xmark = -0.00502, ymark = 0.002288, zmark = 0.067445, kmark = 0,
          density = 2450, markdiameter = 0.0025, coord = 1, xmark = 0.007997,
          ymark = -0.00231, zmark = 0.063724, kmark = 0, density = 2450,
          markdiameter = 0.0025;
max no. (p,l,s,v,b):     26,     52,     39,       9,       3;;

menu:    parameter/particle/append;
pmenu: nmark = 3;
pmenu: coord = 1, xmark = 0.004275, ymark = -0.00573, zmark = 0.063913,
          kmark = 0, density = 2450, markdiameter = 0.0025, coord = 1,
          xmark = 0.000297, ymark = 0.002727, zmark = 0.062873, kmark = 0,
          density = 2450, markdiameter = 0.0025, coord = 1, xmark = 0.004239,
          ymark = 0.004536, zmark = 0.065229, kmark = 0, density = 2450,
          markdiameter = 0.0025;
max no. (p,l,s,v,b):     26,     52,     39,       9,       3;;

menu:    parameter/particle/append;
pmenu: nmark = 3;
pmenu: coord = 1, xmark = 0.002526, ymark = 0.000891, zmark = 0.068779,
          kmark = 0, density = 2450, markdiameter = 0.0025, coord = 1,
          xmark = -0.00134, ymark = -0.0017, zmark = 0.063814, kmark = 0,
          density = 2450, markdiameter = 0.0025, coord = 1, xmark = 0.001949,
          ymark = -0.00376, zmark = 0.061246, kmark = 0, density = 2450,
          markdiameter = 0.0025;
max no. (p,l,s,v,b):     26,     52,     39,       9,       3;;

menu:    parameter/particle/append;
pmenu: nmark = 3;
pmenu: coord = 1, xmark = 0.009072, ymark = -0.0061, zmark = 0.064368,
          kmark = 0, density = 2450, markdiameter = 0.0025, coord = 1,
          xmark = -0.00345, ymark = 0.001692, zmark = 0.062554, kmark = 0,
          density = 2450, markdiameter = 0.0025, coord = 1, xmark = -0.00633,
```

ymark = -0.00592, zmark = 0.063804, kmark = 0, density = 2450,
markdiameter = 0.0025;
max no. (p,l,s,v,b): 26, 52, 39, 9, 3;;

menu: parameter/particle/append;
pmenu: nmark = 3;
pmenu: coord = 1, xmark = -0.00721, ymark = -0.00398, zmark = 0.061127,
kmark = 0, density = 2450, markdiameter = 0.0025, coord = 1,
xmark = -0.00336, ymark = 0.006087, zmark = 0.063401, kmark = 0,
density = 2450, markdiameter = 0.0025, coord = 1, xmark = 0.005587,
ymark = 0.002212, zmark = 0.064026, kmark = 0, density = 2450,
markdiameter = 0.0025;
max no. (p,l,s,v,b): 26, 52, 39, 9, 3;;

menu: parameter/particle/append;
pmenu: nmark = 3;
pmenu: coord = 1, xmark = -0.00049, ymark = 0.009542, zmark = 0.061234,
kmark = 0, density = 2450, markdiameter = 0.0025, coord = 1,
xmark = 0.007651, ymark = -0.00158, zmark = 0.067897, kmark = 0,
density = 2450, markdiameter = 0.0025, coord = 1, xmark = 3.91e-005,
ymark = -0.00194, zmark = 0.061285, kmark = 0, density = 2450,
markdiameter = 0.0025;
max no. (p,l,s,v,b): 26, 52, 39, 9, 3;;

menu: parameter/particle/append;
pmenu: nmark = 3;
pmenu: coord = 1, xmark = -0.00213, ymark = 0.003647, zmark = 0.063592,
kmark = 0, density = 2450, markdiameter = 0.0025, coord = 1,
xmark = 0.001301, ymark = -0.0018, zmark = 0.065121, kmark = 0,
density = 2450, markdiameter = 0.0025, coord = 1, xmark = -0.00058,
ymark = -0.00361, zmark = 0.067897, kmark = 0, density = 2450,
markdiameter = 0.0025;
max no. (p,l,s,v,b): 26, 52, 39, 9, 3;;

menu: parameter/particle/append;
pmenu: nmark = 3;
pmenu: coord = 1, xmark = 0.008378, ymark = -0.00413, zmark = 0.069278,
kmark = 0, density = 2450, markdiameter = 0.0025, coord = 1,

xmark = 0.009602, ymark = -0.00375, zmark = 0.061751, kmark = 0,
density = 2450, markdiameter = 0.0025, coord = 1, xmark = 0.004788,
ymark = -0.00343, zmark = 0.061235, kmark = 0, density = 2450,
markdiameter = 0.0025;
max no. (p,l,s,v,b): 26, 52, 39, 9, 3;;

menu: parameter/particle/append;
pmenu: nmark = 3;
pmenu: coord = 1, xmark = -0.00372, ymark = 0.004935, zmark = 0.068047,
kmark = 0, density = 2450, markdiameter = 0.0025, coord = 1,
xmark = -0.00497, ymark = -0.00329, zmark = 0.069514, kmark = 0,
density = 2450, markdiameter = 0.0025, coord = 1, xmark = -0.00101,
ymark = 0.006572, zmark = 0.0689, kmark = 0, density = 2450,
markdiameter = 0.0025;
max no. (p,l,s,v,b): 26, 52, 39, 9, 3;;

menu: parameter/particle/append;
pmenu: nmark = 3;
pmenu: coord = 1, xmark = -0.00156, ymark = 0.002468, zmark = 0.061229,
kmark = 0, density = 2450, markdiameter = 0.0025, coord = 1,
xmark = -0.00582, ymark = 0.001918, zmark = 0.064053, kmark = 0,
density = 2450, markdiameter = 0.0025, coord = 1, xmark = -0.00575,
ymark = -0.00303, zmark = 0.063402, kmark = 0, density = 2450,
markdiameter = 0.0025;
max no. (p,l,s,v,b): 26, 52, 39, 9, 3;;

menu: parameter/particle/append;
pmenu: nmark = 3;
pmenu: coord = 1, xmark = -0.00257, ymark = -0.00569, zmark = 0.061233,
kmark = 0, density = 2450, markdiameter = 0.0025, coord = 1,
xmark = -0.00331, ymark = -0.00158, zmark = 0.069916, kmark = 0,
density = 2450, markdiameter = 0.0025, coord = 1, xmark = 0.00582,
ymark = 0.00214, zmark = 0.066501, kmark = 0, density = 2450,
markdiameter = 0.0025;
max no. (p,l,s,v,b): 26, 52, 39, 9, 3;;

menu: parameter/particle/append;
pmenu: nmark = 3;

```
pmenu: coord = 1, xmark = 0.00388, ymark = 0.005278, zmark = 0.068114,
        kmark = 0, density = 2450, markdiameter = 0.0025, coord = 1,
        xmark = 0.000526, ymark = -0.00446, zmark = 0.069997, kmark = 0,
        density = 2450, markdiameter = 0.0025, coord = 1, xmark = 0.006964,
        ymark = 0.0032, zmark = 0.065834, kmark = 0, density = 2450,
        markdiameter = 0.0025;
max no. (p,l,s,v,b):     26,     52,     39,       9,       3;;

menu:    parameter/particle/append;
pmenu: nmark = 3;
pmenu: coord = 1, xmark = -0.00327, ymark = -0.00323, zmark = 0.064525,
        kmark = 0, density = 2450, markdiameter = 0.0025, coord = 1,
        xmark = -0.00361, ymark = -0.00361, zmark = 0.067406, kmark = 0,
        density = 2450, markdiameter = 0.0025, coord = 1, xmark = 0.00451,
        ymark = -0.00609, zmark = 0.06964, kmark = 0, density = 2450,
        markdiameter = 0.0025;
max no. (p,l,s,v,b):     26,     52,     39,       9,       3;;

menu:    parameter/particle/append;
pmenu: nmark = 3;
pmenu: coord = 1, xmark = -0.00787, ymark = -0.00142, zmark = 0.065481,
        kmark = 0, density = 2450, markdiameter = 0.0025, coord = 1,
        xmark = 0.005401, ymark = 0.001017, zmark = 0.068807, kmark = 0,
        density = 2450, markdiameter = 0.0025, coord = 1, xmark = -0.00128,
        ymark = 0.007208, zmark = 0.063358, kmark = 0, density = 2450,
        markdiameter = 0.0025;
max no. (p,l,s,v,b):     26,     52,     39,       9,       3;;

menu:    parameter/particle/append;
pmenu: nmark = 1;
pmenu: coord = 1, xmark = -0.00824, ymark = -0.00391, zmark = 0.065005,
        kmark = 0, density = 2450, markdiameter = 0.0025;
max no. (p,l,s,v,b):     26,     52,     39,       9,       3;;

menu:    parameter/particle/append;
pmenu: nmark = 3;
pmenu: coord = 1, xmark = -0.00185, ymark = -0.00342, zmark = 0.051945,
        kmark = 0, density = 2450, markdiameter = 0.0025, coord = 1,
```

xmark = 0.000816, ymark = 0.005154, zmark = 0.053209, kmark = 0,
density = 2450, markdiameter = 0.0025, coord = 1, xmark = 0.00236,
ymark = -0.00119, zmark = 0.051248, kmark = 0, density = 2450,
markdiameter = 0.0025;
max no. (p,l,s,v,b): 26, 52, 39, 9, 3;;

menu: parameter/particle/append;
pmenu: nmark = 3;
pmenu: coord = 1, xmark = 0.00236, ymark = -0.00119, zmark = 0.051248,
kmark = 0, density = 2450, markdiameter = 0.0025, coord = 1,
xmark = -0.00132, ymark = 0.000256, zmark = 0.058042, kmark = 0,
density = 2450, markdiameter = 0.0025, coord = 1, xmark = -0.00285,
ymark = -0.00508, zmark = 0.059304, kmark = 0, density = 2450,
markdiameter = 0.0025;
max no. (p,l,s,v,b): 26, 52, 39, 9, 3;;

menu: parameter/particle/append;
pmenu: nmark = 3;
pmenu: coord = 1, xmark = 0.00126, ymark = -0.00593, zmark = 0.053792,
kmark = 0, density = 2450, markdiameter = 0.0025, coord = 1,
xmark = 0.004484, ymark = -0.00497, zmark = 0.056314, kmark = 0,
density = 2450, markdiameter = 0.0025, coord = 1, xmark = -0.00472,
ymark = 0.003795, zmark = 0.052903, kmark = 0, density = 2450,
markdiameter = 0.0025;
max no. (p,l,s,v,b): 26, 52, 39, 9, 3;;

menu: parameter/particle/append;
pmenu: nmark = 3;
pmenu: coord = 1, xmark = -0.00107, ymark = -0.00154, zmark = 0.056353,
kmark = 0, density = 2450, markdiameter = 0.025, coord = 1,
xmark = -0.00506, ymark = -0.00604, zmark = 0.051638, kmark = 0,
density = 2450, markdiameter = 0.025, coord = 1, xmark = -0.001518,
ymark = 0.004025, zmark = 0.051226, kmark = 0, density = 2450,
markdiameter = 0.025;
max no. (p,l,s,v,b): 26, 52, 39, 9, 3;;

menu: parameter/particle/append;
pmenu: nmark = 3;

pmenu: coord = 1, xmark = -0.00185, ymark = -0.00342, zmark = 0.051945,
kmark = 0, density = 2450, markdiameter = 0.0025, coord = 1,
xmark = 0.000816, ymark = 0.005154, zmark = 0.053209, kmark = 0,
density = 2450, markdiameter = 0.0025, coord = 1, xmark = 0.00236,
ymark = -0.00119, zmark = 0.051248, kmark = 0, density = 2450,
markdiameter = 0.0025;
max no. (p,l,s,v,b): 26, 52, 39, 9, 3;;

menu: parameter/particle/append;
pmenu: nmark = 3;
pmenu: coord = 1, xmark = 0.003479, ymark = -0.00135, zmark = 0.056256,
kmark = 0, density = 2450, markdiameter = 0.0025, coord = 1,
xmark = -0.00132, ymark = 0.000256, zmark = 0.058042, kmark = 0,
density = 2450, markdiameter = 0.0025, coord = 1, xmark = -0.00285,
ymark = -0.00508, zmark = 0.059304, kmark = 0, density = 2450,
markdiameter = 0.0025;
max no. (p,l,s,v,b): 26, 52, 39, 9, 3;;

menu: parameter/particle/append;
pmenu: nmark = 3;
pmenu: coord = 1, xmark = 0.00126, ymark = -0.00593, zmark = 0.053792,
kmark = 0, density = 2450, markdiameter = 0.0025, coord = 1,
xmark = 0.004484, ymark = -0.00497, zmark = 0.056314, kmark = 0,
density = 2450, markdiameter = 0.0025, coord = 1, xmark = -0.00472,
ymark = 0.003795, zmark = 0.052903, kmark = 0, density = 2450,
markdiameter = 0.0025;
max no. (p,l,s,v,b): 26, 52, 39, 9, 3;;

menu: parameter/particle/append;
pmenu: nmark = 2;
pmenu: coord = 1, xmark = -0.00107, ymark = -0.00154, zmark = 0.056353,
kmark = 0, density = 2450, markdiameter = 0.0025, coord = 1,
xmark = -0.00506, ymark = -0.00604, zmark = 0.051638, kmark = 0,
density = 2450, markdiameter = 0.0025;
max no. (p,l,s,v,b): 26, 52, 39, 9, 3;;

menu: parameter/particle/append;
pmenu: nmark = 1;

```
pmenu: coord = 1, xmark = 0.001518, ymark = 0.004025, zmark = 0.051226,
        kmark = 0, density = 2450, markdiameter = 0.0025;
max no. (p,l,s,v,b):     26,     52,     39,       9,       3;;

menu:    parameter/particle/append;
pmenu: nmark = 3;
pmenu: coord = 1, xmark = 0.00431, ymark = -0.00116, zmark = 0.05881,
        kmark = 0, density = 2450, markdiameter = 0.0025, coord = 1,
        xmark = -0.00308, ymark = 0.004573, zmark = 0.051245, kmark = 0,
        density = 2450, markdiameter = 0.0025, coord = 1, xmark = 0.003467,
        ymark = 0.001702, zmark = 0.055339, kmark = 0, density = 2450,
        markdiameter = 0.0025;
max no. (p,l,s,v,b):     26,     52,     39,       9,       3;;

menu:    parameter/particle/append;
pmenu: nmark = 3;
pmenu: coord = 1, xmark = 0.005328, ymark = -0.00373, zmark = 0.058695,
        kmark = 0, density = 2450, markdiameter = 0.0025, coord = 1,
        xmark = -0.00293, ymark = 0.007384, zmark = 0.051296, kmark = 0,
        density = 2450, markdiameter = 0.0025, coord = 1, xmark = 0.006822,
        ymark = 0.000256, zmark = 0.05325, kmark = 0, density = 2450,
        markdiameter = 0.0025;
max no. (p,l,s,v,b):     26,     52,     39,       9,       3;;

menu:    parameter/particle/append;
pmenu: nmark = 3;
pmenu: coord = 1, xmark = -0.00256, ymark = -0.00068, zmark = 0.051239,
        kmark = 0, density = 2450, markdiameter = 0.0025, coord = 1,
        xmark = 0.004767, ymark = 0.003803, zmark = 0.051364, kmark = 0,
        density = 2450, markdiameter = 0.0025, coord = 1, xmark = 0.006021,
        ymark = 0.001559, zmark = 0.051332, kmark = 0, density = 2450,
        markdiameter = 0.0025;
max no. (p,l,s,v,b):     26,     52,     39,       9,       3;;

menu:    parameter/particle/append;
pmenu: nmark = 3;
pmenu: coord = 1, xmark = -0.00541, ymark = 0.001583, zmark = 0.059769,
        kmark = 0, density = 2450, markdiameter = 0.0025, coord = 1,
```

xmark = -0.00103, ymark = 0.000636, zmark = 0.053182, kmark = 0,
density = 2450, markdiameter = 0.0025, coord = 1, xmark = -0.00535,
ymark = -0.00547, zmark = 0.056263, kmark = 0, density = 2450,
markdiameter = 0.0025;
max no. (p,l,s,v,b): 26, 52, 39, 9, 3;;

menu: parameter/particle/append;
pmenu: nmark = 3;
pmenu: coord = 1, xmark = 0.000198, ymark = -0.00592, zmark = 0.051253,
kmark = 0, density = 2450, markdiameter = 0.0025, coord = 1,
xmark = 0.004868, ymark = -0.00095, zmark = 0.051288, kmark = 0,
density = 2450, markdiameter = 0.0025, coord = 1, xmark = 0.006841,
ymark = -0.00439, zmark = 0.052505, kmark = 0, density = 2450,
markdiameter = 0.0025;
max no. (p,l,s,v,b): 26, 52, 39, 9, 3;;

menu: parameter/particle/append;
pmenu: nmark = 3;
pmenu: coord = 1, xmark = -0.00069, ymark = 0.005251, zmark = 0.051233,
kmark = 0, density = 2450, markdiameter = 0.0025, coord = 1,
xmark = -0.00567, ymark = 0.001489, zmark = 0.051454, kmark = 0,
density = 2450, markdiameter = 0.0025, coord = 1, xmark = 0.00342,
ymark = 0.001351, zmark = 0.051279, kmark = 0, density = 2450,
markdiameter = 0.0025;
max no. (p,l,s,v,b): 26, 52, 39, 9, 3;;

menu: parameter/particle/append;
pmenu: nmark = 3;
pmenu: coord = 1, xmark = 0.002038, ymark = -0.00246, zmark = 0.05951,
kmark = 0, density = 2450, markdiameter = 0.0025, coord = 1,
xmark = 0.005871, ymark = -0.00014, zmark = 0.0555522, kmark = 0,
density = 2450, markdiameter = 0.0025, coord = 1, xmark = -0.00182,
ymark = 0.005647, zmark = 0.0555, kmark = 0, density = 2450,
markdiameter = 0.0025;
max no. (p,l,s,v,b): 26, 52, 39, 9, 3;;

menu: parameter/particle/append;
pmenu: nmark = 3;

pmenu: coord = 1, xmark = -0.00614, ymark = 0.000179, zmark = 0.055744,
kmark = 0, density = 2450, markdiameter = 0.0025, coord = 1,
xmark = 0.001449, ymark = 0.003271, zmark = 0.058057, kmark = 0,
density = 2450, markdiameter = 0.0025, coord = 1, xmark = 0.003215,
ymark = 0.003234, zmark = 0.053274, kmark = 0, density = 2450,
markdiameter = 0.0025;
max no. (p,l,s,v,b): 26, 52, 39, 9, 3;;

menu: parameter/particle/append;
pmenu: nmark = 3;
pmenu: coord = 1, xmark = 0.004132, ymark = 0.00019, zmark = 0.053365,
kmark = 0, density = 2450, markdiameter = 0.0025, coord = 1,
xmark = -0.00465, ymark = 0.00375, zmark = 0.055458, kmark = 0,
density = 2450, markdiameter = 0.0025, coord = 1, xmark = -0.00648,
ymark = -0.00305, zmark = 0.056965, kmark = 0, density = 2450,
markdiameter = 0.0025;
max no. (p,l,s,v,b): 26, 52, 39, 9, 3;;

menu: parameter/particle/append;
pmenu: nmark = 3;
pmenu: coord = 1, xmark = 0.001463, ymark = 0.000101, zmark = 0.053516,
kmark = 0, density = 2450, markdiameter = 0.0025, coord = 1,
xmark = 0.000669, ymark = -0.00481, zmark = 0.056145, kmark = 0,
density = 2450, markdiameter = 0.0025, coord = 1, xmark = -0.00568,
ymark = -0.00165, zmark = 0.051382, kmark = 0, density = 2450,
markdiameter = 0.0025;
max no. (p,l,s,v,b): 26, 52, 39, 9, 3;;

menu: parameter/particle/append;
pmenu: nmark = 3;
pmenu: coord = 1, xmark = -0.00147, ymark = -0.0053, zmark = 0.053675,
kmark = 0, density = 2450, markdiameter = 0.0025, coord = 1,
xmark = 0.0031, ymark = -0.00594, zmark = 0.051583, kmark = 0,
density = 2450, markdiameter = 0.0025, coord = 1, xmark = 0.000969,
ymark = 0.007377, zmark = 0.05427, kmark = 0, density = 2450,
markdiameter = 0.0025;
max no. (p,l,s,v,b): 26, 52, 39, 9, 3;;

menu: parameter/particle/append;
pmenu: nmark = 3;
pmenu: coord = 1, xmark = 0.003501, ymark = 0.005844, zmark = 0.053021,
kmark = 0, density = 2450, markdiameter = 0.0025, coord = 1,
xmark = 0.002168, ymark = 0.00603, zmark = 0.055982, kmark = 0,
density = 2450, markdiameter = 0.0025, coord = 1, xmark = -0.00964,
ymark = -0.00532, zmark = 0.05672, kmark = 0, density = 2450,
markdiameter = 0.0025;
max no. (p,l,s,v,b): 26, 52, 39, 9, 3;;

menu: parameter/particle/append;
pmenu: nmark = 3;
pmenu: coord = 1, xmark = 0.003052, ymark = -0.00286, zmark = 0.053698,
kmark = 0, density = 2450, markdiameter = 0.0025, coord = 1,
xmark = -0.00356, ymark = -0.00055, zmark = 0.053665, kmark = 0,
density = 2450, markdiameter = 0.0025, coord = 1, xmark = -0.0004,
ymark = 0.00101, zmark = 0.055608, kmark = 0, density = 2450,
markdiameter = 0.0025;
max no. (p,l,s,v,b): 26, 52, 39, 9, 3;;

menu: parameter/particle/append;
pmenu: nmark = 3;
pmenu: coord = 1, xmark = -0.0021, ymark = 0.003228, zmark = 0.057182,
kmark = 0, density = 2450, markdiameter = 0.0025, coord = 1,
xmark = 0.000492, ymark = 0.000895, zmark = 0.051222, kmark = 0,
density = 2450, markdiameter = 0.0025, coord = 1, xmark = -0.003,
ymark = 0.001477, zmark = 0.055655, kmark = 0, density = 2450,
markdiameter = 0.0025;
max no. (p,l,s,v,b): 26, 52, 39, 9, 3;;

menu: parameter/particle/append;
pmenu: nmark = 3;
pmenu: coord = 1, xmark = 0.00097, ymark = -0.00077, zmark = 0.057487,
kmark = 0, density = 2450, markdiameter = 0.0025, coord = 1,
xmark = -0.00263, ymark = 0.001808, zmark = 0.059441, kmark = 0,
density = 2450, markdiameter = 0.0025, coord = 1, xmark = 0.002264,
ymark = -0.00559, zmark = 0.058277, kmark = 0, density = 2450,
markdiameter = 0.0025;

```
max no. (p,l,s,v,b):     26,     52,     39,       9,       3;;

menu:    parameter/particle/append;
pmenu: nmark = 3;
pmenu: coord = 1, xmark = 0.00983, ymark = 0.003201, zmark = 0.0552,
          kmark = 0, density = 2450, markdiameter = 0.0025, coord = 1,
          xmark = -0.00502, ymark = 0.002288, zmark = 0.057445, kmark = 0,
          density = 2450, markdiameter = 0.0025, coord = 1, xmark = 0.007997,
          ymark = -0.00231, zmark = 0.053724, kmark = 0, density = 2450,
          markdiameter = 0.0025;
max no. (p,l,s,v,b):     26,     52,     39,       9,       3;;

menu:    parameter/particle/append;
pmenu: nmark = 3;
pmenu: coord = 1, xmark = 0.004275, ymark = -0.00573, zmark = 0.053913,
          kmark = 0, density = 2450, markdiameter = 0.0025, coord = 1,
          xmark = 0.000297, ymark = 0.002727, zmark = 0.052873, kmark = 0,
          density = 2450, markdiameter = 0.0025, coord = 1, xmark = 0.004239,
          ymark = 0.004536, zmark = 0.055229, kmark = 0, density = 2450,
          markdiameter = 0.0025;
max no. (p,l,s,v,b):     26,     52,     39,       9,       3;;

menu:    parameter/particle/append;
pmenu: nmark = 3;
pmenu: coord = 1, xmark = 0.002526, ymark = 0.000891, zmark = 0.058779,
          kmark = 0, density = 2450, markdiameter = 0.0025, coord = 1,
          xmark = -0.00134, ymark = -0.0017, zmark = 0.053814, kmark = 0,
          density = 2450, markdiameter = 0.0025, coord = 1, xmark = -0.001949,
          ymark = -0.00376, zmark = 0.051246, kmark = 0, density = 2450,
          markdiameter = 0.0025;
max no. (p,l,s,v,b):     26,     52,     39,       9,       3;;

menu:    parameter/particle/append;
pmenu: nmark = 3;
pmenu: coord = 1, xmark = 0.009072, ymark = -0.0061, zmark = 0.054368,
          kmark = 0, density = 2450, markdiameter = 0.0025, coord = 1,
          xmark = -0.00345, ymark = 0.001692, zmark = 0.052554, kmark = 0,
          density = 2450, markdiameter = 0.0025, coord = 1, xmark = -0.00633,
```

ymark = -0.00592, zmark = 0.053804, kmark = 0, density = 2450,
markdiameter = 0.0025;
max no. (p,l,s,v,b): 26, 52, 39, 9, 3;;

menu: parameter/particle/append;
pmenu: nmark = 3;
pmenu: coord = 1, xmark = -0.00721, ymark = -0.00398, zmark = 0.051127,
kmark = 0, density = 2450, markdiameter = 0.0025, coord = 1,
xmark = -0.00336, ymark = 0.006087, zmark = 0.053401, kmark = 0,
density = 2450, markdiameter = 0.0025, coord = 1, xmark = 0.005587,
ymark = 0.002212, zmark = 0.054026, kmark = 0, density = 2450,
markdiameter = 0.0025;
max no. (p,l,s,v,b): 26, 52, 39, 9, 3;;

menu: parameter/particle/append;
pmenu: nmark = 3;
pmenu: coord = 1, xmark = -0.00049, ymark = 0.009542, zmark = 0.051234,
kmark = 0, density = 2450, markdiameter = 0.0025, coord = 1,
xmark = 0.007651, ymark = -0.00158, zmark = 0.057897, kmark = 0,
density = 2450, markdiameter = 0.0025, coord = 1, xmark = 3.91e-005,
ymark = -0.00194, zmark = 0.051285, kmark = 0, density = 2450,
markdiameter = 0.0025;
max no. (p,l,s,v,b): 26, 52, 39, 9, 3;;

menu: parameter/particle/append;
pmenu: nmark = 3;
pmenu: coord = 1, xmark = -0.00213, ymark = 0.003647, zmark = 0.053592,
kmark = 0, density = 2450, markdiameter = 0.0025, coord = 1,
xmark = 0.001301, ymark = -0.0018, zmark = 0.055121, kmark = 0,
density = 2450, markdiameter = 0.0025, coord = 1, xmark = -0.0058,
ymark = -0.00361, zmark = 0.057897, kmark = 0, density = 2450,
markdiameter = 0.0025;
max no. (p,l,s,v,b): 26, 52, 39, 9, 3;;

menu: parameter/particle/append;
pmenu: nmark = 3;
pmenu: coord = 1, xmark = 0.008378, ymark = -0.00413, zmark = 0.059278,
kmark = 0, density = 2450, markdiameter = 0.0025, coord = 1,

xmark = 0.009602, ymark = -0.00375, zmark = 0.051751, kmark = 0,
density = 2450, markdiameter = 0.0025, coord = 1, xmark = 0.004788,
ymark = -0.00343, zmark = 0.051235, kmark = 0, density = 2450,
markdiameter = 0.0025;
max no. (p,l,s,v,b): 26, 52, 39, 9, 3;;

menu: parameter/particle/append;
pmenu: nmark = 3;
pmenu: coord = 1, xmark = -0.00372, ymark = 0.004935, zmark = 0.058047,
kmark = 0, density = 2450, markdiameter = 0.0025, coord = 1,
xmark = -0.00497, ymark = -0.00329, zmark = 0.059514, kmark = 0,
density = 2450, markdiameter = 0.0025, coord = 1, xmark = -0.00101,
ymark = 0.006572, zmark = 0.0589, kmark = 0, density = 2450,
markdiameter = 0.0025;
max no. (p,l,s,v,b): 26, 52, 39, 9, 3;;

menu: parameter/particle/append;
pmenu: nmark = 3;
pmenu: coord = 1, xmark = -0.00156, ymark = 0.002468, zmark = 0.051229,
kmark = 0, density = 2450, markdiameter = 0.0025, coord = 1,
xmark = -0.00582, ymark = 0.001918, zmark = 0.054053, kmark = 0,
density = 2450, markdiameter = 0.0025, coord = 1, xmark = -0.00575,
ymark = -0.00303, zmark = 0.053402, kmark = 0, density = 2450,
markdiameter = 0.0025;
max no. (p,l,s,v,b): 26, 52, 39, 9, 3;;

menu: parameter/particle/append;
pmenu: nmark = 3;
pmenu: coord = 1, xmark = -0.00257, ymark = -0.00569, zmark = 0.051233,
kmark = 0, density = 2450, markdiameter = 0.0025, coord = 1,
xmark = -0.00331, ymark = -0.00158, zmark = 0.059916, kmark = 0,
density = 2450, markdiameter = 0.0025, coord = 1, xmark = 0.00582,
ymark = 0.00214, zmark = 0.056501, kmark = 0, density = 2450,
markdiameter = 0.0025;
max no. (p,l,s,v,b): 26, 52, 39, 9, 3;;

menu: parameter/particle/append;
pmenu: nmark = 3;

```
pmenu: coord = 1, xmark = 0.00388, ymark = 0.005278, zmark = 0.058114,
        kmark = 0, density = 2450, markdiameter = 0.0025, coord = 1,
        xmark = 0.000526, ymark = -0.00446, zmark = 0.059997, kmark = 0,
        density = 2450, markdiameter = 0.0025, coord = 1, xmark = 0.006964,
        ymark = -0.0032, zmark = 0.055834, kmark = 0, density = 2450,
        markdiameter = 0.0025;
max no. (p,l,s,v,b):     26,     52,     39,       9,       3;;

menu:    parameter/particle/append;
pmenu: nmark = 3;
pmenu: coord = 1, xmark = -0.00327, ymark = -0.00323, zmark = 0.054525,
        kmark = 0, density = 2450, markdiameter = 0.0025, coord = 1,
        xmark = -0.00361, ymark = -0.00361, zmark = 0.057406, kmark = 0,
        density = 2450, markdiameter = 0.0025, coord = 1, xmark = 0.00451,
        ymark = -0.00609, zmark = 0.05964, kmark = 0, density = 2450,
        markdiameter = 0.0025;
max no. (p,l,s,v,b):     26,     52,     39,       9,       3;;

menu:    parameter/particle/append;
pmenu: nmark = 3;
pmenu: coord = 1, xmark = -0.00787, ymark = -0.00142, zmark = 0.055481,
        kmark = 0, density = 2450, markdiameter = 0.0025, coord = 1,
        xmark = 0.005401, ymark = 0.01017, zmark = 0.058807, kmark = 0,
        density = 2450, markdiameter = 0.0025, coord = 1, xmark = -0.00128,
        ymark = 0.007208, zmark = 0.053358, kmark = 0, density = 2450,
        markdiameter = 0.0025;
max no. (p,l,s,v,b):     26,     52,     39,       9,       3;;

menu:    parameter/particle/append;
pmenu: nmark = 1;
pmenu: coord = 1, xmark = -0.00824, ymark = -0.00391, zmark = 0.055005,
        kmark = 0, density = 2450, markdiameter = 0.0025;
max no. (p,l,s,v,b):     26,     52,     39,       9,       3;;

menu:    parameter/particle/delete;
max no. (p,l,s,v,b):     26,     52,     39,       9,       3;;

menu:    parameter/particle/append;
```

```
pmenu: nmark = 3;
pmenu: coord = 1, xmark = -0.005377, ymark = -0.002595, zmark = 0.053242,
        kmark = 0, density = 2450, markdiameter = 0.0025, coord = 1,
        xmark = -0.004595, ymark = -0.001008, zmark = 0.051266, kmark = 0,
        density = 2450, markdiameter = 0.0025, coord = 1, xmark = 0.000337,
        ymark = -0.006001, zmark = 0.052252, kmark = 0, density = 2450,
        markdiameter = 0.0025;
max no. (p,l,s,v,b):     26,     52,     39,       9,       3;;

menu:    parameter/particle/append;
pmenu: nmark = 3;
pmenu: coord = 1, xmark = -0.000533, ymark = -0.003515, zmark = 0.05349,
        kmark = 0, density = 2450, markdiameter = 0.0025, coord = 1,
        xmark = 0.006127, ymark = 0.001289, zmark = 0.051235, kmark = 0,
        density = 2450, markdiameter = 0.0025, coord = 1, xmark = 0.007795,
        ymark = -0.004712, zmark = 0.055467, kmark = 0, density = 2450,
        markdiameter = 0.0025;
max no. (p,l,s,v,b):     26,     52,     39,       9,       3;;

menu:    parameter/particle/append;
pmenu: nmark = 3;
pmenu: coord = 1, xmark = 0.002662, ymark = -0.005836, zmark = 0.051266,
        kmark = 0, density = 2450, markdiameter = 0.0025, coord = 1,
        xmark = -0.006327, ymark = -0.005179, zmark = 0.053862, kmark = 0,
        density = 2450, markdiameter = 0.0025, coord = 1, xmark = -0.003479,
        ymark = -0.001852, zmark = 0.055448, kmark = 0, density = 2450,
        markdiameter = 0.0025;
max no. (p,l,s,v,b):     26,     52,     39,       9,       3;;

menu:    parameter/particle/append;
pmenu: nmark = 3;
pmenu: coord = 1, xmark = 0.003786, ymark = -0.004587, zmark = 0.058091,
        kmark = 0, density = 2450, markdiameter = 0.0025, coord = 1,
        xmark = -0.002522, ymark = -0.002374, zmark = 0.051484, kmark = 0,
        density = 2450, markdiameter = 0.0025, coord = 1, xmark = 0.007069,
        ymark = 2.5e-005, zmark = 0.053198, kmark = 0, density = 2450,
        markdiameter = 0.0025;
max no. (p,l,s,v,b):     26,     52,     39,       9,       3;;
```

menu: parameter/particle/append;
pmenu: nmark = 3;
pmenu: coord = 1, xmark = 0.000736, ymark = 0.009718, zmark = 0.051572,
kmark = 0, density = 2450, markdiameter = 0.0025, coord = 1,
xmark = 0.005292, ymark = -0.003906, zmark = 0.053467, kmark = 0,
density = 2450, markdiameter = 0.0025, coord = 1, xmark = 0.006734,
ymark = -0.003443, zmark = 0.051397, kmark = 0, density = 2450,
markdiameter = 0.0025;
max no. (p,l,s,v,b): 26, 52, 39, 9, 3;;

menu: parameter/particle/append;
pmenu: nmark = 3;
pmenu: coord = 1, xmark = -0.002513, ymark = 0.006752, zmark = 0.054714,
kmark = 0, density = 2450, markdiameter = 0.0025, coord = 1,
xmark = 0.003544, ymark = 0.005611, zmark = 0.052382, kmark = 0,
density = 2450, markdiameter = 0.0025, coord = 1, xmark = -0.005995,
ymark = -0.00139, zmark = 0.055346, kmark = 0, density = 2450,
markdiameter = 0.0025;
max no. (p,l,s,v,b): 26, 52, 39, 9, 3;;

menu: parameter/particle/append;
pmenu: nmark = 3;
pmenu: coord = 1, xmark = -0.005263, ymark = 0.000134, zmark = 0.053325,
kmark = 0, density = 2450, markdiameter = 0.0025, coord = 1,
xmark = 0.002388, ymark = 0.001189, zmark = 0.057274, kmark = 0,
density = 2450, markdiameter = 0.0025, coord = 1, xmark = -0.001913,
ymark = -5.9e-005, zmark = 0.051221, kmark = 0, density = 2450,
markdiameter = 0.0025;
max no. (p,l,s,v,b): 26, 52, 39, 9, 3;;

menu: parameter/particle/append;
pmenu: nmark = 3;
pmenu: coord = 1, xmark = 0.008323, ymark = -0.001576, zmark = 0.05126,
kmark = 0, density = 2450, markdiameter = 0.0025, coord = 1,
xmark = 0.001578, ymark = -0.002247, zmark = 0.053188, kmark = 0,
density = 2450, markdiameter = 0.0025, coord = 1, xmark = -0.003938,
ymark = -0.005794, zmark = 0.05488, kmark = 0, density = 2450,

markdiameter = 0.0025;
max no. (p,l,s,v,b): 26, 52, 39, 9, 3;;

menu: parameter/particle/append;
pmenu: nmark = 3;
pmenu: coord = 1, xmark = -0.006941, ymark = -0.000346, zmark = 0.057422,
kmark = 0, density = 2450, markdiameter = 0.0025, coord = 1,
xmark = 0.003111, ymark = -0.002726, zmark = 0.054947, kmark = 0,
density = 2450, markdiameter = 0.0025, coord = 1, xmark = -0.004542,
ymark = -0.001765, zmark = 0.057849, kmark = 0, density = 2450,
markdiameter = 0.0025;
max no. (p,l,s,v,b): 26, 52, 39, 9, 3;;

menu: parameter/particle/append;
pmenu: nmark = 3;
pmenu: coord = 1, xmark = 0.000852, ymark = 0.005921, zmark = 0.054638,
kmark = 0, density = 2450, markdiameter = 0.0025, coord = 1,
xmark = 0.000207, ymark = 0.002805, zmark = 0.057292, kmark = 0,
density = 2450, markdiameter = 0.0025, coord = 1, xmark = 0.004552,
ymark = 0.003468, zmark = 0.051209, kmark = 0, density = 2450,
markdiameter = 0.0025;
max no. (p,l,s,v,b): 26, 52, 39, 9, 3;;

menu: parameter/particle/append;
pmenu: nmark = 3;
pmenu: coord = 1, xmark = 0.004889, ymark = -0.000852, zmark = 0.053915,
kmark = 0, density = 2450, markdiameter = 0.0025, coord = 1,
xmark = 0.003724, ymark = -0.003008, zmark = 0.051284, kmark = 0,
density = 2450, markdiameter = 0.0025, coord = 1, xmark = 0.00621,
ymark = 0.000323, zmark = 0.055573, kmark = 0, density = 2450,
markdiameter = 0.0025;
max no. (p,l,s,v,b): 26, 52, 39, 9, 3;;

menu: parameter/particle/append;
pmenu: nmark = 3;
pmenu: coord = 1, xmark = -0.008529, ymark = -0.002486, zmark = 0.054787,
kmark = 0, density = 2450, markdiameter = 0.0025, coord = 1,
xmark = 0.002168, ymark = -0.004733, zmark = 0.053462, kmark = 0,

density = 2450, markdiameter = 0.0025, coord = 1, xmark = -0.001851,
ymark = -0.005937, zmark = 0.053365, kmark = 0, density = 2450,
markdiameter = 0.0025;
max no. (p,l,s,v,b): 26, 52, 39, 9, 3;;

menu: parameter/particle/append;
pmenu: nmark = 3;
pmenu: coord = 1, xmark = -0.002965, ymark = 0.005925, zmark = 0.051921,
kmark = 0, density = 2450, markdiameter = 0.0025, coord = 1,
xmark = -0.001856, ymark = -0.001166, zmark = 0.05349, kmark = 0,
density = 2450, markdiameter = 0.0025, coord = 1, xmark = 0.000437,
ymark = -0.000121, zmark = 0.053126, kmark = 0, density = 2450,
markdiameter = 0.0025;
max no. (p,l,s,v,b): 26, 52, 39, 9, 3;;

menu: parameter/particle/append;
pmenu: nmark = 3;
pmenu: coord = 1, xmark = 0.00174, ymark = -0.005035, zmark = 0.056348,
kmark = 0, density = 2450, markdiameter = 0.0025, coord = 1,
xmark = 0.004196, ymark = 0.004612, zmark = 0.055293, kmark = 0,
density = 2450, markdiameter = 0.0025, coord = 1, xmark = 0.002259,
ymark = 0.007123, zmark = 0.058237, kmark = 0, density = 2450,
markdiameter = 0.0025;
max no. (p,l,s,v,b): 26, 52, 39, 9, 3;;

menu: parameter/particle/append;
pmenu: nmark = 3;
pmenu: coord = 1, xmark = -0.00094, ymark = -0.000258, zmark = 0.055578,
kmark = 0, density = 2450, markdiameter = 0.0025, coord = 1,
xmark = -0.003935, ymark = 0.004082, zmark = 0.053655, kmark = 0,
density = 2450, markdiameter = 0.0025, coord = 1, xmark = -2.5e-005,
ymark = -0.005986, zmark = 0.05486, kmark = 0, density = 2450,
markdiameter = 0.0025;
max no. (p,l,s,v,b): 26, 52, 39, 9, 3;;

menu: parameter/particle/append;
pmenu: nmark = 3;
pmenu: coord = 1, xmark = -0.003203, ymark = -0.003867, zmark = 0.053465,

kmark = 0, density = 2450, markdiameter = 0.0025, coord = 1,
xmark = 0.000295, ymark = 0.001926, zmark = 0.051347, kmark = 0,
density = 2450, markdiameter = 0.0025, coord = 1, xmark = -0.002009,
ymark = 0.002438, zmark = 0.055539, kmark = 0, density = 2450,
markdiameter = 0.0025;
max no. (p,l,s,v,b): 26, 52, 39, 9, 3;;

menu: parameter/particle/append;
pmenu: nmark = 3;
pmenu: coord = 1, xmark = -0.00625, ymark = -0.005173, zmark = 0.057222,
kmark = 0, density = 2450, markdiameter = 0.0025, coord = 1,
xmark = -0.000538, ymark = -0.002748, zmark = 0.055809, kmark = 0,
density = 2450, markdiameter = 0.0025, coord = 1, xmark = -0.009831,
ymark = -0.004116, zmark = 0.051601, kmark = 0, density = 2450,
markdiameter = 0.0025;
max no. (p,l,s,v,b): 26, 52, 39, 9, 3;;

menu: parameter/particle/append;
pmenu: nmark = 3;
pmenu: coord = 1, xmark = -0.002729, ymark = 0.000372, zmark = 0.057366,
kmark = 0, density = 2450, markdiameter = 0.0025, coord = 1,
xmark = -0.006548, ymark = 0.000911, zmark = 0.051248, kmark = 0,
density = 2450, markdiameter = 0.0025, coord = 1, xmark = 0.005442,
ymark = 0.002499, zmark = 0.053322, kmark = 0, density = 2450,
markdiameter = 0.0025;
max no. (p,l,s,v,b): 26, 52, 39, 9, 3;;

menu: parameter/particle/append;
pmenu: nmark = 3;
pmenu: coord = 1, xmark = -0.000259, ymark = 0.008835, zmark = 0.053978,
kmark = 0, density = 2450, markdiameter = 0.0025, coord = 1,
xmark = -0.005222, ymark = -0.006048, zmark = 0.051854, kmark = 0,
density = 2450, markdiameter = 0.0025, coord = 1, xmark = 0.007373,
ymark = -0.005343, zmark = 0.052904, kmark = 0, density = 2450,
markdiameter = 0.0025;
max no. (p,l,s,v,b): 26, 52, 39, 9, 3;;

menu: parameter/particle/append;

pmenu: nmark = 3;
pmenu: coord = 1, xmark = 0.000382, ymark = 0.009331, zmark = 0.057132,
kmark = 0, density = 2450, markdiameter = 0.0025, coord = 1,
xmark = 0.001351, ymark = -0.003798, zmark = 0.051202, kmark = 0,
density = 2450, markdiameter = 0.0025, coord = 1, xmark = -0.00731,
ymark = -0.003922, zmark = 0.051676, kmark = 0, density = 2450,
markdiameter = 0.0025;
max no. (p,l,s,v,b): 26, 52, 39, 9, 3;;

menu: parameter/particle/append;
pmenu: nmark = 3;
pmenu: coord = 1, xmark = 0.002009, ymark = 0.004628, zmark = 0.05673,
kmark = 0, density = 2450, markdiameter = 0.0025, coord = 1,
xmark = 0.005114, ymark = 0.003108, zmark = 0.058174, kmark = 0,
density = 2450, markdiameter = 0.0025, coord = 1, xmark = -0.001105,
ymark = -0.004334, zmark = 0.051211, kmark = 0, density = 2450,
markdiameter = 0.0025;
max no. (p,l,s,v,b): 26, 52, 39, 9, 3;;

menu: parameter/particle/append;
pmenu: nmark = 3;
pmenu: coord = 1, xmark = -0.000478, ymark = -0.000248, zmark = 0.058232,
kmark = 0, density = 2450, markdiameter = 0.0025, coord = 1,
xmark = -0.005722, ymark = 0.00177, zmark = 0.058041, kmark = 0,
density = 2450, markdiameter = 0.0025, coord = 1, xmark = -0.002497,
ymark = -0.003814, zmark = 0.051183, kmark = 0, density = 2450,
markdiameter = 0.0025;
max no. (p,l,s,v,b): 26, 52, 39, 9, 3;;

menu: parameter/particle/append;
pmenu: nmark = 3;
pmenu: coord = 1, xmark = -0.000418, ymark = 0.007101, zmark = 0.052108,
kmark = 0, density = 2450, markdiameter = 0.0025, coord = 1,
xmark = -0.003987, ymark = 0.001506, zmark = 0.051251, kmark = 0,
density = 2450, markdiameter = 0.0025, coord = 1, xmark = 0.003671,
ymark = -0.001455, zmark = 0.057478, kmark = 0, density = 2450,
markdiameter = 0.0025;
max no. (p,l,s,v,b): 26, 52, 39, 9, 3;;

menu: parameter/particle/append;
pmenu: nmark = 3;
pmenu: coord = 1, xmark = -0.000411, ymark = 0.00425, zmark = 0.053109,
kmark = 0, density = 2450, markdiameter = 0.0025, coord = 1,
xmark = -0.000127, ymark = -0.001845, zmark = 0.051264, kmark = 0,
density = 2450, markdiameter = 0.0025, coord = 1, xmark = 0.007701,
ymark = -0.003084, zmark = 0.053722, kmark = 0, density = 2450,
markdiameter = 0.0025;
max no. (p,l,s,v,b): 26, 52, 39, 9, 3;;

menu: parameter/particle/append;
pmenu: nmark = 3;
pmenu: coord = 1, xmark = 0.002789, ymark = 0.00606, zmark = 0.053516,
kmark = 0, density = 2450, markdiameter = 0.0025, coord = 1,
xmark = -0.002573, ymark = -0.004037, zmark = 0.056392, kmark = 0,
density = 2450, markdiameter = 0.0025, coord = 1, xmark = 0.001694,
ymark = -0.000599, zmark = 0.055481, kmark = 0, density = 2450,
markdiameter = 0.0025;
max no. (p,l,s,v,b): 26, 52, 39, 9, 3;;

menu: parameter/particle/append;
pmenu: nmark = 3;
pmenu: coord = 1, xmark = -0.002516, ymark = 0.006214, zmark = 0.057033,
kmark = 0, density = 2450, markdiameter = 0.0025, coord = 1,
xmark = 0.002037, ymark = -0.000676, zmark = 0.051279, kmark = 0,
density = 2450, markdiameter = 0.0025, coord = 1, xmark = 0.004281,
ymark = -0.005349, zmark = 0.055419, kmark = 0, density = 2450,
markdiameter = 0.0025;
max no. (p,l,s,v,b): 26, 52, 39, 9, 3;;

menu: parameter/particle/append;
pmenu: nmark = 3;
pmenu: coord = 1, xmark = 0.000315, ymark = 0.002229, zmark = 0.0547,
kmark = 0, density = 2450, markdiameter = 0.0025, coord = 1,
xmark = 0.009314, ymark = -0.004374, zmark = 0.052122, kmark = 0,
density = 2450, markdiameter = 0.0025, coord = 1, xmark = 0.006665,
ymark = -0.005517, zmark = 0.057668, kmark = 0, density = 2450,

markdiameter = 0.0025;
max no. (p,l,s,v,b): 26, 52, 39, 9, 3;;

menu: parameter/particle/append;
pmenu: nmark = 3;
pmenu: coord = 1, xmark = -0.001985, ymark = -0.002033, zmark = 0.057794,
kmark = 0, density = 2450, markdiameter = 0.0025, coord = 1,
xmark = 0.001181, ymark = -0.002231, zmark = 0.058148, kmark = 0,
density = 2450, markdiameter = 0.0025, coord = 1, xmark = 0.006157,
ymark = -0.000832, zmark = 0.058508, kmark = 0, density = 2450,
markdiameter = 0.0025;
max no. (p,l,s,v,b): 26, 52, 39, 9, 3;;

menu: parameter/particle/append;
pmenu: nmark = 3;
pmenu: coord = 1, xmark = -0.002154, ymark = 0.001574, zmark = 0.053071,
kmark = 0, density = 2450, markdiameter = 0.0025, coord = 1,
xmark = 0.008026, ymark = -0.003238, zmark = 0.057876, kmark = 0,
density = 2450, markdiameter = 0.0025, coord = 1, xmark = 0.004561,
ymark = -0.000695, zmark = 0.05127, kmark = 0, density = 2450,
markdiameter = 0.0025;
max no. (p,l,s,v,b): 26, 52, 39, 9, 3;;

menu: parameter/particle/append;
pmenu: nmark = 3;
pmenu: coord = 1, xmark = 0.003055, ymark = 0.003231, zmark = 0.053355,
kmark = 0, density = 2450, markdiameter = 0.0025, coord = 1,
xmark = 0.002836, ymark = 0.001716, zmark = 0.051311, kmark = 0,
density = 2450, markdiameter = 0.0025, coord = 1, xmark = -0.007055,
ymark = -0.001562, zmark = 0.051238, kmark = 0, density = 2450,
markdiameter = 0.0025;
max no. (p,l,s,v,b): 26, 52, 39, 9, 3;;

menu: parameter/particle/append;
pmenu: nmark = 3;
pmenu: coord = 1, xmark = -0.005031, ymark = -0.003294, zmark = 0.056022,
kmark = 0, density = 2450, markdiameter = 0.0025, coord = 1,
xmark = -0.000472, ymark = -0.005029, zmark = 0.057133, kmark = 0,

density = 2450, markdiameter = 0.0025, coord = 1, xmark = -0.01018,
ymark = -0.006386, zmark = 0.052823, kmark = 0, density = 2450,
markdiameter = 0.0025;
max no. (p,l,s,v,b): 26, 52, 39, 9, 3;;

menu: parameter/particle/append;
pmenu: nmark = 3;
pmenu: coord = 1, xmark = -0.003497, ymark = 0.000564, zmark = 0.05499,
kmark = 0, density = 2450, markdiameter = 0.0025, coord = 1,
xmark = -0.003898, ymark = 0.003717, zmark = 0.056569, kmark = 0,
density = 2450, markdiameter = 0.0025, coord = 1, xmark = 0.001611,
ymark = 0.004147, zmark = 0.051454, kmark = 0, density = 2450,
markdiameter = 0.0025;
max no. (p,l,s,v,b): 26, 52, 39, 9, 3;;

menu: parameter/particle/append;
pmenu: nmark = 3;
pmenu: coord = 1, xmark = -0.001972, ymark = 0.003173, zmark = 0.051201,
kmark = 0, density = 2450, markdiameter = 0.0025, coord = 1,
xmark = -0.002917, ymark = -0.005993, zmark = 0.051176, kmark = 0,
density = 2450, markdiameter = 0.0025, coord = 1, xmark = -0.005813,
ymark = 0.001702, zmark = 0.055392, kmark = 0, density = 2450,
markdiameter = 0.0025;
max no. (p,l,s,v,b): 26, 52, 39, 9, 3;;

menu: parameter/particle/append;
pmenu: nmark = 1;
pmenu: coord = 1, xmark = -0.004773, ymark = 0.003789, zmark = 0.051238,
kmark = 0, density = 2450, markdiameter = 0.0025;
max no. (p,l,s,v,b): 26, 52, 39, 9, 3;;

menu: parameter/multi-phase flow;
pmenu: nphase = 1, idrift = 0, isdgsl = 0, iresta = 1, dtalph = 0,
alpha(min) = 0, rgsl = 0.0025, rhogsl = 2450, visco = 0,
sftension = 0, vterm0 = 0, stokes = 3, nonstokes = 1.5, speh = 0,
therco = 0, degx = 0, degy = 0, degz = 0, overx = 0, overy = 0,
overz = 0;
max no. (p,l,s,v,b): 26, 52, 39, 9, 3;;

menu: parameter/property;
pmenu: density = 1.205, sigma = 0;
max no. (p,l,s,v,b): 26, 52, 39, 9, 3;;

menu: parameter/acceleration;
pmenu: g = 0, 0, -9.80665, bf = 0, 0, 0, rotate0 = 0, rot_p = 0, 0, 0,
rot_v = 0, 0, 1;
max no. (p,l,s,v,b): 26, 52, 39, 9, 3;;

menu: parameter/viscosity;
pmenu: viscosity = 1.822e-005, newton = 0, nvistemp = 0, uplowvis = 1e+020,
0, 1e+020, 0, 1e+020, -273;
max no. (p,l,s,v,b): 26, 52, 39, 9, 3;;

menu: parameter/io;
pmenu: nintpo = 0, tintpo = 0.001, nowpost = 0, iwstrs = 0, iwchtr = 0,
iwpost = 0, iwmean = 0, itypos = 0, nfview = 0, nintre = 0,
iwrest = 0, ityres = 0, npower = 0, nforce = 0, iprint = 0,
pre.file = pre.txt, restart.file = restart.bin;
max no. (p,l,s,v,b): 26, 52, 39, 9, 3;;

menu: physical variable/set value/flow velocity;
click: total no. = 3, block = 3, block = 2, block = 1;
pmenu: select = velocity(x), value = 0, 0, 0;
max no. (p,l,s,v,b): 26, 52, 39, 9, 3;;

End of Read Session=I:¥andrey¥particle¥re-create yoshino¥100 particle 10^-6¥restart¥pre.his
menu: parameter/control;
pmenu: title = , nousr = 0, istead = 1, iturb = 1, nmax = -1, tmax = 10,
elapsed time(max) = 0, dt = 1e-006, couran = 0, irest = 1, iveloc = 1,
istokes = 0, imvgrd = 1, imvgsc = 1;
max no. (p,l,s,v,b): 26, 52, 39, 9, 3;;

menu: physical variable/set value/flow velocity;
click: total no. = 1, block = 3,
no. of mesh_range = 1, mesh range = 0,-1,0,0,0,-1;

```
pmenu: select = velocity(x), value = 0, 0, 1;
max no. (p,l,s,v,b):     26,     52,     39,       9,       3;;

menu:    physical variable/set value/flow velocity;
click: total no. = 1, block = 2,
          no. of mesh_range = 1, mesh range = 0,-1,0,0,0,-1;
pmenu: select = velocity(x), value = 0, 0, 1;
max no. (p,l,s,v,b):     26,     52,     39,       9,       3;;

menu:    physical variable/set value/flow velocity;
click: total no. = 1, block = 1,
          no. of mesh_range = 1, mesh range = 0,-1,0,0,0,-1;
pmenu: select = velocity(x), value = 0, 0, 1;
max no. (p,l,s,v,b):     26,     52,     39,       9,       3;;

menu:    parameter/particle/control;
pmenu: nintpg = 0, tintpg = 0, nptscal = 0, irestp = 0, iturbp = 0,
          nptclmax = 0, nptgmax = 0, rclenwpt = 0, nptcompt = 0, plencopt = 0,
          ireversp = 0, nwphis = 1, nwptcl = 1, ityptcl = 12, nopts_wr = 1,
          nopte_wr = -1, noptd_wr = 1, nwptwall = 1;
max no. (p,l,s,v,b):     26,     52,     39,       9,       3;;

menu:    parameter/dem/basic settings;
pmenu: idem = 1, idemrot = 1, idemiof = 1, sprcn = 100, sprct = 0,
          rescn = 0.95, resct = -1, fricc = 0.2, friccw = -1, rsrohnrp = 0,
          ndtfdem = 1, rdpdem = 1, rdpcont = 1, chtrpp = 0, chtrpw = 0,
          chtrpf = -1, idemcoh = 0;
max no. (p,l,s,v,b):     26,     52,     39,       9,       3;;
```